PHYSICAL VOLCANOLOGY OF RED CRATER, TONGARIRO.

A thesis
submitted in partial fulfillment
of the requirements for the degree

of

Master of Science in Earth Sciences

at
The University of Waikato
by

CANDICE JOY BARDSLEY

THE UNIVERSITY OF
WAIKATO
Te Whare Wānanga o Waikato

The University of Waikato
2004

ABSTRACT

The Tongariro Volcanic Centre (TVC) is New Zealand's most recently active volcanic centre and comprises two large active andesitic cones, Ruapehu and Tongariro. Tongariro is a dominantly andesitic cone complex, yet located at its centre is Red Crater, a basaltic andesite vent with an eruptive nature in striking contrast to the rest of Tongariro. The main aim of this research was to reconstruct the eruption history of this vent and provide the basis to model the impact of a range of future eruption scenarios from Tongariro.

The Red Crater basaltic andesite vent occupies a small scoria cone (~ 0.3 km^3) which has also erupted eleven lava flows including the single largest preserved lava flow on Tongariro, with a length of ~ 7 km and a volume of ~ 0.3 km^3. This flow was erupted between 9.7 ka and 3.4 ka, providing a maximum age for the vent. A distinctive feature of this vent is the exposed drained dike in the eastern wall.

Clast density (vesicularity), SEM, grain size, and petrographic analysis were undertaken on the deposits erupted from Red Crater, and used to constrain the timing of the lava flows in relation to the construction of the scoria cone. Average vesicularities for the Red Crater scoria deposits, exposed in the eastern and southern crater walls in particular, range from 51.5% to 76.8%, while the range of individual clasts is from 30.5% to 82.1%. These values classify Red Crater scoria as highly vesicular. This scoria section is ~ 60 metres thick and possibly erupted within a 48 hour period. The five lava flows erupted prior to this scoria cone construction (pre-1.85ka Taupo eruption) are andesitic blocky flows, with lengths up to ~7 km and thicknesses up to ~ 50 metres. Five basaltic andesite aa flows were erupted post 1.85 ka and coincided with the construction of the scoria cone. Maximum thicknesses are ~ 5 metres with lengths up to 0.98 km. The change in composition of the lava flows at this time is reflected by a change in the eruptive processes. Effusive activity dominated pre 1.85 ka while strombolian style eruptions producing discrete gas bursts dominated during the scoria cone construction post 1.85 ka. Two dikes are intruded into the scoria cone; one is the eastern wall and the other in the western wall.

The eruptive history of Red Crater can be divided into three phases. Phase one was probably initiated with a violent phreatic eruption caused by the interaction of an intruding dike with groundwater. The loss of volatiles during this phreatic eruption and through the permeable country rock lead to sustained effusive activity which produced the five andesite flows into Oturere Valley. Phase two began when more basaltic magma was injected into the system, with strombolian eruptions rapidly building the scoria cone and erupting the remaining six basaltic andesite lava flows. The basaltic andesite flow (flow 9) into Central Crater has the most mafic composition of any lava flow from the entire Tongariro cone complex. Phase three began when the withdrawal of magma from the dike caused a series of phreatic explosions originating from the deeper section of the NE-SW orientated dike, which violently excavated the NE trending Emerald Lakes explosion pits, the northern section of the scoria cone and the explosion pit on the south face of the cone. Minor ash and steam eruptions have been observed at the end of the last century, but it is the active fumaroles surrounding the vent which reveal Red Crater's currently active state, and potential for future eruptions.

ACKNOWLEDGMENTS

Undertaking the field work for this thesis proved to be one of the most difficult and yet rewarding endeavors I have ever attempted. The difficulties associated with field work in such a remote area were quickly forgotten whenever I stopped and looked at where I was. I consider myself incredibly lucky to have had the opportunity to work in such a spectacularly beautiful and awe-inspiring part of New Zealand.

In order to make the most of the time I spent in the field, weeks at a time were spent based at either Mangatapopo or Oturere Huts on the slopes of Tongariro. A huge thanks goes to the Department of Conservation and especially Jimmy Johnson for allowing me to make these huts (especially Oturere) my second home. Also hi and thanks to all the hut wardens I met while up there (especially Rach!), the nightly candle-lit card extravaganzas and debates were always entertaining!

I'm entirely indebted to everyone who volunteered to assist with field work and lug great weights of rocks off the mountain (Arne, Ailsa, Anthony, Darrin, Simon, Leigh, Kim, Sarah, Bec, Sue, Sam, Tim, Nicola, Shane and Jo). Whether you were faced with the five hour uphill slog to Oturere or the delights of conquering the devils staircase, I'm sure you all enjoyed it anyway! A big hug has to go to Arne for helping me find my stride in the field (and for keeping Rach and I entertained and safe from the clutches of cabin fever during the week the sun forgot to shine). Thanks to Sarah for all the photos (many of which are used in this thesis) and for forcing me to keep walking on the inaugural hike into Oturere. Huge thanks have to go to Jo, for sending me over the edge of an active crater on the end of a rope (see I do trust you!). Jo, Darrin, Sarah and Sam, I can't thank you guys enough for carrying all the abseil gear up to the top of Red Crater, the day turned out to be fantastic albeit very long! A thank you has to be put in here to my osteopaths (Geraldine and Liz in particular) for fixing me back up after each week in the field, I couldn't have kept going without the constant repairs.

Thanks to all the staff in the Earth Science department who have made the last six years enjoyable and for sharing your knowledge with us all. In particular Roger and Richard who make Volcanology a delight to learn! Thank you Richard for answering any questions I had, for editing and re-sculpting my chapters and for making sure I did a thesis in Volcanology. Your patience was greatly appreciated!

To my fellow strivers in thesis perfection, cheers for keeping me sane and always providing some light entertainment in the form of the joke board. Rachel, JK, Amy, Sarah, and Ross thanks for finishing three months ago and showing us all that yes there is a way out! To my extensionare compatriots, yay for not having to hand in all alone, Pete, Mike and Jennifer its being great to be able to feed off your knowledge in these last few weeks. A huge thanks also has to go to Steve, Arne, Xu, Kyle, Dave and Will, all of whom have helped enormously in the various areas where my knowledge was lacking!

Thanks to Karen for fuelling my interest in geography and life and being a great movie buddy, we need more teachers like you! Sherida, sorry for being so busy, but don't worry I have time to talk to you now! Thank you for listening to my grips and general venting of steam and always sharing in and encouraging my healthy eating habits!

To my family, Mum, Dad, Sam, Grandma and Grandad (and Patch and Bubbles), I can't thank you enough for all the encouragement and financial support you have provided me with over the past six years. Mum and Dad, you have had to put up with a lot and I thank you for being so understanding and encouraging. None of this would have being possible without you. Finally to Grandad, this thesis is for you as you have being a huge source of inspiration throughout my life, constantly encouraging me to do what I enjoy the most. Thank you.

TABLE OF CONTENTS

FIGURES

CHAPTER ONE – INTRODUCTION

CHAPTER TWO – STRATIGRAPHY

CHAPTER THREE – TEXTURAL AND COMPONENTRY ANALYSIS

CHAPTER FOUR – ERUPTIVE PROCESSES

CHAPTER FIVE – ERUPTIVE HISTORY

TABLES

CHAPTER ONE

INTRODUCTION

1.0 INTRODUCTION

Within this chapter an outline of the aim of this research will be given, identifying the key areas examined and the outcome which was hoped to be achieved. This will be followed by a detailed look at the geological and tectonic setting at both a regional and local scale.

1.1 AIM OF STUDY

The Tongariro Volcanic Centre (TVC) is New Zealand's most recently active volcanic centre and comprises two large active andesitic cones, Ruapehu and Tongariro. Numerous ash and lava eruptions have being produced from a number of different vents within historic times, most recently from Ngauruhoe in 1975 and Ruapehu in 1996. Despite this frequent activity there is still only a poor understanding of the range of sizes, types and frequencies of past eruptions in particular from the numerous vents on the Tongariro cone complex. A detailed understanding of the nature and dynamics of past Tongariro eruptions is absolutely critical for the successful reduction of future volcanic risk at Tongariro. With the ever-increasing numbers of tourists hiking the Tongariro Crossing each day, the need to understand the behavior of Red Crater (which the track cuts across) becomes even more critical.

Tongariro is a dominantly andesitic cone complex, yet located at its centre is Red Crater, a basaltic andesite vent with an eruptive nature in striking contrast to the rest of Tongariro. The aim of this research is therefore to characterize, quantify and model the recent eruptive behavior of the Red Crater vent, which is one of the most productive of the five active vents on the Tongariro cone complex. The Red Crater vent occupies a small scoria cone, but a number of small to large volume lava flows have also been erupted from the Red Crater vent. Most recently it was active in the late 1800's (Gregg, 1961b).

This research has involved a detailed geological investigation of the cone deposits and associated lava flows, which has allowed the determination of the magnitudes, styles

and timing of eruptions which have constructed this cone. Fieldwork has characterized the deposits and volcanic features, while sampling of both scoria and lava has quantified the factors controlling the generation, storage and eruption of magma from Red Crater.

With this field and laboratory data, the main aim of this research was to reconstruct the eruption history of this vent and provide the basis to model the impact of a range of future eruption scenarios from Tongariro.

1.2 Geological and Tectonic Setting

Late Cenozoic volcanism in New Zealand is dominatly the result of subduction beneath the North Island of the Pacific Plate along the Hikurangi trench at a rate of approximately 50 mm/yr (Bibby et al., 1995). This subduction setting, also known as a continental magmatic arc system (Gamble and Price, 2000; Price, 2000), has rotated south over time, currently fuelling the active Taupo Volcanic Zone (TVZ). This zone encompasses the majority of New Zealand's active volcanism, extending some 300 km from White Island in the north (its northern most sub-aerial expression), to Ruapehu in the south (Wilson et al., 1995).

The TVZ has a current width of approximately 60 km, which increases by 7-18 mm each year (Wilson et al., 1995). This extension is occurring asymmetrically, widening faster at its northern extent, whilst barely extending in the south (Gamble and Price, 2000). The Tonga-Kermadec Arc, of which the TVZ is the southern-most extent of, therefore pinches out at the central North Island volcanoes (Gamble and Price, 2000). The TVZ trends NE-SW and comprises of three main areas of volcanic activity. A central zone dominated by eight rhyolitic calderas, and southern and northern areas dominated by andesite cone volcanoes, as can be seen in Figure 1.1(Houghton et al., 1995).

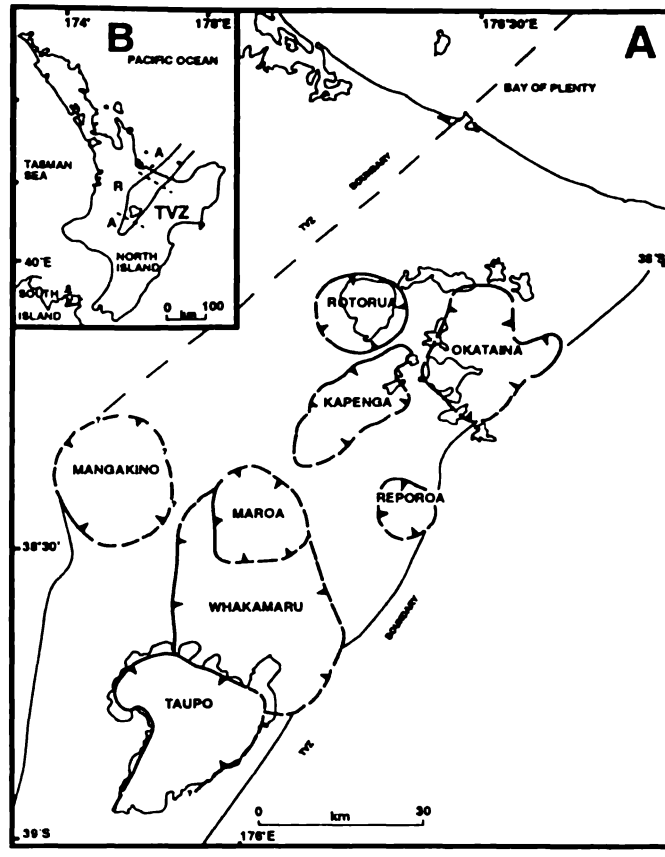

Figure 1.1 – A - The eight rhyolitic centers within the TVZ. **B** – TVZ showing the northern, central and southern section with A = Andesite and R = Rhyolite. Modified from Houghton et al. (1995).

The northern and southern sections of the TVZ have being active for the past 2.0 ma erupting predominantly andesite and dacite, while the central region is dominated by rhyolites and has being active for 1.6 ma (Houghton et al., 1995). In total, approximately 20 000 km^3 of material has being erupted (Wilson et al., 1995).

The Tongariro Volcanic Centre is itself ~55 km in length and is dominated by the two andesitic composite cones of Ruapehu and Tongariro. The oldest dated lavas from Tongariro are ~275 ka (Hobden et al., 1996). However, andesite-bearing gravels and lavas underneath the 0.34 ma Whakamaru ignimbrite suggest activity at Tongariro is at least as old (Topping, 1974).

Ruapehu and Tongariro have been modified by glacial erosion during the most recent glaciation between 26 and 15 thousand years ago (Mathews, 1967). Till deposits found in Oturere Valley and moraine ridges in Mangatapopo Valley are evidence of glaciers on Tongariro (Mathews, 1967). These glaciers carved out huge valleys such as the Mangatapopo and Oturere Valleys on Tongariro. Glaciers extended down as low as 1200 meters during the peak of the last glaciation. Volcanic activity at Tongariro cone complex can be roughly divided into three age groups: 1) deposits from activity prior to the last glaciation (>26,000 years old), 2) activity after the glaciation but before the 1.85 ka Taupo eruption, and 3) the recent eruptives deposited since the Taupo eruption (Hobden, 1997). The presence of the Taupo Ignimbrite upon Tongariro acts as an important stratigraphic age marker for recent volcanic activity.

The volcanic vents within the Tongariro complex can be divided into two chains as Figure 1.2 shows.

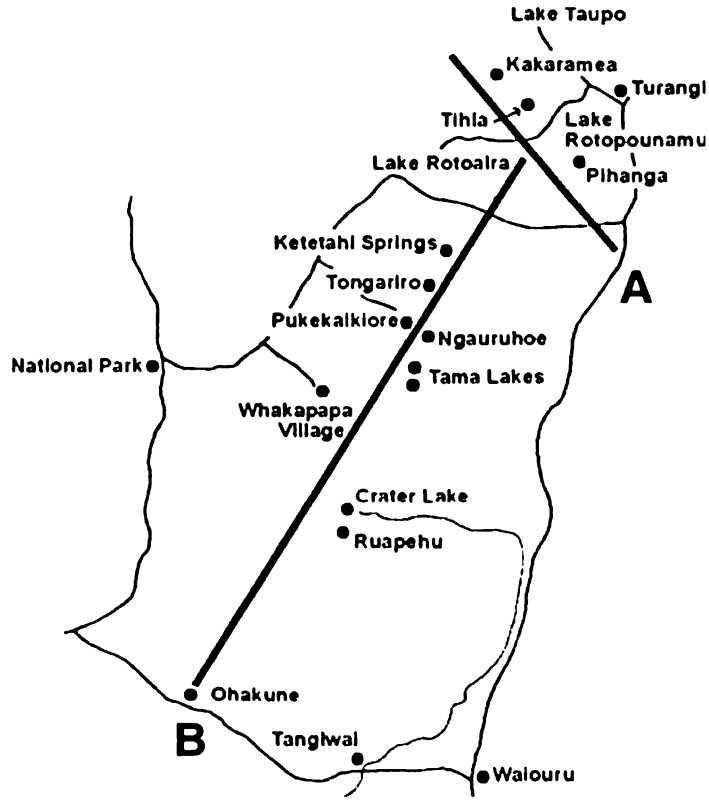

Figure 1.2 – **A** – NW-SE volcanic chain. **B** – NE-SW volcanic chain, modified from Williams (2001).

Fig 1.3a shows a cross section through the 10 km long, NW-SE trending vents which include Pihanga and Kakaramea. This NW-SE trending zone last erupted greater than 26 ka (Cole, 1978; Topping, 1974; Williams, 2001).

Figure 1.3b shows the NE-SW trending eruptive zone which is some 18 km long and 5 km wide and encompasses all the vents on Tongariro and Ruapehu. The point source of eruptions on Tongariro has changed numerous times over its life time. While there is no logical order or progression of active vents, all have occurred within the NE-SW trending eruptive zone and all have erupted in the last 26 ka as seen in Figure 1.4 (Cole, 1978; Price et al., 2003; Williams, 2001).

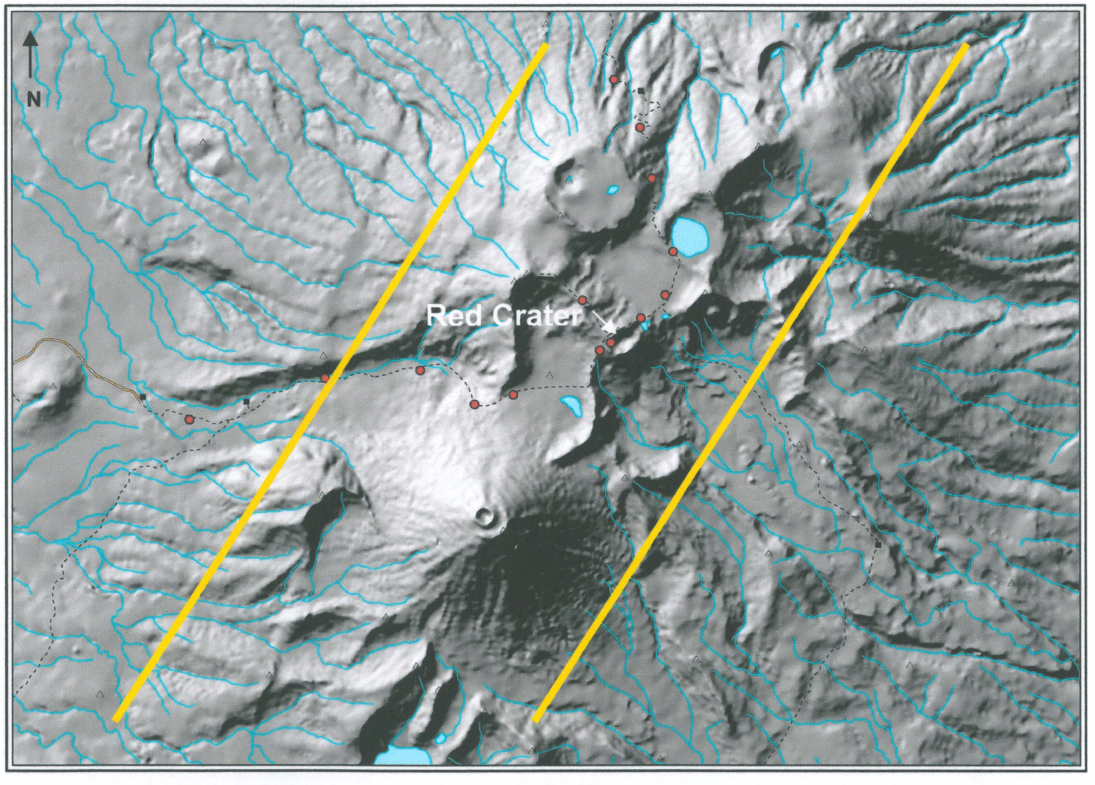

Figure 1.4 – NE-SW trending vent lineament as seen on Tongariro, modified from Price et al (2003).

Faults within the Tongariro Volcanic Centre predominantly strike NNE, as Figure1.5 shows (Gregg, 1961a; Gregg, 1961b). These are predominantly normal faults, and are associated with extension (Gregg, 1961a; Gregg, 1961b). Displacements along these faults are up to 15 metres.

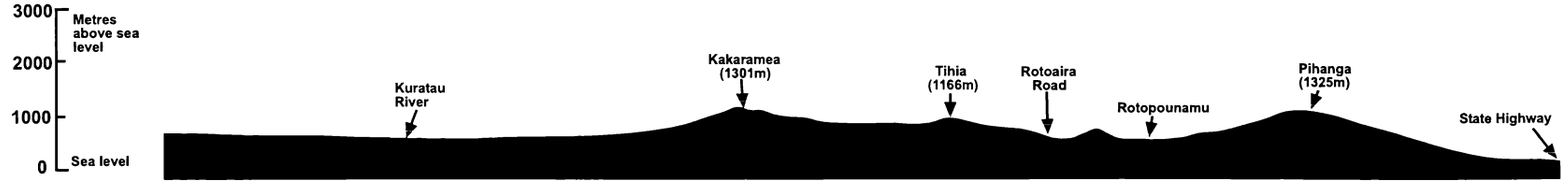

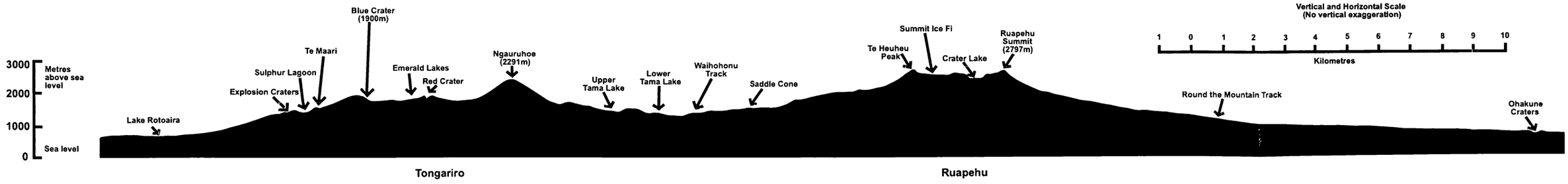

Figure 1.3 - Vent Lineaments of the Tongariro Volcanic Centre. **A** - NW-SE trending linement. **B** - NE-SW trending linement.

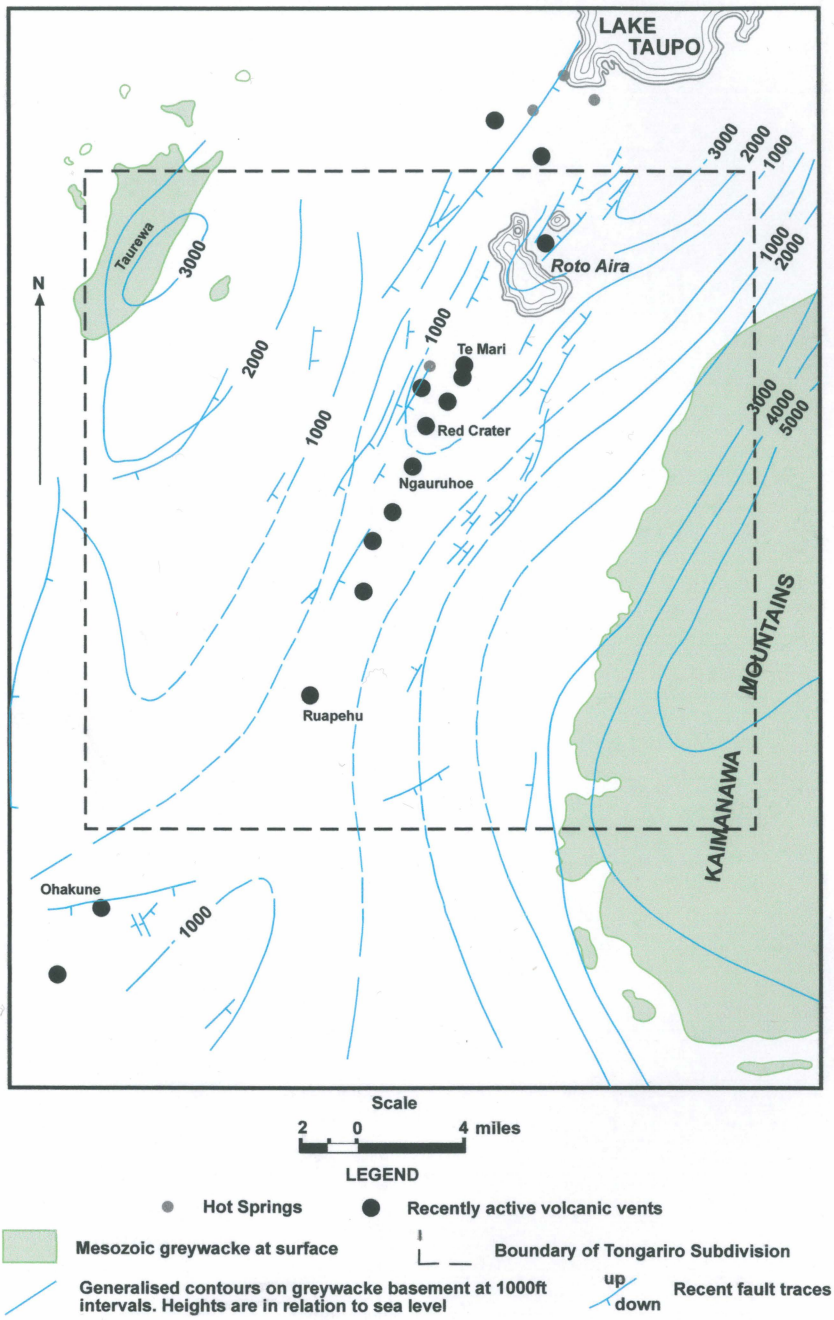

Figure 1.5 – Fault traces through the Tongariro National Park, modified from Gregg (1961b).

1.3 PREVIOUS WORK

1.3.1 19TH CENTURY WORKERS

Tongariro Volcanic Complex has being the focus of many research projects over the years, with one of the first published works occurring in Nature in 1870. This journal published an account of an eruption from Tongariro, witnessed by Dr J.D. Hooker. His records talk of an eruption beginning in April 1869 and continuing until at least the 18th of July. Explosions occurred approximately every five minutes, while ash clouds, lava flows and bursts of magma jets were all witnessed from Taupo (Hector, 1870). Based on the view of Tongariro from Taupo, it is likely that this was an eruption of the Te Mari Craters, which was confirmed by Dibble et al (1985). A second eruption of the Te Mari Craters on the north face of Tongariro, was witnessed by H. Hill in 1892. Hill (1893), also makes note of the increase in activity from the Tongariro Volcanic Complex vents since the 1886 AD Tarawera eruption. Hill (1893), also mentions that the western side of Red Crater was unusually active at the time of his ascent (January 1st, 1893).

1.3.2 20TH CENTURY WORKERS

The tectonic setting of Tongariro was illustrated by Gregg in 1961(a), emphasizing or highlighting how the fault traces were aligned in the same NE-SW trending zone as the volcanic vents. Matthews (1967) provides a close up look at the faults Gregg (1961a) discussed (Figure 1.6), and shows that apart from a poorly defined fault marked through Red Crater and the Emerald Lakes explosion pits, they are largely limited to the outer slopes of Tongariro and few structures are evident on the summit area.

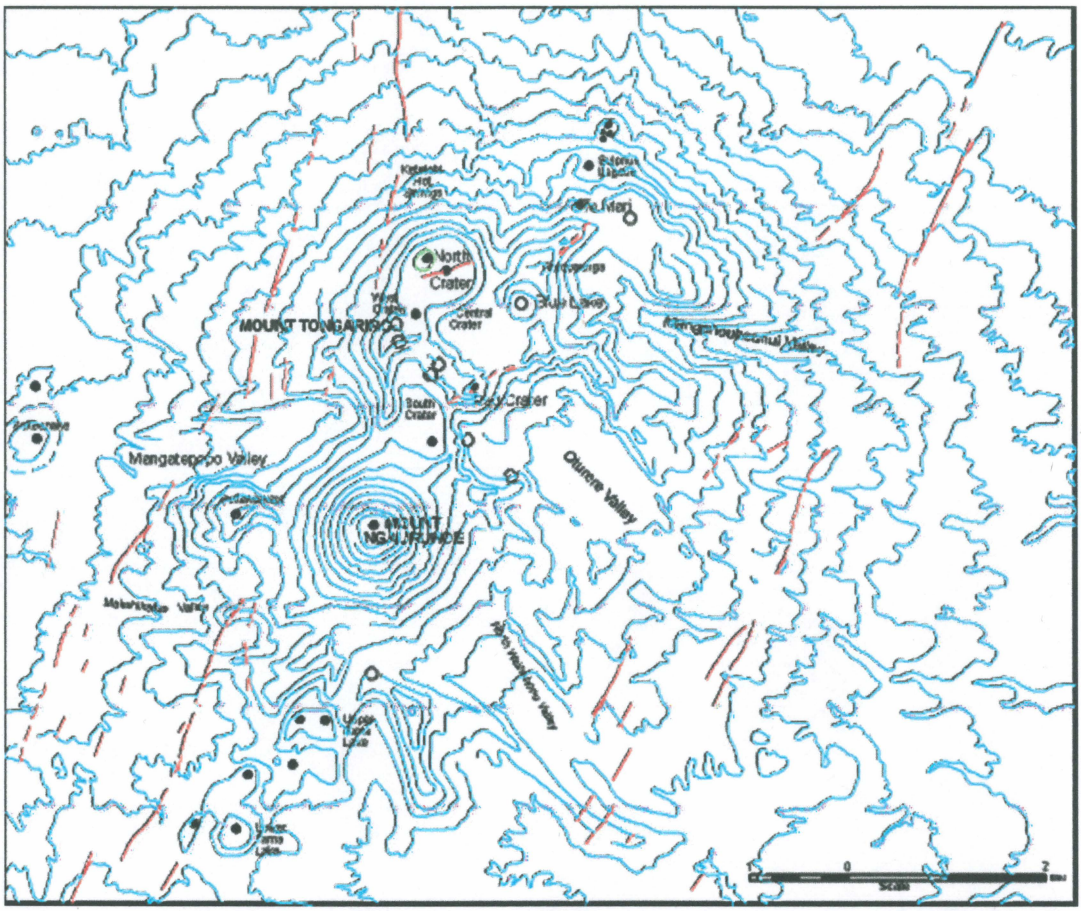

Figure 1.6 – Fault localities (in red) modified from map by Matthews (1967).

During the 1970's, Nairn (1976), documented the atmospheric shock waves from Ngauruhoe's 1975 eruptions, while Cole (1978) presented his findings on the andesites within the Tongariro Volcanic Centre. Cole (1978), confirmed the two vent lineaments seen within the complex, being the older NW-SE zone and the more recent lineament trending NE-SW. This vent alignment was fuelled from the underlying subduction zone (Cole, 1978), but while passing through the crust, involved crustal contamination. Cole et al (1983), examined rare-earth elements within the Taupo Volcanic Zone, finding that Red Crater basalts are 'low-Al' basalts with light rare-earth element values similar to the andesites they erupted through. Red Crater is the only location in the TVZ that these 'low-Al' basalts are found (Cole et al., 1983). The most comprehensive study of Tongariro carried out during the 1970's was by W.W. Topping (1974), who wrote his PhD on "Some aspects of Quaternary History of Tongariro Volcanic Centre". References to his work are made throughout this thesis.

Moore and Brock (1981) found that the Ketetahi hot springs in the northern face of Tongariro, are infact the surface expression of a steam-dominated geothermal system. While research into the volcanic hazards of the North Island in by Dibble et al (1985), found that the communication and energy networks around Tongariro were likely to be the most affected by future eruptions. The population is small in the area, so evacuation could be undertaken and lahar warning systems on Ruapehu have being installed (Dibble et al., 1985).

Hochstein (1985) undertook research looking at the steaming ground around both Te Mari and Red Craters. Steaming ground was characterized as all ground with ground temperatures above 70°C (Hochstein, 1985). Around Red Crater ~ 8 x 10^3 m^3 of steaming ground exists (Figure1.7) (Hochstein, 1985).

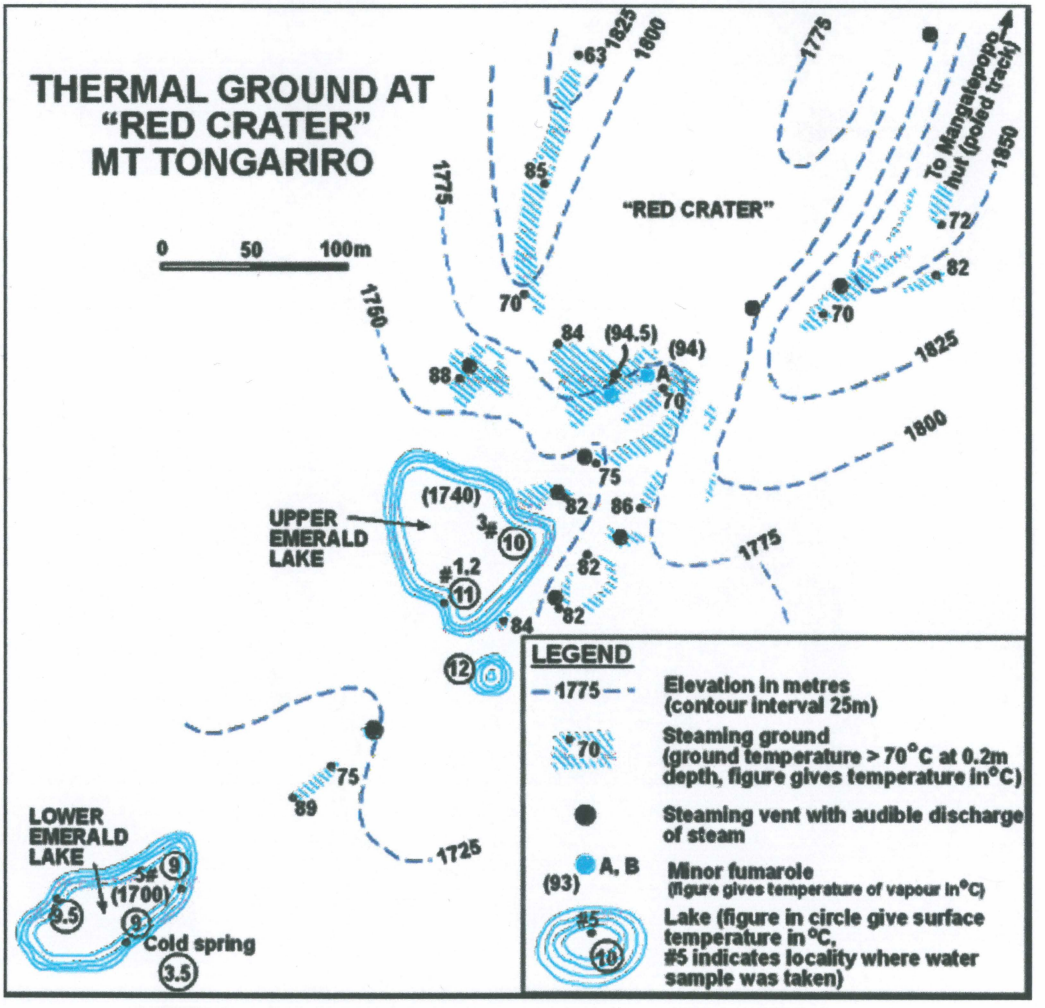

Figure 1.7 – Steaming ground at Red Crater modified from(Hochstein, 1985).

Steaming ground was also observed at the head of the Central Crater lava flows, at the same elevation as the steaming ground shown in Figure 1.7 beneath Red Crater (Hochstein, 1985). Hochstein (1985), stated this was due to, "...an enhanced natural draught of steam which presumably moves laterally beneath the valley floor." Due to this steaming ground being at an elevation of 1775 metres, it is the highest geothermal field in the TVZ and has a boiling temperature of 94.1°C

The greywacke and argillite, Mesozoic Torlesse basement terrane underlying the Tongariro complex was confirmed by Graham et al (1988), based on buchitic metagreywacke xenoliths erupted from Ngauruhoe.

The 1990's produced a great amount of research on Tongariro. Ruapehu and the Tama Lakes saddle were targeted by Zeng and Ingham (1993) for modeling of gravity data, with their findings showing andesites, pyroclastics and basement rock in three layers through a cross section of Ruapehu. This research was linked with AMT soundings on the Tama Lakes saddle by the same authors, identifying an andesitic intrusion beneath the lakes. Rogan and Blake (1994), confirmed mixing, contamination and crystallization had occurred in the magma system beneath Ngauruhoe, based on trace element zonations in Plagioclase crystals.

An in depth study on the andesitic tephra deposits from the Tongariro Volcanic Centre was carried out by Donoghue et al (1995). There findings revised earlier work of Topping (1974), grouping all Tongariro Volcanic Centre tephras into two groups – those being the Tongariro Subgroup and the Tukino Subgroup. Donoghue and Neall (1996) state that several of the tephras erupted from the Tongariro Volcanic Centre can be used as valuable chronostratigraphic marker beds, which is a new revelation given that marker beds are usually rhyolitic tephras (due to their greater dispersal area). Further work on tephrostratigraphy by Cronin and Neall (1997) reveals 15 lahar episodes from Ruapehu between >65 and 5 ka, and five lahar episodes from Tongariro between >24 and 14 ka.

A second comprehensive PhD, modeling magmatic trends to determine the eruptive and magmatic history of Tongariro, was completed by Hobden (1997). Reference to this work is made throughout this thesis. Hobden et al (1996) looked at K-Ar age determinations to understand the growth of the Tongariro cone complex. While Topping (1974), determined the post-glacial history using ^{14}C age determinations, Hobden et al. (1996), were able to target times of rapid cone growth at Tongariro – those being between 210-200 ka, 130-70 ka and 25 ka to the present day (Figure 1.8). Further research by Hobden et al. (1999) found that the complex plumbing system feeding Tongariro has produced, "...numerous small (<0.1 km3) and short-lived (≤1 ka) magma batches.

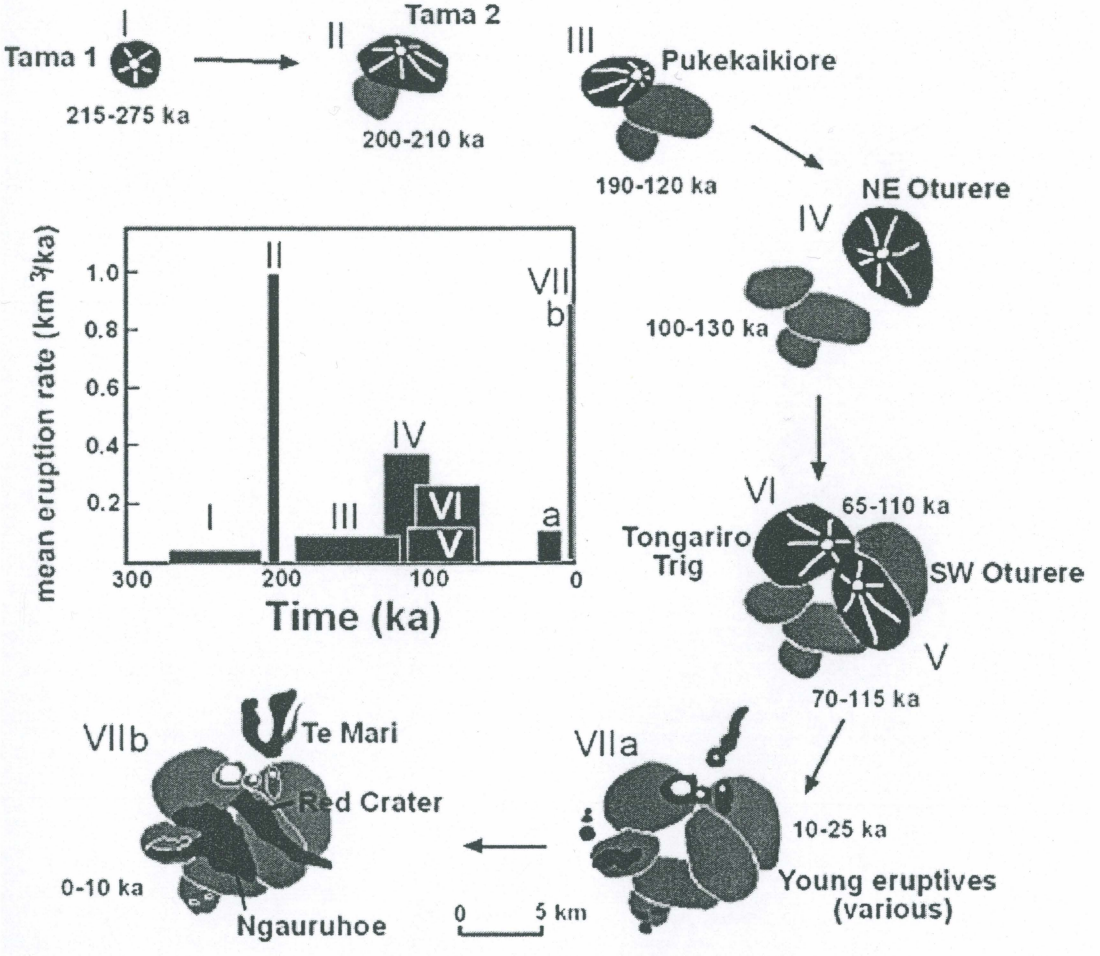

Figure 1.8 – Growth of the Tongariro Complex (Hobden, 1999).

Nairn et al. (1998) looked specifically at the six major pyroclastic eruptions which came from the Tongariro Volcanic Centre at around 10 ka. This research showed that multiple vents were active in the Centre at the same time, all located within the NNE striking vent lineament (Nairn et al., 1998). Accelerated rifting or extension right across the Centre was determined to be the reason for this increased activity, which involved several discrete magma bodies. This event was not specific to the Tongariro Volcanic Centre, but a regional event, with large rhyolitic tephras also erupted from Taupo volcano at the same time, inferring regional extension was occurring. Nakagawa et al (1998), showed that crystallization of dacitic magmas was occurring at ~ 8 km depth, while andesites and basaltic andesite magmas were crystallizing at ~ > 20 km depth.

Monitoring at Tongariro has increased of late due to the recent occurrence of Tornillos or low frequency seismic events beneath the volcano (Hagerty and Benites, 2003). Tornillos have preceded ash eruptions at Galeras Volcano in Colombia (Hagerty and Benites, 2003).

As established earlier in this chapter, Tongariro is a composite cone volcano which has being heavily eroded over time. Research by Lecointre et al (2002) showed that the Te Whaiau Formation (55-60 ka) located on the north western Tongariro ring plain is a massive debris flow, sourced from the area of the current summit of Tongariro. This study provides an understanding of how the three massive original cones of Tongariro (Hucks, 2000) could have being eroded.

Further research in 2002 was carried out by Hobden et al, who detailed the growth of the frequently active Ngauruhoe cone. Ngauruhoes history consists of numerous eruptive styles, including effusive, strombolian, vulcanian and sub-plinian (Hobden, 2002).

The first research to be done solely on Red Crater was undertaken by Stevens (2002), who used airborne interferometric radar to determine the size and emplacement behavior of the largest Red Crater lava flow. Stevens (2002) concluded that this 7 km long andesite flow has a volume of ~ 371 – 640 million m^3 and was emplaced between

3400 and 9700 years ago, and along with Hobden (1997), concluded it was likely to have represented a major emptying of the magma chamber. This lava flow was erupted as a single flow, with folding resulting from the slowing of the flow front (Stevens, 2002).

1.3.3 RECENT ERUPTIONS

The late 1800's saw a number of small eruptions from Red Crater recorded by Hochstetter, Thompson, Keam, Gregg, Hill, Thomas, Cussen, Speight, Turner and Thompson (Gregg, 1961b). Based on Gregg's (1961b) accounts of these papers, the following summary of activity in the late 1800s early 1900s can be listed.

1855 Ash eruption
1859 Steam eruption
1886 Collapse and disappearance of 'chimney-like cone, which stood near the verge of the Red Crater.' (Gregg, 1961b).
1887 Vigorous steaming
1888 Small lava-stream inside crater
1890 Vigorous steaming
1891 Violent steaming, suffocating sulphur fumes
1893 Western side very active
1897 Only two fumaroles active
1908 Vigorous steaming, very noisy
1911 Activity rapidly decreasing
1926 Vigorous steaming

CHAPTER TWO

STRATIGRAPHY

2.0 INTRODUCTION

The stratigraphy seen within Red Crater is complex and variable, with units often showing little continuity between the east, west and southern inner crater walls where units are exposed.

This chapter will begin by describing the structure and stratigraphy of the Red Crater scoria cone, which is based on detailed descriptions of the full thickness of the eastern inner-wall (outer wall facies) of the cone and seven other stratigraphic columns from the crater rim. Figure 2.1 illustrates the location within the crater where the full thickness of the eastern inner-wall was described, while Figure 2.2 shows the dip of the inner and outer facies of the Red Crater scoria cone. This will give a detailed understanding of the scoria cone lithofacies which make up Red Crater. Detailed descriptions of the lava flows which have originated from Red Crater will follow, with their link to the scoria cone stratigraphy being made.

2.1 SETTING

Red Crater occupies a small scoria cone perched on a glacially eroded slope at the head of Oturere Valley. The Red Crater vent system has been one of the most active and productive post-glacial vents on the Tongariro cone complex in the last 10 ka. It is bounded by Central Crater to its north-west and South Crater to its south-west, with the Oturere Valley expanding out from its entire eastern flank, as can be seen in Figure 2.3.

While the cone itself is the main focus of this research, the associated lava flows, emerald lakes explosion pits, plus the explosion pit on the south face of the cone will also be discussed. These last two features can be seen in Figure 2.4. Within the cone itself this chapter will be discussing the stratigraphy of the Eastern inner-wall, Eastern crater rim and Southern crater rim. These three localities are shown in Figure 2.5.

There are eleven main lava flows will be discussed within this chapter, six of which were erupted post c. 1.85 ka, and a further five prior to 1.85 ka.

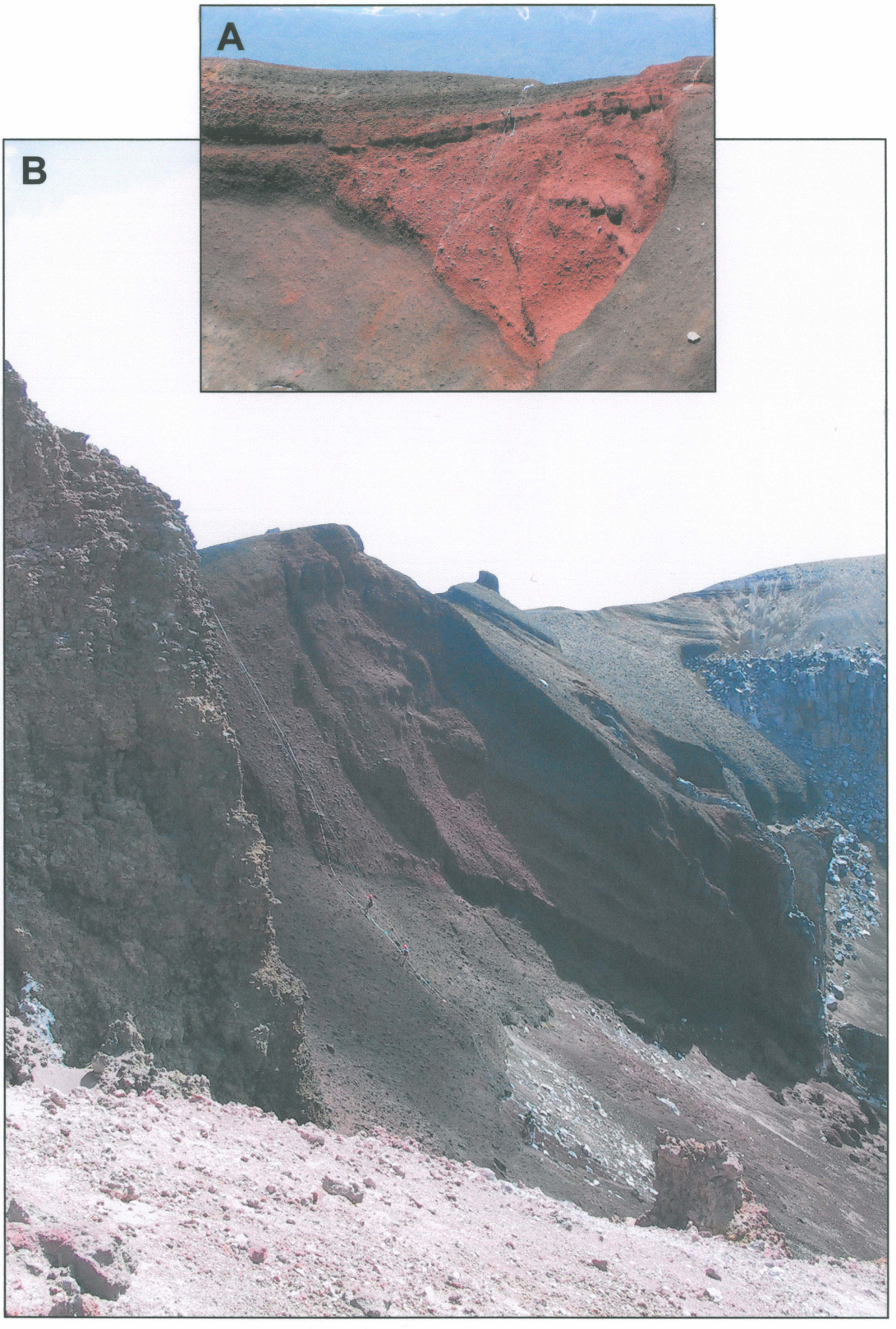

Figure 2.1 – Eastern inner-wall section, obtained via abseil. **A** – Looking east. **B** – Looking south.

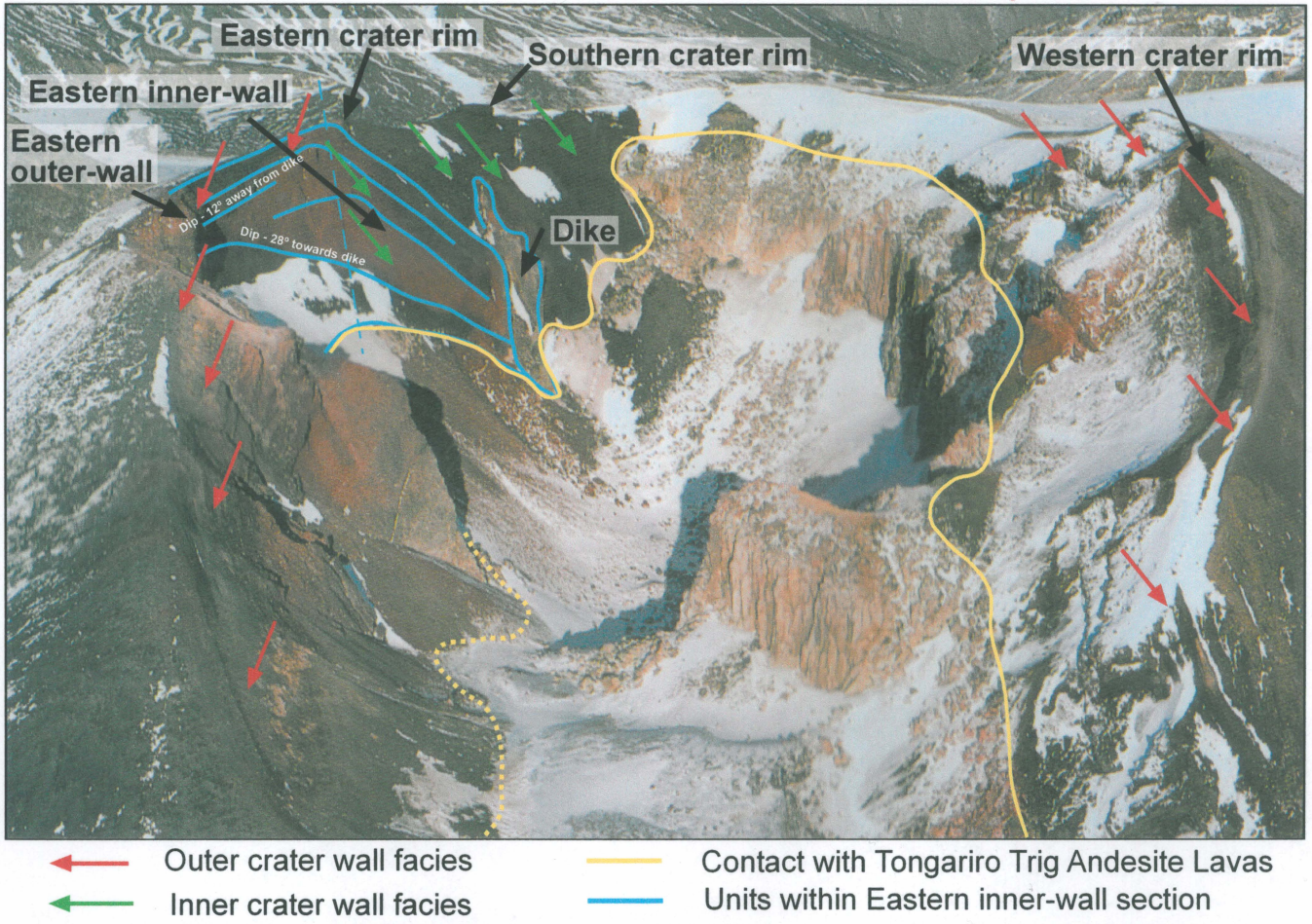

Figure 2.2 - Oblique photo of Red Crater, highlighting dip directions of scoria beds and contact with Tongariro Trig andsites.

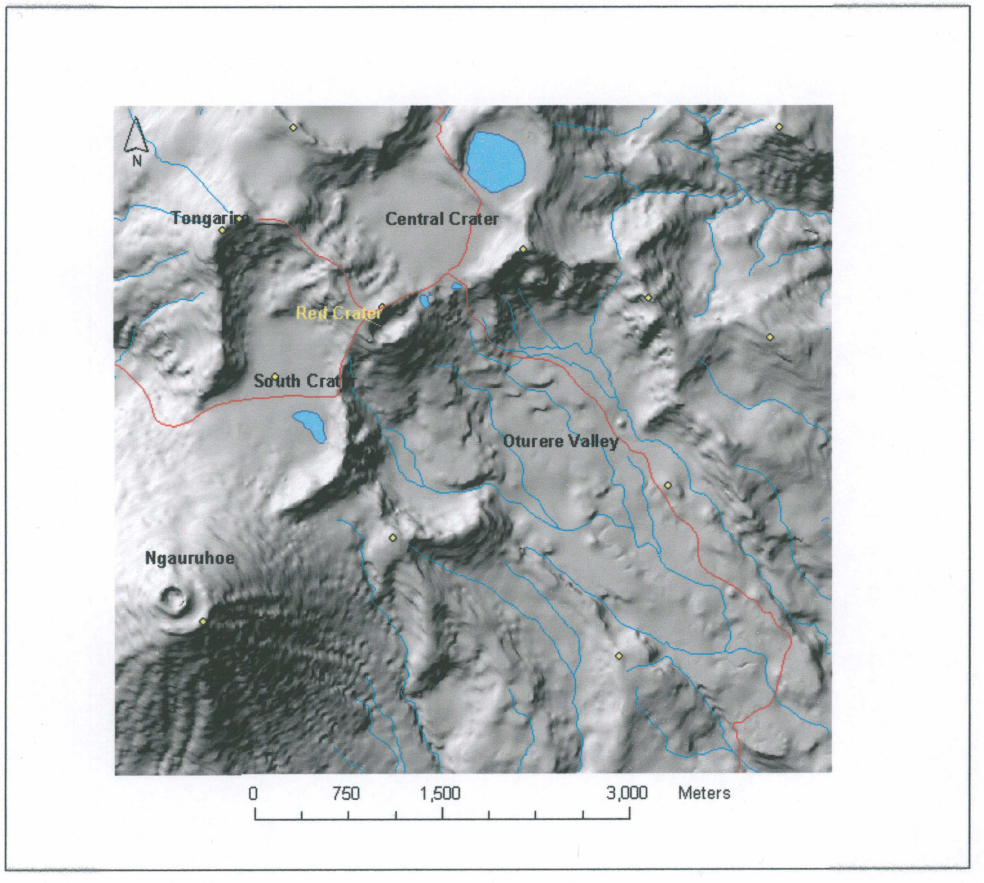

Figure 2.3 – DEM of Red Crater and surrounding features.

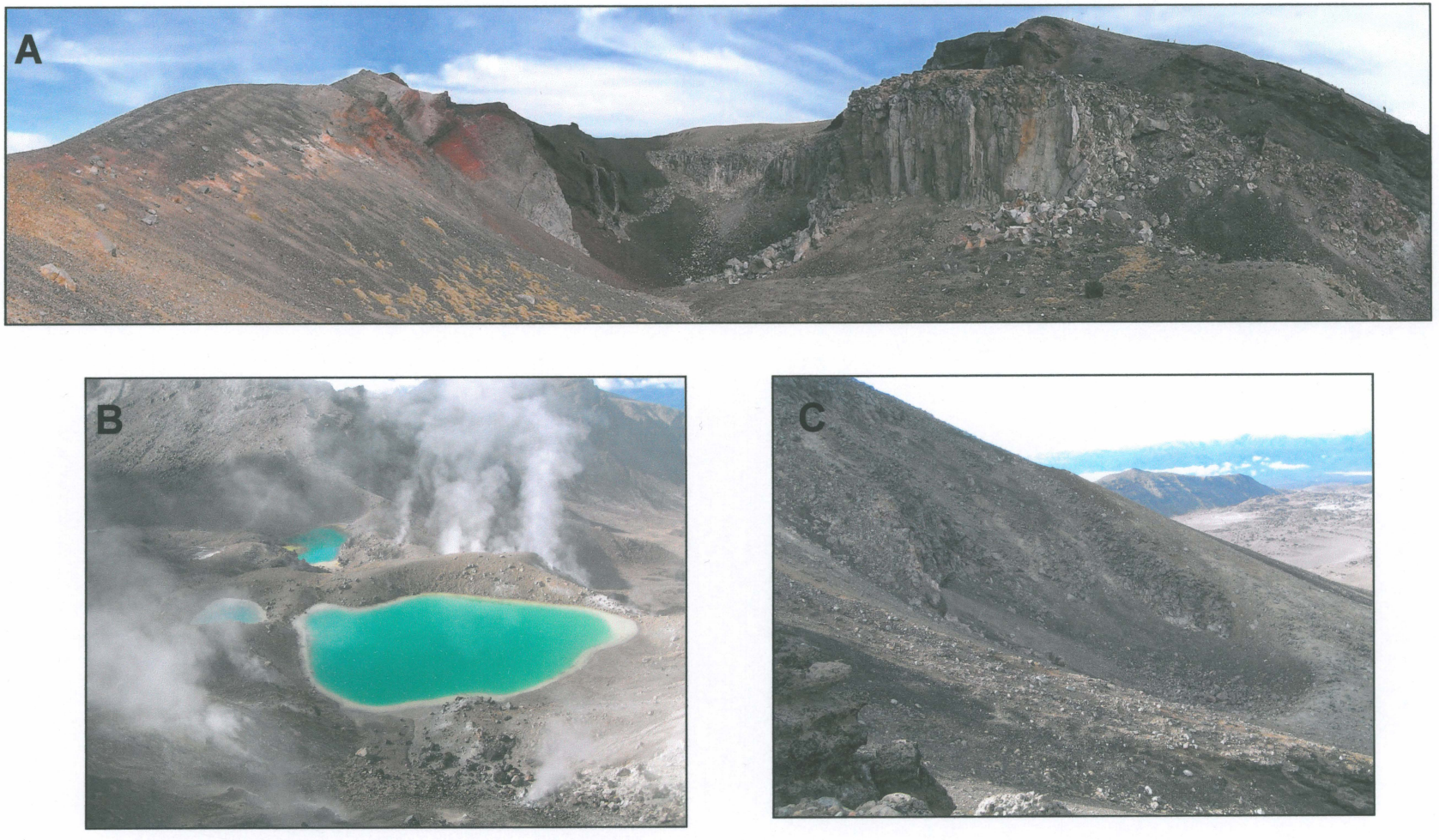

Figure 2.4 – **A** - Red Crater Cone as seen looking towards the south. **B** - Emerald Lakes, filling several explosion craters that extend NE from Red Crater. **C** - Explosion pit on the south face of Red Crater.

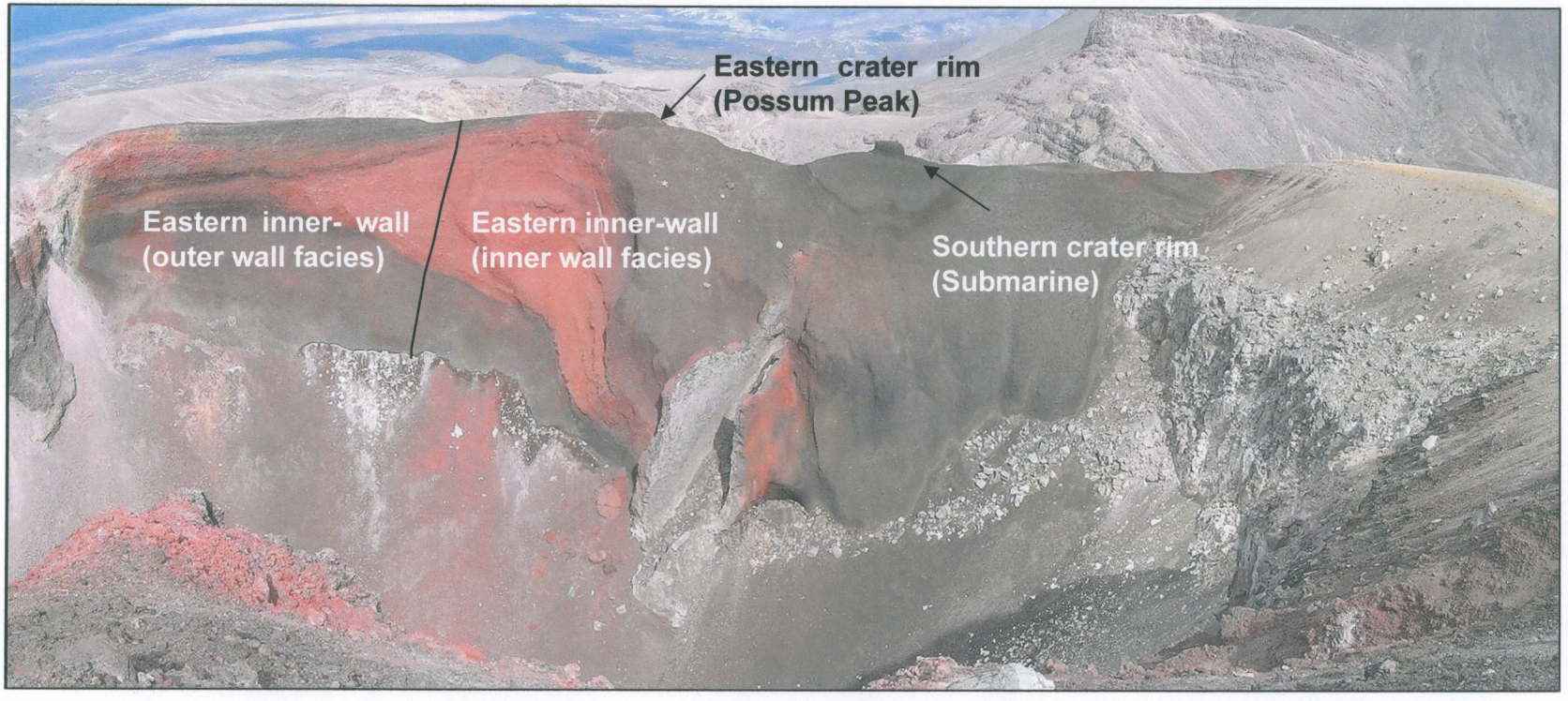

Figure 2.5 – Locations of stratigraphic column descriptions within the Red Crater scoria cone.

2.2 SCORIA CONE STRATIGRAPHY

2.2.1 EASTERN CRATER WALL

The eastern crater wall of Red Crater is the first and often only part of the crater many walkers on the Tongariro crossing see. Its main component is the 50-60 metres of scoria which radiates out from the exposed drained dike in the SE wall. Figure 2.6 shows a photo of this exposed drained dike.

This section of scoria is described in full within the stratigraphic column section of this chapter, by both the Eastern inner-wall and Eastern crater rim sections. Both the western and southern walls of Red Crater clearly show the contact with older andesitic Tongariro Trig lavas on which the scoria cone is constructed upon.

This contact within the eastern wall is merely a few andesite blocks at the base of the scoria section. These blocks can be inferred to represent the presence of the Tongariro Trig lavas just beneath the scoria scree slope for two reasons. Firstly, because of the high amount of water seepage occurring along this contact. This water seepage is the result of rain water percolating down through the highly permeable scoria and then encountering the very poorly permeable andesite and escaping sideways out into the inner crater. While water seepage is one clue as to the underlying presence of the Tongariro Trig lavas, the other is the shattered andesite lava exposed on the eastern outer crater wall at approximately the same level as the contact on the inner eastern crater wall. Figure 2.7 shows a photo of this inner crater wall andesite as well as a close up version of this inner crater wall contact.

The further north you travel along the eastern crater wall, the greater the hydrothermal alteration becomes, in particular the area where ECR-b is located. This part of the eastern wall is of interest because it appears as though the large v-section which cuts into the inner crater has infact collapsed into this position as the result of a rotational slump.

Figure 2.6 – Basaltic andesite exposed drained dike, eastern crater wall.

Figure 2.7 – A - Contact with Tongariro Trig andesite within eastern crater wall of Red Crater. **B** – Close up of this contact.

As Figure 2.8 shows, the stratigraphic units identified within the Eastern inner-wall section can be continued north, through this collapsed block and linking up with the units exposed even further north of it.

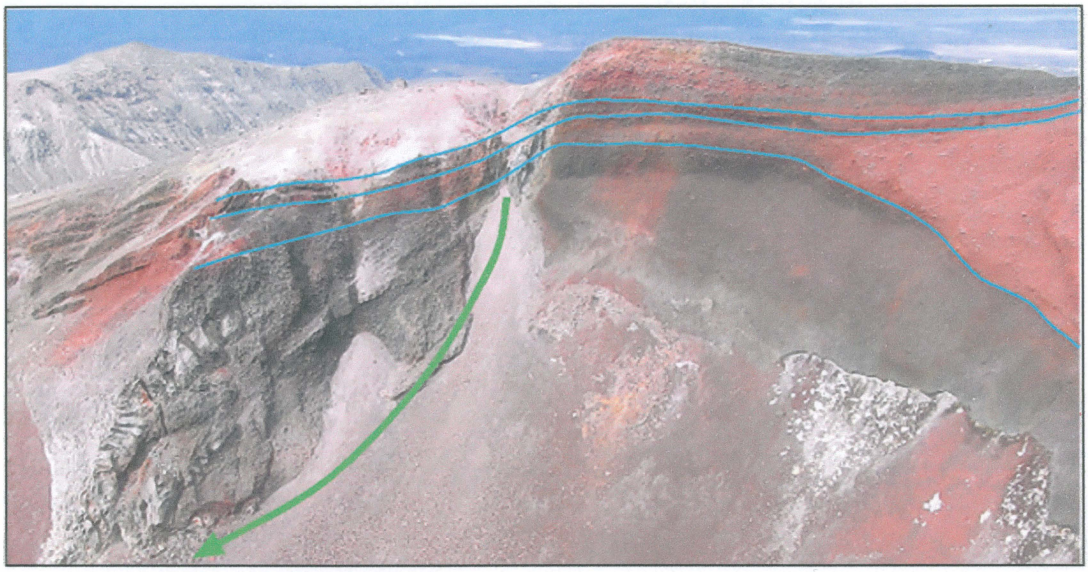

Figure 2.8 – Eastern crater collapsed section with lines linking stratigraphy up to the south of it

What was originally thought to be Tongariro Trig lava within this collapsed section, is infact of similar composition to the exposed drained dike, indicating that this is infact an agglutinated scoria unit. This similarity can be seen in the photo-micrographs in Figure 2.9 below, which show photomicrographs of the agglutinated scoria unit, a Tongariro Trig andesite ballistic block and the exposed basaltic andesite drained dike (corresponding University of Waikato sample numbers for all samples can be seen in Appendix 7). As can be seen, the crystal sizes and matrix are more comparable with the exposed drained dike sample than with the Tongariro Trig andesite sample, indicating this unit has been erupted from this dike and not the same source as the Tongariro Trig andesite. This collapse probably occurred as a result of the late stage phreatic eruptions which ripped through the area creating the emerald lakes, removing the northern section of Red Crater, and exploding out the explosion pit on the south face of the cone. This caused instability in the north-eastern crater wall, causing the collapse. Erosion has since removed the scoria deposits from the northern face of the more agglutinated scoria unit. Figures 2.10 and 2.11 show photos of this agglutinated scoria unit in situ, plus a close up of a fallen part of this unit.

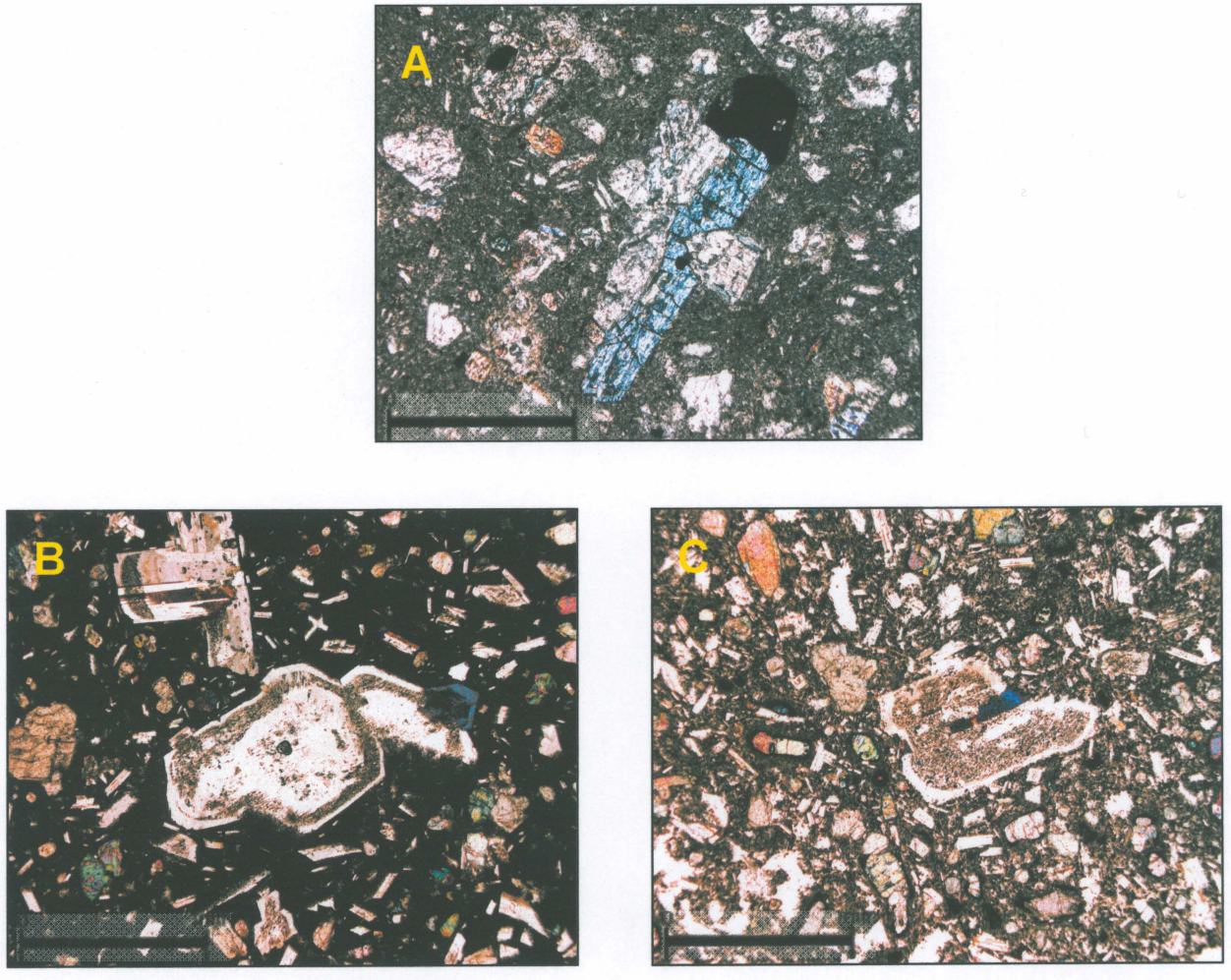

Figure 2.9 – Photomicrographs – **A** - Tongariro Trig andesite. **B** – Exposed basaltic andesite drained dike. **C** – Agglutinated scoria unit.

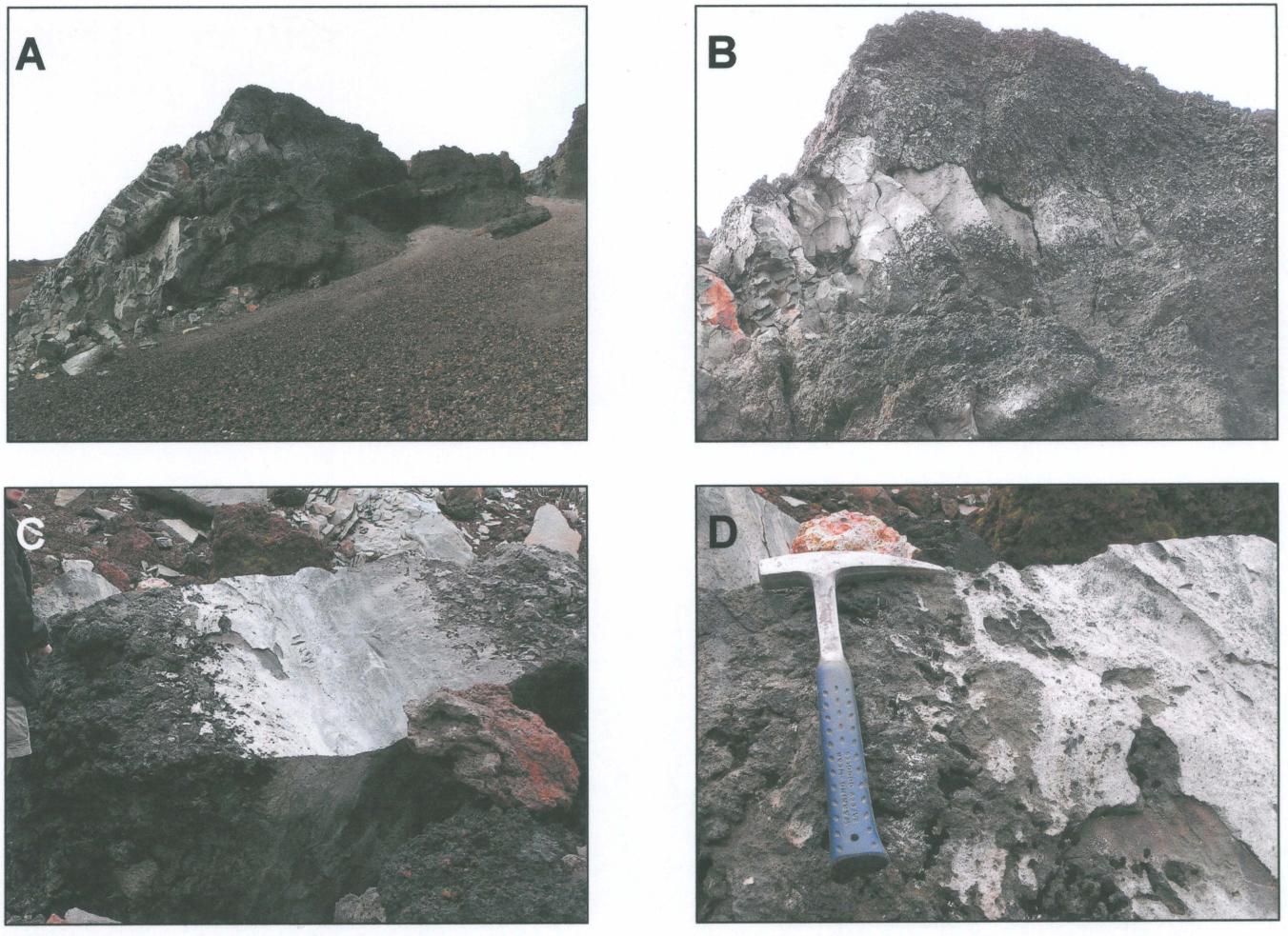

Figure 2.10 – Agglutinated scoria unit in eastern inner-wall collapsed section. Progressive close ups **(A-D)**

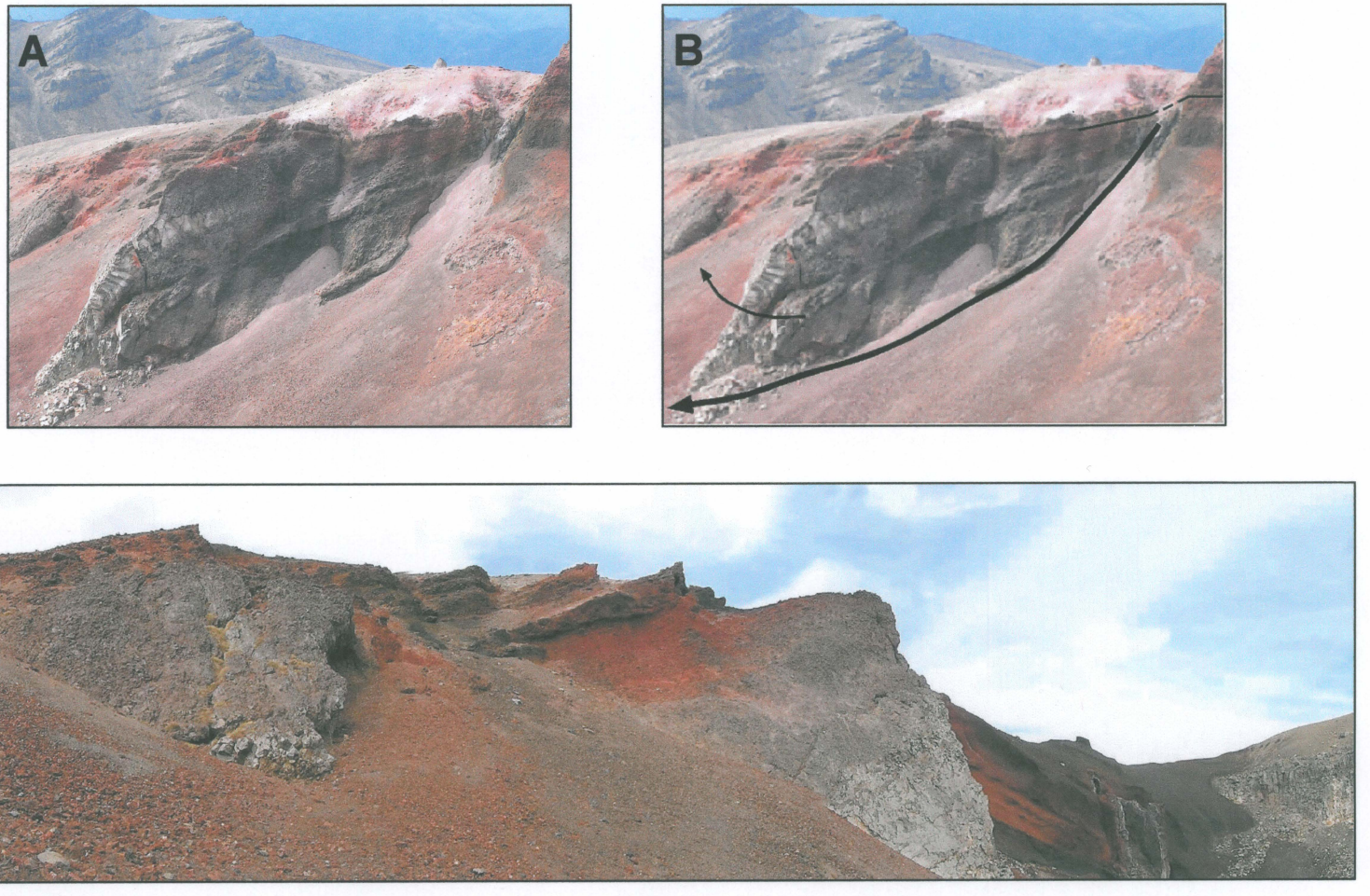

Figure 2.11 – Eastern inner crater wall agglutinated scoria unit. **A** – Looking north. **B** – Sketch showing the rotational slump of this section of the crater wall. **C** – Looking South.

The close up photo (Figure 2.10d) shows the contact between the agglutinated scoria unit and the loose scoria deposits. As can be seen in this figure the contact between the two is not sharp, as it would be if this unit was an intruded dike.

The hydrothermal alteration above this collapse has caused the formation of denser, slabey rocks as seen in Figure 2.12. These extend approximately 20 metres down the outer crater rim and cover a width of approximately 10 metres. These slabs are of the same composition as the surrounding unaltered rock, but have being lithified as a result of the intense hydrothermal alteration and groundwater effects at this localized spot.

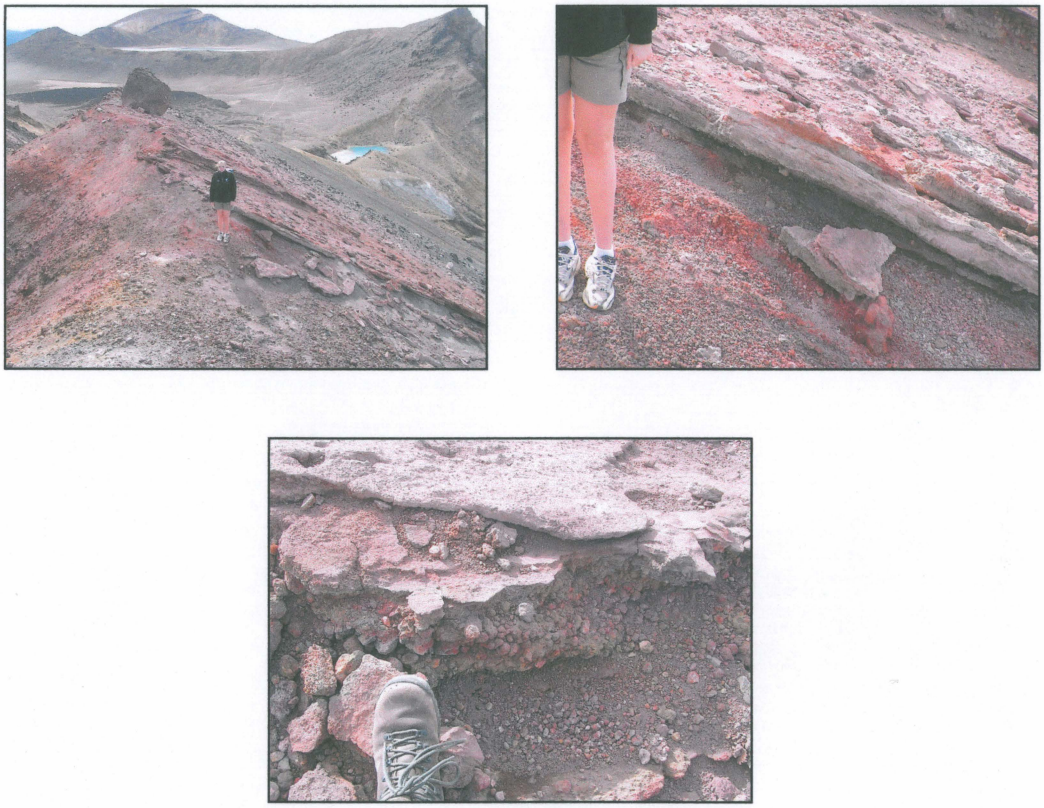

Figure 2.12 – Hydrothermal alteration on the north eastern crater wall

2.2.1A EASTERN INNER-WALL SECTION

An approximately 52 metre section was logged through the Eastern inner-wall, to the north of the exposed drained dike, from a height of 1838 metres on the rim, to 1786

metres within the crater as seen in Figure 2.1. Based on changes of grain size, sorting and color, this section was divided into eleven main units, with a further two units identified on the rim above this section. The stratigraphic columns for this section and the others to follow can all be viewed in Enclosure 1. Each individually highlighted unit can be referred to in Figure 2.13 when reading the eleven unit descriptions to follow.

The upper 2.8 metres defines unit eleven, which is continuous along the entire eastern crater wall. This is a non-bedded unit, which is very poorly sorted and non-welded. Grain sizes range from the 1-2mm clasts of the matrix, to the 10-15cm clasts which are randomly scattered throughout. This unit is dark grey in color and clasts are highly vesicular with an average vesicularity of 68.2%.

The contact between unit eleven and the tenth unit is gradational, with unit 10 extending from 2.8 – 4.2 metres and like the unit above, it can be traced continuously along the eastern crater wall. Once again, this unit is very poorly sorted, massive and non-welded. The grain size ranges from 3-4mm up to 15-20cm. Some larger scoria clasts exhibit spatter like cow-pat morphologies within this unit. Clasts are dark grey in color with an average vesicularity of 65.9%.

A color change from dark grey to a dull red marks the start of the ninth unit which extends from 4.2 - 5.3 metres, with a gradational contact with unit 10. Like the units above, this is a laterally continuous unit, massive, very poorly sorted and non-welded. Clast sizes range from 1-2mm to 10-15cm and typically are highly vesicular but the average clast vesicularity is slightly less than the units above at 62.3%. A notable difference in this unit is the more angular nature of the clasts as if they had broken on impact after cooling in flight, as opposed to still being fluid on impact (producing the spatter textures of the second unit).

The eighth unit is defined by its fine grain size of 1-5mm. The average grain size is 5.66mm. It extends from 5.3 – 5.6 metres and pinches out laterally approximately 20 metres to the north of this columns locality, while thickening towards the vent (as the column at the base of Eastern crater rim shows). This pinching out is not the result of

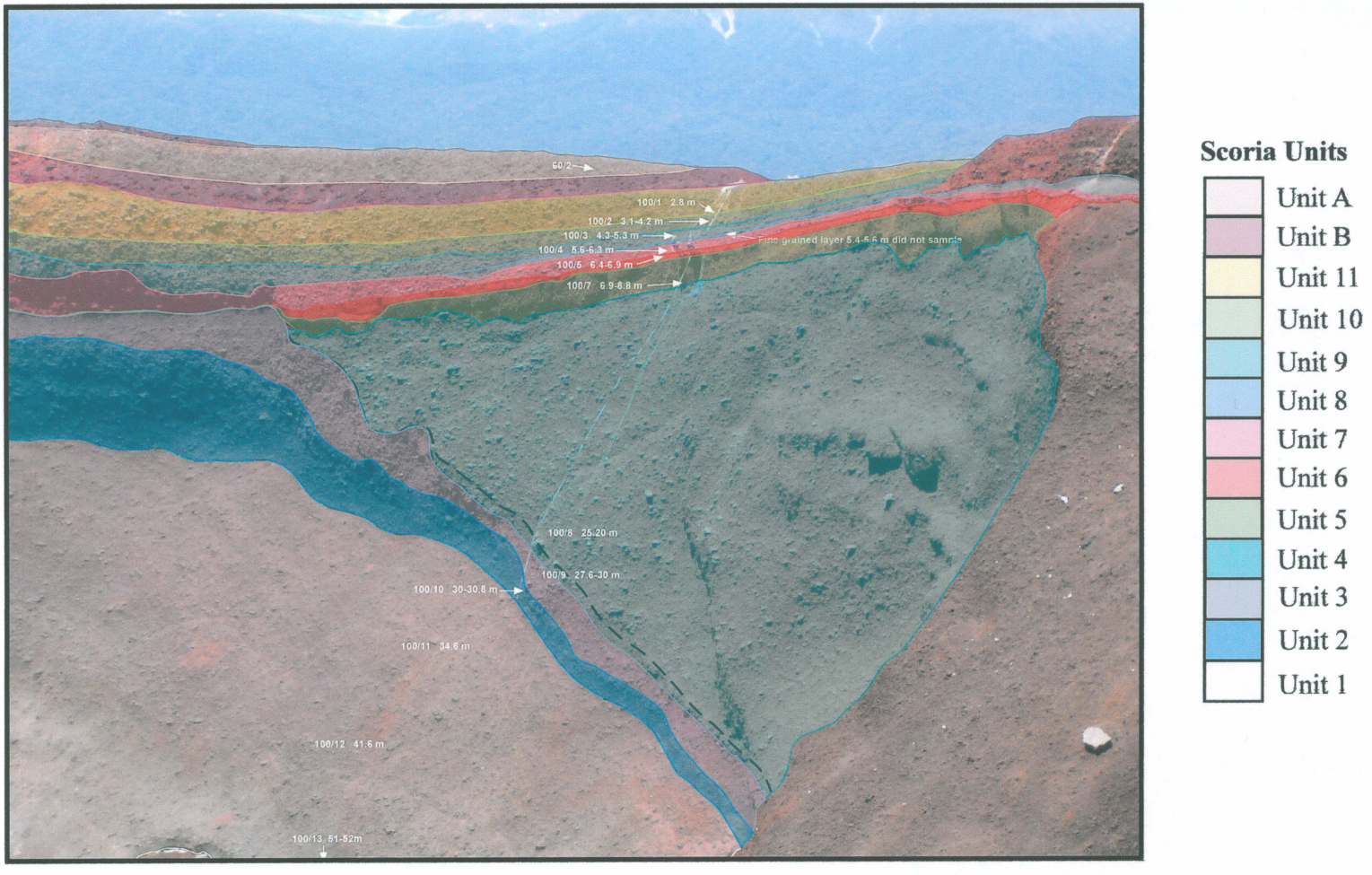

Figure 2.13 - Eastern inner crater wall stratigrahpy, which represents outer crater wall facies and is divided into eleven main units

an unconformity but simply reflects how this unit was deposited, possibly thinning due to a declining magma discharge rate. It is well sorted, massive and non-welded. Sharp contacts above and below define this unit, which also has a bright red-orange color and clasts are uniformly highly vesicular.

Unit seven extends from 5.6 – 6.3 metres, is laterally continuous, poorly sorted, non-welded and shows no bedding structures. It is a similar colour to the unit above, but is coarser grained with clast up to 30cm. Clasts within this unit exhibit dominantly fluidal morphologies as seen in Figure 2.14. These clasts are not as angular as unit nine indicating fluidicity upon impact. Clast vesicularity is high, with an average of 66.0%.

Fig 2.14 – Clasts within unit 7 exhibit fluidal morphologies as this broken spindal bomb shows.

Unit six is laterally continuous towards the vent (southwards), but pinches out approximately 20 metres northwards of this columns location. It shows the same characteristics as unit eight, well sorted, burnt red colour, massive, non-welded and grain sizes of 1-5mm. The mean grain size is also 5.66mm. This unit extends from 6.3 – 6.9 metres. The contacts between this unit and those above and below are sharp.

Extending from 6.9 – 8.8 metres is unit five which does not dip towards the rim (as opposed to the previous six which all have shallow dips towards the rim). This unit is very poorly sorted with grain size ranging from 3-4mm up to 10-15cm. This unit has the highest average vesicularity of all the units within the eastern inner-wall, peaking at 72.5%. There is one band which runs horizontally through this unit at approximately

the 7.9 – 8.0 metre mark. This band consists of larger clasts of 15-20cm diameters and is simply the thickness of these clasts. No other bedding is evident, and the unit is non-welded. This unit pinches out to the north at the same place as units six and eight, while increasing in thickness towards the vent (southwards).

The thickest unit within this section, known as unit four, extends from 8.8 – 27.6 meters at this locality and has a gradational contact with the unit above. This unit forms a large wedged shape deposit which pinches out 20 metres north (at the same place as previous units have pinched out), of the column locality, and thickens dramatically towards the vent or dike. This unit is deposited on the upper 4/5ths of the northern dike wall. South of the column locality, five or six welded bands are evident within this unit (Figure 2.1), dipping steeply towards the vent. These bands are likely to be either variations within the eruption rather than a separate event, or a facies change as a result of distance from the vent. No variations of colour are evident through this unit. Grain size is dominantly 5-10cm but large (40-50cm) spatter bombs are common. Clasts are highly vesicular with an average vesicularity of 69.1%. There is strong evidence that clasts within this unit were still fluid upon impact, due to the spatter like textures and the lack of angular clasts. There is also the occasional very large outsize clast of 80-100cm as the photo in Figure 2.15 shows.

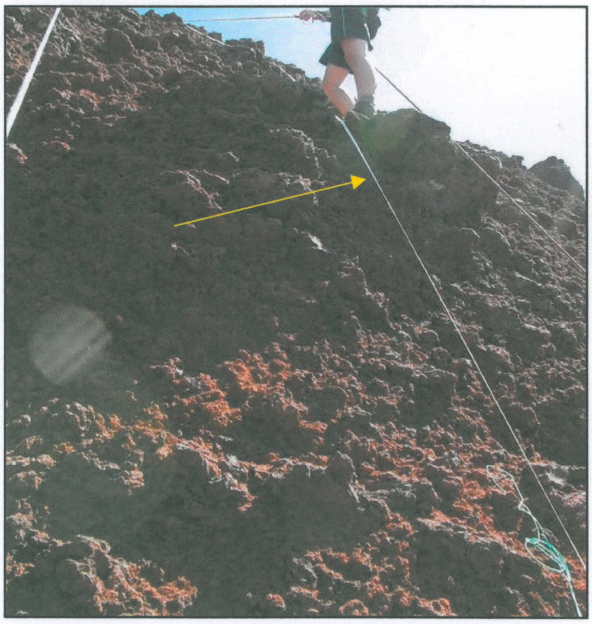

Fig 2.15 – Outsize clast (arrow pointing to it) of 0.9m in Eastern inner-wall section.

Unit three, which extends from 27.6 – 30 metres, is a continuous layer which extends past the point of the unit 4 wedge, and appears to mantle the inside of a vent mouth, as Figure 2.16 shows (which has later being filled by unit eight, hence the wedge shape). The colour has changed to a duller red, sorting is still very poor with clasts ranging from 1-2mm up to 10-15cm. These larger clasts often have spatter like textures, but overall the unit is less spatter rich than the wedge shaped unit eight. No bedding was evident at the location of the column, but towards the vent, a more highly welded cohesive band appears, once again likely to be variation within the eruptive episode or changes due to distance from the vent. The average clast vesicularity of this unit is 67.0%.

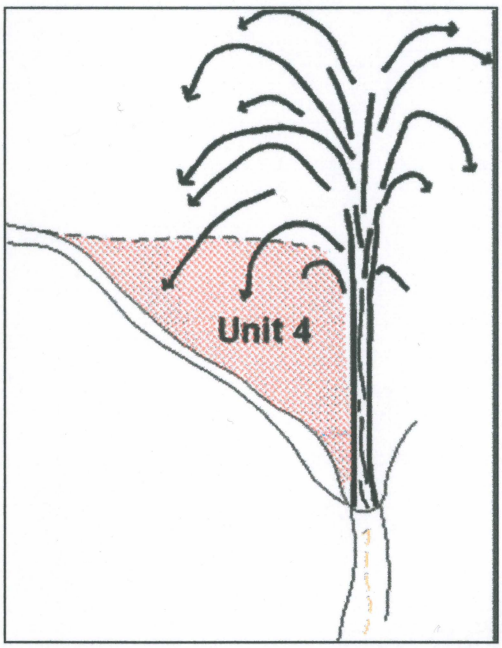

Fig 2.16 – Deposition of unit 4 results in partial infilling of the vent, creating a wedged-shaped deposit.

Unit two extends from 30.0 – 30.8 metres, and is marked by a change to a very deep red colour. Like unit three, it is laterally continuous in both directions, with bedding attitude becoming horizontal in its northern most reaches, indicating the change from inner crater wall facies to deposition on the crater rim. Unit is poorly sorted with a matrix of 3.4mm and clasts getting up to 5-10cm, with no bedding evident. This unit exhibits some of the most vesicular clasts in the section, with an average vesicularity of

71.5%. There is an increase in thickness away from the vent where the unit becomes flat-lying.

The basal unit of the inner crater is unit one, which extends from 30.8 – 52.0 metres. This unit slopes down to the scree slope at an angle of approximately 45-50 degrees, with that slope increasing to ~75 degrees at 47.6 metres and to near vertical for the final metre (51 – 52 metres). This unit is continuous and increases in thickness away from the vent, and has no bedding evident. Occasional spatter bombs greater than 20cm are present, one of which contained a large (15 cm diameter) hydrothermal altered and reworked scoria inclusion. This unit has very poor sorting with a matrix of 1-2mm and clasts of up to 20cm present. Average vesicularity over this unit is 67.6%. Dark grey/black, highly vesicular scoria makes up this compacted but non-welded unit, which is also strongly welded. The colour of the scoria becomes lighter towards the base, possibly due to the high volume of ground water which leaches out at this level. This water pathway is the result of the permeable scoracious layers above, all allowing water to pass through, and unit one's underlying contact with the impermeable old Tongariro Trig lavas, causing the water to exit at this level. The amount of moss growing at the base is evidence of the damp lower section of the unit. At the base of this unit there is approximately 20cm of clay-like material which appears to be highly weathered old Tongariro Trig lavas, as seen in Figure 2.17.

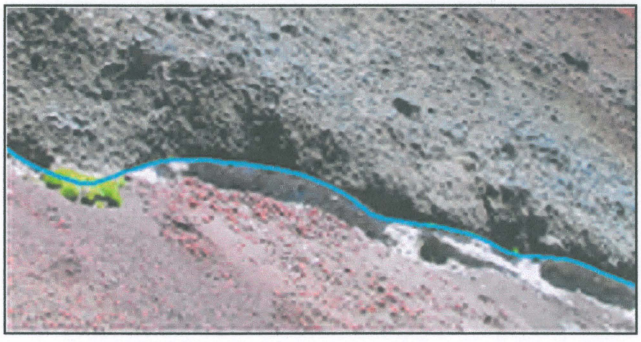

Figure 2.17 – Highly weathered Tongariro Trig lavas marking the contact with the basal scoria cone unit.

The two units above the Eastern inner-wall section which have not being included in the stratigraphic column are Unit A and Unit B. Both units are laterally continuous and flat-lying suggesting emplacement on the crater rim. Unit B is poorly sorted, non-welded with clast sizes typically in the 10-15cm range. Unit A differs in that while the clast sizes, sorting and welding are similar to Unit B, the clasts themselves are denser overall (as observed in the field) with an average vesicularity of 51.5%.

2.2.1B EASTERN INNER-WALL – CORRELATION OF UNIT 1

This stratigraphic column was located approximately five metres to the north of the vent, in the lower 0.6 metres of unit one of the Eastern Inner-wall section. This locality was approximately 15 metres to the south of where unit one's description was based. The unit is massive, non-bedded and poorly sorted. The matrix consists of clasts of very fine (1mm or less) scoria which is non-welded. The largest grain sizes present are the 15-20cm black scoria clasts which are denser and less vesicular than the scoria seen on the upper crater rim. The base of the unit is in contact with old Tongariro Trig lavas and alteration is evident, either hydrothermal or as a result of water discharge.

2.2.1C EASTERN CRATER RIM – ECR-A1 TO ECR-A4

The next stratigraphic column to be described was logged on the Eastern crater rim, approximately 30 metres southwards along the eastern crater wall, from the Eastern inner-wall section. The locality of the Eastern Crater Rim section can be seen in Figure 2.4. This section is 3.8 metres in height, with the three units within it representing the southern most extent of units eleven, ten, nine and eight of the Eastern inner-wall section. Units ECR-a1 and ECR-a2 merge into each other and are described as a single unit extending down to 2.6 metres. The clasts are black in colour, highly vesicular and very poorly sorted. Grain sizes range from 5mm to 20cm. The upper part of this unit displays high degrees of copper oxidization distinctive by the peacock blues, greens and purples in the rock. Nearer the base of this unit some clasts start to become a little more orange as grading into the next unit occurs.

The second unit within this column, ECR-a3, which correlates to unit nine in the Eastern inner-wall section, is moderately sorted and has a more dominant orange/black colouring. Grain sizes are ranging from 5-12cm within this unit, which is totally clast supported. While the unit above was highly vesicular, this unit also contains some denser clasts with smaller vesicles which greatly out number the larger vesicles seen in more vesicular clasts.

The final unit within this column, ECR-a4, correlates to unit eight in the Eastern inner-wall section. The clasts within this unit are predominantly homogenous with a size range of 5-20mm (slightly bigger than in the unit 8 of the Eastern inner-wall section due to closer proximity to the vent). The big difference in this unit at this locality is the presence of random 10cm by 15cm spindal bombs. Because of these, the unit is very poorly sorted. No grading or bedding is evident, clasts are both highly vesicular and angular with a deep red colour.

2.2.1D EASTERN CRATER RIM – ECR–B

50 metres further north along the upper eastern crater wall from the Eastern Inner-wall section, is the next stratigraphic column. This section is a single unit with no bedding and extensive hydrothermal alteration. It has a thickness of 0.7 metres and is very poorly sorted with grain sizes ranging from 1mm up to 7cm. This unit is essentially scoria, but it has being so hydrothermally altered that some of the more angular blocks have the appearance of Tongariro Trig lavas. There is major vesiculation in the smaller clasts but not so much in the larger clasts, however these contain 1-2mm diameter plagioclase phenocrysts. Due to the hydrothermal alteration the unit is strongly welded, but originally clast supported. While not present at this particular column locality, the top of this section would normally be a hard, flat surface similar to the hydrothermally altered slabs 10 metres to the north of it. The entire unit is a pinky, reddey, white colour.

2.2.2 SOUTHERN CRATER WALL

The southern face of Red Crater marks the transition between the western domination of andesitic Tongariro Trig lavas and the eastern domination of basaltic andesite scoria deposits. As Figure 2.18 shows there is a sudden change in the exposure and height of the contact with these older Tongariro Trig lavas. This shows how dominant the exposed drained dike is on the south eastern wall.

Figure 2.18 – Southern Crater wall.

The most prominent landmark on the southern rim of the crater is that of the submarine outcrop, which is where the Southern crater-rim section was based. Consisting entirely of black basaltic andesite scoria, it stands alone, behind and slightly to the west of the exposed dike as Figure 2.19 shows.

Figure 2.19 – Submarine outcrop on southern crater rim.

Whilst consisting predominantly of scoria, unlike the stratified and defined units of the eastern wall, the scoria of the southern wall drapes down into the crater in one apparently homogeneous unit. Apart from the bedding used to divide the Southern Crater Rim outcrops into sub-units, the rest of the inner wall shows no such stratigraphy. This is the result of the final fire fountaining episode which occurred after the phreatic explosions had cleared out the center of the crater. This final episode was intense but small in height, leading to the very localized, draped deposits only found above and to the west of the exposed dike. The small dribble of aa basaltic andesite lava into South Crater was feed by the spatter deposits from this fire fountain.

Further to the west of this draped scoria is the transition zone between this draped black scoria deposit and the black scoria which is sitting on top of the Tongariro Trig andesite. This particular black scoria correlates to unit one in the Eastern inner-wall section and also with the southern section of the western wall. Figure 2.20 shows this transition zone.

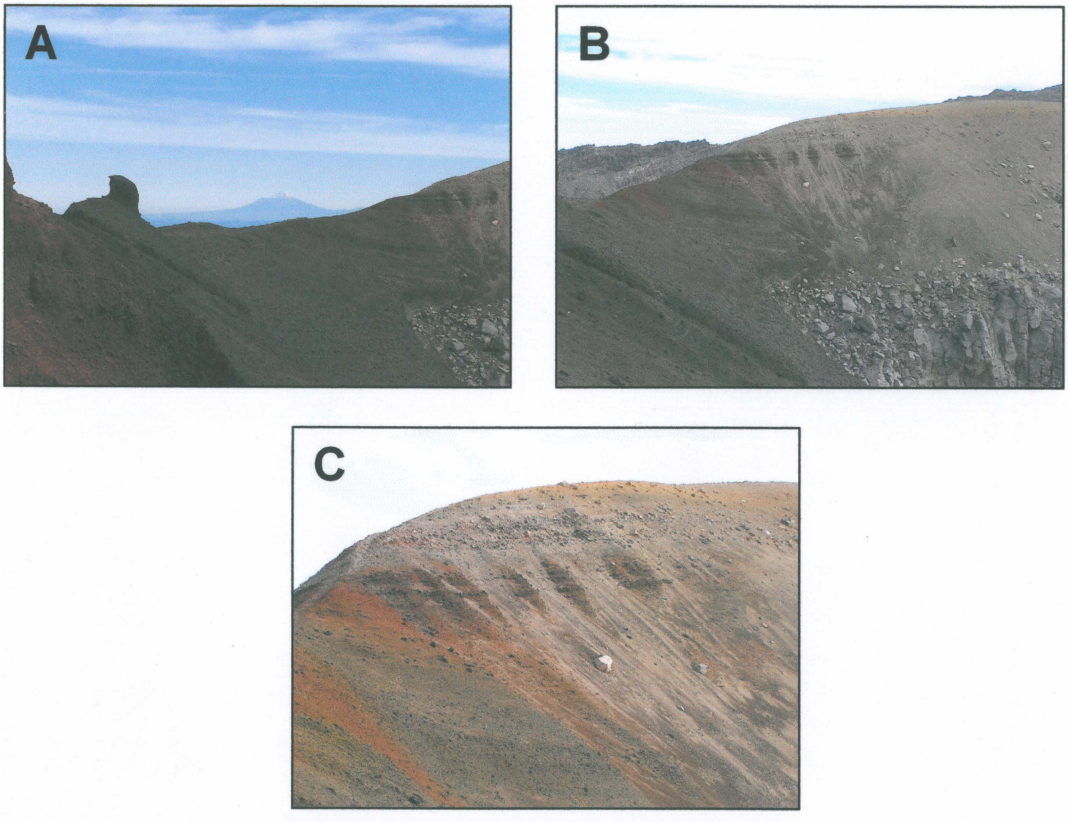

Figure 2.20 – Progressive close-ups (**A** – **C**) of transition Zone on the southern crater wall.

Sitting above this is a series of horizontal, flat-lying, well bedded layers, alternating between coarse 10-70 cm andesite clasts and finer grained ash-rich layers of similar composition. The coarser layers are lithic rich and have been deposited by the late stage phreatic eruption, while the finer layers include some outwash from the summit of Tongariro to the west.

2.2.2A SOUTHERN CRATER RIM – SCR6 TO SCR8

The next stratigraphic column to be described is the Southern Crater Rim. This section is on the south-eastern rim of the crater and is part of the inner crater wall facies. This section dips towards the vent, which is approximately 10 metres to the north of it. It is also approximately 20 metres south of the earlier described Eastern Crater Rim section. This outcrop differs completely from the previous two, in that beds all dip towards the crater as opposed to dominantly away from the crater, as most beds in the Eastern Crater Wall and Eastern Inner-wall sections do. This section is part of the outer crater wall facies of the scoria cone. Other than that it also stands alone. It is 2.4 metres high and 4.0 metres wide and is composed of entirely black scoria as seen in Figure 2.19.

The 2.4 metres of this section of the Southern Crater Rim can be subdivided into three main units based on major grain scale changes and will be termed SCR8 to SCR6. Within these units, fine subdivisions can be made and 12 individual subunits recognized; SCR-a1 makes up SCR8, with SCR-a2 to SCR-a9 occuring within SCR7, and SCR-a10 – SCR-a13 occuring within SCR6. Figure 2.21 highlights the eight SCR units.

SCR-a1 extends from the top (0m) down to 0.55 metre, is very poorly sorted and contains clasts ranging from 2cm up to 40cm. The ratio of black to red scoria in this section is 3:1, all of which is very jagged and sharp and highly vesicular. SCR-a1 is totally clast supported, some of which have denser centres with many tiny vesicles, while others are full of larger vesicles. Lithics of Taupo Pumice were also found within this unit.

Figure 2.21 - Units of the Southern crater wall section

SCR-a2 extends from 0.55 – 0.70 metres, is moderately sorted, with clasts ranging from 1mm up to 2cm. The bigger clasts are highly vesicular and no grading is evident.

SCR-a3 encompasses 0.70 – 1.0 metres and exhibits slight normal bedding, with clast sizes increasing towards the bottom. These clasts are very angular with the ratio of black to red scoria increasing to 5:1. Clasts are highly vesicular with copper oxidation evident and a high amount of Plagioclase phenocrysts obvious to the naked eye. The unit is poorly sorted, ranging from 1cm up to 7cm. Two small (2cm) lithics of Taupo Pumice were found.

SCR-a4 is a very thin layer extending from 1.0 – 1.03 metres. The unit is fine grained, strongly welded and very well sorted. Comprises of totally black scoria within the 1mm range.

SCR-a5 comprised large dense scoria clasts with diameters of 17cm wide by 8cm high, which had waxy, red vesicular inner cores with very dense outer rims. The majority of the unit is poorly sorted with clast sizes ranging from 1cm to 7cm with some copper oxidation evident. SCR-a5 encompassed 1.03 – 1.21 metres.

SCR-a6 is nearly identical to unit S4. It is fine grained, strongly welded and very well sorted. This unit is composed of black scoria 1mm in size and extending from 1.21 – 1.24 metres.

SCR-a7 consists of very jagged scoria, which is poorly sorted with clasts ranging from 1mm to 5cm. This unit is totally clast supported with larger clasts displaying highly vesicular centres and denser thin, blue (copper oxidation) rims. SCR-a7 extends from 1.24 – 1.48 meters.

SCR-a8 is a 12cm thick unit extending from 1.48 – 1.60 metres. The large scoria clasts of 9cm diameters exhibit a thin, dense, blue rim (2mm wide) and a redder vesicular centre (vesicles up to 2cm wide). The matrix consists of 3-4cm angular scoria clasts.

SCR-a9 is a zone of poorly sorted ragged scoria, ranging in size from 3mm up to 5cm. The scoria is moderately welded, entirely black and is matrix supported. No rounding is evident on the clasts, all are angular. This unit extends from 1.60 – 1.90 metres.

SCR-a10 is a 17cm thick band which is the thicknesses of the clasts within it, extending from 1.90 – 2.07 metres. This unit contains a large (17cm wide by 20cm high) black scoria clast with a 2-3cm rim of vesicular, blue oxidising copper, with a center of very vesicular red scoria containing 1mm plagioclase crystals.

SCR-a11, extending from 2.07 – 2.16 metres is a zone of ragged scoria varying in size from 1mm to 2cm. It is poorly sorted and matrix supported.

The final unit of the submarine outcrop is SCR-a12 which contains a large (20cm high by 40cm wide) clast, contrasting totally with the one described in unit SCR-a10. This clast has a similar 2mm, very vesicular, blue oxidizing copper rim, but the inner core is dense with planes or lines of tiny vesicles within. The core is redder in colour and contains abundant 2mm diameter plagioclase crystals.

2.2.2B SOUTHERN CRATER RIM – SCR4 TO SCR2

The next stratigraphic column to be described is approximately one metre beneath unit SCR6 described above. The upper 0.6 metres of this unit, known as SCR4 in the Southern Crater Rim section is dominated by 5-10cm clasts within a matrix of clasts ranging from <1mm to 3cm. This unit is non-bedded, very poorly sorted and slopes towards the inner crater at a 30 degree angle as Figure 2.22 shows. Occasional lithics of Taupo Pumice present. Some clasts show denser outer rims and highly vesicular centres. The contact with the unit below is gradational and could potentially be part of the same unit with slight bedding, but was divided due to the change in slope at this contact.

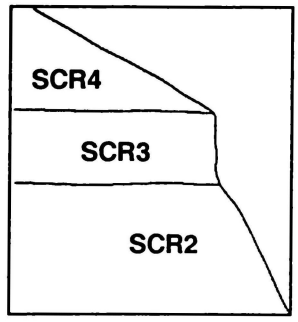

Fig 2.22 – Sketch showing slope angles SCR4 to SCR2.

From 0.60 – 0.70 metres the second unit or SCR3 is exhibits no slope towards the crater rim and consists of larger black scoria clasts (4-9cm diameters) within a matrix of 2-3cm clasts. No grading is evident and large plagioclase phenocrysts are present. The contact with the unit beneath is sharp, marked by both a change in grain size and slope angle.

The final unit in this section, known as SCR2 slopes at 64 degrees towards the crater rim and is dominated by black scoria clasts of 1-3cm diameters. The occasional 5cm diameter clast is also present. There is a slight normal grading within this unit with the smaller (<1cm) grains in a 5cm band at the top. Occasional pumice lithics also found.

2.2.2c Southern Crater Rim – SCR1

The next stratigraphic column is located beneath the one above, still dipping in towards the crater rim. Like SCR6-SCR8, this section can be subdivided into finer units, known as SCR-b1 to SCR-b3, all of which occur within SCR1. The upper portion of this unit, SCR-b1 is 1.15 metres thick and is massive with no bedding. Very poor sorting and non-welding dominates. Clast sizes range from the matrix of 3-4cm black scoria clasts, to the larger, randomly placed 15cm clasts. There is a mixture of denser clasts with vesicular rims and highly vesicular clasts with dense rims. SCR1 is the base unit for the Southern crater rim section.

SCR-b2 is a zone of large (15-20cm diameter) clasts extending from 1.15 – 1.3 metres. These large clasts are supported by a matrix of 2-3cm clasts of black scoria; hence the unit is very poorly sorted. These larger clasts have dense, often copper oxidized rims and very vesicular inner cores.

The basal unit of this section, SCR-b3, extends from 1.3 – 2.4 metres, and is the same as SCR-b1. While large plagioclase phenocrysts are present in all subunits within SCR1, SCR-b3 contains pumice lithics.

2.2.3 Northern Crater Wall

The northern section of Red Crater was all but blown away in the phreatic eruptions which followed the cone construction. Figure 2.23 shows a photo looking north and one looking back towards the south, showing the gaping hole that is the northern section of the cone.

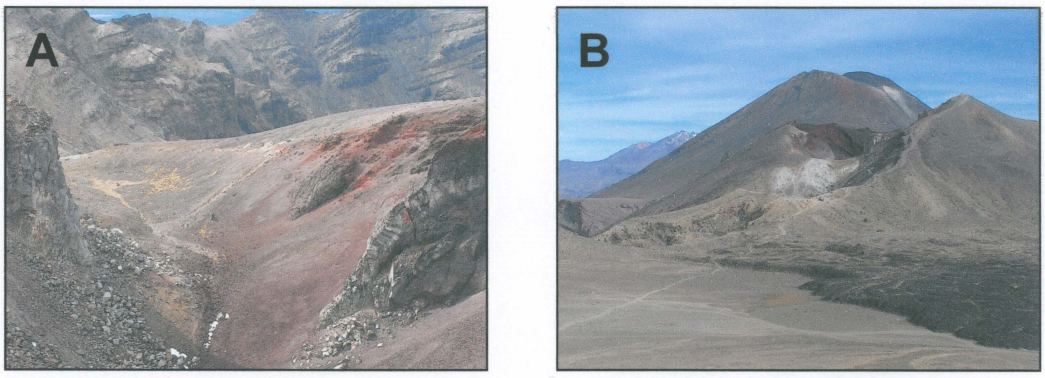

Figure 2.23 – Missing northern section. **A** - Looking north. **B** - Looking south.

A stratigraphic column was interpreted from the tiny section on the very northern rim, which is another hydrothermally altered slab zone similar to that located above the collapsed eastern wall. The explosion that created the upper emerald lake has exposed the North Slope, down which the Tongariro Crossing track follows, as can be seen in Figure 2.24.

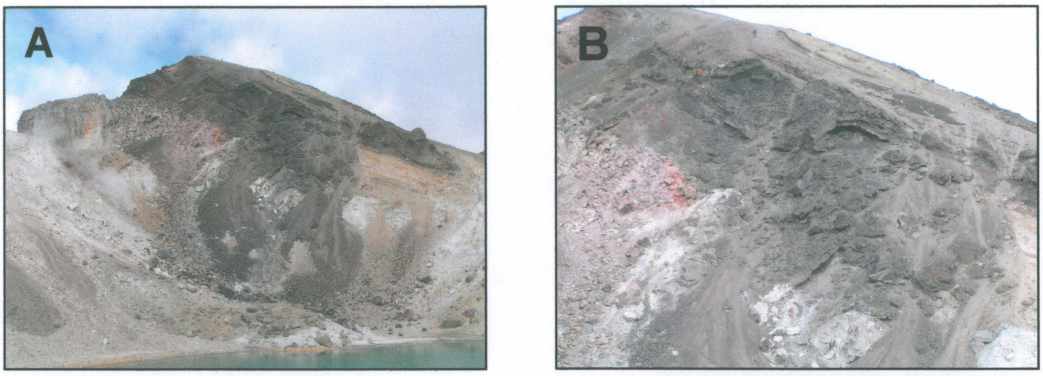

Figure 2.24 – **A** - North face of Red Crater showing partially welded scoria draping hydrothermally altered old Tongariro Trig lavas. **B** – Close up of A.

Two clear things can immediately be seen in these photos, firstly the sharp contact with the Tongariro Trig lavas continues on from the western face, while slatly, scoracious black lava can also be seen. This black lava has a fabric similar to that of the flow into South Crater, indicating it was also feed by spatter from a series of sustained gas bursts. This would also result in the short distance it has flowed due to increased cooler of the magma during flight causing higher viscosity than is usual for basaltic magma during the flow phase. If the discrete gas bursts or fire fountaining were intermittent this would also add to enhanced cooling and slower flow rates. Originally deposited parallel to the underlying Tongariro Trig lavas, the collapse in towards the upper emerald lake has occurred since the phreatic eruptions weakened the northern wall. Figure 2.25 shows the exposure of this flow into Central Crater and the evidence that it is therefore the likely source of a second flow identified on top of the original single Central Crater flow.

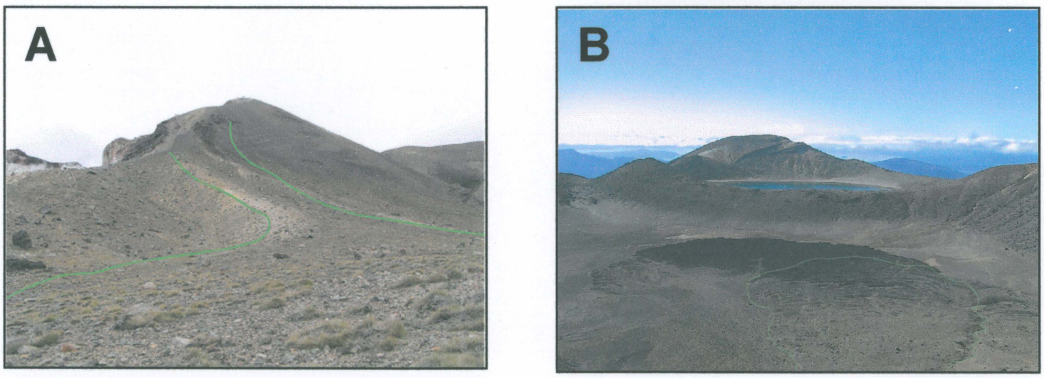

Figure 2.25 – **A** – Path down which upper Central Crater flow (Flow 10) traveled (looking south). **B** – Flow 10 looking north.

As can also be seen from Figure 2.26, the northern section of Red Crater is a zone of intense, very active hydrothermal activity.

Figure 2.26 – Intense hydrothermal activity at the northern face of Red Crater (looking north).

2.2.3A NORTHERN CRATER RIM

The northern lip of Red Crater provided only one locality for a stratigraphic column and is described below. Although only 0.5 metres high, this section is divided into five distinct units, NCR1-NCR5. NCR1 extends from 0 – 0.12 meters, consisting of very well cemented grey lithics within red cement. These grey lithics range from 1cm to 4cm in the lapilli size range, while the matrix is very fine grained. NCR1 is moderately sorted, matrix supported and dominated by angular clasts.

NCR2 extends over the next 0.10 metres and is well cemented, not frittery and moderately well sorted. Grain sizes range from coarse ash to lapilli (1mm to 1cm). Clasts are both angular and rounded and have a brown/red colour.

The next 0.08 metres, NCR3, is marked by a slope change, with this unit being vertical as opposed to the 45 degree inward slope of the two previous units. This unit consists

of well rounded clasts in a matrix of fine white ash sized particles. Grain size ranges from 1cm to 1.5cm and is well sorted and matrix supported.

Unit NCR4 extends from 0.3 – 0.42 metres and returns to the 45 degree inward sloping angle. Bedding is evident within this unit, with layers of 3-4cm clasts interspersed with 1-2cm clasts in between. As a whole the unit is poorly sorted, but individual beds are moderately sorted. Clasts are angular, have a red and grey colour and a well cemented matrix.

NCR5 extends the final 0.8 metres, is moderately sorted and contains rounded clasts ranging from 1mm to 1cm in size. Clasts have white hydrothermal altered deposits on them, while the matrix is well cemented.

2.2.4 WESTERN CRATER WALL

While the eastern wall is dominated by scoria deposits, the western wall is dominated by columnar jointed andesite lava erupted from the old Tongariro Trig cone between 65-110ka (Hobden et al., 1996). Figure 2.27 shows the full western crater wall, with approximately 40 metres of columnar jointed andesite being overlain by a chaotic and disrupted 30 metres of scoria deposits. Unlike the distinct layering seen in the Eastern inner-wall, the scoria on the western wall displays only minor bedding and lacks any definite distinctions between what bedding there is.

A key to the hap-hazard nature of this western wall is the intrusion of a clearly defined dike as Figure 2.28 shows. Outlined in yellow and green on this figure are two agglutinated scoria beds which are likely to have been erupted at the same time as the agglutinated scoria bed seen in the eastern crater wall. The effect that the intrusion of this dike has had on the scoria deposits is to disrupt and confuse them.

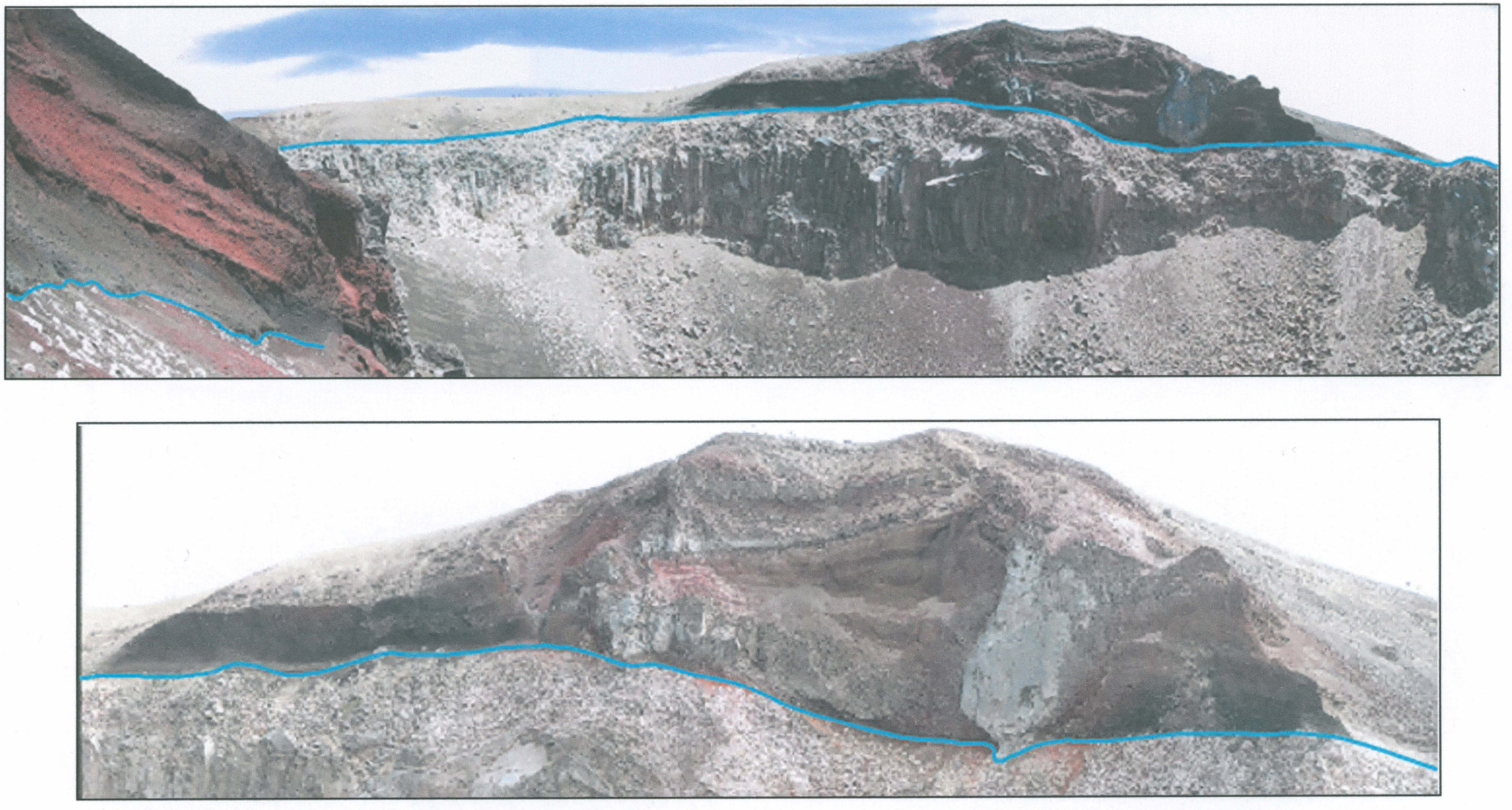

Figure 2.27 – Western inner crater wall, showing contact with underlying Tongariro Trig andesite lavas.

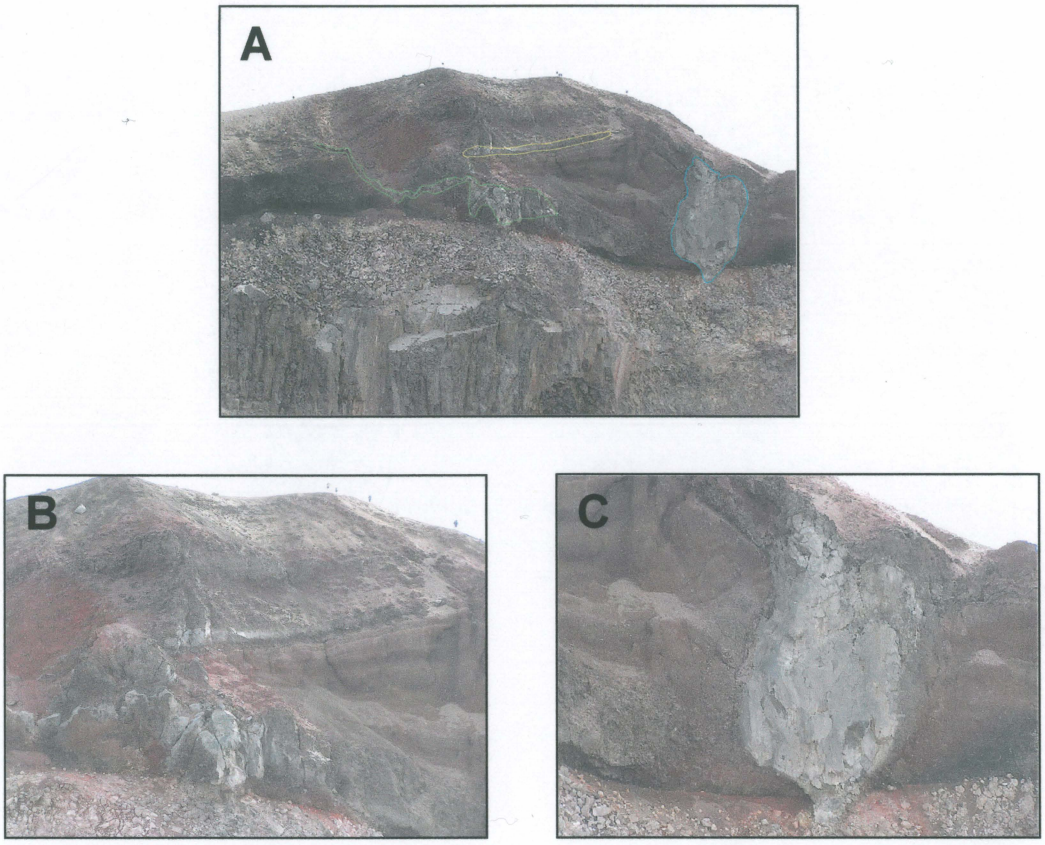

Figure 2.28 – **A** - Western crater wall dike and agglutinated scoria beds. **B** – Close up of the two agglutinated scoria beds. **C** – Close up of dike.

The southern end of this western face exhibits the most continuous scoria layers, but due to their inaccessible location they have not being closely examined. They consist of black scoria and given their locality in relation to the Tongariro Trig lavas, they have being interpreted to correlate with unit one from the Eastern inner-wall section. The increased distance from the vent compared to the Eastern inner-wall section is the reason for the difference in thicknesses seen on either side of the crater. As seen in Figure 2.27, the contact with the andesitic Tongariro Trig lavas is sharp, allowing only a tiny intrusion by the dike to interrupt this contact. The intrusions in the western wall have being intruded after the main exposed drained dike located in the eastern crater wall, and after the main deposition period of the scoria cone.

2.3 LAVA FLOW DESCRIPTIONS

Throughout the course of the fieldwork undertaken, eleven separate lava flows which have originated from Red Crater have been identified. Whilst past workers (Hobden and Houghton, 2000; Topping, 1974) have also identified eleven flows, these descriptions differ by splitting the Central Crater flow into two and keeping the triple lobe flow in southern Oturere Valley as one flow. Therefore five lava flows were erupted prior to the 1.85 ka Taupo eruption (which is known due to the presence of Taupo Pumice on top), and six erupted post 1.85 ka. The order of extrusion of the eleven flows can be seen in Figure 2.29, while photos of each can be seen in Figures 2.30 (a, b, c, d).

The largest preserved lava flow on Tongariro is also the first flow erupted from Red Crater. This flow fills the glaciated Oturere Valley, stretching seven kilometers to the east with a thickness of ≤100 metres (Hobden and Houghton, 2000). This flow is an andesitic blocky flow. Given the volume of this flow (~0.3 km^3) is an order of magnitude greater than the total volume of all other Red Crater flows combined (~0.034 km^3), it is thought that this initial flow may have emptied or nearly emptied the magma chamber (Hobden et al., 1996; Stevens, 2002). Figure 2.31 gives a comparison between the volume of this single flow compared with the total volume of all other Red Crater flows.

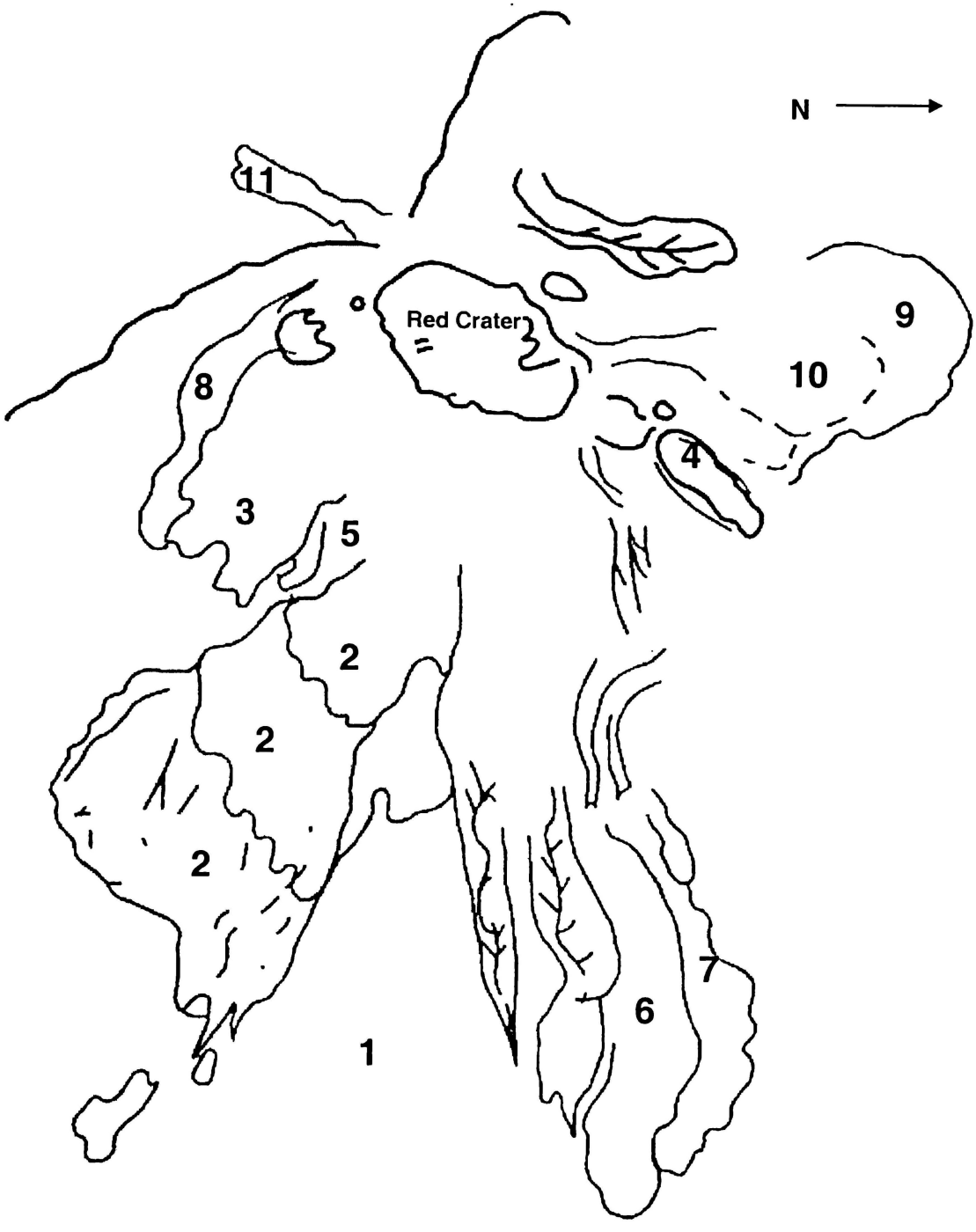

Figure 2.29 – Eleven lava flows erupted from Red Crater. Numbers 1 – 11 refer to the possible order in which they were extruded in (Flow 1 oldest, flow 11 youngest).

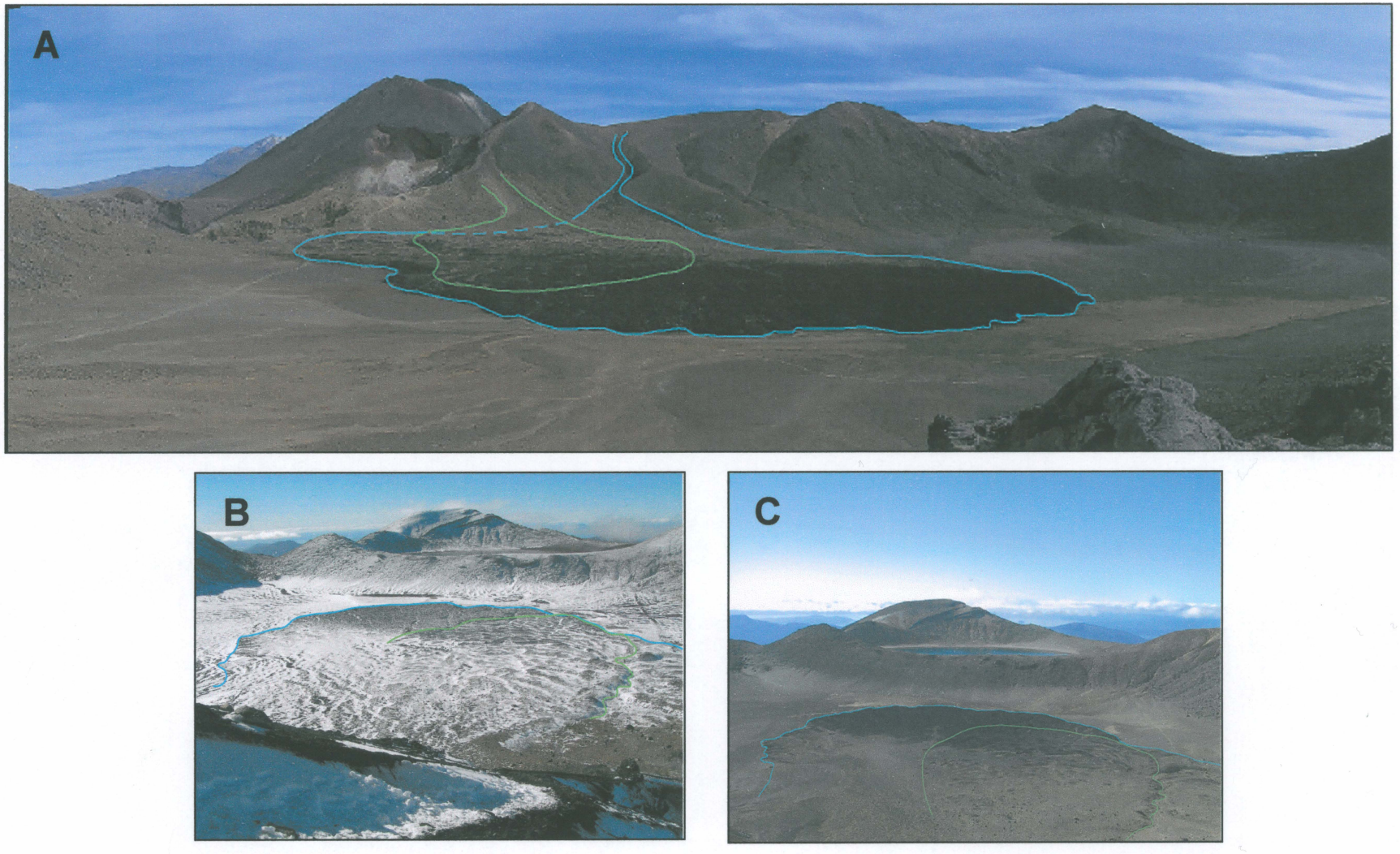

Figure 2.30a – Lava flows erupted from Red Crater into Central Crater. **A** – Looking south. **B, C** – Looking north (Flows 9 and 10).

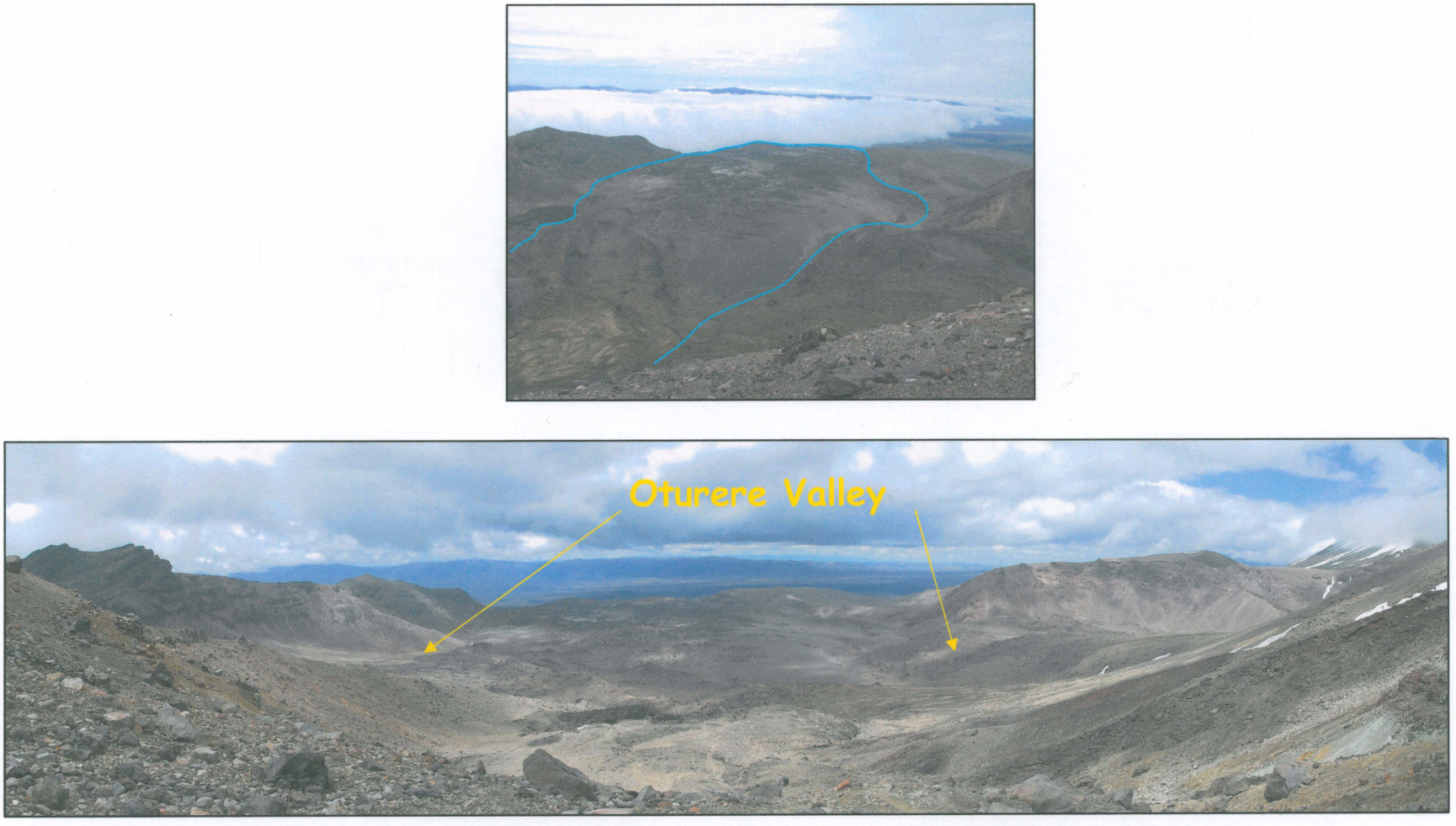

Figure 2.30b – 7km long andesitic Red Crater flow (Flow 1).

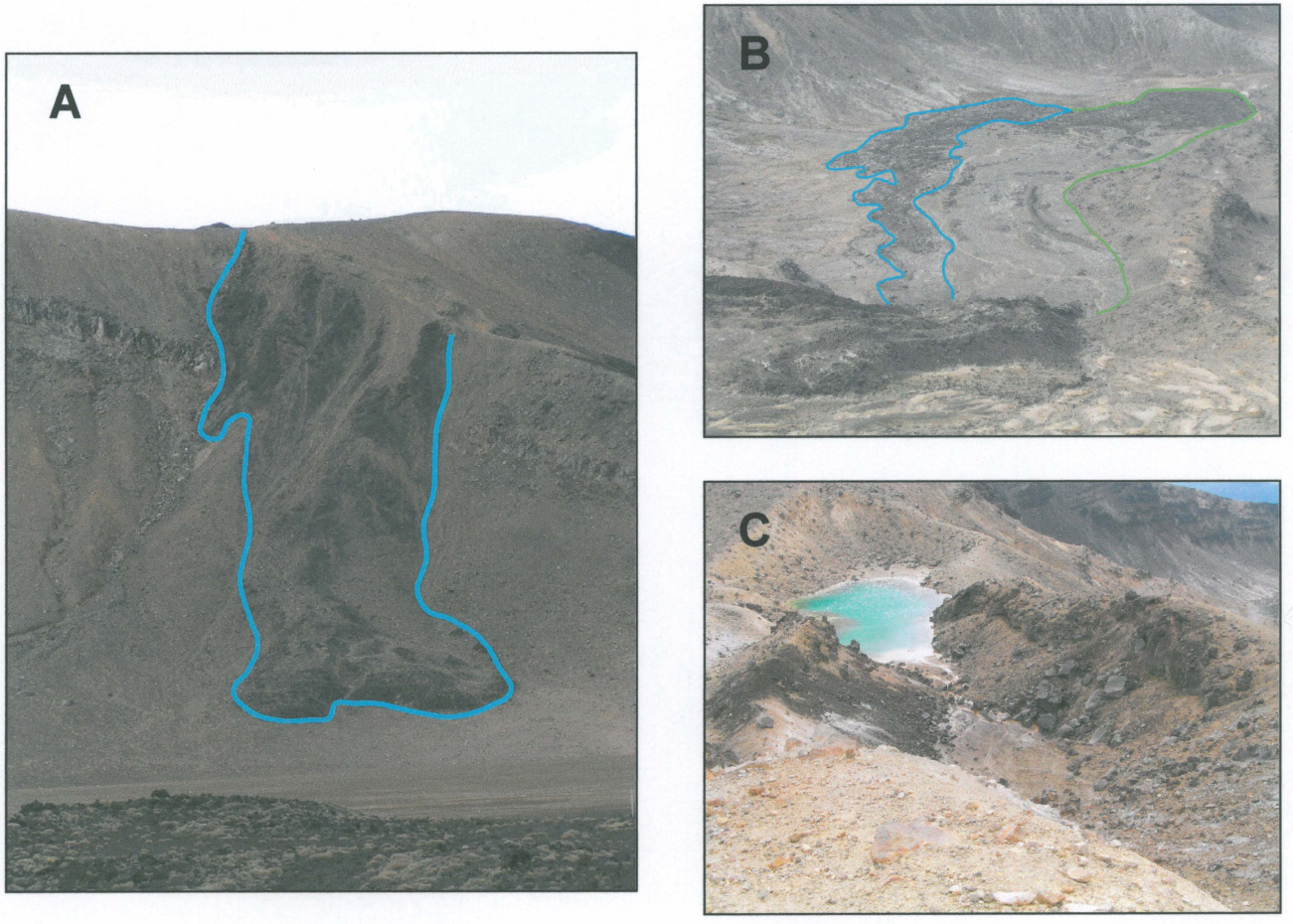

Figure 2.30c – **A** - South Crater basaltic andesite flow (Flow 11). **B**- Aa basaltic andesite flows into NE Oturere Valley (Flows 6 and 7). **C** - Andesite flow exposed at the lower emerald lake (Flow 4).

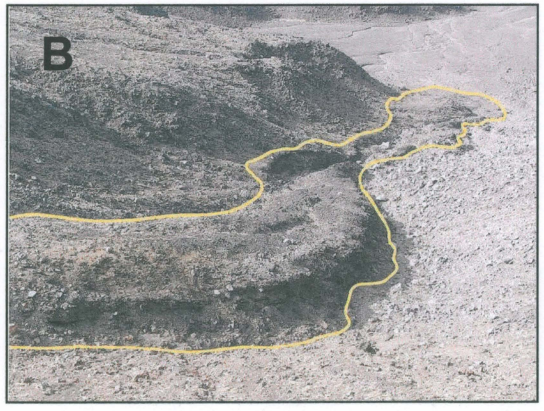

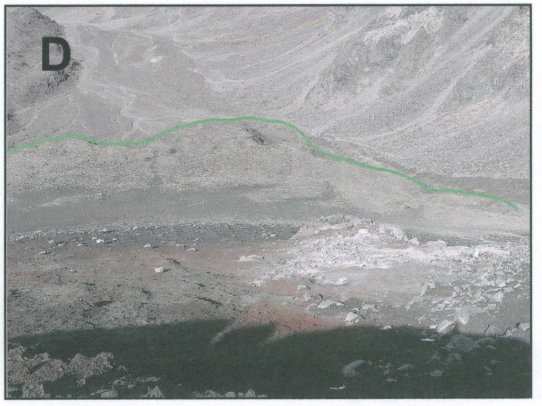

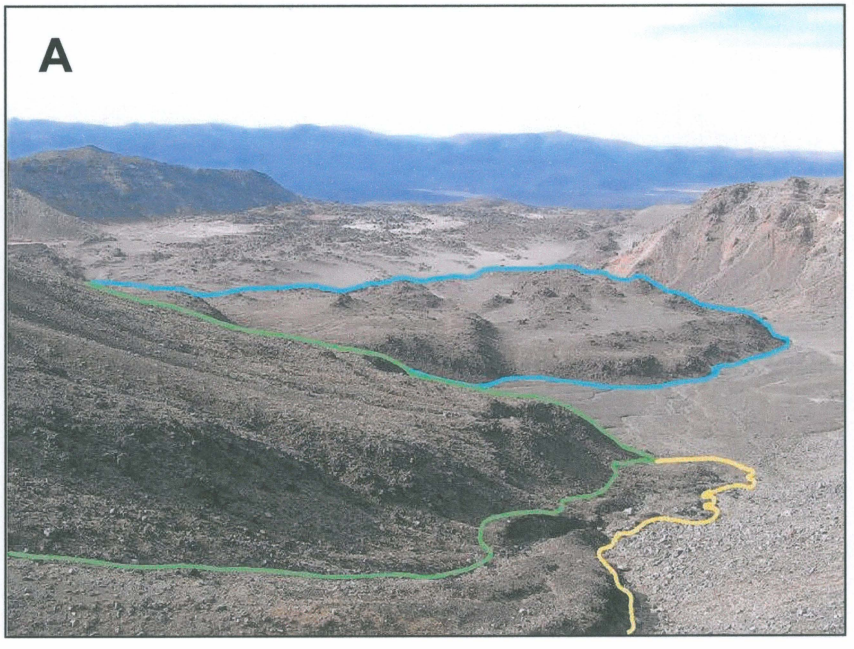

Figure 2.30d – **A** - Lava flows into SE Oturere Valley

B - Aa SE Oturere flow (Flow 8).
C - Triple lobe flow (Flow 2).
D - Andesite SE Oturere flow (Flow 3).

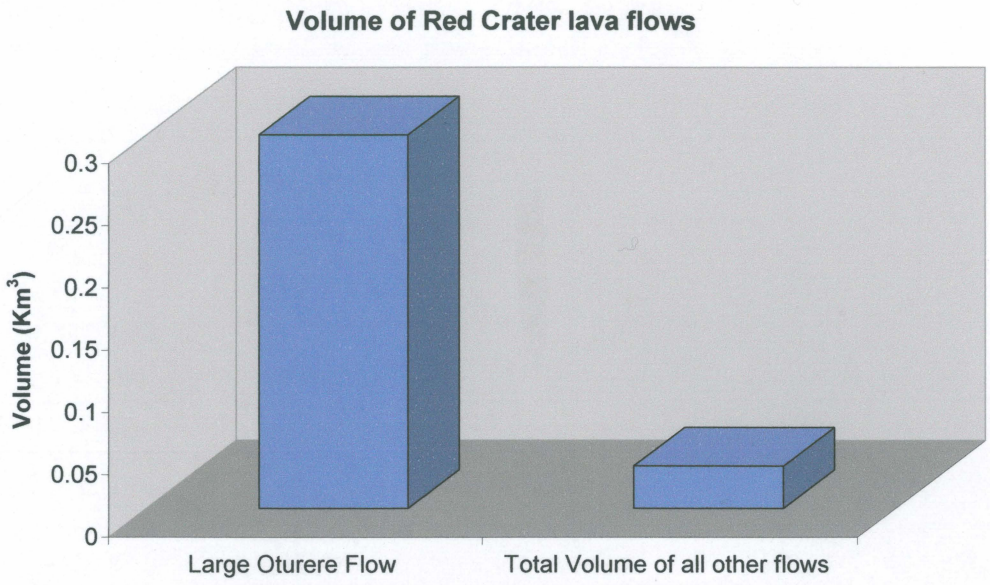

Figure 2.31 – Volume of single Oturere Valley filling flow compared with total volume of all other Red Crater flows.

The second flow to be erupted is the triple lobe flow into southern Oturere Valley. This flow is also a blocky andesitic flow with a flow front some 98 metres high and length of ~980 metres. Each lobe rises 20 metres higher than the one below it. The total volume of this flow and flow four combined is ~ 0.016 km^3.

Flow three, also into southern Oturere Valley is a short, stubby flow, with a flow front rising approximately 60 metres high and length ~ 350 metres. This flow is blocky in nature with an andesitic composition and total volume of ~ 0.007 km^3.

Flow four is a blocky andesite flow which is partially exposed within the lower emerald lake. This flow has a thickness of approximately four metres within unknown volume and length due to underlying the more recent explosion debris from the creation of the emerald lakes.

The final flow to be erupted prior to the 1.85 ka Taupo eruption is flow five, which outcrops between flows two and three and is ~70 metres long. This is merely a small

tongue of a flow which fills the gap between the two large andesitic flows (flows two and three) without reaching the valley floor. It is also an andesitic blocky flow.

Not only have these five flows erupted prior to the 1.85 ka Taupo eruption, they have probably also erupted prior to any construction of the existing scoria cone.

The first flows erupted after the 1.85 ka Taupo eruption are flows six and seven into northern Oturere Valley. These flows mark the first major change in lava composition and style as more mafic magma was injected into the system. Both flows are aa in style and of basaltic andesite composition. The lava channels which feed these flow down the north-eastern face of Red Crater are still preserved as Figures 2.32 and 2.33 show. Flows six and seven wind their way ~0.9 kilometers around the northern flank of flow one, with a thickness of up to three metres. The surface of both these flows is loose and rubbly with little cohesion. Combined flows six and seven have a total volume of ~ 0.00038 km^3 and extend for ~ 800 – 900 metres.

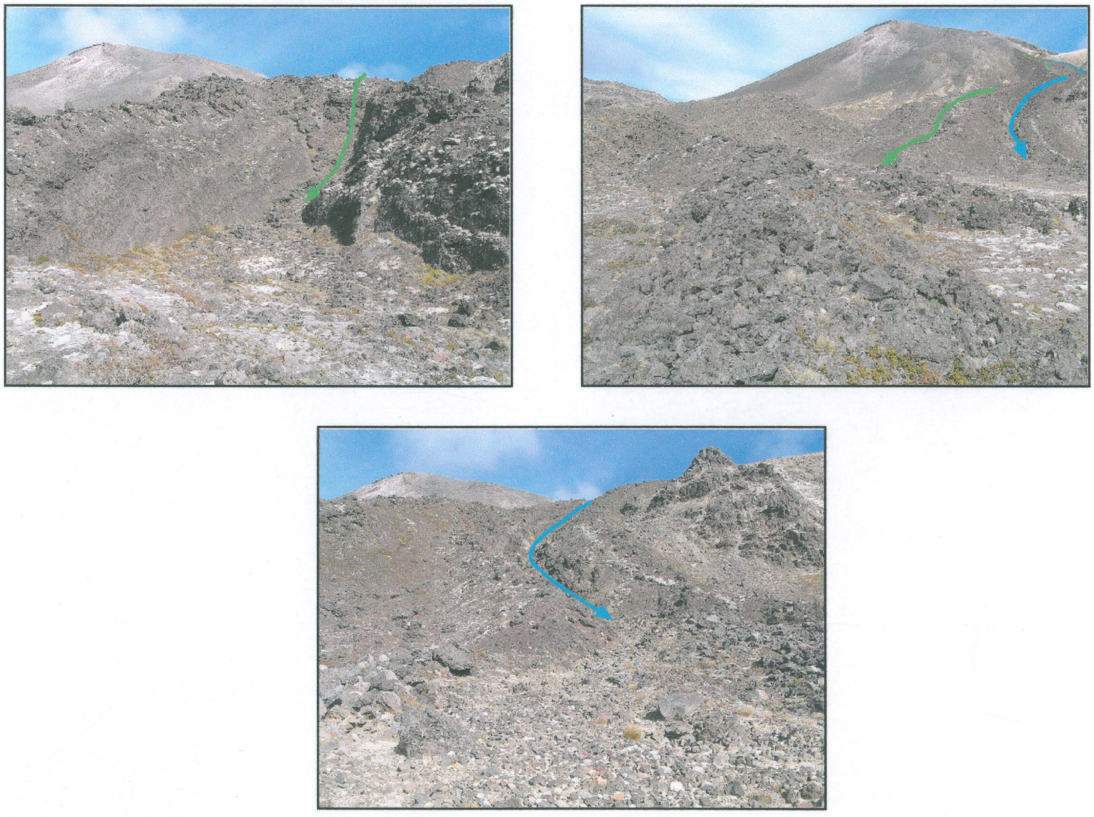

Fig 2.32 – Lava channels feeding flows 6 and 7 into NE Oturere Valley.

Figure 2.33 - Lava channels feeding two aa basaltic flows into NE Oturere Valley

The eighth flow erupted from Red Crater is the small aa, basaltic andesite flow which has oozed ~ 810 metres down into southern Oturere Valley, in between the valley wall and flow three. This flow has a flow front thickness of up to three metres and a volume of ~0.00008 km^3.

The next two flows to be erupted are flows nine and ten, both erupting short time spans apart (hours to days) and in the order just listed. These flows are 400 metres wide and ~ 500 metres long together and have thicknesses ranging from one to five metres. Transverse pressure ridges are evident on the flows surfaces, and it is the change in style of these pressure ridges which defines the two flows as separate. Basaltic andesite in composition, containing large phenocrysts of mainly olivine but also plagioclase. These flows are aa in style. This thin, wide character is also known as a low aspect ratio flow (as opposed to a high aspect ratio flow, such as the andesitic flows into Oturere Valley which are shorter and higher). The surface of flow nine is rubbly and broken black basaltic lava. This flow was feed by a lava channel, seen in Figure 2.34, flowing down the western side of Red Crater, having originated at the south-western ridge of the crater. These two flows have a combined volume of ~ 0.00069 km^3.

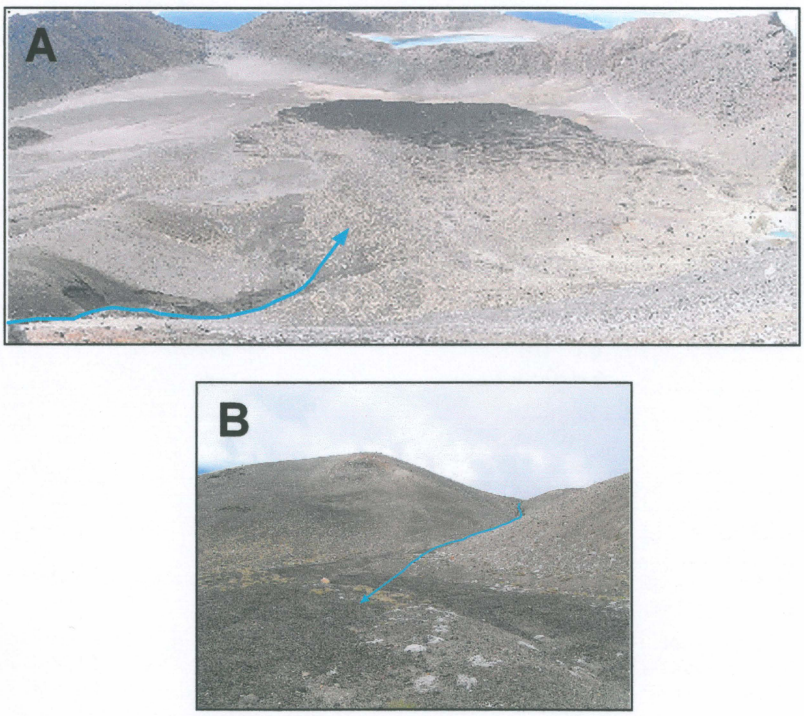

Fig 2.34 – Photos of lava channel feeding Central Crater Flow 9. **A** - Looking south. **B** - Looking north.

The final flow to be erupted from Red Crater has a total volume of ~0.00002 km^3. This flow (eleven) has erupted into South Crater, dribbling over the southern rim of Red Crater. This flow is narrow (~10 metres wide), ~ 330 metres long and one metre thick.

The lava flows erupted from Red Crater can be divided into two groups. The first group consists of flows one, two, three, four and five, which are all the result of sustained effusive activity issuing from the vent. This group has been erupted prior to the main cone construction. Flows six, seven, eight, nine, ten and eleven make up the second group, are basaltic andesites and are produced by molten scoria during sustained discrete gas bursts which have produced the flow.

The basaltic andesitic aa flows 6 and 7 into NE Oturere Valley are likely to have originated as clastogenic flows, perhaps flowing from the point where the agglutinated scoria unit in the eastern wall is preserved, and being channeled down into Oturere Valley by the lava channels which formed on the north eastern slope of the cone. The remaining basaltic andesite aa flows erupted from Red Crater (flows 8, 9, 10 and 11) are also clastogenic flows, with evidence been the partially welded scoria deposits seen at the potential origins of these lava flows.

While flow one emptied or nearly emptied the magma chamber, later injections of fresh magma (of more basaltic composition each time) into the chamber is a likely trigger for the later eruptive episodes.

2.3.1 LAVA FLOW MORPHOLOGY

The eleven lava flows of Red Crater have been analysed petrographically and geochemically by both Hodben (1997) and Topping (1974). What this section sets out to achieve is to clearly determine an order of extrusion for the lava flows (or groups of lava flows) and how these may be correlated with the construction of the Red Crater scoria cone. From GPS data recorded in the field, the lengths, widths and thicknesses of the flows could be determined, which could then be used to calculate the volume of each flow. Figure 2.35 below shows a scatter plot of length versus thickness.

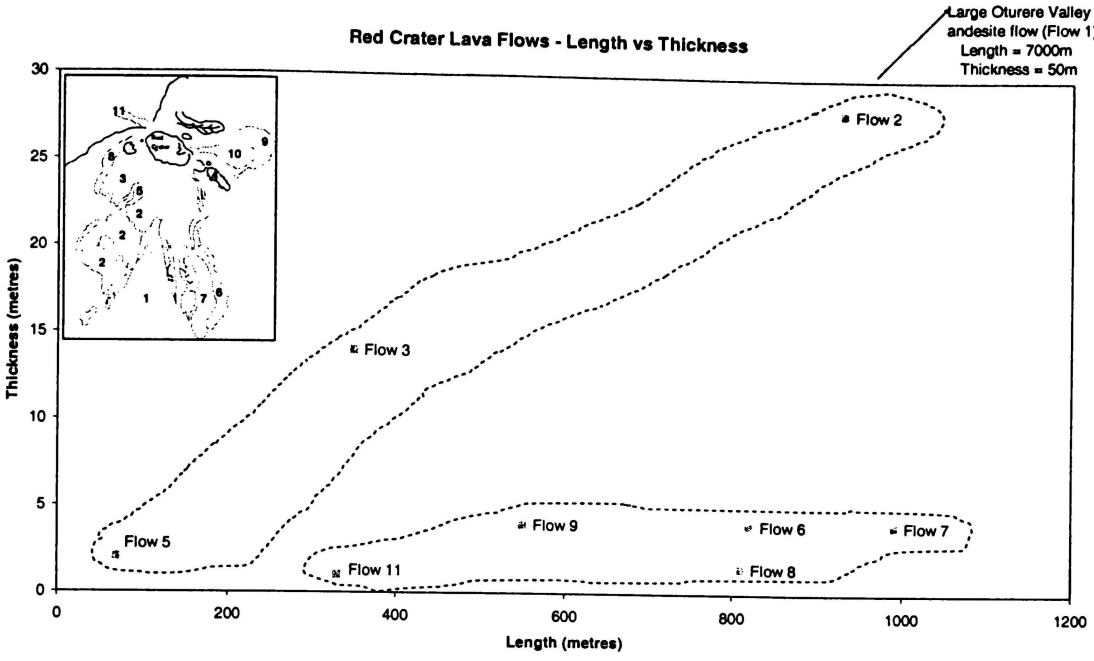

Figure 2.35 – Scatter plot of length versus thickness for eight Red Crater lava flows.

Flows 4 and 10 are not included, as Flow 10 is incorporated into Flow 9 (as overlying each other) and Flow 4 was buried under and hence unable to be calculated. This figure clearly shows the difference between the andesite flows and the basaltic andesite flows. The andesite flows follow an almost 1:1 relationship, in that as their length increases so does their thickness. On the other hand, the basaltic andesite flows remain less than five metres thick no matter what length they extend to.

Figure 2.36 shows two scatter plots, the first of length versus composition and the second of volume versus composition (based on SiO_2 measurements made by Topping, 1974). These plots both show two clearly defined groups, but both extend horizontally across the graph, indicating that composition is not the main controlling factor determining the length of Red Crater lava flows. The composition of the scoria cone fits into the same group as the basaltic andesite lava flows in both cases. Figure 2.37 plots volume versus length and shows that the basaltic andesite flows have lower volumes than the andesites, but similar lengths. This indicates that the more basaltic magma injected into the system after emplacement of the andesites, was smaller in volume than the initial andesite. Each of the basaltic andesite flows may reflect the

volume of a new batch of magma. Although the R^2 value is only 0.4381, there is still a correlation between length and volume, with the volume increasing as the length does.

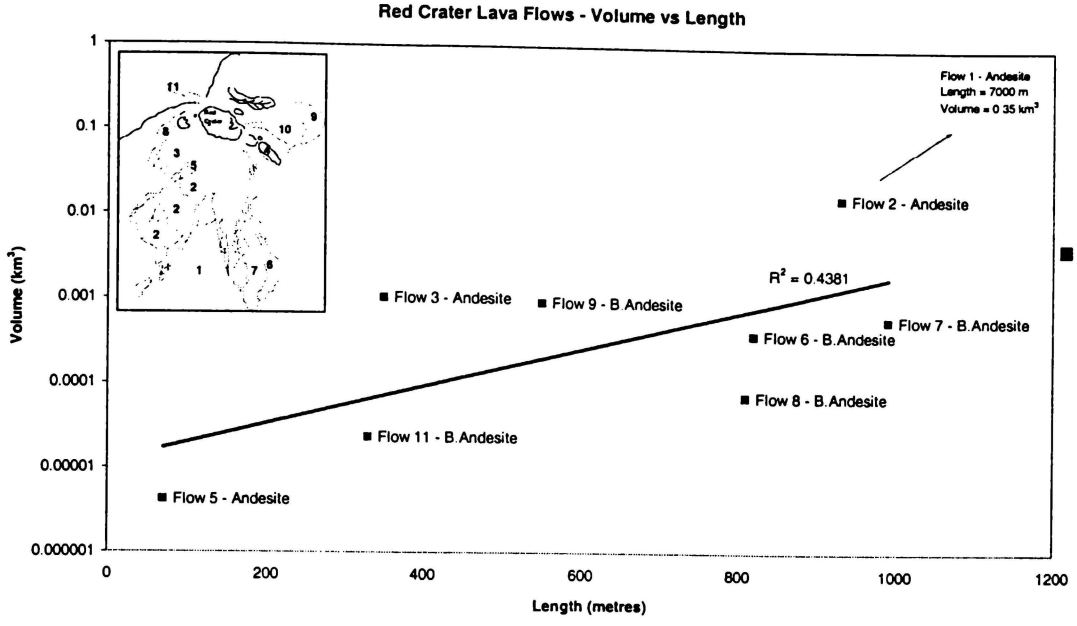

Figure 2.37 – Scatter plot of volume versus length for Red Crater lava flows.

The slope angles were calculated for three of the Red Crater flows, namely the Central Crater flow, South Crater flow and the Triple Lobe flow. These were chosen because they represent the three different ways in which the Red Crater lava flows were emplaced. The andesitic Triple Lobe flow was the result of sustained effusive activity prior to the cone construction, the Central Crater basaltic andesite flow resulted from the magma flowing out the base of a fire fountain during cone construction, while the South Crater basaltic andesite flow was feed by spatter from the same fire fountain or at the close of scoria cone construction. Figure 2.38 below shows profiles through the three flows and their slope angles. The shortest and thinnest flow, that into South Crater, has come to rest on a 23° slope and has only just reached the floor of South Crater below. The characteristics of this flow are therefore defined by the effusion rate of the eruption that fed it, rather than the slope angle or composition.

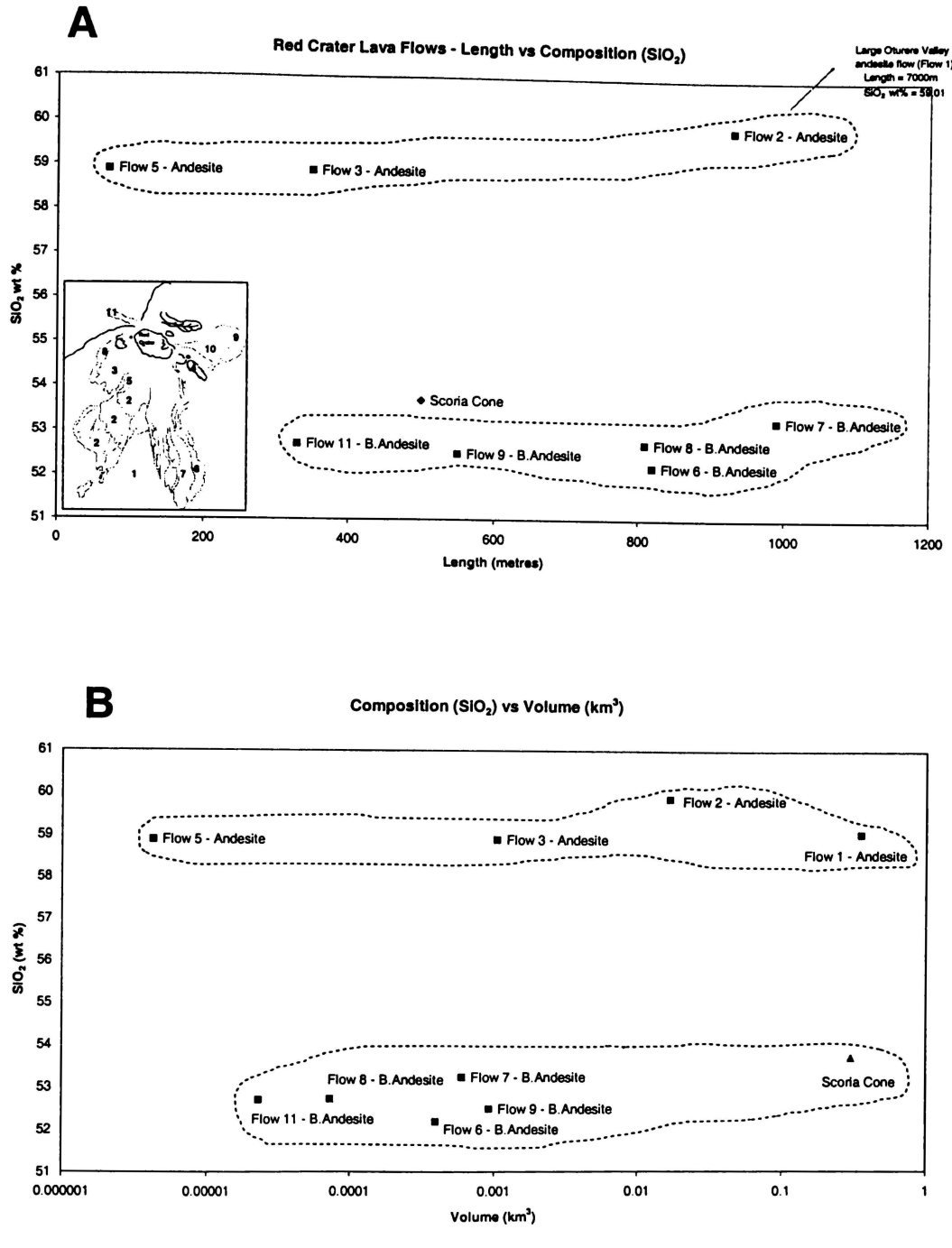

Figure 2.36– A - Scatter plot of length versus composition (SiO_2) for Red Crater lava flows. Scoria cone was plotted using a fictitious length in order to show the composition of the scoria cone in relation to the lava flows. **B** – Scatter plot of volume versus composition (SiO_2) for all Red Crater lava flows except Flow 4 (as this flow was not geochemically analysed by Topping (1974).

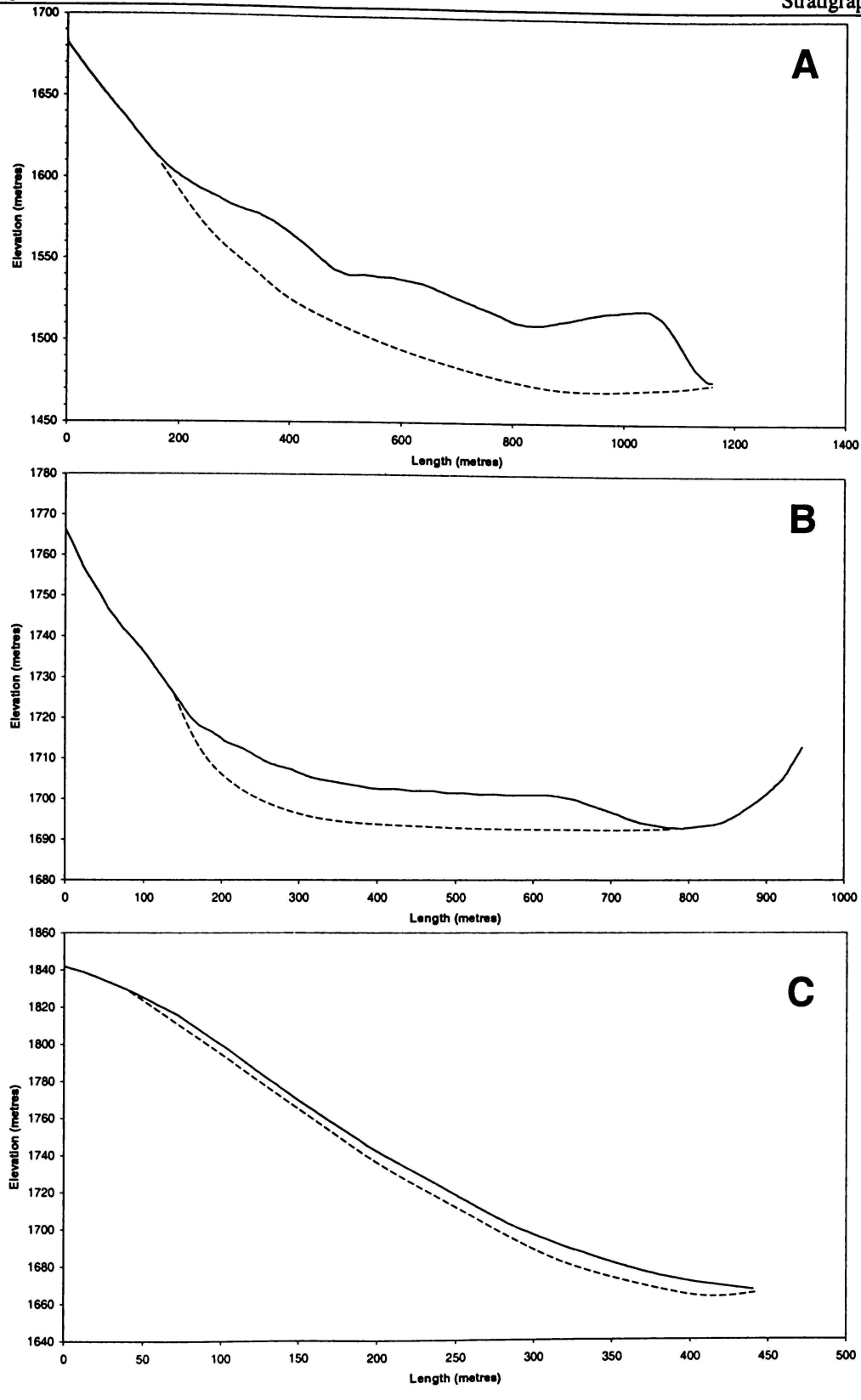

Figure 2.38 – Profiles showing slope differing slope angles which Red Crater flows are emplaced on. **A** – Andesite flow (Flow 2). **B** – Basaltic andesite flow (Flow 9). **C** – Basaltic andesite flow (Flow 11).

The South Crater flow, along with the Central Crater flow (emplaced on a slope angle of 2°) are examples of low aspect ratio flows, meaning they are defined as being long and thin, with low viscosities and therefore more mafic compositions. As Figure 2.39 shows, the basaltic andesites all plot along the bottom of the thickness versus area scatter plot, which is a characteristic of a low aspect ratio flow.

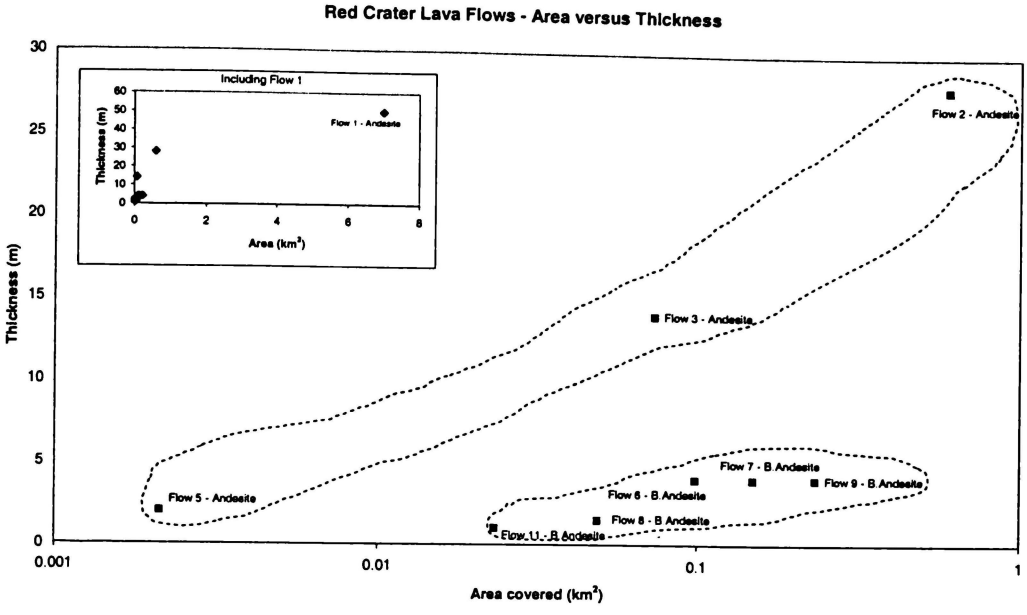

Figure 2.39 – Scatter plot of area versus thickness for Red Crater lava flows.

The andesites on the other hand plot at either side of the area axis because, as high aspect flows they are typically thicker and often shorter than there basaltic andesite counterparts. In the case of the Red Crater flows, it is only the thickness that clearly defines the difference.

Based on the evidence obtained from field observations and petrography, the order of the flow groups can be defined. The presence of Taupo Pumice on top of the Oturere Valley andesites gives a clear marker, indicating they were emplaced prior to the 185 ka Taupo eruption. Topping (1974) gave an age of the largest Red Crater andesite flow (flow 1 on Figure 2.39) to be between 9700 and 3200 years, which gives an approximate maximum age for the vent. Following the eruption of flow 1, the next 4 andesites were emplaced, all prior to 185 ka, these being flows 2, 3, 4 and 5. At this stage cone construction had not yet begun. These five flows were the result of sustained effusive activity probably with minor explosive activity. Following the 1.85 ka Taupo

eruption (Topping, 1974), flows 6 and 7 into the NE Oturere Valley were deposited as the result of the first basaltic magma injection into the magma chamber. Strombolian activity also began at this stage, rapidly constructing the scoria cone during this time, with flows 8, 9, 10 and 11 being emplaced in that order during the later stages of this cone construction and along with flows 6 and 7, as a result of either magma flowing from the base of sustained gas explosions, or from the spatter deposits of a fire fountain. Topping (1974) determined the relative ages of the post-Taupo basaltic andesite flows by using Parker's Index, which is based on the differences between weathered and un-weathered rock.

2.4 EXPLOSION PIT

On the outer southern crater wall is an explosion pit approximately 30 metres wide by 20 metres deep, as shown in Figure 2.40. It exposes the old Tongariro Trig andesite lavas upon which Red Crater is constructed. This andesite lava is columnar jointed, as it is within the crater itself, but is decidedly more rubbly and unstable. On the floor of the explosion pit is mainly the fallen blocks of andesite lava as well as five, metre-diameter blocks of black scoriacious lava. These blocks have the same composition as the spatter feed flows into South Crater and the SE Oturere flow which passes to the west of this explosion pit.

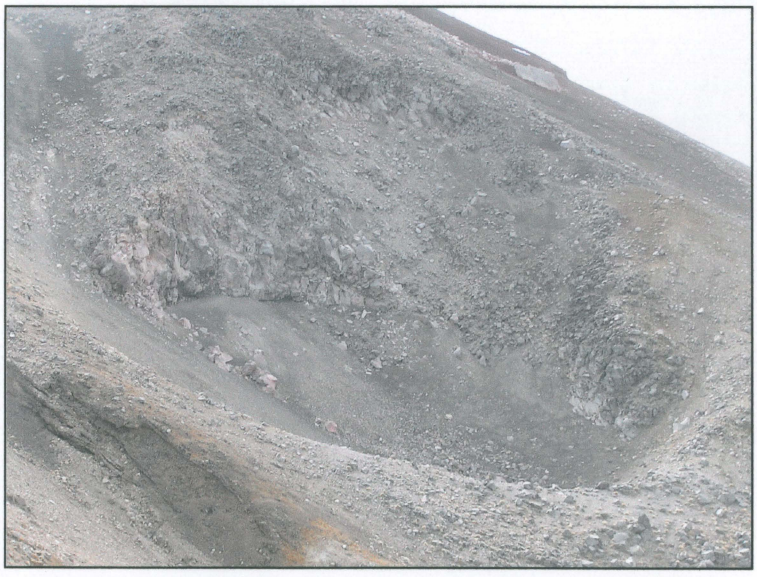

Figure 2.40 – Explosion pit, southern outer wall of Red Crater.

2.5 EMERALD LAKES

Created since the 1.85 ka Taupo eruption (Topping, 1974), the emerald lakes explosion pits are one of the youngest features of Red Crater. Consisting not only of the three lake-filled pits but also a further two smaller pits to the north east of the lower lake. These pits are the result of phreatic eruptions and extend out to the NE of the Red Crater cone. Their pH ranges from 3 – 5, with depths of up to 4.5 metres. While they slope at 30° - 40° into their centres, with temperatures of 9 - 11°C (Hochstein, 1985). Sulphur leaching into the lakes from the surrounding fumaroles is what gives them their distinct turquoise green colour (Hobden and Houghton, 2000).

The upper emerald lake is the largest with a diameter of approximately 110 metres. Around its flanks are a number of ballistic blocks ranging in size from 1.5 metre diameters up to the largest, which has a diameter of 6.7 metres. While debris from these explosions is found on top of both the Central Crater flows and the north face of Red Crater, these larger ballistic blocks are limited to the rims or within 30 meters of the explosion pits, giving an indication as to the explosiveness of these eruptions. Figure 2.41 below shows the line of explosion pits, a ballistic block, plus the sulphur leaching into the bottom emerald lake.

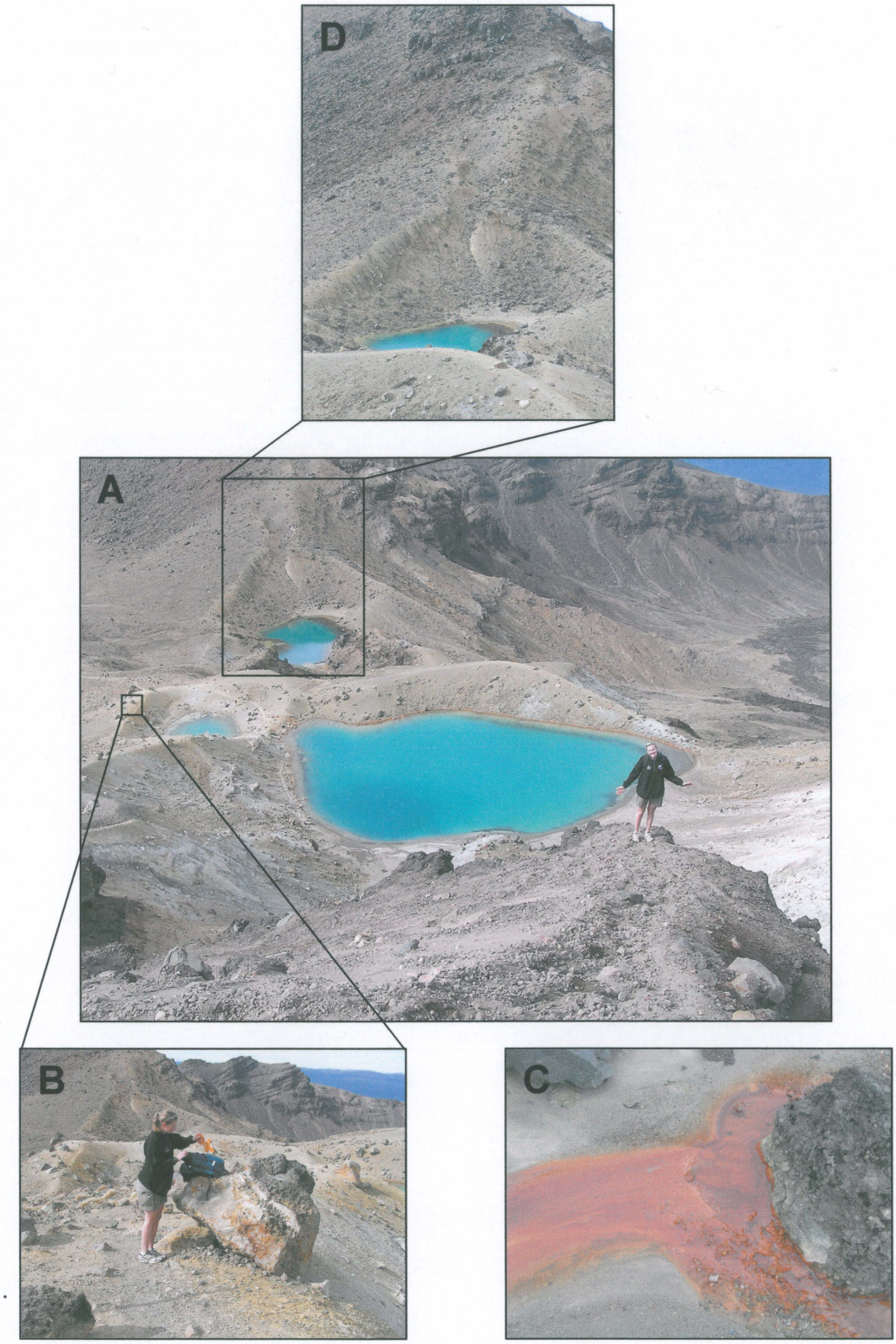

Figure 2.41 – **A** - Emerald Lake explosion pits looking north. **B** – Ballistic block 1.9m diameter. **C** - Sulphur leaching into lower emerald lake (within box in A). **D** – Full extension of explosion pits.

2.6 DISTAL DEPOSITS

Topping (1974) excavated a number of pits within the Oturere Valley in order to find evidence of past Red Crater eruptions and marker bed tephras that could help constrain the ages of the lava flows and tephra deposits. Two sites were examined during the course of this thesis, the first (seen in Figure 2.42) being located approximately half way along the northern circuit track, between Oturere Hut and the base of Red Crater, and the second (Figure 2.43) approximately 300 metres closer to the vent, on top of Flow 1, as the map in Figure 2.44 shows.

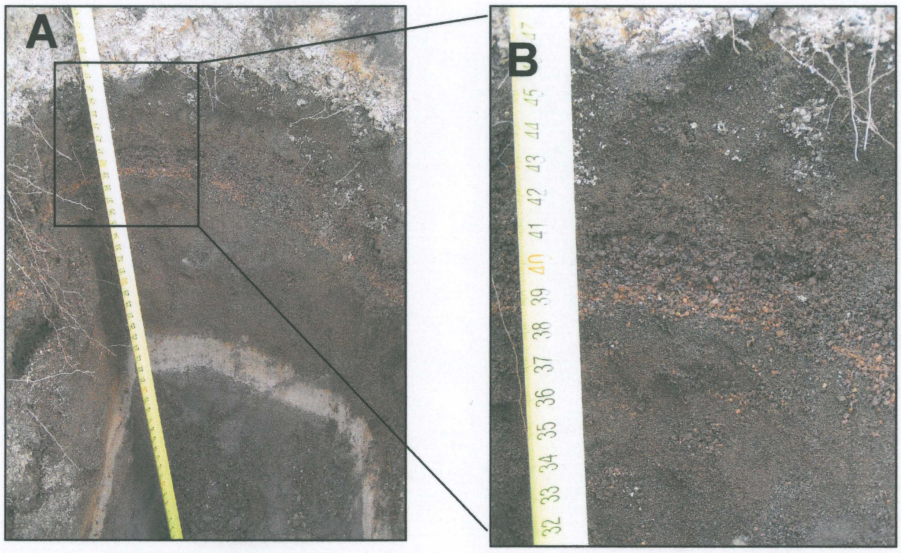

Figure 2.42 – **A** - Site 1 located half way between Oturere Hut and Red Crater. **B** – Close up of scoria layer.

The bottom 18cm of this section has a silty texture, is dark brown and very fine grained. Between 18 and 22cm, is a pale grey ash with clay like texture which is well compacted. 22-38cm is identical to the initial 18cm, except is more reddy brown. Above this is a 3cm unit of scoracious lapilli, reddy orange in colour, totally clast supported, and very well sorted with grain sizes of 1-2mm. Between 41 and 47cm occurs the very fine grained, silty textured reddy brown soil seen in horizons 1 and 3 already. The second pale grey, ash with clay like texture occurs, but this unit is less compacted and 13cm thick. Between 60 and 72cm, a mustard colored, sandy ash is

deposited and is capped by 55cm of the very fine grained, silty textured, reddy brown material of horizons 1, 3 and 5.

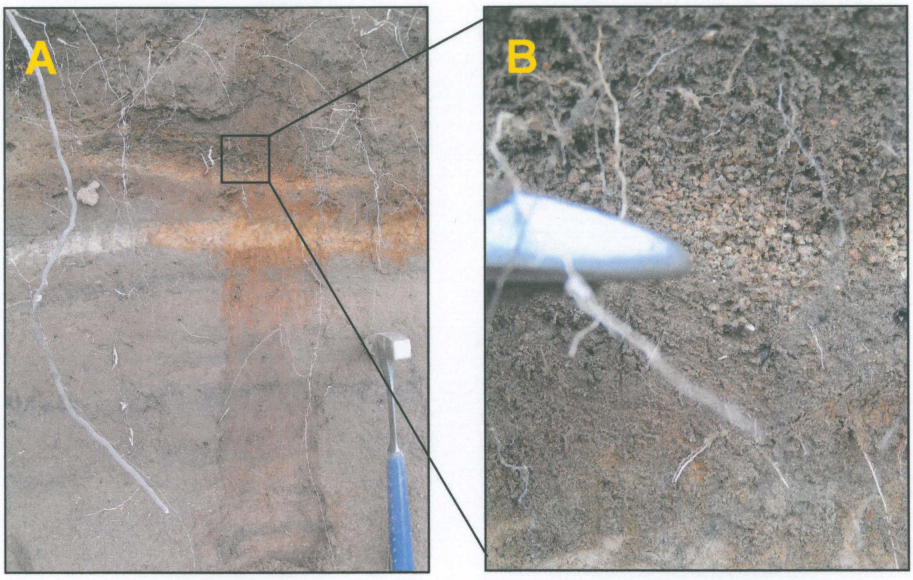

Figure 2.43 – **A** - Site 2 located ~ 300 metres closer to the vent than Site 1. **B** – Close up of A.

Starting from the top this time, the upper 11cm is a brown silty layer, which directly overlies the 2cm of scoracious lapilli, which is very well sorted and pinches out periodically. Beneath this is 3cm of the reddy brown silty layer of the upper horizon. The same pale grey, clayey horizon as described in the first section occurs between 16 and 19cm. The remaining 30cm alternates between the reddy brown silty layer of horizon 1 and a light black, fine grained unit.

The pale grey/yellow clayey units described in these two sections are of hydrothermal origin and according to Topping (1974) could represent the phreatic eruptions which followed intense fumerolic activity and cleared the vent of Red Crater. The scoria here is primarily fall associated with the scoria cone units, hence the hydrothermal ash layer is most likely to have erupted during phase one, and possibly correlates to the clay layer at the base of the scoria cone units interpreted to be altered Tongariro Trig andesites.

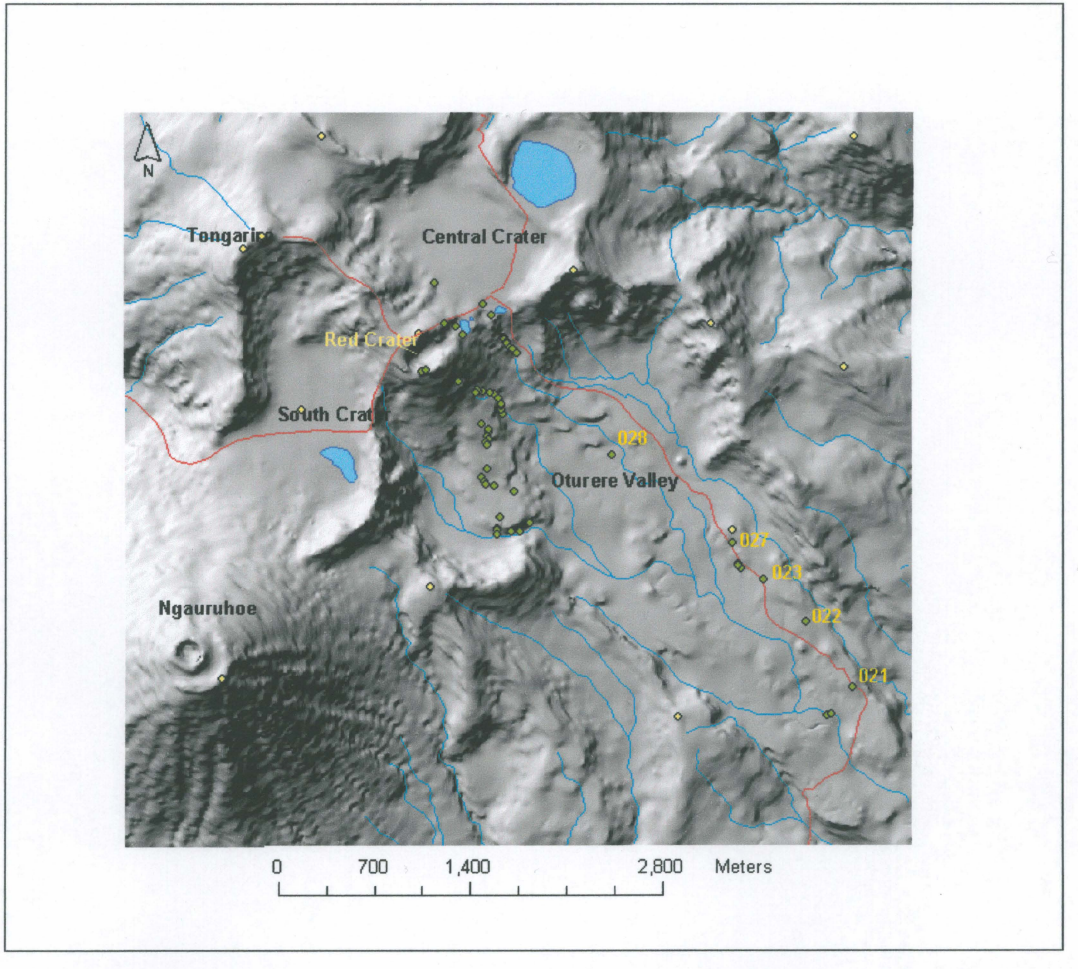

Figure 2.44 – DEM showing site localities. Site 1 is marked as 022, while Site 2 is marked as 027 (which are there corresponding waypoint numbers.

CHAPTER THREE

TEXTURAL AND COMPONENTRY ANALYSIS

3.0 VESICULARITY

3.0.1 INTRODUCTION

Red Crater is a scoria cone of 0.3 km^3 volume (Hobden, 2000). This scoria cone has units within it clearly defined by grain size variations and colour changes of the deposits. Clast density analysis was undertaken to see if the vesicularities and hence gas content of these units changed throughout the sequence and how this corresponds to subunit stratigraphy defined by grain size and colour.

3.0.2 METHODOLOGY

For the full methodology for this analysis, which is adapted from Houghton and Wilson (1989), please see Appendix 1. In order to obtain an accurate portrayal of the entire units' vesicularity, 30-40 scoria clasts within the size range of 4-10cm were selected from a narrow stratigraphic interval of 10-15cm. These scoria clasts were then dried for a period of two weeks before being individually weighed. Following weighing, each clast was then wrapped in squares of parafilm until the clast was watertight. Due to the nature of scoria being so sharp, a double layer of parafilm was necessary to prevent any leakages. Once wrapped and sealed, clasts were weighed again, this time in water. Due to the generally highly vesicular nature of Red Crater scoria clasts, most had to be ballasted with a lead weight, which was taken into account during the later calculations. The first calculation to be undertaken was to obtain the clasts Specific Gravity (S.G.) or density. This formula being:

$$S.G. = \frac{(W_{clast}{}^{air})}{(W_{clast}{}^{air}) + (W_{sheet}{}^{water}) - (W_{clast+sheet}{}^{water})}$$

If a lead weight was also used, then this becomes:

$$S.G. = \frac{(W_{clast}{}^{air})}{(W_{clast}{}^{air}) + (W_{sheet}{}^{water}) - ((W_{clast+sheet}{}^{water} + sinker^{water}) - (W_{sinker}{}^{water}))}$$

From this the vesicularity of each clast can then be calculated using this formula:

$$V\ (\%) = \frac{100\ (\text{D.R.E density} - \text{clast density})}{\text{D.R.E density}}$$

The D.R.E or dense rock equivalent value used for the basaltic scoria density was 2.74 g/cm^{-3} (Wohletz and Heiken, 1992). The full results for each unit and individual clast can be seen in Appendix 2.

3.0.3 RESULTS

Two main sections were targeted for vesicularity analysis, those being the Southern crater rim and the Eastern inner-wall which together provide a near complete stratigraphy of the scoria deposits.

As can be seen in Figure 3.1, the mean vesicularities for each unit vary through the section. Numbers of clasts analysed range from 30 to 42 for each sample. The average vesicularities are all between 60-80% vesicularity which classifies them as highly vesicular (Houghton and Wilson, 1989). The vesicularity ranges as low as 41% and as high as 81%, which means there are clasts ranging from moderately vesicular to extremely vesicular within the deposits.

According to Houghton and Wilson (1989), in the case of magmatic 'dry' eruptions, if the magma rises and erupts fast enough to prevent any non-explosive degassing, then the vesicularities should have a small range about 75-83%. In the case of the Red Crater scoria deposits, the mean vesicularities lie between 62-75% often with large vesicularity ranges. These lower average vesicularities are the result of the gas/bubbles within the magma rising faster than the magma itself, resulting in vesicles not yet fully developed at the point of the eruption. This means fragmentation and vesiculation had not reached their peak at the point of the eruption (Houghton and Wilson, 1989; Mastrolorenzo et al., 2001). This is a feature of strombolian eruptions, which have far greater ratios of gas to magma solid in the upper, shallow portion of the magma

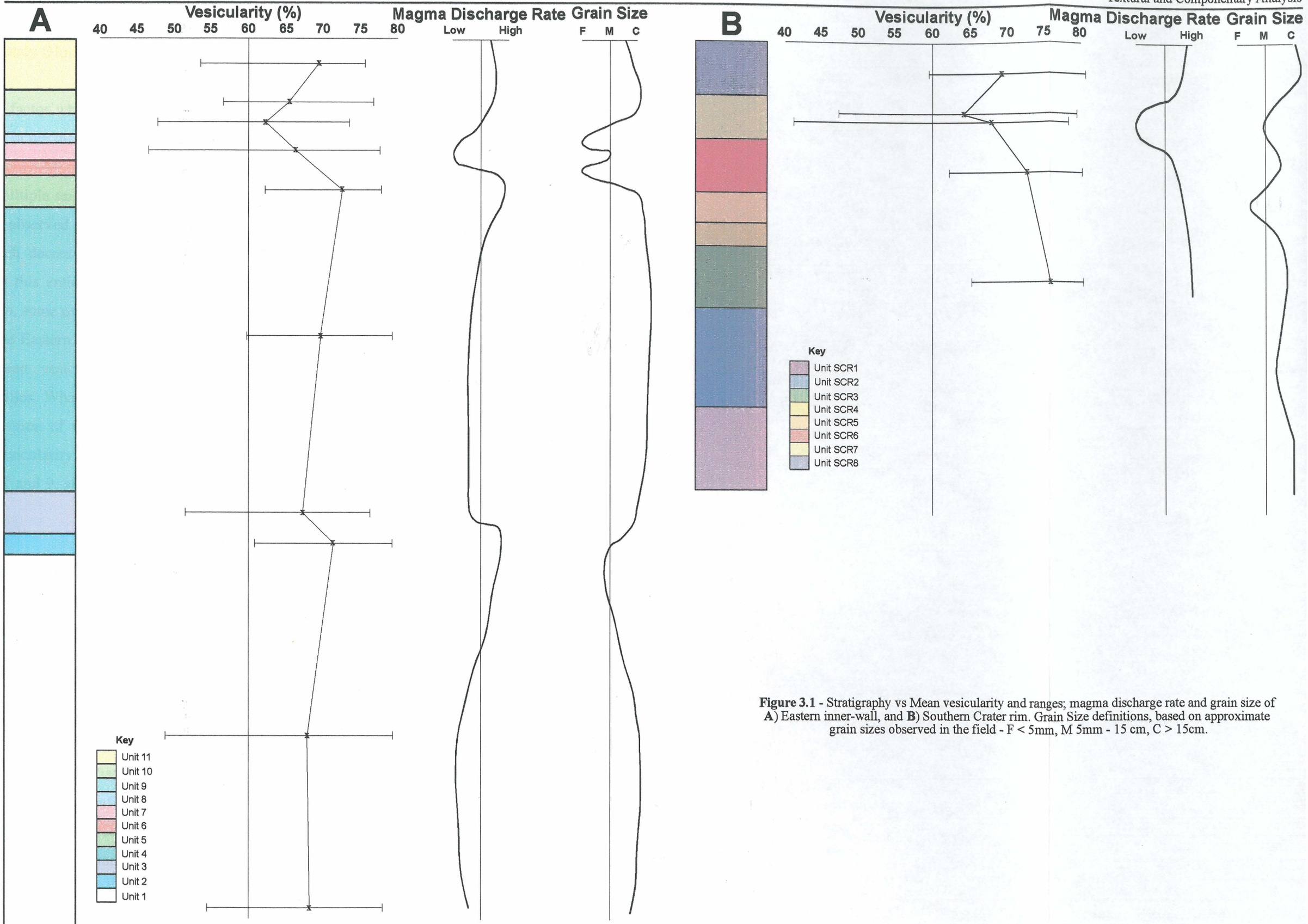

Figure 3.1 - Stratigraphy vs Mean vesicularity and ranges; magma discharge rate and grain size of **A**) Eastern inner-wall, and **B**) Southern Crater rim. Grain Size definitions, based on approximate grain sizes observed in the field - F < 5mm, M 5mm - 15 cm, C > 15cm.

column as a result of the bubbles rapidly streaming up through the slower moving magma body (Houghton and Wilson, 1989).

Another factor which affects the clast vesicularities is the magma discharge rate. A decrease in the discharge rate is reflected in the clast vesicularities by the vesicularity range increasing. Unit 1 of the Eastern inner-wall section was the only unit from which multiple samples were collected and within this unit an increase in vesicularity range is observed towards the top of the unit, indicating an initially high discharge rate which decreased over the deposition time of the unit. While the logistics of sampling this entire 52 metre section via abseiling precluded sampling at a higher resolution, some overall trends can be seen. Two peaks in the mean vesicularity occur within the Eastern inner-wall section, one in Unit 5 and the other in Unit 2, both of these mean vesicularity peaks also correspond with the narrowest range in vesicularities. What this means is that the magma discharge rate was highest during the deposition of these two units. Conversely the greatest vesicularity ranges and lowest vesicularity means indicate the lowest magma discharge rates, and occur in Units 3, 7 and 9, all of which occur immediately after the highest peaks in discharge rate.

The 52 metres of scoria deposited on the eastern wall of Red Crater has accumulated in a continuous fashion, with fluctuations in magma discharge rate occurring in an apparently cyclic fashion throughout the section. The rise rate of the bubbles within the magma also fluctuates in the same cyclic fashion as the discharge rate. A curve of this discharge rate is plotted alongside the vesicularities in Figure 3.1.

The Southern crater rim section shows a stark contrast in appearance to the Eastern inner-wall section, in that it is entirely black, with the units being defined by grain size in the field and confirmed by vesicularity measurements. Given there is such a marked difference between the Southern crater rim and the stratigraphic top of the Eastern inner-wall section, there may have been a short break in time between the deposition of the two sections.

This initial phase of the Southern crater rim section, which deposited units SCR1-3, probably involved a relatively high magma discharge rate, given the very narrow vesicularity range, and the high mean vesicularities. After the deposition of unit SCR3, the vesicularity ranges increase and the average vesicularities decrease suggesting a decline in the magma discharge rate. This decrease hits a minimum low at unit SCR7, before increasing again during the deposition of the final unit, SCR8.

3.0.4 SEM (SCANNING ELECTRON MICROPROBE)

In order to quantify physical differences in vesicularity, 13 samples from across the Red Crater vesicularity spectrum were examined. To determine which 13 clasts were to be used, the vesicularities for every clast analysed were placed in a spreadsheet and sorted from highest to lowest vesicularities. A graph was then made, from which the two end members were firstly selected and then eleven evenly spaced lines were drawn in between, with each line intersecting a point which corresponded with a unit sampled and the clast within that unit. Appendix 3a shows this graph and the lines used to select each clast, while Appendix 3b shows the frequency curve of the Red Crater samples and where the selected 13 clasts fit into this curve.

Figure 3.2 shows the 13 samples used for SEM analysis, with the photos on the left taken before the clasts were cut up into blocks 2cm x 2cm x 3mm (thickness). Due to the fragile nature of the scoria clasts, they were all impregnated in resin prior to being cut and mounted onto glass slides. For a detailed description on preparing these samples for SEM analysis, see Appendix 4.

One of the first things that is apparent when looking at this figure is that vesicle coalescence occurs in all the samples. Figure 3.3 below is a really clear example of coalescence.

60/02 (12)

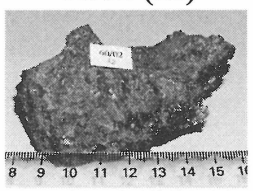

30.5%

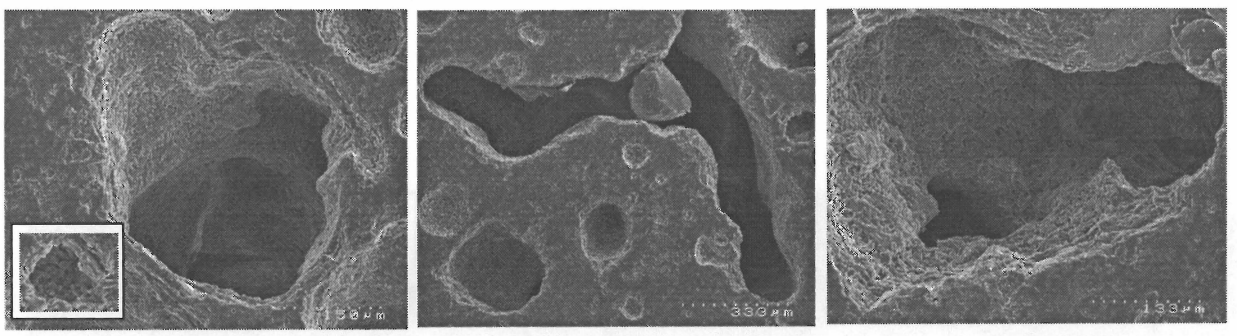

60/02 (17)

45.1%

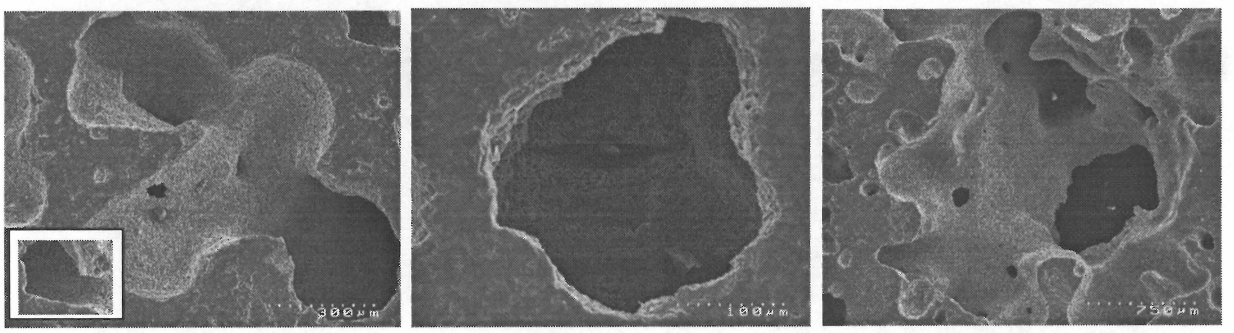

60/02 (1)

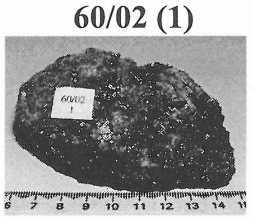

49.7%

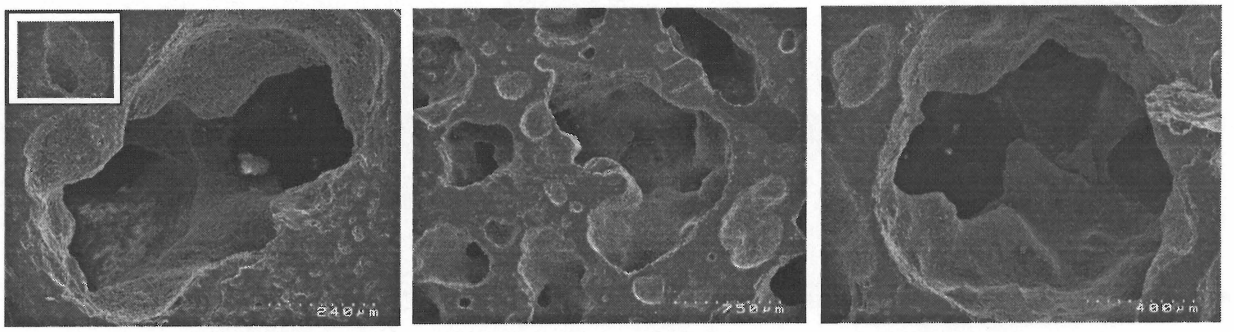

60/02 (21)

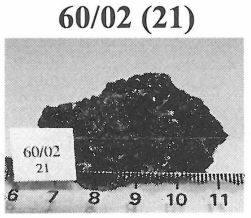

54.6%

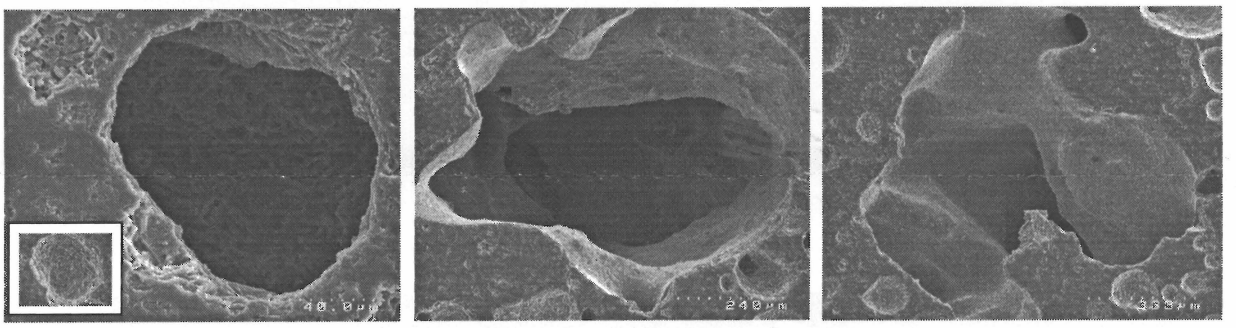

58/01 (1)

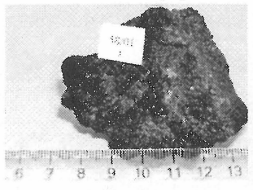

59.5%

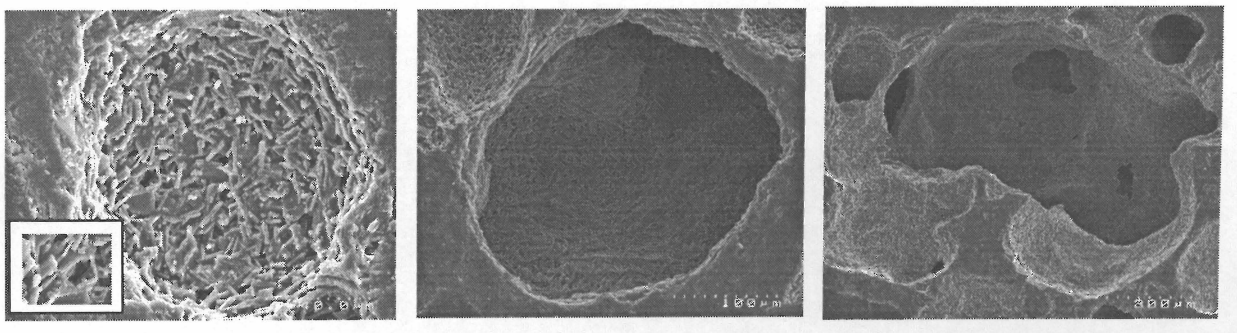

67/3 (26)

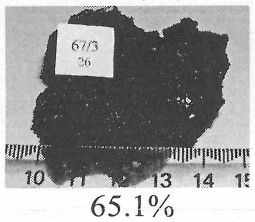

65.1%

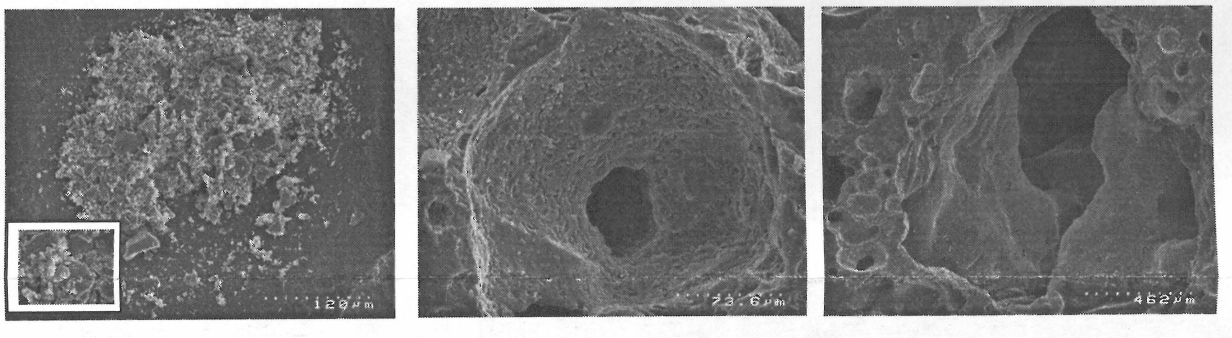

67/4 (27)

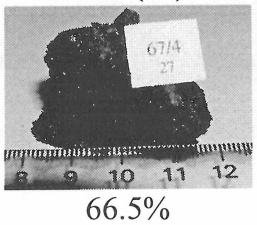

66.5%

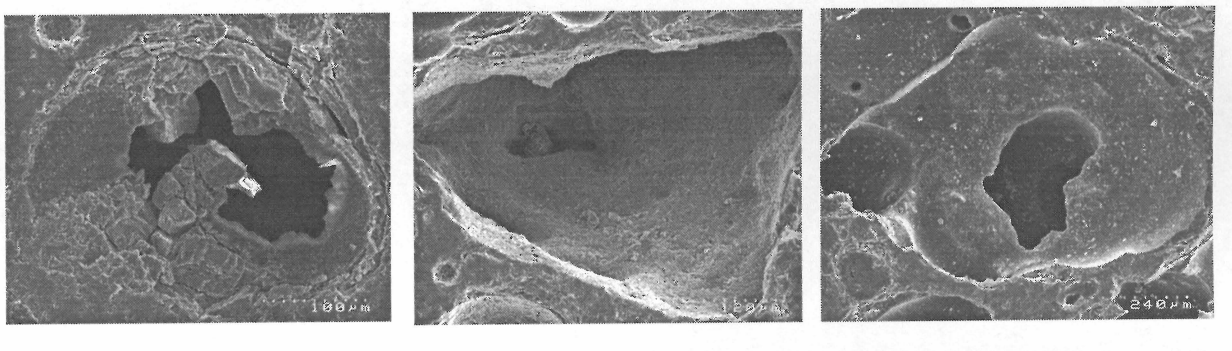

Figure 3.2a - SEM pictures of the full range of vesicularites seen in the Red Crater scoria deposits. 30.5% to 66.5% vesicularities.

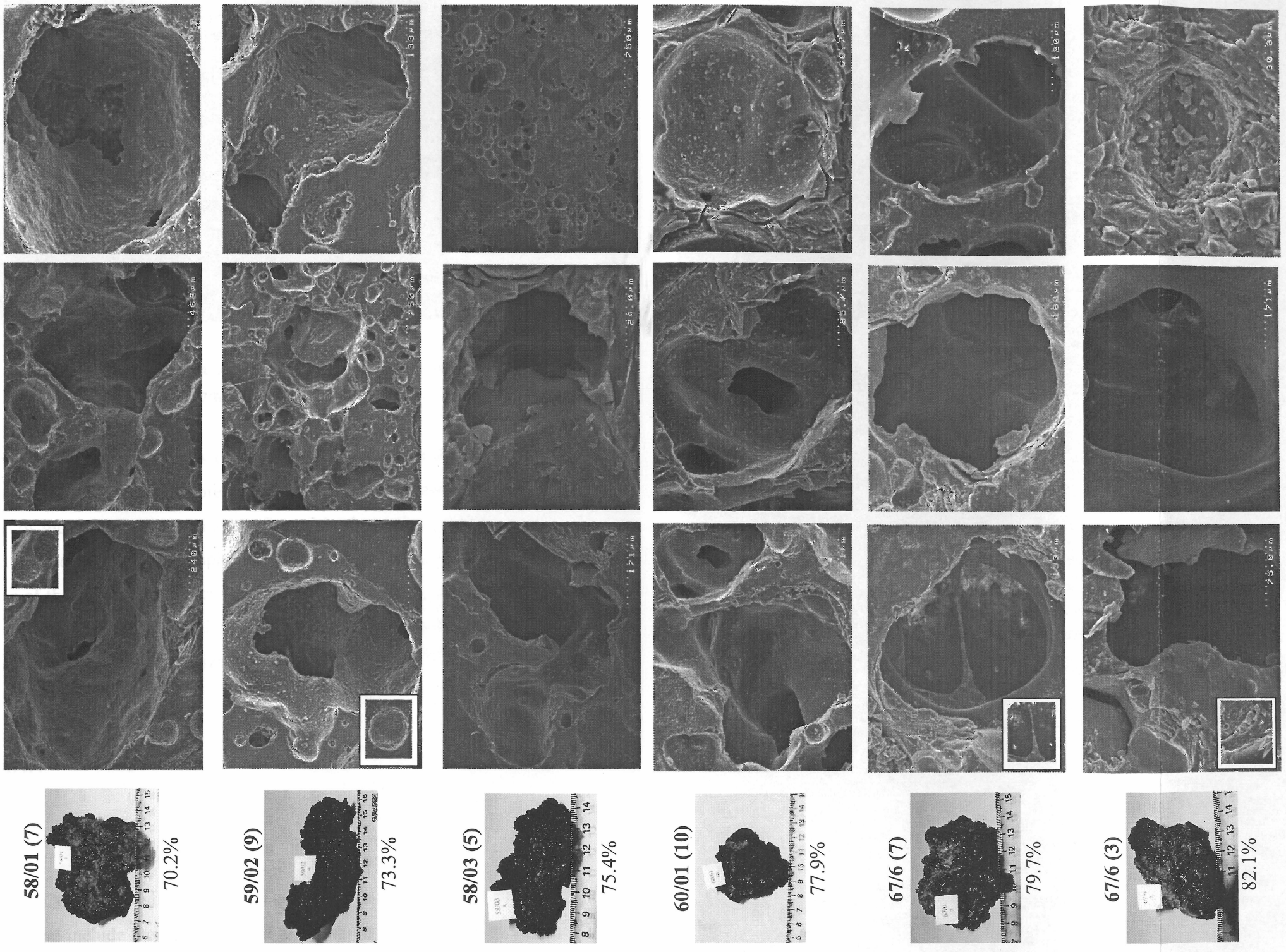

Figure 3.2b - SEM pictures of the full range of vesicularites seen in the Red Crater scoria deposits. 70.1% to 82.1% vesicularities.

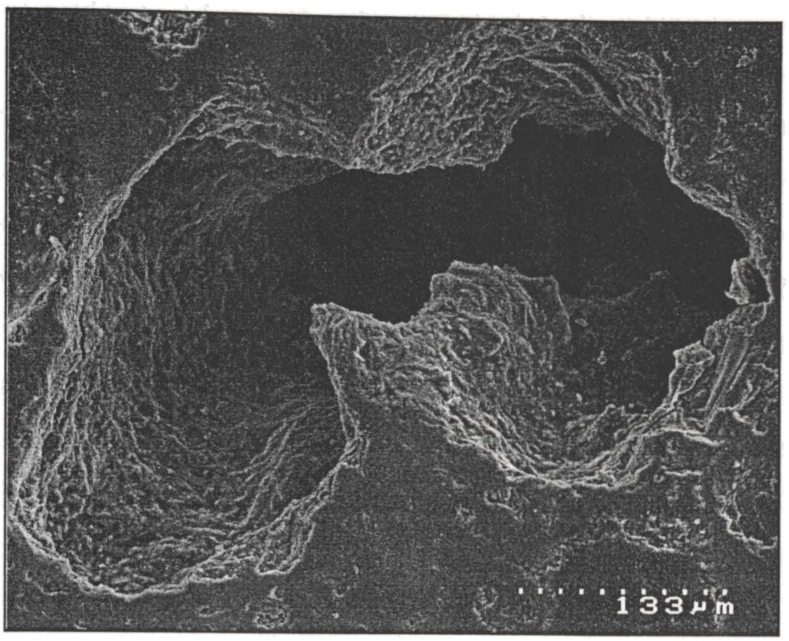

Figure 3.3 – Coalescence seen in sample 60/02, clast number 1 (this clast has a vesicularity percentage of 49.7%).

As the vesicularity increases, the chambers or cavities within the scoria increase as the bubbles expand and coalesce even more. The higher the vesicularity the more ragged the exterior of individual clasts. This is reflected in the vesicle shapes, with the low vesicularity vesicles being more spherical, compared to the more elongate and irregular shapes of the vesicles in higher vesicularity clasts as seen in Figure 3.2. This elongate shape is a result of several small vesicles coalescing. Some clasts exhibit evidence of vapour-phase mineralization within vesicle cavities as seen in Figure 3.2 (sample 58/01).

3.1 PETROGRAPHY

3.1.1 INTRODUCTION

The lava flows of Red Crater erupted from the vent system have diverse compositions (52 – 59 wt% SiO2) and include the most mafic of all Tongariro eruptions (Hobden, 1997; Topping, 1974). Given the maximum age of Red Crater is only between 9700

and 3800 years (Topping, 1974), this range and contrast in compositions is unusual. Topping (1974), and Hobden (1997), have both looked at the composition and petrography of the Red Crater lava flows but have not established relationships with the scoria cone. This section has the aim of showing the relationships between flows, which will later help in determining an extrusion order and relationship to the scoria cone deposits. Figure 3.4 shows a location map and outline of the eleven Red Crater lava flows, while all thin section descriptions can be seen in Appendix 5. In all of the graphs which are presented in this chapter, the largest Red Crater flow (flow 1) into Oturere Valley has been included as an inset in the upper corner of each graph. This is because this flow is magnitudes greater that the other ten flows, and if graphed on the same scale, then the ten flows would be bunched in one corner and no relationships would be able to be interpreted.

3.1.2 RESULTS

Fresh, fist sized samples of all eleven Red Crater lava flows were collected in the field over the course of this study. These were then cut and mounted on thin sections in order for analysis to be undertaken. Thin section preparation is described in Appendix 4. Once made into thin sections the first thing to do was determine the composition of the samples and in particular, the types of phenocrysts present. Percentages of mineral phases were determined by point counting 21 samples and all data are summarized in Table 3.1.

Plagioclase by far and away dominates in all samples ranging from 9.4% up to 32.2%. Olivine and Augite were the next two most dominant phenocrysts, with Hypersthene and Opaques occurring to a lesser degree. The percentage of crystals present in each sample gave a good indication as to how the lava flows could be subdivided into groups. As Figure 3.5 shows, the andesite lavas erupted into Oturere Valley have the highest crystal percentage, ranging from 36.8 to 49.2%.

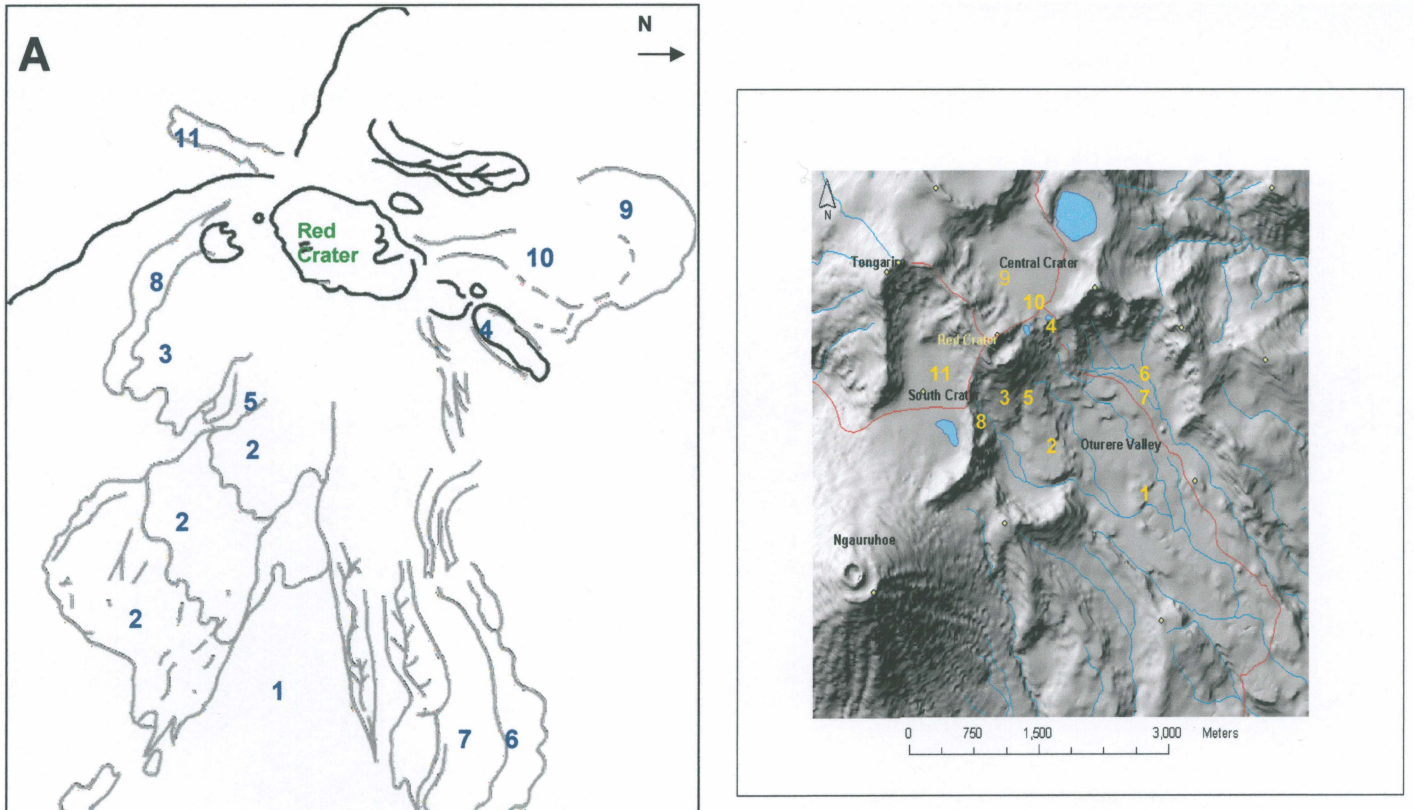

Figure 3.4 – **A** - Outline of the eleven lava flows erupted from Red Crater, with numbers referring to the order in which they were erupted, 1 been the oldest flow, 11 the youngest. **B** – DEM of Red Crater showing the location of the eleven lava flows.

Petrography Summary Statistics											
	Glassy Matrix as % of 500	Microlite Matrix as % of 500	% Crystals	Vesicles as % of 500	Plagioclase as % of 500	Hypersthene as % of 500	Augite as % of 500	Olivine as % of 500	Opaques as % of 500	Location	Waypoint
53/2 (5)	5	49.8	45.2	0	28.8	3.4	4.2	4	4.8	Large valley filling Oturere flow (Flow 1)	123 (25/4/03)
53/1 (14)	7	36.8	39.6	16.6	18.2	2	6.4	11.2	1.8	Large valley filling Oturere flow (Flow 1)	122 (25/4/03)
50/1 (7)	1.2	51.8	41	6	22.6	1.2	3.8	11.4	2	1st lobe (upper) Tripple Lobe flow (Flow 2)	114 (25/4/03)
52/1 (11)	2.8	55.8	36.8	4.6	22.2	2	7	4.6	1	2nd lobe Triple lobe flow (Flow 2)	119 (25/4/03)
52/3 (19)	4.6	35.6	39.6	20.2	28	2.2	2.4	4.6	2.4	3rd lobe Triple lobe flow (Flow 2)	121 (25/4/03)
51/2 (15)	1.8	49.8	40.8	7.6	25	2.6	4.6	6.6	2	2nd large andesite Oturere flow (Flow 3)	117 (25/4/03)
51/1 (1)	14.6	36.2	49.2	0	30.8	3.4	7.2	5	2.8	Little andesite SE Oturere flow (Flow 5)	116 (25/4/03)
47/4 (10)	4.4	48	30.2	17.4	12.2	1.8	7.4	8.8	0	Lava channel Sth track NE Oturere Valley (Flow 6)	101 (24/4/03)
48/2 (21)	3.4	53	34	9.6	15.8	1.8	6.2	10.2	0	Lava channel Nth track NE Oturere Valley (Flow 7)	104 (24/4/03)
47/1 (1)	16.8	32.2	23.2	27.8	10	0.8	6	6.4	0	SE aa flow NE Oturere Valley (Flow 6)	95 (24/4/03)
49/1 (16)	11.4	45	30	13.6	14	1.2	7.4	7.4	0	NE aa flow NE Oturere Valley (Flow 7)	105 (24/4/03)
36/1 (12)	3.2	52.2	42.2	2.4	24	5.4	8.2	2.2	2.4	Tongariro Trig lava within explosion pit	53 (6/3/03)
34/3 (4)	24.2	40	35.8	0	12.6	2.2	12.2	8.8	0	Vent Breccia	50 (5/3/03)
34/1 (3)	11.4	43.2	45.4	0	32.2	4	3.4	3.6	2.2	Tongariro Trig lava - Possum Peak	47 (5/3/03)
62/1 (23)	0.8	52	39	8.2	26.4	4	3.2	3.2	2.2	Extension dike Sth face	006 (18/5/03)
39/1 (7)	8.6	32.2	21	38.2	10.4	0.8	.4	5.8	0	Central Crater flow (Flow 9)	80 (15/3/03)
40/1 (2)	4.6	40.6	24.4	30.4	10.8	1.4	2.8	9.4	0	Lava channel feeding Central Crater flow (Flow 9)	87 (16/3/03)
51/3 (13)	10.4	41.2	53.6	14.6	12.6	1.4	16	23.6	0	aa flow SE Oturere Valley (Flow 8)	118 (25/4/03)
18/2 (20)	5.4	34.8	35	24.8	18.8	2.4	5	8.8	0	South Crater flow (Flow 11)	25 (21/1/03)
65/2 (25)	11.8	30.4	28.4	29.4	17	0.4	4.4	4.4	2.2	Lava to right of track down Nth Face (Flow 10)	
56/2 (22)	8.2	32.2	19.2	40.4	9.4	0.6	3.8	5.4	0	Lava to left of track down Nth Face (Flow 10)	
TG128	5.6	22.6	26	45.8	12.8	1.8	3.2	8.2	0	Lava bomb, western crater rim (Scoria Cone)	

Table 3.1 – Petrography summary statistics for Red Crater lava flows and a representative sample from the scoria cone.

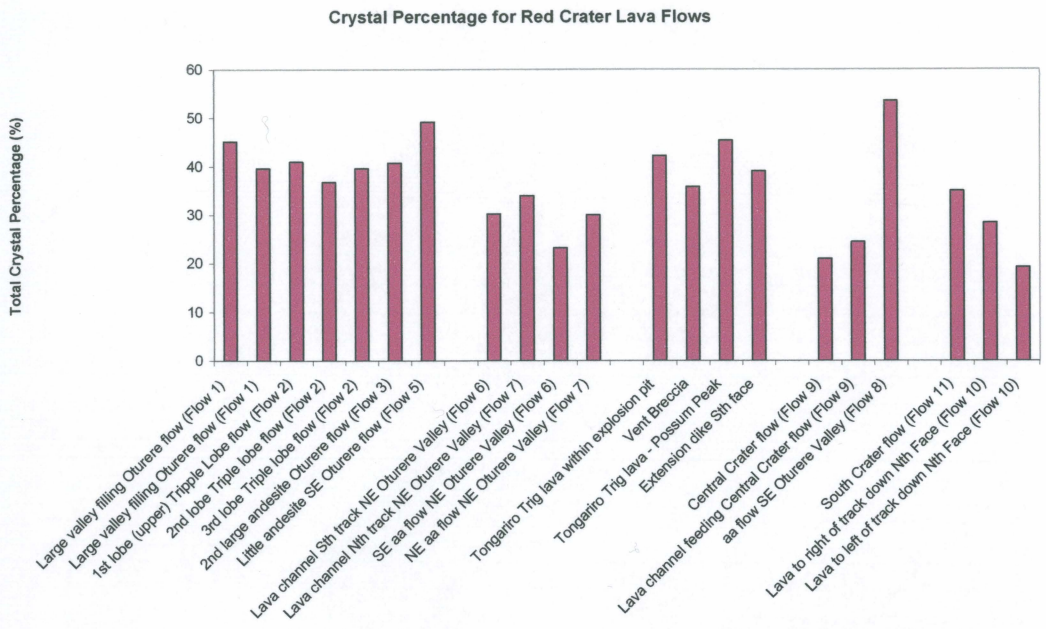

Figure 3.5 – Crystal Percentages in all Red Crater lava flows, plus four Tongariro Trig lava samples.

Overall, these are only slightly greater than the various samples of older Tongariro Trig lavas sampled from within the explosion pit on the south face of the cone; the large ballistic block above this explosion pit (named vent breccia); the ballistic block on top of the Eastern crater rim; and what was originally thought could be an extension through the crater wall of the drained dike, but what is another ballistic block. Figure 3.6 below shows two photomicrographs taken to show the similarities between these two groups.

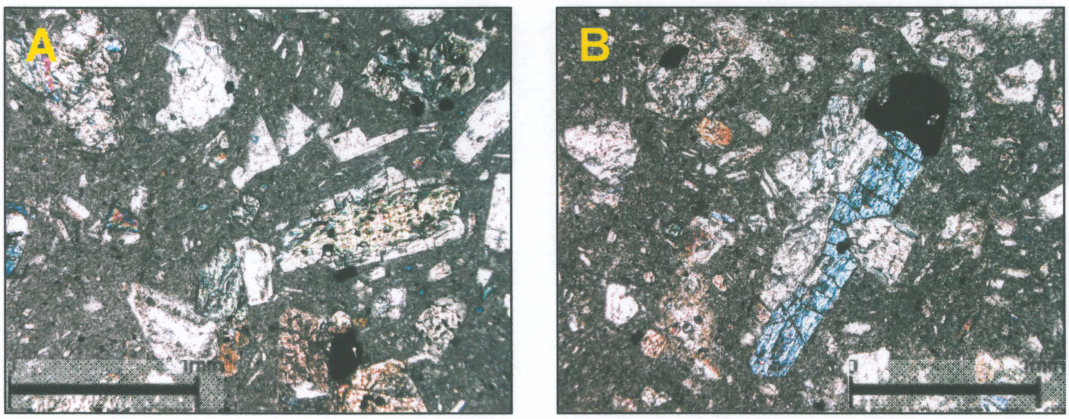

Figure 3.6 – Photomicrographs of the andesite Triple Lobe flow erupted from Red Crater (**A**) sample 52/1, and the older andesitic Tongariro Trig lavas (**B**) from within explosion pit, sample 36/1.

The group of samples with the next highest crystal percentage is the NE Oturere Valley, basaltic andesite aa flows and their associated lava channels. The final group is the remaining basaltic andesite aa flows into Central Crater and South Crater, which have similar crystal percentages to the NE Oturere basaltic andesite flows. The odd ball in all these flows is the basaltic andesite aa flow into SE Oturere Valley which has the highest crystal percentage of all the lava flows. As Figure 3.7 shows, Plagioclase dominates alone in the phenocrysts within the andesite flows, whereas in the basaltic andesite aa flows, there is less of a difference between the plagioclase, olivine and augite phenocrysts percentages.

The other noticeable thing about the figure for the basaltic andesite aa flows (3.7a) is that the vesicles dominate the phenocrysts, giving a clear indication as to the change in eruption style. In NE Oturere Valley, two very similar basaltic andesite aa flows are deposited. Above them on the NE slope of the cone itself are two lava channels, which meander down the side of the cone towards these flows. As Figure 3.8 shows, these lava channels did infact feed these two flows due, which can be concluded from the near identical nature of the phenocrysts percentages between them.

Another lava flow to be confirmed as one flow and not three is the Triple Lobe flow into Oturere Valley. Samples were collected at each of the three lobes, and as Figure 3.9 shows, the three lobes have phenocrysts percentages that are close to matching. The three groups of lava flows are represented in Figure 3.10, by the andesite Triple Lobe flow, the Central Crater basaltic andesite aa flow, and the basaltic andesite aa flow into South Crater. This figure shows the decrease in plagioclase and the increase in both olivine and vesicles, which in turn show the change in composition between the early erupted andesites and the later erupted basaltic andesites.

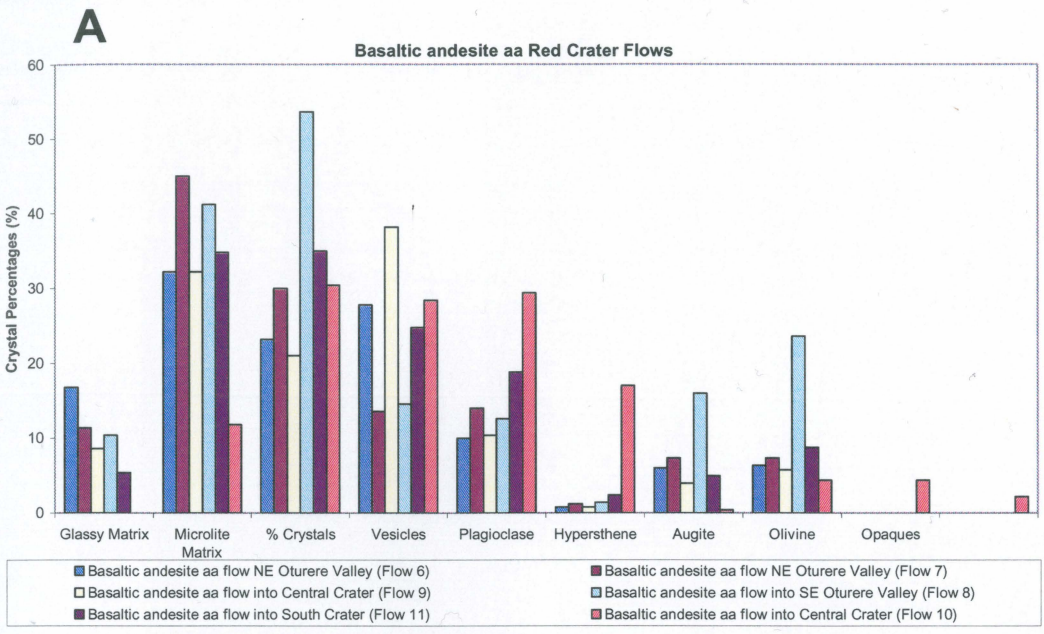

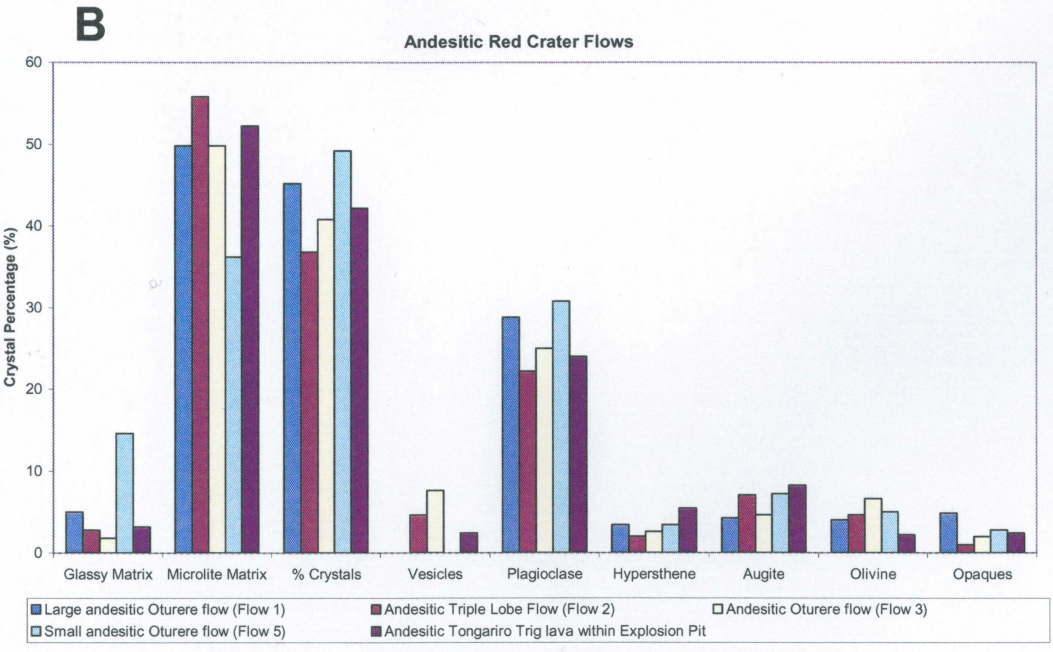

Figure 3.7 – Crystal percentages in Red Crater lava flows. **A** - Basaltic andesite aa flows. **B** – Andesitic blocky flows.

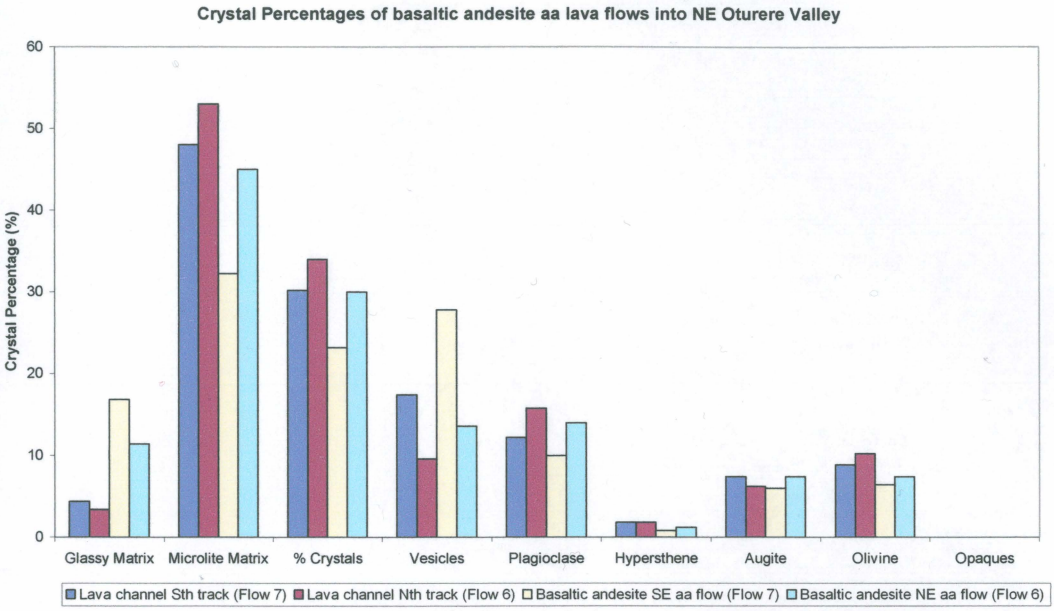

Figure 3.8 – Crystal percentages in basaltic andesite aa flows into NE Oturere Valley, showing the lava channels are of similar composition to the lava flows.

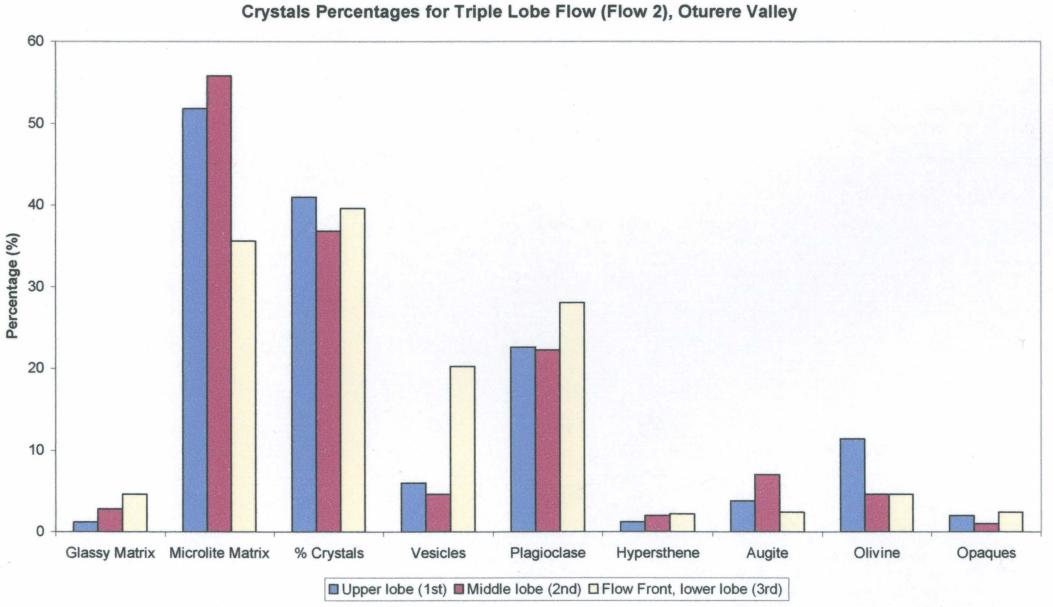

Figure 3.9 – Crystal Percentages for the three lobes of the Triple Lobe flow, Oturere Valley.

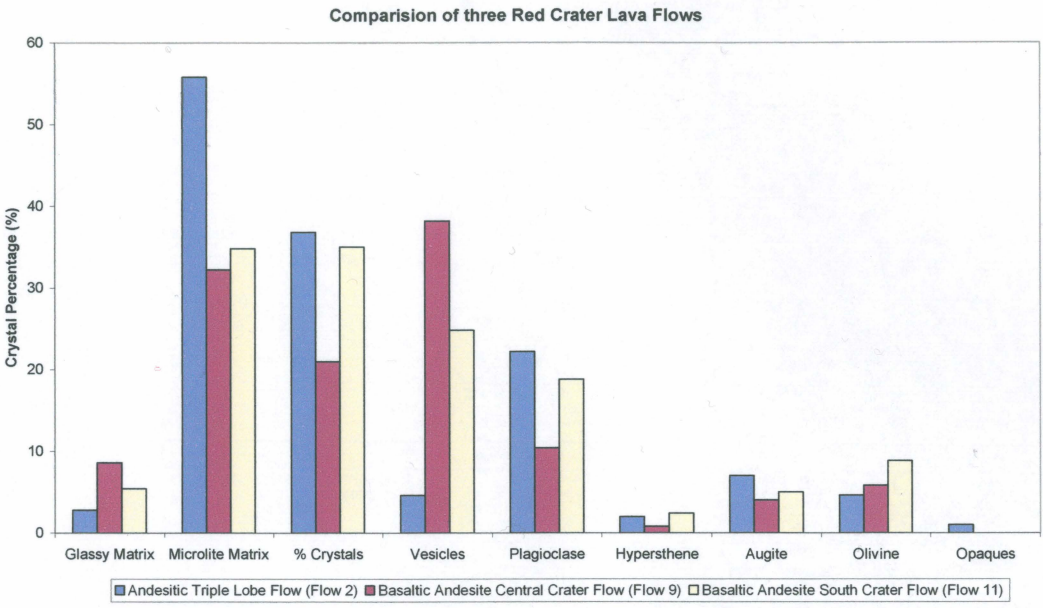

Figure 3.10 – Comparison of plagioclase, olivine and augite in andesitic Triple Lobe flow (flow 2), basaltic andesite Central Crater flow (flow 9) and basaltic andesite South Crater flow (flow 11).

When comparing specific phenocrysts percentages against each other for the four flow groups defined, some clear patterns emerge. Figure 3.11 is a scatter plot of olivine versus plagioclase, the two most dominant phenocrysts in all the Red Crater lava flows.

The two groups of basaltic andesite aa flows fall within the same area, with small percentages of plagioclase and as a combined group, the highest percentages of olivine overall. They can therefore be defined as a single group. Once again, the SE Oturere basaltic andesite aa flow plots apart from all other groups, with a plagioclase percentage of 12.6% and an olivine percentage of 23.6%. The andesite flows are clustered together at variable olivine percentages, but high plagioclase percentages. This figure shows a clearer distinction between the Red Crater andesites and the Tongariro Trig andesites, with the Tongariro Trig andesites having similar plagioclase percentages, but much lower olivine percentages.

The second scatter plot which confirms the subdivision of flows into three main groups is Figure 3.12, which plots hypersthene versus augite percentages.

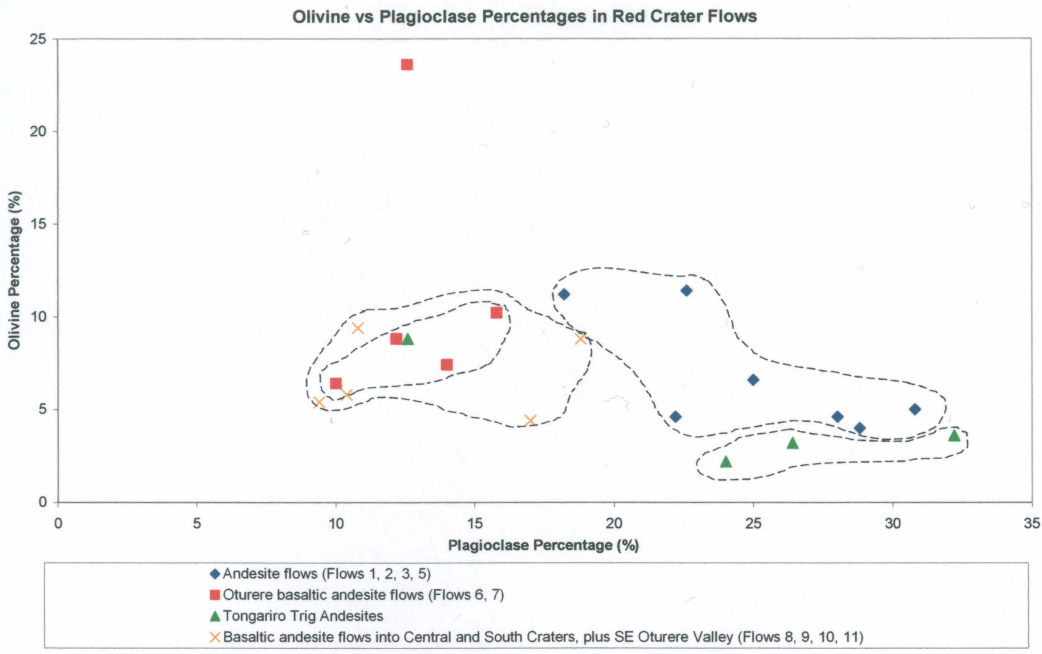

Figure 3.11 – Scatter plot of olivine versus plagioclase, showing the four lava flow groupings.

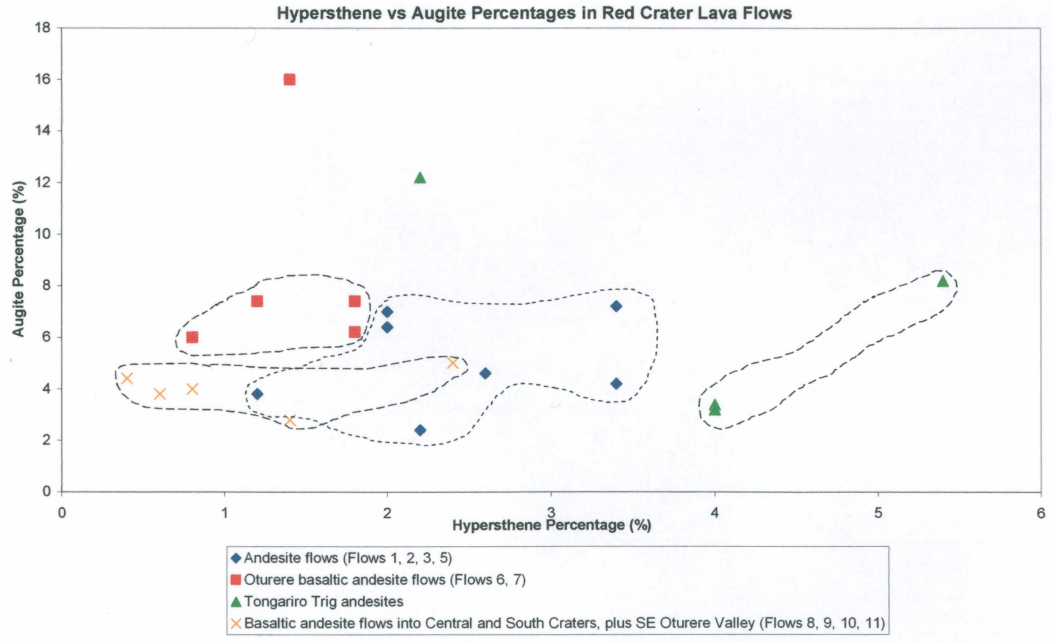

Figure 3.12 – Scatter plot of hypersthene versus augite, showing the three lava flow groupings the Red Crater lavas can now be split into.

Once again, the two groups of basaltic andesite aa flows can be combined into one, while the Tongariro Trig andesites are grouped apart from the Red Crater andesites due to their higher hypersthene percentages. Figure 3.13 below shows photomicrographs of the three main groups, plus the SE Oturere basaltic andesite aa flow which is plotted apart from the other groups.

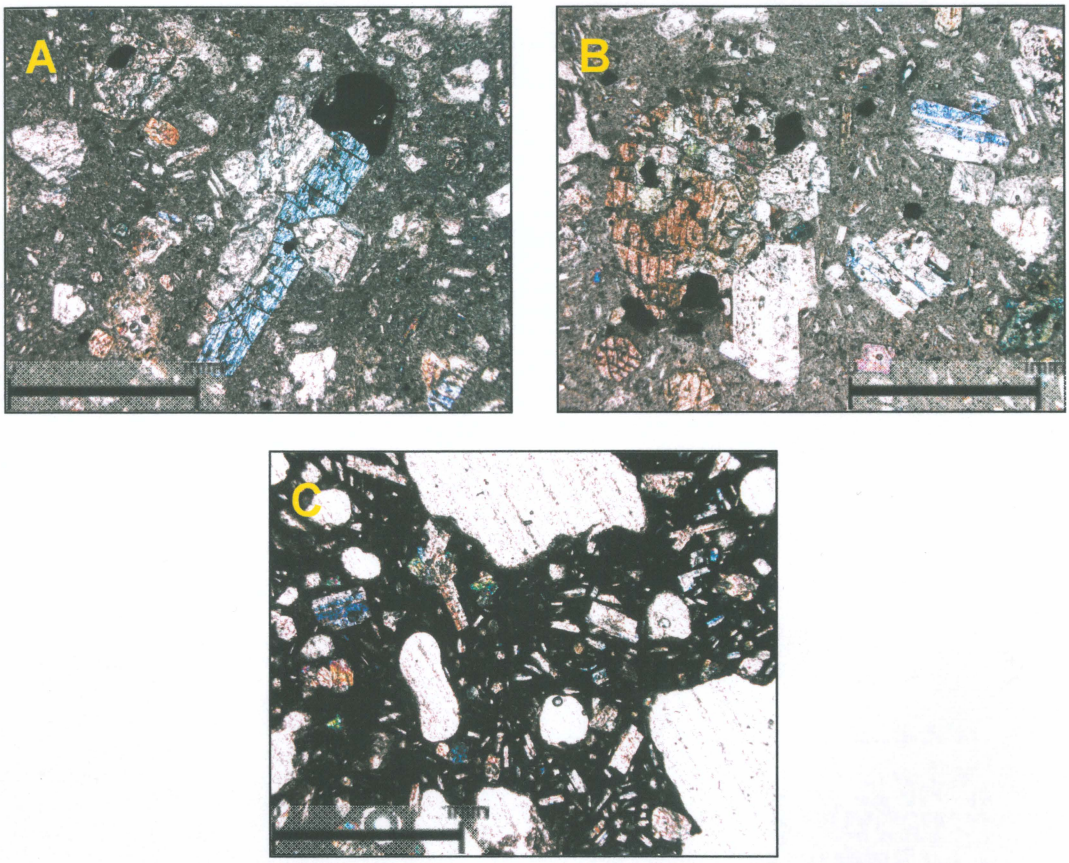

Figure 3.13 – Representative photomicrographs of the three main Red Crater lava groups. **A** - Tongariro Trig andesites. **B** - Red Crater andesites (Flow 3). **C** - Red Crater basaltic andesites (Flow 9).

With the first aim of dividing Red Craters lava flows into petrographic groups completed, the second aim of the petrography chapter is to show the evidence for magma mixing and mingling. Given the compositional differences already highlighted, there is an assumption that magma mixing and mingling has to have occurred in order to get the range of lava flows seen. Proof of this can be seen by examining the thin sections sampled. Hobden (1997), stated that compositional

banding, sieve textures, reverse and patchy zoning, disequilibrium mineral assemblages and disparate crystallization temperature estimates, are five features which suggest magma mixing. From the samples analysed, evidence of sieve textures and reverse and patchy zoning were found.

The plagioclase crystals seen in both the andesite and basaltic andesite lavas of Red Crater show strong oscillatory zoning and also both patchy and reverse zoning, as the photomicrographs in Figure 3.14 show. This is an indication of magma mixing as this is often associated with partial resorption of the plagioclase back into the melt (Hobden, 1997).

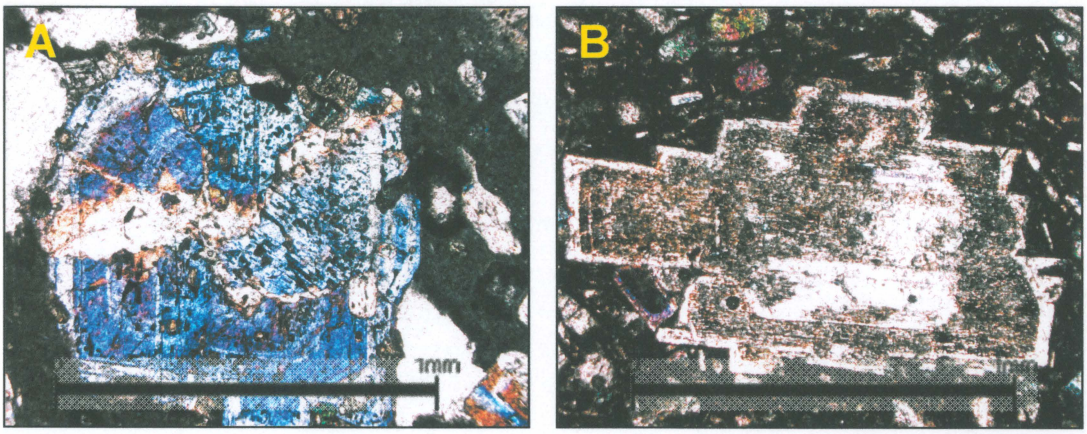

Figure 3.14 – Photomicrographs showing plagioclase zoning in Red Crater lavas. **A** – Andesite from Triple Lobe flow (flow 2). **B** - Basaltic andesite from NE Oturere aa flow (Flow 6).

The second indicator of magma mixing beneath Red Crater is the sieve textures that are seen in the plagioclase phenocrysts. These sieve textures are more prolific in the basaltic andesites than in the andesites (Hobden, 1997), and can be seen in Figure 3.15.

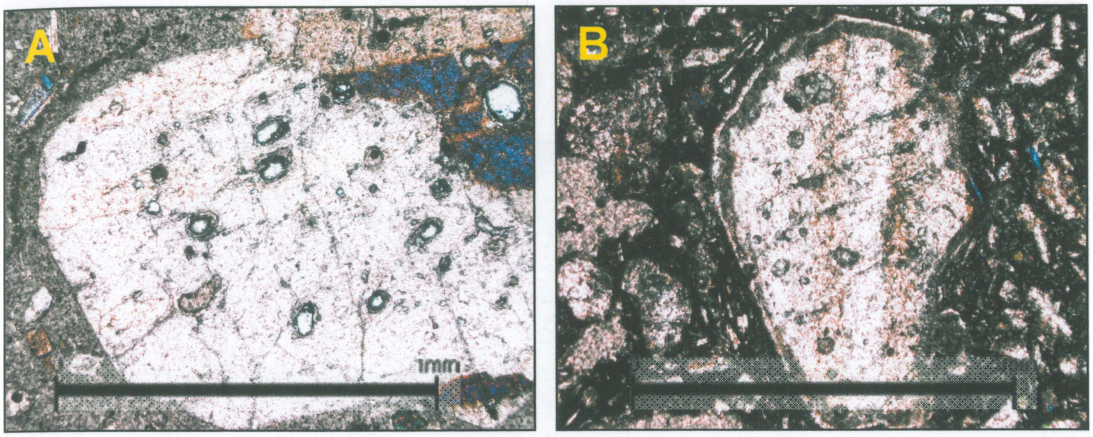

Figure 3.15 – Sieve textures seen in plagioclase phenocrysts within Red Crater lavas. **A** – Andesite from mini Oturere flow (Flow 5). **B** - Basaltic andesite from SE Oturere aa flow (Flow 8).

3.2 GRAIN SIZE

3.2.1 INTRODUCTION AND RESULTS

Determining the grain size parameters of a unit are often a good way of defining differences between units and quantifying changes in eruption dynamics. Within the Red Crater scoria deposits, vesicularities and colour changes were used to determine the stratigraphic intervals, with grain size parameters confirming these units where possible. Due to the generally large grain sizes seen at Red Crater, the only way to gain an accurate grain size analysis was to hand sieve in the field. The logistics of getting the sieving equipment two hours by foot to the top of Red Crater meant that 90% of the samples selected were of a size (< -5 phi) which allowed an A4 bag full to be carried out for laboratory sieving. The second reason for not undertaking grain size analysis on all the units was the large amount of each unit that would have to be destroyed in order to gain a representative sample of each unit. In total 11 samples were collected for laboratory sampling, using sieves from -5 phi down to 4 phi. Each size fraction was weighed and a cumulative total and percentage was calculated. Exponential frequency curves for each sample were drawn, with the percentiles from these curves being used to calculate the mean size, sorting, skewness and kurtosis. Full grain size results can be seen in Appendix 6.

Table 3.2 shows this summary data for each sample, while Figure 3.1 shows the grain size curve for the Eastern inner-wall and Southern crater rim sections, estimated from photos taken in the field. As was expected, given the fragile nature of scoria, all units were either poorly or very poorly sorted. The grain size parameters calculated were best used to show the difference between the southern and eastern crater walls. Figure 3.16 shows a scatter plot of sorting verses mean grain size.

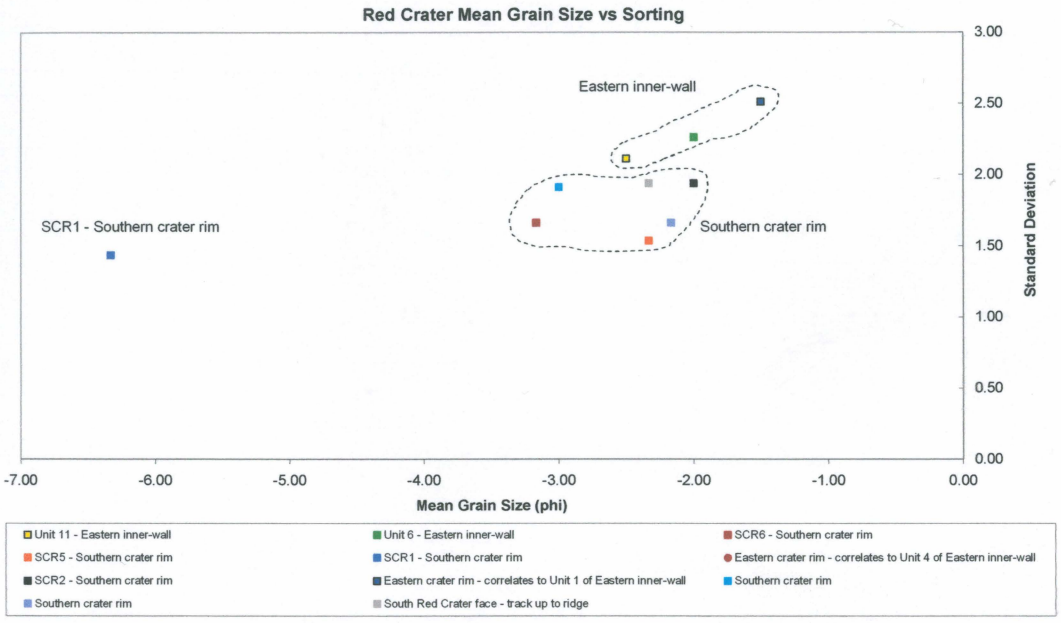

Figure 3.16 – Scatter plot of mean grain size versus sorting, showing the two groupings of Southern and Eastern crater walls.

It should be remembered at this stage that these data are only for units with grain sizes less than -5 phi. As can be seen in this figure, the southern and eastern walls can be divided into two clear groups, indicating the two depositional periods that occurred during the construction of the scoria cone, as was described earlier in the vesicularities section. The only unit which does not fall into one of these groups is SCR8 of the Southern crater wall section. This unit was the only one to be sieved in the field and hence was the only one with grain sizes greater than -5 phi to be sampled.

Sample	Location	Mean Size	Sorting	Skewness	Kurtosis	Description
100/13	Unit 1 - Eastern inner-wall	-2.50	2.11	0.44	1.07	Very poorly sorted, very poorly skewed and mesokurtic
100/5	Unit 6 - Eastern inner-wall	-2.00	2.26	0.33	1.02	Very poorly sorted, very poorly skewed and mesokurtic
67/2	SCR3 - Southern crater rim	-3.17	1.66	0.42	1.23	Poorly sorted, very poorly skewed and leptokurtic
67/1	SCR4 - Southern crater rim	-2.33	1.53	0.27	1.23	Poorly sorted, poorly skewed and leptokurtic
58/1b	SCR8 - Southern crater rim	-6.33	1.43	-0.11	0.61	Poorly sorted, negative skewed and very platykurtic
35/2	Eastern crater rim - ECR-a4	-2.17	1.66	0.33	1.23	Poorly sorted, very poorly skewed and leptokurtic
33/4	SCR7 - Southern crater rim	-2.00	1.94	0.36	1.43	Poorly sorted, very positively skewed and leptokurtic
20/1	Eastern crater rim - ECR-a1	-1.50	2.51	0.24	0.88	Very poorly sorted, positive skewed and platykurtic
18/4	Southern crater rim	-3.00	1.91	0.17	0.82	Poorly sorted, positive skewed and platykurtic
18/3	Southern crater rim	-2.17	1.66	0.33	1.23	Poorly sorted, very positively skewed and leptokurtic
18/1	South Red Crater face - track up to ridge	-2.33	1.94	0.21	1.43	Poorly sorted, positive skewed and leptokurtic

Table 3.2 – Grain size summary statistics for selected scoria sample from Red Crater.

3.3 HAND SPECIMANS

3.3.1 GREY, ANDESITIC, BLOCKY LAVA FLOWS

These lava flows represent the first phase of eruptive activity at Red Crater. Flows 1, 2, 3, 4 and 5 into Oturere Valley occurred as a result of the effusive activity which followed the initial phreatic eruption which heralded the intrusion of the dike into the eastern crater wall. In hand specimen these lavas are light grey in colour, with a ratio of 70:30 of mafic to felsic minerals and an overall crystallinity of approximately 85%. Plagioclase crystals up to 4mm in diameter can be seen with the naked eye, with the occasional olivine crystal of similar size also being visible. Lavas are medium grained, with irregular shaped vesicles displaying very minor coalescence and only 10% vesicularity as a whole. Figure 3.17 shows a photo of this lava as a hand specimen.

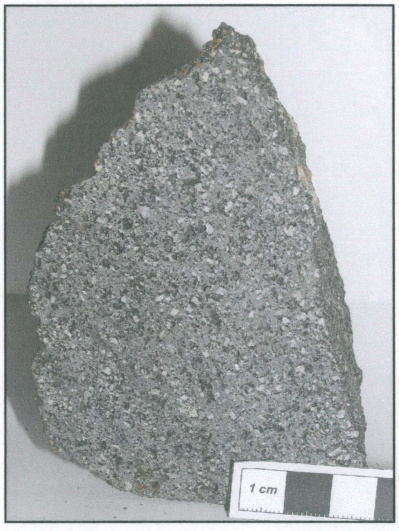

Figure 3.17 – Grey, andesitic, blocky lava flow hand speciman

In thin section these lavas have an intergranular groundmass dominated by plagioclase laths. Phenocrysts of Plagioclase dominate overall, with maximum sizes of 3.75mm. Augite, olivine and hypersthene are also common and occur in order of abundance as just listed. Figure 3.18 shows a photomicrograph of a Red Crater andesite lava flow.

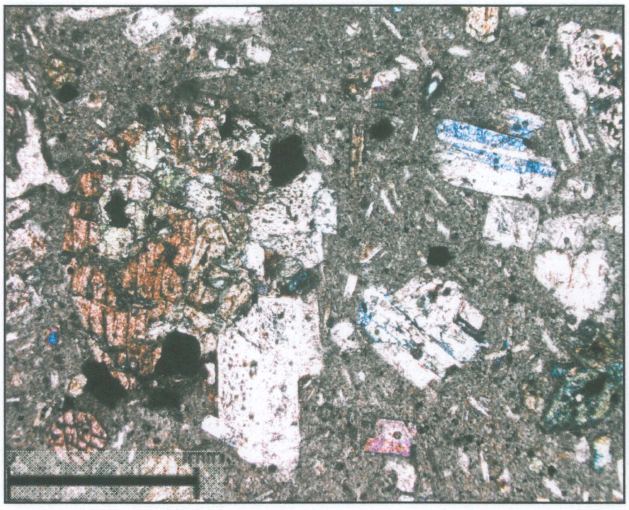

Figure 3.18 – Photomicrograph of grey, andesitic, blocky lava flow.

3.3.2 BLACK, HIGHLY VESICULAR, BASALTIC ANDESITE AA LAVA FLOWS

The second and third eruptive phases of Red Crater are dominated by the main period of scoria cone construction as well as emplacement of lava flows 6, 7, 8, 9, 10 and 11 into NE and SE Oturere Valley, South Crater and Central Crater. These lava flows are dark grey to black in colour as the hand specimen in Figure 3.19 shows.

Figure 3.19 – Black, highly vesicular, basaltic andesite aa lava flow.

Lavas are porphyritic in nature with a mafic to felsic mineral ratio of 80:20. The proportion of crystals is only 30% in these lavas due to the vesicularity being around 75%. Plagioclase crystals once again stand out in the hand specimen, with sizes ranging from 0.5mm to 7mm, occasional olivine crystals up to 7mm are also seen, and are more prolific in these lavas than in the andesite flows.

Lava is medium grained with sub rounded to elongate vesicles indicating that coalescence is occurring. The largest vesicles are up to 4 x 7 mm and dominate over the smaller 1 mm sized vesicles. This gives a snapshot as to the highly vesicular nature of the magma as it was erupting. In thin section these lavas have a fine-grained, intergranular groundmass, dominated by plagioclase laths but also containing blebs of plagioclase, olivine and augite. Hence as with the andesitic lavas of Red Crater, these lavas are dominated by a microlite matrix. While plagioclase is still the most prolific phenocryst (with maximum lengths of 1.5mm), augite and olivine are both only half as dominant as plagioclase. The percentage of vesicles seen in the section is almost equal with the percentage of plagioclase. Figure 3.20 shows a photomicrograph of these lavas.

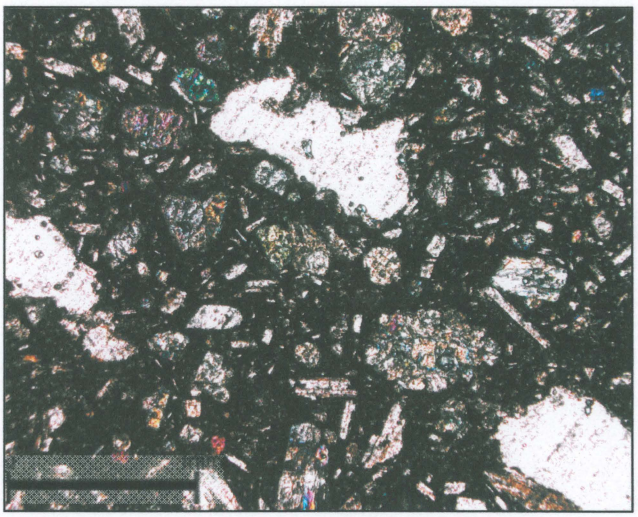

Figure 3.20 – Photomicrograph of black, highly vesicular, basaltic andesite aa lava flows.

3.4 COMPONENTRY

3.4.1 WALL ROCK LITHICS

Within the scoria deposits of the eastern and southern crater walls, a variety of wall rock lithics have been identified, both as discrete clasts and as inclusions. The first example can be seen in Figure 3.21.

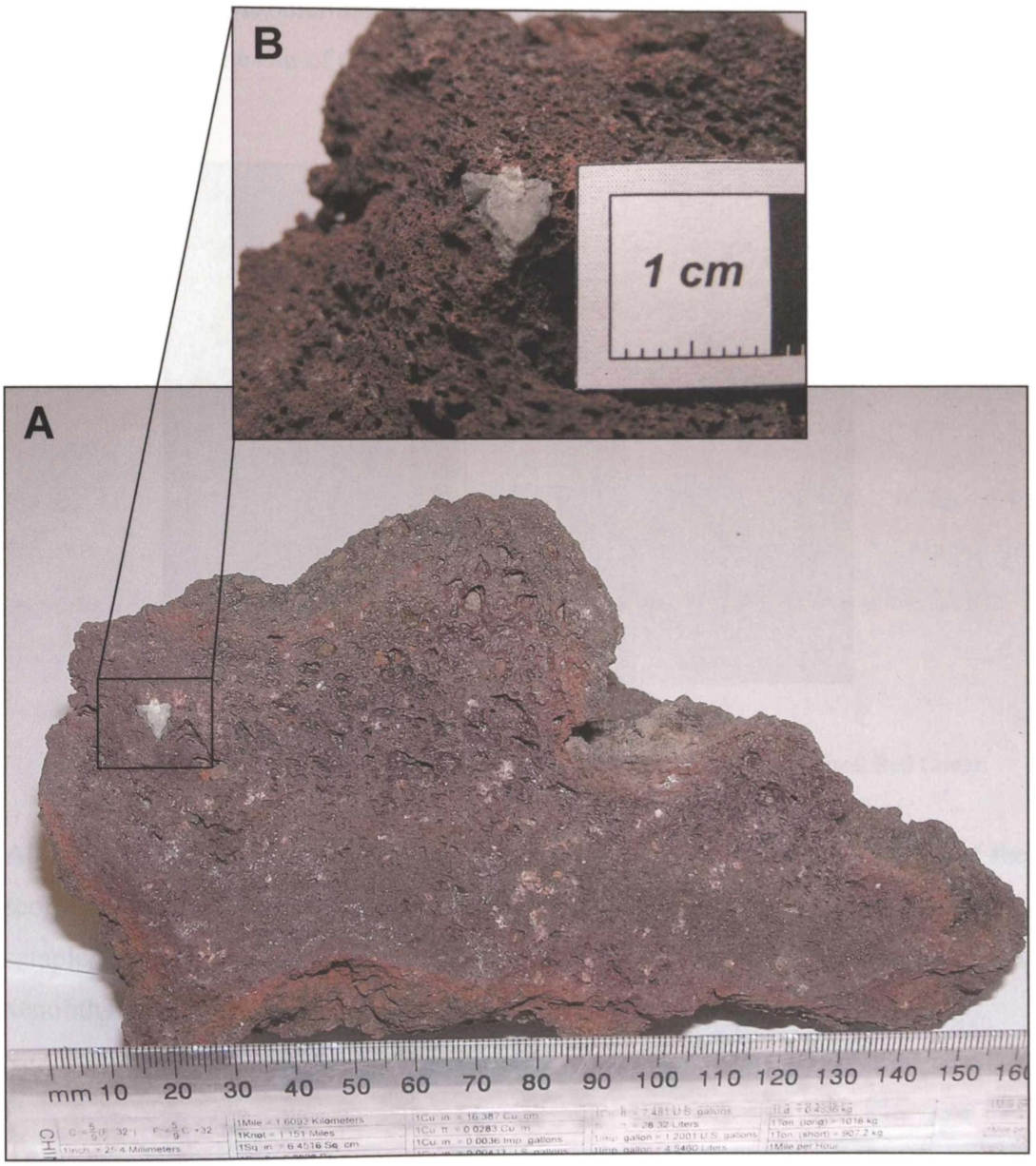

Figure 3.21 – **A** – Metasedimentary xenolith inclusion within scoria clast. **B** – Close up of A.

This sample is a dark red basaltic scoria clast with approximately 70% vesicularity, collected from the centre of the crater as a loose block. Within this scoria clast is a 6 x 5mm lithic, green in colour and bearing no resemblance to any rock seen within the Red Crater area. This is a basement metasedimentary greywacke xenolith, originating from deep (~10 – 15km) within the mantle, which was floating in the magma as it rose to the. Figure 3.22 shows a photo of the lithics sampled from the base of the submarine outcrop on the southern rim of the crater, and also a lithic of similar composition but hydrothermally altered, which was collected from the highest point of Red Crater on the rim of the western crater wall.

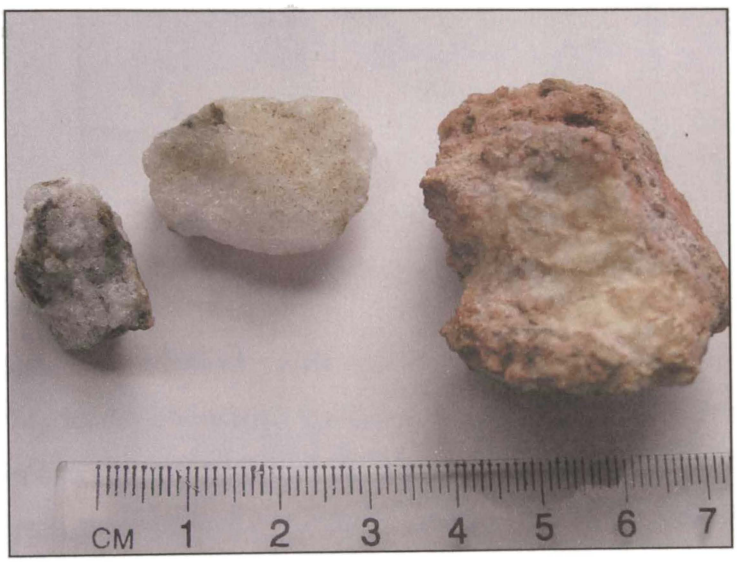

Figure 3.22 – Quartz xenoliths sampled from the southern and western crater rims, Red Crater.

All three lithics are quartz, with the darker patches on them being remnants of the scoria clasts they were originally erupted with. These are unlikely to have been sampled from the andesitic volcanic edifice and probably represent remnant basement xenoliths incorporated into the magma deep (~10 – 15 km) in the mantle.

3.4.2 PUMICE INCLUSIONS

The black scoria deposits around the submarine outcrop on the southern rim of the crater include scoria clasts with large pumice inclusions. Figure 3.23 below shows a photo of the two largest pumice lithics discovered, these were loose clasts lying at the base of the submarine outcrop.

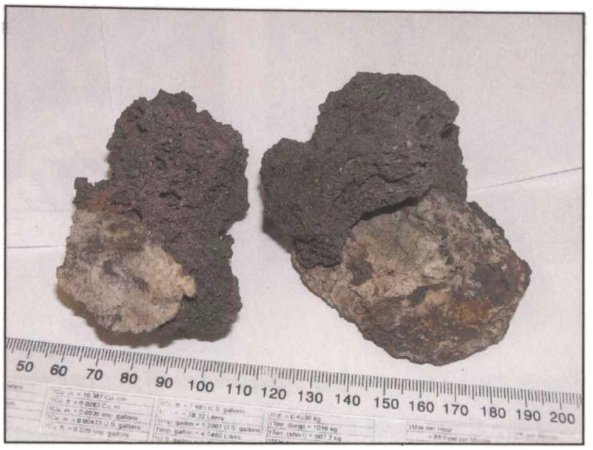

Figure 3.23 – Pumice lithic inclusions in black scoria clasts.

Both are inclusions within black scoria and measure 70 x 40 mm (largest of the two). Topping (1974) identified pumice from the 1.85 ka Taupo eruption on top of the andesite flows from Red Crater, so the presence of this pumice as an inclusion in the youngest erupted units from Red Crater confirms that the scoria cone was indeed constructed post-Taupo. Pumice is both re-melted and re-vesiculated, and was identified as Taupo pumice due to a lack of any other pumice in the Red Crater vicinity. These pumice clasts have being brought up from a shallow depth (~ 60 m) in the conduit compared to the quartz xenoliths lithics which would have traveled from greater depths (~ 10-15 km).

3.4.3 REWORKED LITHIC

A large, extremely altered scoria clast was sampled from Unit 1, of the Eastern inner-wall section. As Figure 3.24 shows, this clast measures 12 x 15 cm and is a mustard, brown colour. This has been interpreted to be an original piece of scoria (from earlier

initial strombolian eruptions) which has being blown out of the dike, undergone intense hydrothermal alteration due to its close proximity to the dike.

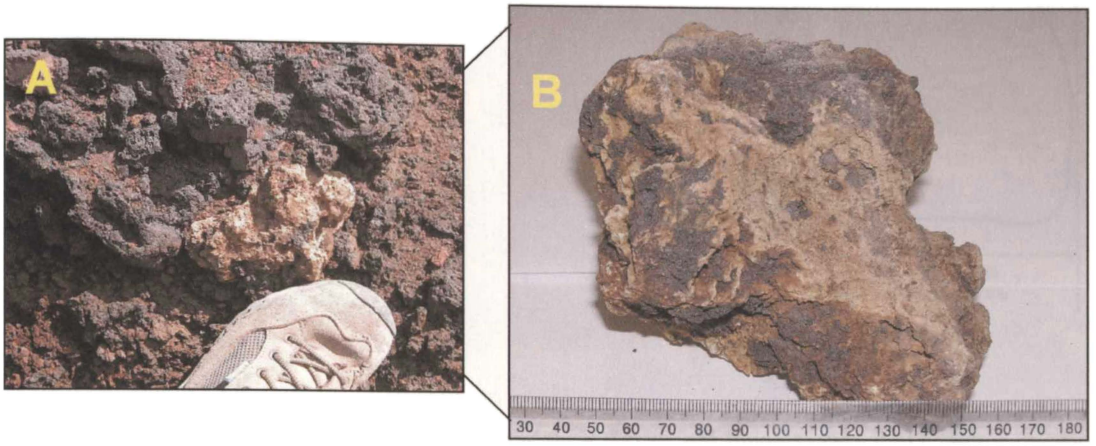

Figure 3.24 – **A** - Re-worked and hydrothermally altered scoria clast, sampled from Unit 1 Eastern inner-wall section. **B** – Close up of scoria clast.

It has then fallen back into the dike to be reworked and blown out again shortly after and deposited in Unit 1. When erupted for the second time, this scoria clast was mixed with fresh, black scoria, which is how reworking was determined (Houghton and Smith, 1993).

3.4.3 ANDESITIC LITHIC BLOCKS

There are numerous lithic blocks located around the rims of Red Crater and the Emerald Lakes. The blocks on the eastern wall rim have dimensions of 2.35 m x 2.19 m x 1.32 m, while those around the emerald lakes have varying sizes but mostly in the range of 1.9 m diameters. Figure 3.25 gives an illustration of the sizes and shapes of some of these ballistic blocks.

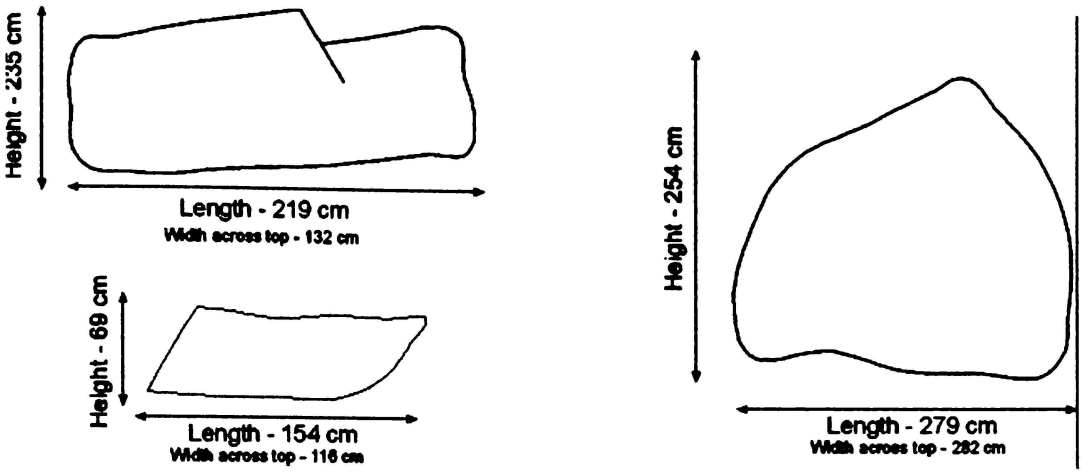

Figure 3.25 – Various ballistic blocks and their dimensions found around Red Crater.

In hand specimen (Figure 3.26) these blocks are light grey, are dense, medium grained and crystal rich (60%). Crystals visible to the naked eye are mostly plagioclase (up to 3mm), plus very rare olivine.

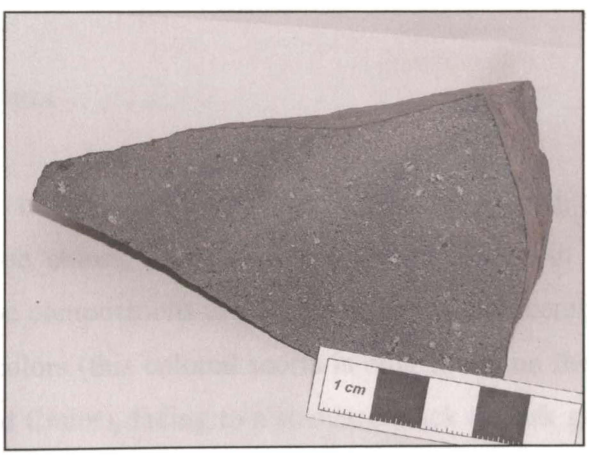

Figure 3.26 – Hand specimen of andesitic ballistic blocks.

In thin section, groundmasses are typically fine-grained and intersertial with plagioclase dominant over hypersthene, olivine and augite (Figure 3.27).

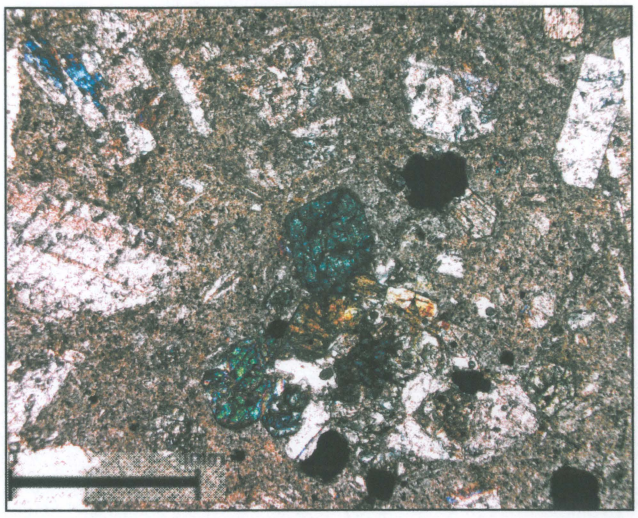

Figure 3.27 – Photomicrograph of andesitic ballistic block.

These blocks are interpreted as shallow wallrock lithics from older (65 – 110 ka) Tongariro Trig andesite lavas that outcrop beneath the scoria cone (Hobden et al., 1996). These blocks were ejected as ballistic blocks during the late stage phreatic eruptions which created the explosion pits and quarried out the centre of the scoria cone.

3.4.5 SCORIA

The scoria deposits of Red Crater are found in three colors, red, black and black with bright peacock blue colors. All three variations are seen in Figure 3.28. While different colors, the compositions are all the same. Most recently erupted scoria has the peacock blue colors (this colored scoria is only found on the southern and south eastern rims of Red Crater), fading to a standard black to dark grey over time. When steam percolates up through the scoria deposits, it causes the iron in the scoria to oxidize, resulting in the deep red colour seen (Francis, 1993). Given both the phreatic steam eruptions known to have created Red Crater, and the very active hydrothermal steaming ground around it, there is plenty of steam around to cause this oxidation. Due to their high vesicularity of 70% or above (in most cases), the proportion of crystals is only approximately 15%. Clasts are medium grained, with sub rounded

vesicles up to 15 x 7 mm. Vesicles this size are the result of coalescence which has occurred in all clasts. The larger scoria clasts are referred to as bombs and discussed

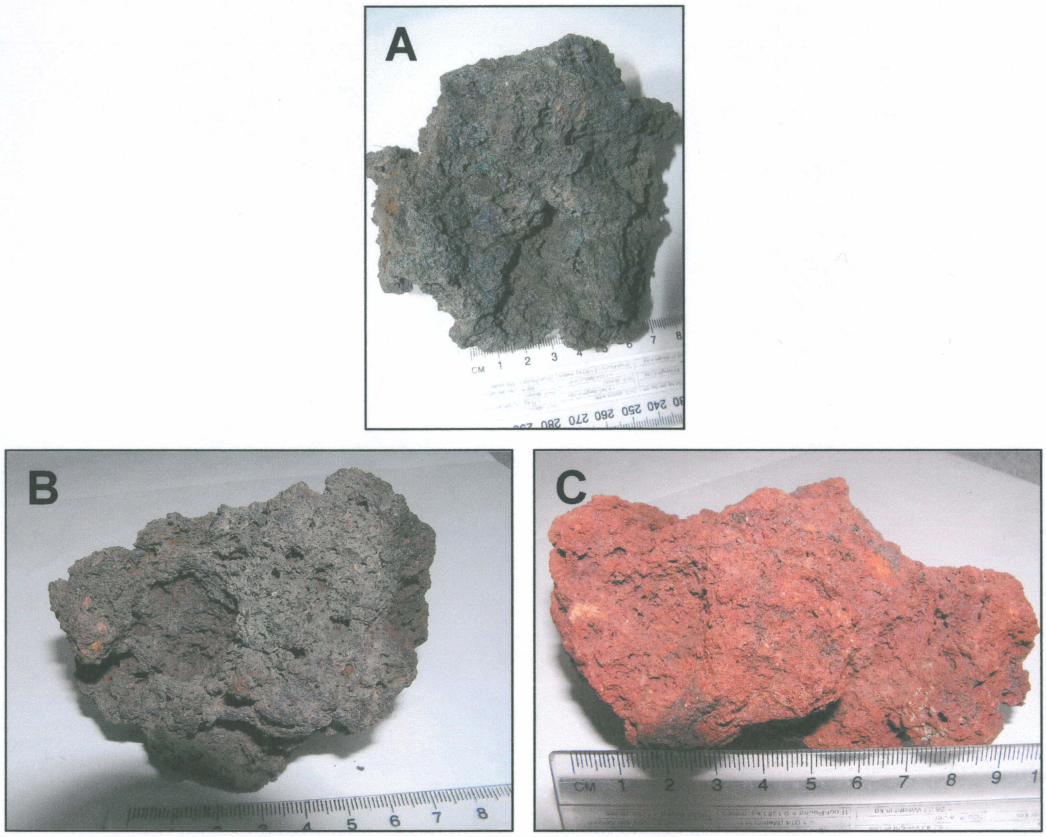

Figure 3.28 – Three variations of Red Crater scoria deposits. **A** – Peacock blue (Eastern Crater Rim). **B** – Black (Unit 11 Eastern inner-wall). **C** – Red (Unit 3 Eastern inner-wall section).

in Chapter Four. Figure 3.29 shows a photomicrograph of a scoria clast from Red Crater. In thin section, vesicles dominant over the groundmass at 45.8%, while the microlite matrix matrix accounts for 22.6%. Plagioclase is the most prolific phenocryst at 12.8%, with olivine, augite, and hypersthene also featuring.

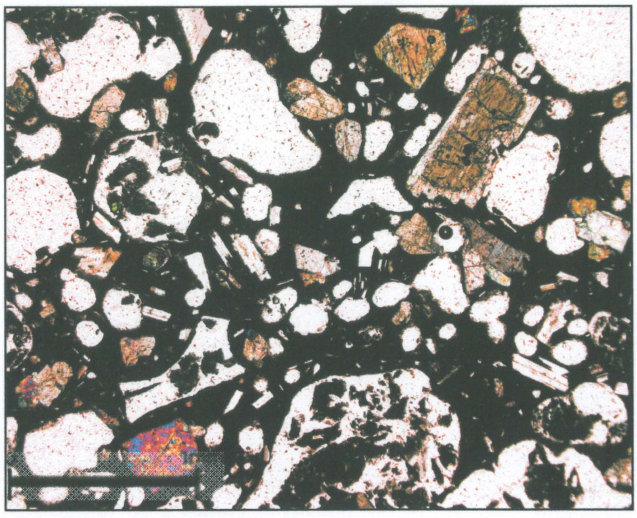

Figure 3.29 – Photomicrograph of Red Crater scoria clast.

3.4.6 AGGLUTINATED SCORIA

Within the collapsed portion of the north eastern wall of Red Crater, is an extremely compacted and dense horizon which is shown in a series of close-ups in Figure 2.10 This is thought to be a horizon of agglutinated scoria which forms when clasts greater than 1 cm and with viscosities lower than 1000 Pa s are erupted, coalescing and deforming upon deposition (Cas and Wright, 1987; Wolff and Sumner, 2000). The inner fountain of a strombolian fire fountain (as described in Chapter Five – Eruptive Processes), produces these low viscosity, larger clasts (Wolff and Sumner, 2000). This agglutinated scoria unit dips towards the north, and is part of the outer crater wall facies. It is possible that this vent is a rampart down which the basaltic andesite aa lava flows in NE Oturere Valley originated from. Columnar joints often occur at 90° to the deposition surface, while the contact between the agglutinated and non-agglutinated scoria is ragged as the photos in Figure 2.10 show (Cas and Wright, 1987).

CHAPTER FOUR

ERUPTIVE PROCESSES

4.0 INTRODUCTION

Over its short lifetime, Red Crater has displayed a wide range of eruptive magnitudes and processes which make it unique compared with the other active and older vents on the Tongariro cone complex. These unique features include:

- Produced the single largest lava flow on the Tongariro cone complex.
- During the first ~ 8 ka of its lifetime, Red Crater erupted five large andesitic lava flows, without any construction of the cone occurring.
- Flows 9 and 10 into Central Crater have the most mafic compositions of all lava flows erupted from the Tongariro vent systems.
- This vent system has produced the single largest scoria cone deposit of all Tongariro vent systems.
- Red Crater provides the best exposed example on Tongariro of a dike feeder structure.

The nature of strombolian activity will be a major part of this chapter, and will also include case studies on two similar systems, the first being Italy's Mt Etna, and the second, Mexico's Paricutin. Phreatic activity, different bomb types, magma dikes, magma rise rates and lava flow morphology will also be fully discussed within this chapter.

4.1 ERUPTION PROCESSES

4.1.1 STROMBOLIAN ACTIVITY

Strombolian eruptions are characterized as 'dry' magmatic eruptions, meaning that little or no water interaction is involved, with the eruption drawing its energy from the high gas fluxes and expansion within the basaltic to basaltic andesite magma (Cas and Wright, 1987; Parfitt and Wilson, 1995; Vergniolle and Mangan, 2000). Along with Hawaiian eruptions they are the least explosive (Figure 4.1) which is a direct consequence of the low viscosity magmas involved (Vergniolle and Mangan, 2000).

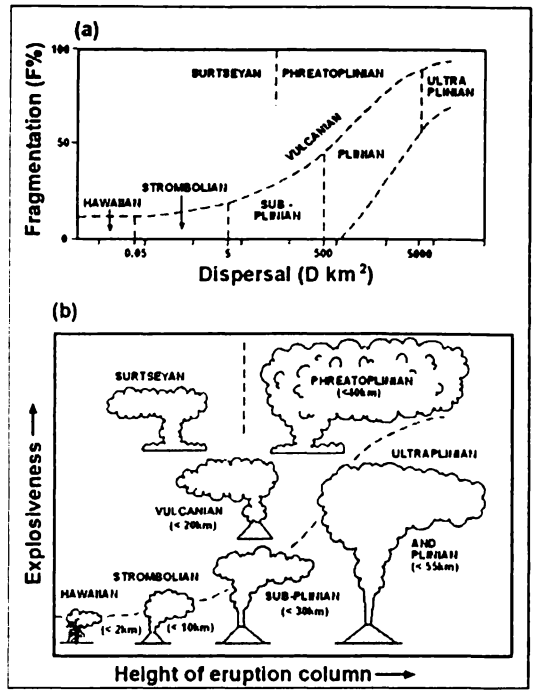

Figure 4.1 – Eruption Styles and Sizes (Cas and Wright, 1987).

Both styles of eruptions produce fire fountains (more commonly found in Hawaiian style eruptions) and in the case of strombolian eruptions, smaller scale bursts or discrete gas explosions (Cas and Wright, 1987; Jaupart and Vergniolle, 1988; Parfitt and Wilson, 1995; Vergniolle and Brandeis, 1996). In regards to eruption dispersal and fragmentation, strombolian eruptions are cone-forming and produce coarse grained deposits of vesicular juvenile material (Cas and Wright, 1987). The low water to magma ratios in strombolian eruptions is illustrated in Figure 4.2, which shows the overlapping nature of Hawaiian and strombolian eruption style (Vespermann and Schmincke, 2000).

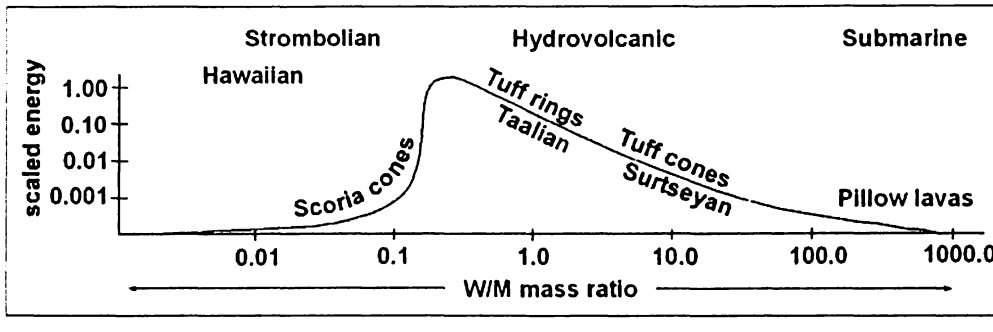

Figure 4.2 – Strombolian eruptions are described as 'dry' magmatic eruptions, with low water : magma rations as this figure shows (Vespermann and Schmincke, 2000).

Coarse clasts, lack of or minor bedding and high depositional temperatures further define the nature of 'dry' magmatic eruptions (Vespermann and Schmincke, 2000).

The gas rise rate in strombolian eruptions, relative to magma column ascent, is higher than in Hawaiian eruptions. The gas streams up through the magma column at a faster rate than the magma itself, coalescing with smaller bubbles on the way. By the time all this gas reaches the surface on the magma column, it has coalesced into a 'slug' of gas bubbles, with zones of bubbly magma in between these 'slugs' (Figure 4.3) (Parfitt and Wilson, 1995; Parfitt, 2004; Vergniolle and Brandeis, 1996; Vergniolle and Mangan, 2000). The controlling factor on how these gas bubbles originate in the magma chamber and hence travel through the magma column, either as annular (Hawaiian) or slug (Strombolian) flow, is the viscosity of the magma (Jaupart and Vergniolle, 1988). Within the magma chamber gas bubbles rise from the bottom up to the roof of the chamber, forming a foam layer which collapses and generates pockets of gas (Jaupart and Vergniolle, 1988). In low viscosity magmas such as basalts, a single gas pocket is formed and flows up the conduit as annular flow, generating Hawaiian style fire fountains (Jaupart and Vergniolle, 1988). Basaltic andesite magmas have higher viscosities and hence when the foam layer collapses, many pockets of gas are formed, flowing up the conduit as slugs of gas, generating the discrete gas explosions that define Strombolian style eruptions (Jaupart and Vergniolle, 1988).

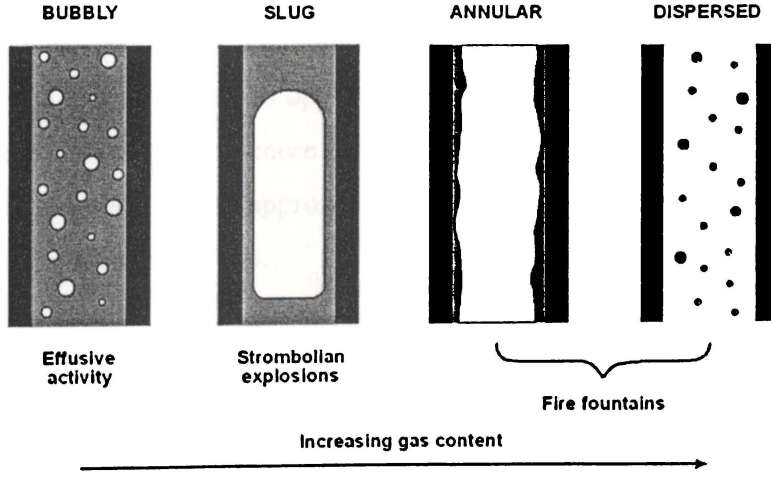

Figure 4.3 – Effect on gas flow within the magma column as the gas content increases (Cas and Wright, 1987; Vergniolle and Mangan, 2000).

When this slug of gas reaches the top of the magma column or lava pond it explodes which, depending on the frequency of these slugs, either leads to fire fountaining (if the frequency of gas slugs is high) or more commonly, discrete gas explosions (Figure 4.4). These discrete gas explosions can send the cooled skin of the top of the magma column or lava pond up to hundreds of metres into the air (Cas and Wright, 1987; Jaupart and Vergniolle, 1988; Parfitt and Wilson, 1995; Vergniolle and Brandeis, 1996). At Stromboli the time between these discrete gas explosions varies from 10 minutes to 1 hour (Parfitt, 2004).

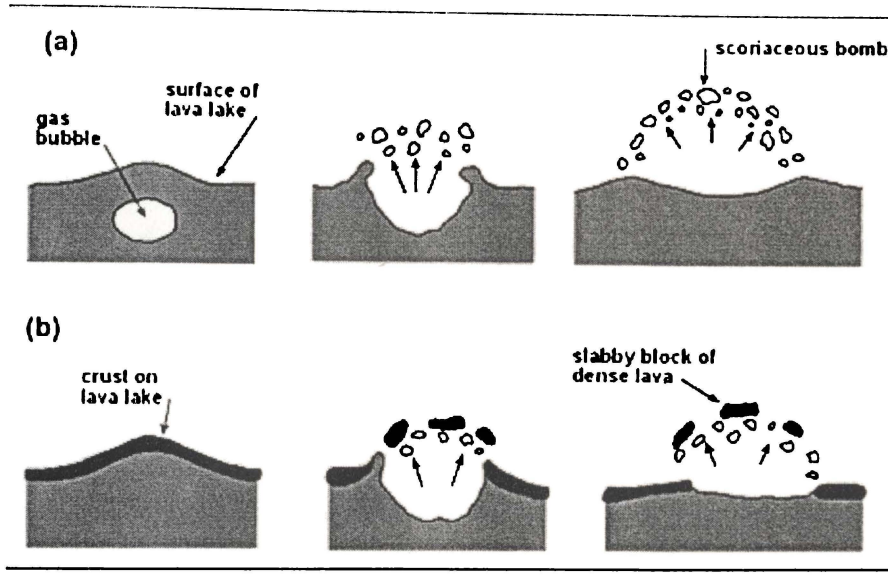

Figure 4.4 – Creation of scoria clasts during discrete gas bursts at the surface of a lava lake (Cas and Wright, 1987).

This high gas flux in strombolian eruptions is a result of the magma and hence the gas being confined to the conduit, as opposed to an open fissure system as in a Hawaiian style eruption where gas can more readily escape (Vergniolle and Mangan, 2000). The gas volume needs to be approximately 70% in order for slug flow to develop (Vergniolle and Mangan, 2000).

Research by Chouet et al. (1999) has provided evidence for the 'slug' model of gas ascension. Broadband seismic experiments used seismometers to pick up the very-long period signals (in the 2 – 50 s band) which strombolian eruptions produce (Chouet et al., 1999). The signals picked up by these seismometers followed the

ascent of a gas slug beneath Stromboli. Pressurisation and dilation of the conduit occurs first as the gas slug enters the conduit and is followed by depressurization and deflation as the gas slug is erupted due to such a large volume of gas and magma been removed from the conduit (Chouet et al., 1999). Injection of fresh magma into the conduit repressurizes the system until the gas builds up and the cycle repeats (Chovet, 1999). The magma residence times in the chamber which feeds the conduits at Stromboli was estimated at ~19 years by Francalanci et al (1999), based on a Sr isotope survey, from a chamber only ~0.3 to 0.04 km^3 in volume.

Vergniolle and Mangan (2000), state that the gas: lava volume ratios in a strombolian eruption are in the range of 10^5:1, with clasts being ejected from the vent at 40 – 100 ms^{-1}, at angles of 45° to 75°, and reaching to 100 metres or higher (Parfitt, 2004). A strombolian eruption often does not begin as a strombolian eruption, instead transitioning into this style from either a Hawaiian style fissure eruption or a Vulcanian style, vent clearing phreatic eruption (Vergniolle and Mangan, 2000).

Parfitt and Wilson (1995), after looking at the transition between Hawaiian and Strombolian activity, concluded that magma rise speed was the most important control on eruption styles, with strombolian magma rising slower, allowing gas to decouple and stream up through it faster. Frequent gas slugs maintain a constant strombolian eruption (Parfitt and Wilson, 1995). If the conduit is inclined, coalescence is encouraged more than if the conduit was vertical, and hence a lower frequency of gas slugs can maintain a strombolian eruption the same size as from a vertical conduit with higher frequencies of gas slugs (James et al., 2003). Houghton et al. (1999) and Parfitt and Wilson (1995) agree that magma rise rate defines the degree of degassing occurring in the magma, and hence that Hawaiian and Strombolian style eruptions can be determined by the magma rise rate.

4.1.1A FIRE FOUNTAINING

Welded and agglutinated scoria layers erupted during a strombolian eruption are the result of a fluctuation to fire fountaining more commonly associated with Hawaiian

style eruptions. Fire fountains in Hawaiian style eruptions are feed by sustained annular to dispersed gas flows (Wolff and Sumner, 2000). Fire fountains can be either high and spreading or high and narrow, depending on their driving force (Wolff and Sumner, 2000). High and spreading is the result of high gas content, while high and narrow results from high effusion rates (Wolff and Sumner, 2000). As Figure 4.5 shows, the structure of a fire fountain has two parts, an inner fountain where clasts are the hottest and take longest to cool, and an outer fountain where more air contact causes more rapid cooling (Wolff and Sumner, 2000).

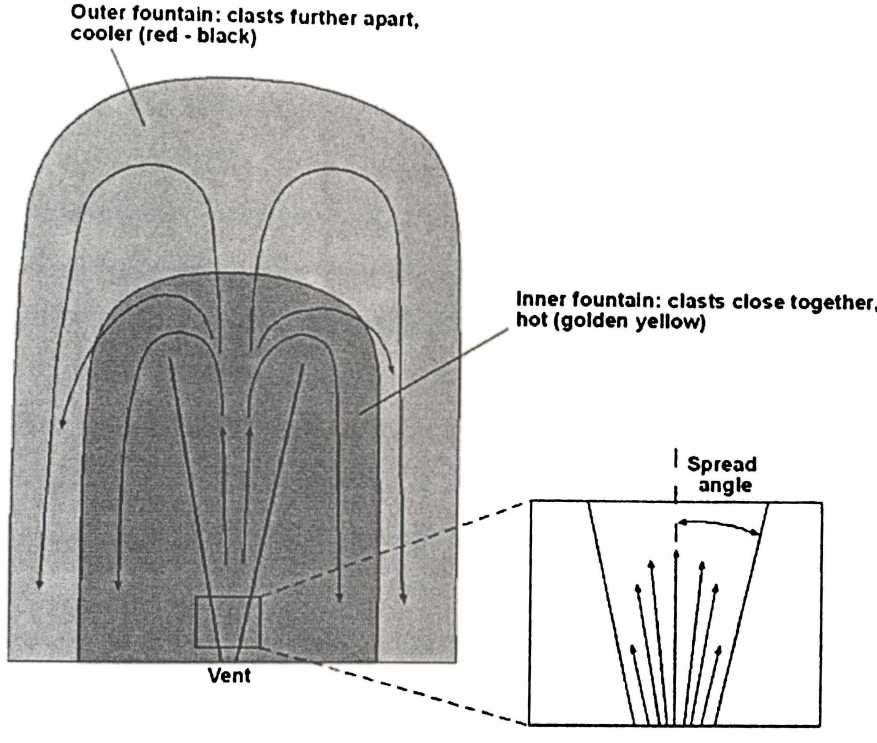

Figure 4.5 – Structure of a fire fountain (Wolff and Sumner, 2000).

The inner fountain remains very hot (magmatic temperatures of erupting basalt are 1000-1300°C (Spera, 2000)), so material which falls back around the base of the vent is still molten, and hence accumulates in ponds often flowing off as lava flows. Lava flows will only occur if the effusion rate is high enough to sustain them (Wolff and Sumner, 2000). This ponding at the base of a fountain can be erupted through by the next discrete gas explosion or fountain event, mixing in the denser material starting to

cool in the lava pond, with new highly vesicular scoria (Vespermann and Schmincke, 2000).

The cooler outer fountain is where the agglutinated scoria deposits have fallen from (Wolff and Sumner, 2000). Vergniolle (1996), determined that in Hawaiian style eruptions, fire fountaining stops when all the large bubble from the base of the magma chamber have risen to the top, leaving only small bubbles that cannot sustain the fountain. With strombolian fire fountains, a high frequency of gas slugs must occur in order to sustain the fire fountain (Vergniolle and Mangan, 2000).

4.1.2 VULCANIAN STYLE VENT CLEARING PHREATIC ERUPTIONS

A vulcanian style eruption can occur as a discrete event, which is what often precedes a strombolian style eruption (Vergniolle and Mangan, 2000). Single vulcanian bursts produce no new juvenile material, exploding out the older vent material which it has erupted through (Francis, 1993). These phreatic explosions are the result of groundwater interacting with a magma body or magmatic heat (MacDonald, 1972). If an intruding dike comes into contact with groundwater, it causes it to flash to steam and create a violent phreatic eruption which opens the pathway for the dike to reach the surface (Harris, 2000; Rittmann, 1962; Williams and McBirney, 1979). Most of the explosiveness of the magma is removed in this initial stage phreatic eruption and effusive activity often follows until enough gas bubbles have coalesced within the magma chamber to form slug flows (Gutmann, 1979). This decline in explosiveness following the initial violent phreatic eruption is possibly due to gas escaping through fractures in the conduit walls created during these eruptions (Jaupart, 1998). Magma withdrawing from the dike could also trigger a violent phreatic eruption, as groundwater enters the drained conduit, flashing to steam (Calvari, 2003).

4.1.3 DIKES

Dikes are the mode by which magma arrives at the surface, and the pathway for shallow transport of magma. Sills on the other hand store magma rather than transport

it, and tend to be horizontal to strata rather than vertical (Marsh, 2000). Dikes propagate out from their source in sheet like, disk shapes, thicker in the center and thinning towards the edges (Hyndman and Alt, 1987; Marsh, 2000).

Experiments carried out by McLeod and Tait (1999) and Hyndman and Alt (1987), have shown with gelatin models, how a dike initially forms from a magma chamber. Increasing pressure due to either the build up of gas or the injection of new magma into the a magma chamber, causes the magma to fill any cracks or fractures (zones of weakness) in the walls of the magma chamber, and continued pressure allows the new dike to propagate towards the earths surface (Carrigan, 2000; McLeod and Tait, 1999). McLeod and Tait (1999) also concluded that higher viscosity magmas are associated with longer times (years) for dike nucleation, whereas with low viscosity basaltic magmas, dike nucleation occurs only hours to days after the injection of new magma into the magma chamber.

Tibaldi (2003) showed at Stromboli that dike orientations are influenced by the cone morphology. The dikes exposed at Stromboli mostly dip outwards, away from the current summit cone and at the same dip as the original cone slope (Tibaldi, 2003). Outward dipping dikes are usually described as ring dikes and are associated with caldera collapse, which is not seen at Stromboli. Tibaldi (2003) proposed that these outward dipping dikes have followed the path of least resistance, which at Stromboli is along old cone surfaces, allowing them to intrude to the surface unimpeded (Tibaldi, 2003). An example at Stromboli was of a dike which curved at its end to the west, mimicking the orientation of the paleo valley it was intruded into (Tibaldi, 2003).

4.2 Eruptive Products

4.2.1 Scoria Cones

Scoria cones are constructed of, as the name suggests, scoria which is an eruptive product of a strombolian eruption. Vast amounts of gas pulse up through the magma

column as discrete gas bursts, exploding out as scoria clasts. The most common compositional range for scoria is basaltic to basaltic andesite (Vespermann and Schmincke, 2000; Williams and McBirney, 1979). Eruptive products of strombolian eruptions include agglutinated or welded beds, vesicular lava bombs and scoracious lapilli (scoria), all of which combine to construct a scoria cone (Calvari, 2003; Vespermann and Schmincke, 2000). While spatter bombs are more common in Hawaiian eruptions, because the two eruptive styles are transitional to each other, spatter bombs are also present to a lesser degree in scoria cones constructed by strombolian eruptions (Vergniolle and Mangan, 2000; Vespermann and Schmincke, 2000). Figure 4.6 shows a cartoon diagram of an idealised cross-section through a scoria cone, highlighting the inner crater facies and the outer wall facies, the two parts of a scoria cone (Vespermann and Schmincke, 2000).

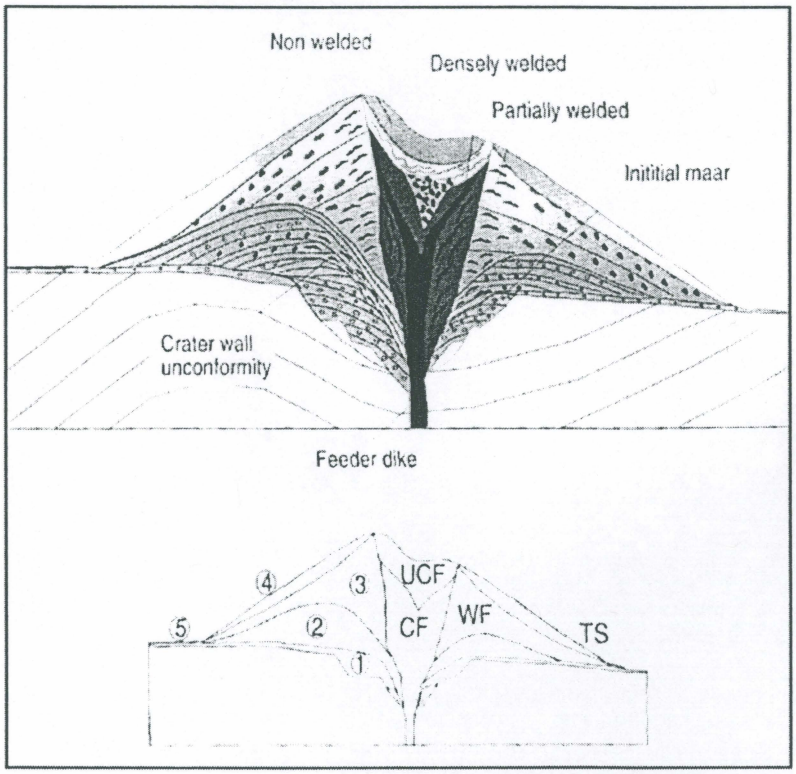

Figure 4.6 – Cross section through an idealized scoria cone showing slopes and depositional nature of units within it. Unit 1 represents initial phreatic or phreatomagmatic deposits, while 2 and 3 are the main strombolian cone building facies. 4 represents the talus or scree slide and 5 is the extent of distal fallout. CF – crater facies (agglutinates, feeder dike). UCF – upper crater facies (bombs within lapilli matrix, re-deposition from slumping). WF – wall facies (scoria breccias, bombs). TS – talus slope (re-deposition due to slope failure).

The crater facies (CF) in the centre of this illustration are dominantly heterogeneous (Vespermann and Schmincke, 2000) when compared to the wall facies (WF). Agglutinated or welded scoria fall units often occur in the lower section of the cone, transitioning into non-welded scoria units (Vespermann and Schmincke, 2000). Scoria and lava bombs deposited close to the vent are coarser and moderately welded, while more distal deposits tend to be finer grained and less compacted and non-welded (Vespermann and Schmincke, 2000).

4.2.1A Cone Construction Rates

According to Vespermann et al (2000), and Francis (1993), scoria cone construction ended in less than 30 days in 50% of the worlds observed scoria cone eruptions. Mount Nuovo in Italy is a fast-building scoria cone, growing to a height of 130 metres in only two days during 1538 (Ollier, 1988)., while Paricutin Volcano in Mexico, grew to a height of 40 metres in only 24 hours (Vespermann and Schmincke, 2000). The slope angle of young scoria cones is approximately 33°, which is the maximum angle loose scoria clasts can rest at without rolling down the slope (Fisher et al., 1997; Francis, 1993). The scoria cones of Pinacate volcanic field in Mexico have slope angles of 26° – 29° (Gutmann, 1979), and basal diameters ranging from 0.25 to 2.5 km (Vespermann and Schmincke, 2000).

4.2.2 Scoria deposits, agglutinated scoria beds and lava bombs

Scoria and lava bombs are two types of strombolian eruptive products. Scoria is formed by rapid quenching during flight of magma blobs erupted in a discrete gas explosion. These clasts, due to their high vesicularities often break on impact with the ground which exposes their fragile nature. This is the most common eruptive product of a strombolian eruption (Vergniolle and Mangan, 2000). Agglutinated scoria beds occur when clasts are still hot on landing, welding together to form an agglutinated bed (Vespermann and Schmincke, 2000). Agglutinated scoria forms when clasts greater than 1 cm and with viscosities lower than 1000 Pa s are erupted, coalescing and deforming upon deposition (Cas and Wright, 1987; Wolff and Sumner, 2000).

The inner fountain of a strombolian discrete gas explosion or fire fountain produces these low viscosity, larger clasts (Wolff and Sumner, 2000).

Spatter bombs are larger than scoria clasts, often greater than 15cm in diameter. Unlike scoria clasts which are fully quenched in flight due to their smaller size, spatter bombs still have a molten interior upon impact as only the outer rim of the clast has being quenched during flight (Vergniolle and Mangan, 2000). Hence upon landing, the clast flattens into whatever shape the underlying topography takes. Usually this underlying topography is one or many scoria clasts, which gives these bombs either a cowpat or buckled iron type texture (MacDonald, 1972). The interior of a spatter bomb is denser than a scoria clast with many fine vesicles, rather than the large vesicles which are uniform throughout an entire scoria clast (Vergniolle and Mangan, 2000). In a spatter bomb the larger vesicles are concentrated in the outer rim. Spindal bombs have similar densities to the inner core of a spatter bomb. The big difference between a spatter and spindal bomb is that the spindal bomb spins in flight, molding the outside into a spindle like structure as it spins (Francis, 1993).

4.2.3 LAVA FLOW MORPHOLOGIES

There are two types of lava flows erupted from Red Crater. The andesitic blocky flows into Oturere Valley and the basaltic andesite aa flows. This section will describe block and aa flow types, pressure ridges and both low and high aspect ratio flows. The fastest moving lava flows are pahoehoe flows, which are basaltic in composition and often have many flow fronts active at the same time (Kilburn, 2000). Pahoehoe flows evolve into aa flows at higher viscosities. Aa flows are often basaltic andesite, and in turn evolve into blocky lavas which generally range from basaltic andesite to rhyolitic in composition (Kilburn, 2000). The yield strengths of both types of flows increases towards there flow fronts due to been exposed to the air and topography longer (Kilburn and Guest, 1993).

4.2.3A BLOCKY FLOWS

Blocky lava flows have surfaces covered in large angular, broken blocks while there flow centres are dense and coherent (Kilburn, 2000; Linneman and Borgia, 1993). These broken surface blocks can be up to a metre in diameter (Kilburn, 2000). Unlike pahoehoe flow fronts that diverge and break away, the flow front of a blocky flow is constantly crumbling yet still moving as a single unit (Kilburn, 2000). Flow fronts increase in thickness as they advance, with those of great length taking months to be emplaced (Kilburn, 2000). Blocky flows have high aspect ratios and are characterized by thick flows which have high viscosities (compared to aa and pahoehoe flows) and hence take longer periods to be emplaced and are fuelled by continuous effusive activity (Kilburn, 2000). Blocky lava flows can be further divided up into a channel zone and a frontal zone (Linneman and Borgia, 1993). The frontal zone is the flow front of the lava flow which is the furthest point on the flow from the vent and is where the levees shown in Figure 4.7 are constructed (Linneman and Borgia, 1993).

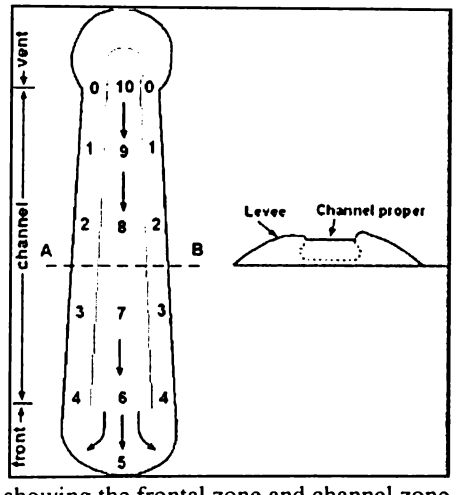

Figure 4.7 – Illustration showing the frontal zone and channel zone of a blocky lava flow, numbers represent age of the lava, 10 been the youngest, 0 been the oldest (Linneman and Borgia, 1993).

Kilburn and Lopes (1991) while researching the patterns of flow field growth in both aa and blocky lavas, deduced that a flow is advanced by the internal lava just behind the flow front. When lava stops flowing into the frontal zone, then the flow stops (Linneman and Borgia, 1993). Within the channel zone, lava flows down the centre

towards the flow front, folding of to each side as it reaches the flow front to form levees which define the boundaries of the channel zone (Linneman and Borgia, 1993).

4.2.3B AA FLOWS

Aa lava flows are commonly basaltic andesite in composition and like blocky flows also develop channel flow, which feeds the flow front (Kilburn, 2000). Aa flows typically have low aspect ratios; that is, they are thin with low viscosities and can be emplaced within hours or days and have flow fronts less than 20 m (Kilburn, 2000). The surfaces of aa flows consist of smaller, more irregular clasts than blocky flows, which are often not welded to the flow and hence makes traversing them difficult. Aa flows can be subdivided further into cauliflower and rubbly textures (Kilburn, 2000; Kilburn and Guest, 1993; Kilburn and Lopes, 1990). The morphological differences between cauliflower and rubbly surfaces is illustrated in Figure 4.8 below. Cauliflower surfaces display irregular protrusions which resemble the heads of cauliflowers (Kilburn and Guest, 1993; Kilburn and Lopes, 1990). These can be up to tens of centimeters in size with dense interiors and grade into the underlying channel lava beneath (Kilburn and Lopes, 1990). Cauliflower protrusions often break off at there stems so the flow surfaces are often loose and fragmented, as illustrated in Figure 4.9 (Kilburn and Guest, 1993).

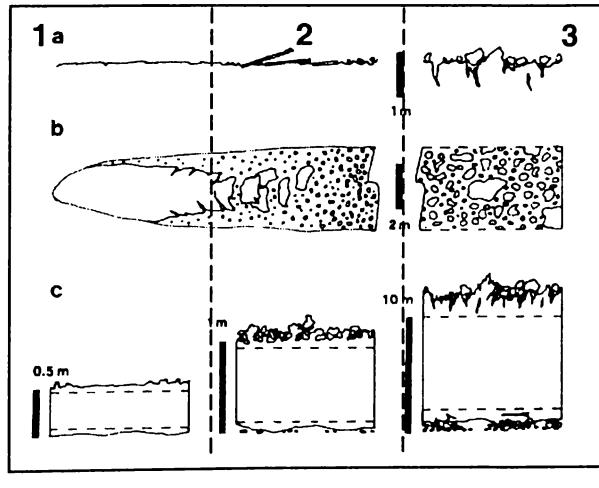

Figure 4.8 – A – Illustration of the transition from cauliflower to rubbly textures in aa lava flows (Kilburn and Guest, 1993). These three profiles (a – longitudinal surface profile, b – plan view, c – transverse profiles) can be divided into three sections. **1** – Slab pahoehoe flow. **2** – Cauliflower aa flow. **3** – Rubbly aa flow.

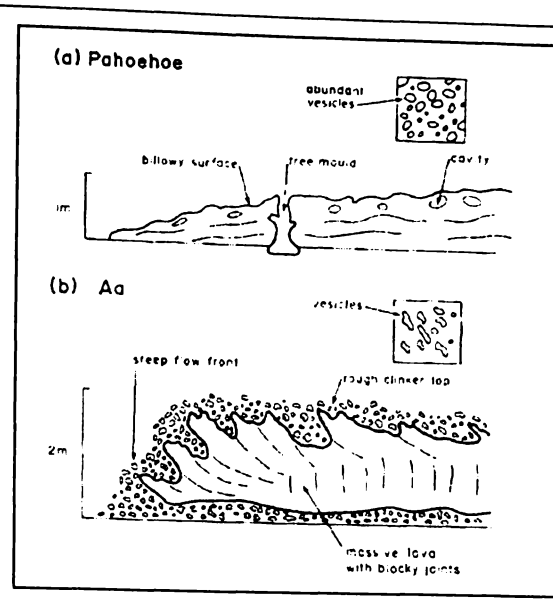

Figure 4.9 –Morphological differences between a pahoehoe and aa lava flow, illustrating the loose cauliflower clasts on the surface of the flow (Cas and Wright, 1987).

Rubbly surfaces are not as irregular as cauliflower surfaces, with debris been subrounded and up to a metre across, with only minor protrusions which look similar to sugar granules (Kilburn, 2000; Kilburn and Guest, 1993). Rubbly surfaces occur closest to the vent, where the channel lava is fractured and irregular, often leading to infilling by the rubbly surface debris (Kilburn and Guest, 1993).

The textural change between cauliflower and rubbly surfaces occurs when the surface of the lava flow is moving slower than the underlying lava due to different cooling rates (Kilburn and Guest, 1993). The faster moving underlying channel lava pulls the cooler crust along with it, while leaving the outer margins attached to the levees, creating deformation in the surface (Kilburn and Guest, 1993).

4.2.3c Pressure Ridges

Lava in the centre or channel of the flow remains hotter than the margins, as the margins are more exposed to the air and topography which increases the cooling rate (Kilburn and Guest, 1993). Due to this, the middle portion of a lava flow travels the fastest. The faster moving lava beneath the cooler surface crust pushes up under this cooler surface, creating pressure ridges. These ridges occur perpendicular to the flow

direction in the centre of the flow, and at ~ 45° at the flow margins (Cas and Wright, 1987).

A study by Cashman et al (1999) on the active lavas at Kilauea concluded that while the system generally produces pahoehoe flows, if the effusion rate is higher, then aa flows will be formed. The higher viscosities due to higher crystallinities, slow the surface of the lava down, allowing cauliflower and rubbly textures to develop (Cashman et al., 1999).

4.3 CASE STUDY I – PARICUTIN, MEXICO.

The eruption of Paricutin Volcano in Mexico is one of the most well documented and well known eruptions in recent times. Paricutin is located within the 1200 km Mexican Volcanic Belt which is part of the Pacific Ring of Fire and is controlled by subduction related volcanism (Luhr, 1993). Frequent earthquakes were recorded in the month leading up to the eruption, with a 30 m fissure opening on the 20th February 1943 (Luhr, 1993). Throughout this day observers recall witnessing the widening of the fissure, eruption plumes above the vent and tongues of flame rising to 800m (Luhr, 1993). By the end of the day the scoria cone was ~ 6 m high (Luhr, 1993). After another 24 hours of periodic strombolian eruptions, Paricutin stood at ~ 50 m and was exploding bombs 500 m above the vent (Luhr, 1993; Vespermann and Schmincke, 2000). During this second day, a lava flow was observed erupting through the east side of the cone at the same time as strombolian eruptions were depositing scoria on the cones flanks (Luhr, 1993). These periodic and violent strombolian eruptions continued until the 4th March, 1952 when all eruptions ceased (Luhr, 1993). Paricutin had grown to 424 m within nine years, with a basal diameter of ~1 km and erupting compositions ranging from basaltic andesite to andesite (Luhr, 1993; Vespermann and Schmincke, 2000).

Paricutin is an excellent example to compare with Red Crater because its history has been so closely watched. The strombolian eruptions which were recorded as reaching heights of 800 m above the vent would have been similar to what occurred during the

initiation of cone building at Red Crater. The thickness of scoria deposited at Paricutin after 48 hours provides a good benchmark to determine the duration of emplacement time of the Red Crater scoria cone.

4.4 Case Study II – Mt Etna, Italy

Etna is the largest volcano in Europe with an area of approximately 500 square miles and can be found at the front of the Apennine-Maghrebian Chain (Aeocella, 2003; Wilcoxson, 1966). Etna is a basaltic volcano, which in the grand scheme of volcanoes means it's not overly hazardous, with lava flows and fire fountains easier to escape than rhyolitic pyroclastic flows. However because volcanic land is so fertile and the hazards appear manageable, its slopes are highly populated which has lead to Etna having one of the highest death tolls to its name as a result of the unexpected, bigger eruptions.

Recent research on Etna includes work on the 2001 eruptions, both on general processes and on flank eruptions from the volcano (Acocella and Neri, 2003; Aeocella, 2003; Behncke and Neri, 2003). While Calvari et al. (2002) estimated effusion rates during the 1999 summit eruptions. This case study is going to focus on the life of a new cinder cone, researched and documented by Calvari and Pinkerton (2003), due to its similarities with Red Crater.

The 'Laghetto' cinder cone as it was termed, is constructed of basaltic scoria to a height of 62 metres in a period of two weeks (Calvari, 2003). Like Red Crater, the cone is asymmetrical, being ~10 metres higher on its eastern side. This asymmetrical nature of scoria cones is common as wind can alter the direction of fire fountaining, favoring increased deposition on one side. The initiation of the 'Laghetto' vent was the result of a phreatomagmatic eruption, caused by magma intruding through rocks with high water contents (Calvari, 2003). At Red Crater, the cone construction began with phreatic eruptions through the existing Tongariro Trig lavas.

Phreatomagmatic eruptions at 'Laghetto' transitioned into magmatic strombolian activity which then constructed the scoria (or cinder) cone (Calvari, 2003). Decreased permeability of the dike walls as a result of magma cooling against them is one of the reasons Calvari and Pinkerton (2003) give for this change in eruption style. Figure 4.10 shows the less permeable inner dike wall, as seen in the exposed drained dike at Red Crater, which would prevent the intrusion of groundwater into the dike. The end of this 2001 eruption was marked by a return to phreatomagmatic activity possibly due to magma withdrawal allowing aquifer water into the dike (Calvari, 2003). This is once again semi-mirrored in the Red Crater construction, with the injection of basaltic magma changing the eruptive style to strombolian. The final stage in Red Craters development was a switch back to phreatic activity which created the NE trending explosion pits. Of particular interest from the 'Laghetto' construction was that the line of fissures and explosion pits thought to have feed the vent(s), was buried by the

Figure 4.10 – Cooling along the dike margin. Red Crater exposed drained dike, eastern inner-wall.

cone itself, leaving little morphological evidence it even existed (Calvari, 2003). This could be the case for Red Crater, with the explosion pits created during the last phreatic eruption infact revealing the underlying fissure which the system was feed by. The dikes intruded into the cone could be linked to this fissure which is in turn linked to a deeper source.

Figure 4.11 shows a cartoon of how this would appear, with the dike at depth to the NE not breeching the surface, while the SW tip is intruded into the main cone. As

magma withdrew from the dike late in Phase Two, the magma in the deeper part of the dike which extends NE-SW interacted with groundwater, causing phreatic steam eruptions.

4.5 RED CRATER INTERPRETED ERUPTIVE PROCESSES

4.5.1 VULCANIAN VENT CLEARING PHREATIC ERUPTIONS AT RED CRATER

Red Crater has being constructed primarily by strombolian eruptions, although fluctuations between this style and hawaiian style eruptions have occurred. An initial phreatic or vulcanian vent clearing eruption erupted up though, and removed a large section of, the Tongariro Trig lavas that the modern cone is constructed upon. Any evidence for this initial phreatic eruption in distal deposits is not seen due to Flow 1 into Oturere Valley burying all evidence for it. A large section of the Tongariro Trig andesites within the scoria cone was removed prior to the cone construction, with this removal been inferred to have occurred before the emplacement of the five andesite flows into Oturere Valley, because there is no evidence of Tongariro Trig andesite ballistic blocks on top of these flows. This initial phreatic eruption was triggered by the intrusion of a dike, which flashed groundwater to steam, blasting a pathway to the surface (Harris, 2000; Williams and McBirney, 1979). Jaupart (1998) links the decline in explosiveness following an initial vent clearing eruption such as this, to gas escaping through cracks in the conduit created during the eruption. The five andesitic lava flows (flows 1, 2, 3, 4 and 5) into Oturere Valley are evidence that effusive activity did indeed follow the initial vent clearing eruption.

Magma withdrawal from the dike late in Red Craters history is likely to have caused the late stage phreatic eruption which created the NE trending explosion pits. As the magma withdrew, the magma within the deeper part of the dike interacted with ground water causing this phreatic eruption. Ballistic blocks and debris from this eruption are scattered around the Emerald Lakes explosion pits and up and around the rims of the scoria cone. The upper grey clay layer identified in the distal sections

described in chapter two, is likely to be derived from hydrothermal deposits erupted out of the Emerald Lakes explosion pits during this late stage phreatic eruption.

4.5.2 STROMBOLIAN ERUPTIONS AT RED CRATER

Strombolian activity is clearly seen at Red Crater, with the ~ 80 metre high scoria cone representing the single largest scoria deposit on the Tongariro cone complex, with a volume of ~ 0.3 km^3 (Hobden, 2000). The majority of the scoria exposed in Red Crater is the product of discrete gas bursts, depositing the scoria clasts, while limited hawaiian style fire fountaining deposited the agglutinated scoria units seen in the north-eastern and western crater walls and exploded out many of the vesiculated lava bombs.

Based on the close proximity of Red Craters scoria to the vent, and the rapid accumulation of that scoria, the discrete gas bursts responsible for it are likely to have being high and narrow and hence the result of high effusion rates (Wolff and Sumner, 2000). Rapid accumulation of molten clasts during these rapid discrete gas bursts has created clastogenic lava flows into South Crater, Central Crater and SE Oturere Valley (flow 8). This can only occur if the effusion rate is high enough, which is why the South Crater lava flow (flow 11), is much smaller than the Central Crater lava flows (flow 9 and 10), because the effusion rate decreased during its emplacement and could no longer feed the flow (Wolff and Sumner, 2000). Coarse clasts and lack of bedding are typical products of strombolian eruptions and characterize the facies seen at Red Crater. The Red Crater scoria cone structure is defined by colour, grain size and vesicularity changes, with the entire scoria cone sequence being non-welded, except for minor beds in the north east and western cone walls.

4.5.3 DIKES EXPOSED AT RED CRATER

Red Crater displays the most well preserved dike on the Tongariro cone complex. Their have being a number of metasedimentary xenoliths (as discussed in Chapter Four), found in the scoria deposits of the eastern and southern rims of Red Crater,

which have been brought up from basement depths (~ 10 – 15 km) which give an indication of the depths the magma feeding Red Crater has risen from. This exposed drained dike in the eastern crater wall of Red Crater, has an exposed diameter of ~ 4 metres, a drained depth of ~ 6 metres and an exposed height of ~ 30 metres. Exposed in the western wall is another bulbous dike (~ 30 m high and 20 m wide), which is possibly represents lateral injection from the large drained dike on the eastern wall during the scoria cone construction.

These two dikes trend NW-SE, cutting across the NE trending vent lineament seen on Tongariro, which the Red Crater cone and explosion pits follows. The connection between these two dikes is not seen because the phreatic eruption which followed scoria cone construction, blew the middle away. It is proposed that the dike feeding Red Crater follows the NE-SW regional vent lineament at depth, but is controlled by the cone topography at the surface, with the upper part of the dike trending NW-SE. Figure 4.11 shows an illustration of this trend.

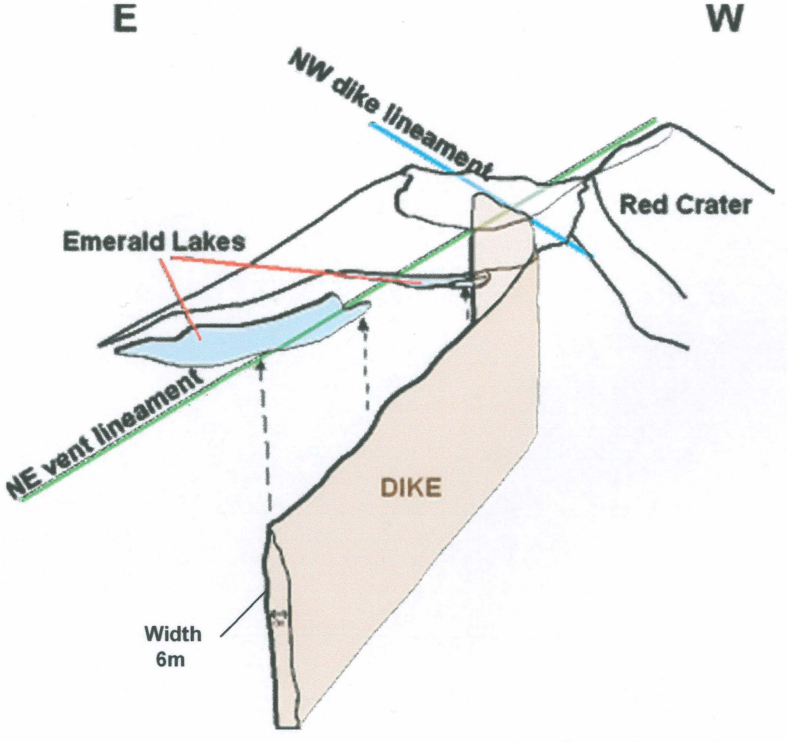

Figure 4.11 – NW-SE alignment of the two Red Crater dikes, their relationship to the NE trending vent lineament and the proposed dike alignment at depth.

Tibaldi (2003) showed on Stromboli that dike orientations are influenced by the cone morphology. This is something that can be related back to Red Crater, as the dike exposed in the western wall is not intruding into the underlying Tongariro Trig andesites upon which the cone is built. This western wall dike was influenced by this paleosurface prior to the late stage phreatic eruption which removed the Tongariro Trig andesites from the centre of the cone. A magma residence time of ~ 19 years was calculated for Stromboli, based on a magma chamber of ~ 0.3 to 0.04 km^3 in volume (Francalanci et al., 1999). This is comparable in volume to individual lava eruptions from Red Crater (Stevens, 2002; Topping, 1974).

4.6 RED CRATER ERUPTIVE PRODUCTS

4.6.1 RED CRATER SCORIA CONE

Units within the illustration of the idealized scoria cone (Figure 4.6) can be identified within Red Crater. The eastern wall of Red Crater represents sections 2 and 3 of this diagram, with the wedged shaped deposit of Unit 4 representing the main cone forming stage. Due to the preservation of the exposed drained dike, Red Crater enables a cross-section through both the inner crater wall facies and the outer wall facies to be seen. Figure 4.12 illustrates the break between inner and outer wall facies, with the outer wall facies sloping outwards towards the base of the cone, while the inner crater wall facies slope inwards towards the vent. Figure 4.13 shows a cross section through the Red Crater scoria cone, highlighting the units discussed above. The collapsed section of Red Craters eastern wall and the western crater wall expose agglutinated scoria fall deposits, which are a common deposit found in the lower parts of scoria cones (Vespermann and Schmincke, 2000).

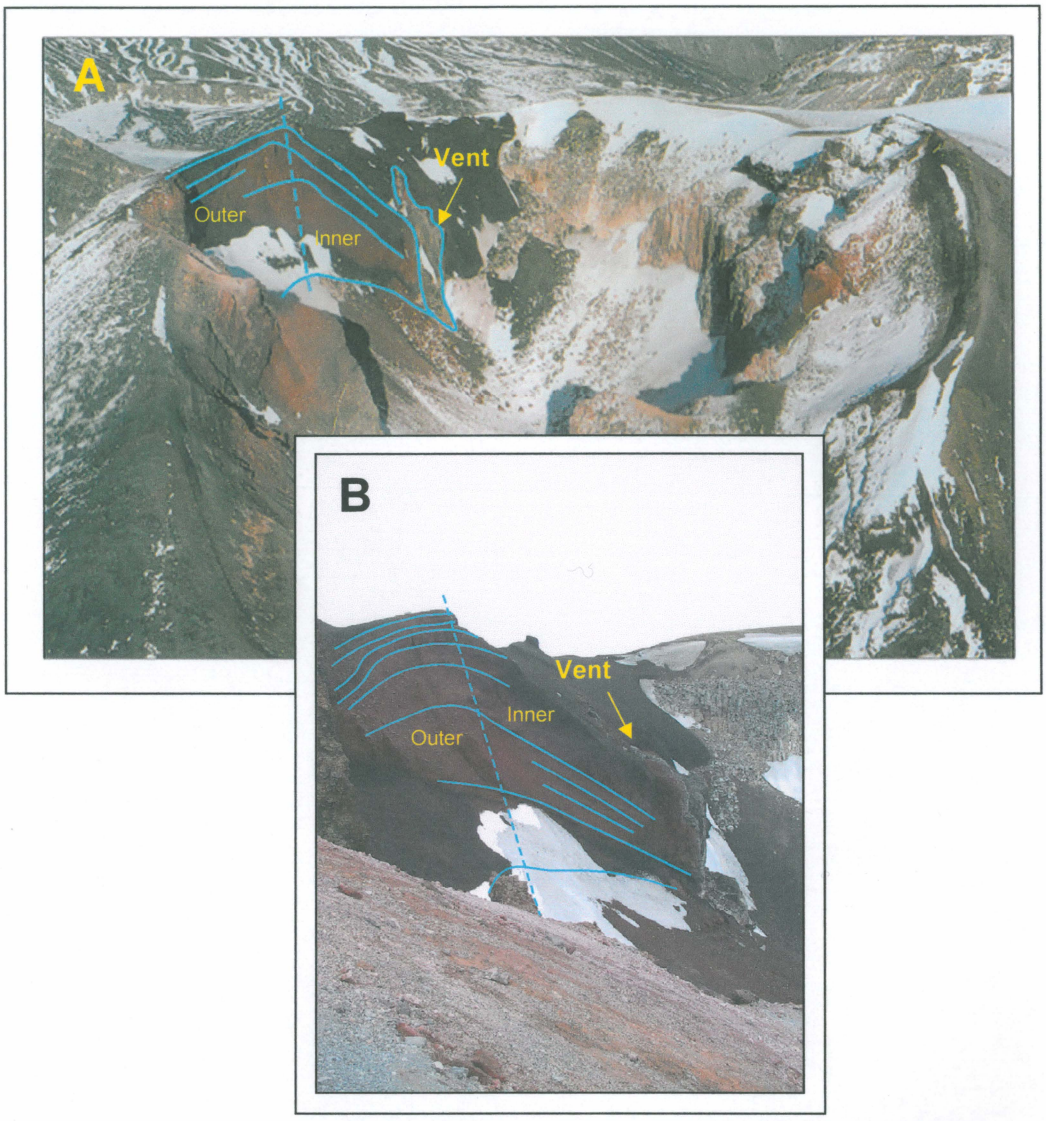

Figure 4.12 – **A** - Oblique photo (Williams, 2001) of Red Crater showing the junction between the outer wall facies and the inner wall facies. **B** – As seen from the eastern crater rim looking south.

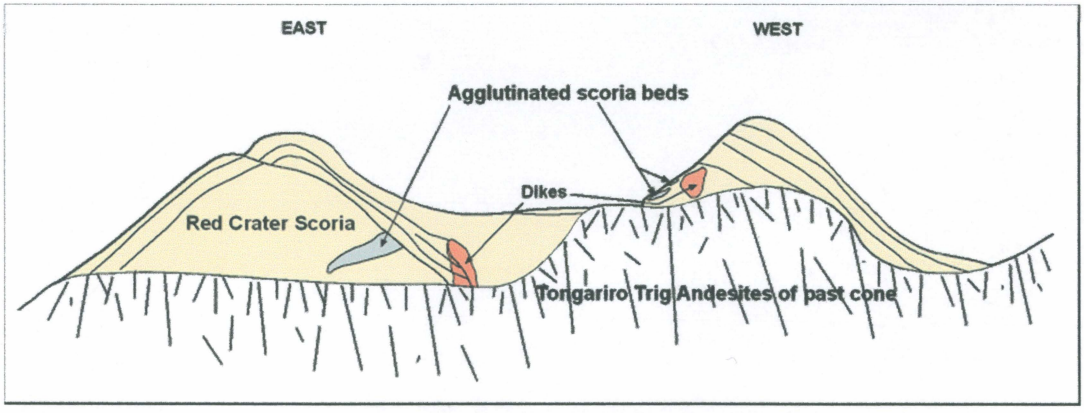

Figure 4.13 – Red Crater scoria units draping older Tongariro Trig andesites, with agglutinated scoria beds shown in yellow.

4.6.2 SCORIA, AGGLUTINATED SCORIA AND LAVA BOMBS IN RED CRATER

Scoria, lava bombs and agglutinated scoria beds are the three strombolian eruptive products found on Red Crater. Scoria is formed by rapid quenching during flight of magma blobs erupted by a discrete gas explosion. These clasts, due to their high vesicularities (up to 80% in Red Craters instance, with sizes ranging from < 1 mm up to 15 – 20 cm), often break on impact with the ground which exposes their fragile nature (Vergniolle and Mangan, 2000). Spatter bombs displaying cow-pat textures are commonly seen at Red Crater, highlighting the transitional boundary between hawaiian and strombolian eruptions (Vergniolle and Mangan, 2000; Vespermann and Schmincke, 2000), with the end members of the two styles changing throughout the scoria cone deposition.

Based on the rates of cone construction at Mount Nuovo in Italy (Ollier, 1988) and Paricutin in Mexico (Vespermann and Schmincke, 2000), it is possible that the entire Red Crater scoria cone was constructed within 48 hours. This is a realistic estimate when compared to Paricutin, which grew to 40 metres in only 24 hours (Vespermann and Schmincke, 2000). The maximum height of the scoria section in the Red Crater cone is ~ 60 metres, and like other young scoria cones, has slope angles of approximately 33°.

Lava bombs are the second eruptive product found at Red Crater. Two types of bombs were identified, the most common being the spatter bombs, while two spindal bombs were also found. Spatter bombs are larger than scoria clasts, often greater than 15cm in diameter. The interior of a spatter bomb is denser than a scoria clast, with the larger vesicles concentrated in the outer rim as Figure 4.14 shows.

Figure 4.14 – Interior of a spatter bomb.

Spindal bombs, as seen in Figure 4.15, have similar densities to the inner core of a spatter bomb, but differ in that the outside is molded into a spindle like structure (Francis, 1993).

Figure 4.15 – Spindal bomb sampled from the southern rim of Red Crater.

Agglutinated scoria beds are seen in both the eastern and western inner crater walls, and represent hot scoria clasts which have welded and become agglutinated on landing, creating the denser units within the scoria cone.

4.6.3 RED CRATER BLOCKY LAVA FLOWS

The andesitic lava flows of Red Crater exhibit the characteristics of blocky flows, with large angular, broken surface blocks littering there surfaces, overlying the dense, coherent centre (Kilburn, 2000; Linneman and Borgia, 1993). These broken surface blocks can be up to a metre in diameter as the photo of Red Craters Triple lobe flow (flow 2) in Figure 4.16 below shows.

Figure 4.16 – Close-up view of Triple lobe flow (flow 2) surface.

The front of the Triple lobe flow (flow 2) is ~ 40 metres compared with the ~ 30 metre thickness of the flow interior, while the tail trails out to a thickness of less than a metre. Figure 4.17a shows a photo of the flow front of the Red Crater andesitic Triple Lobe flow (Flow 2), while Figure 4.17b shows a profile through this lava flow, illustrating the greater thickness of the flow front compared to the rest of the flow. This thicker flow front shows the front cooled faster than the rate of accumulating lava behind it.

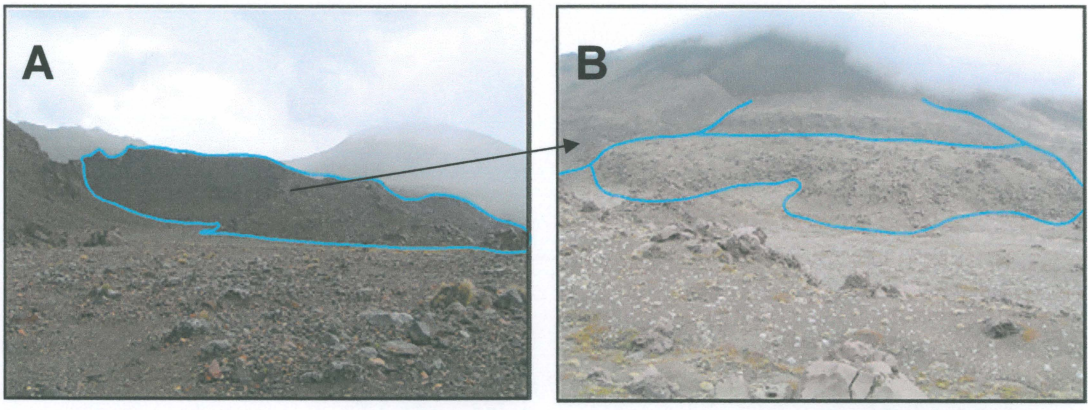

Figure 4.17a – Triple Lobe flow (Flow 2). **A** – Looking west at the flow front. **B** – Standing on top of the flow front looking back towards the west at the upper and middle lobes of the same flow.

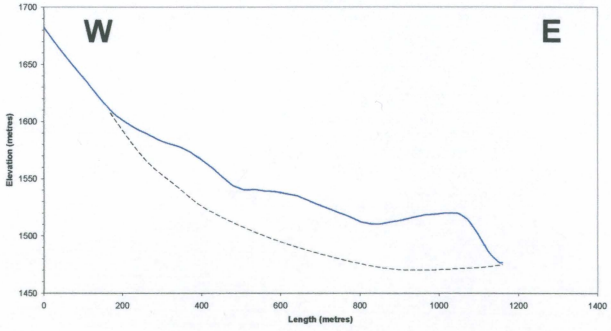

Figure 4.17b – Profile through the andesitic Triple lobe flow (Flow 2), showing the superior thickness of the flow front (looking north).

Linneman (1993) divided blocky flows into frontal zones and channel zones. The andesitic Triple lobe flow (flow 2) from Red Crater has evidence of this channellised flow preserved as Figure 4.18 shows.

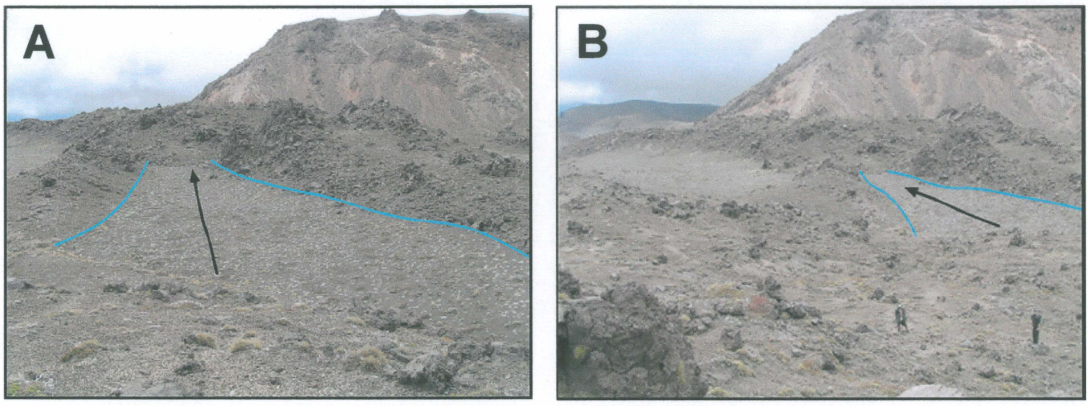

Figure 4.18 – **A** - Chanallised flow in the lower lobe of the Triple Lobe Flow (Flow 2) Red Crater. **B** – Entire lower lobe (flow front) of flow.

4.6.4 RED CRATER AA LAVA FLOWS

Aa lava flow fronts typically do not exceed 20 m (Kilburn, 2000) with the maximum thickness of a Red Crater aa flow front reaching only ~ 5 m. This is typical of a low aspect ratio flow which is produced due to the low viscosity of the basaltic andesite magma. Aa flows are subdivided into cauliflower and rubbly textures (Kilburn, 2000; Kilburn and Guest, 1993; Kilburn and Lopes, 1990). Red Crater aa flows have cauliflower textures but do not display the three sections (Pahoehoe, cauliflower and rubbly) of an aa flow that (Kilburn and Guest, 1993) described.

The two Central Crater flows of basaltic andesite aa lava best display the pressure ridges described by Kilburn (1993), while the Triple lobe andesitic flow also exhibits them on a larger scale.

CHAPTER FIVE

ERUPTIVE HISTORY

5.0 INTRODUCTION

The eruptive history of Red Crater is of interest because it displays an abrupt shift in eruptive style, yet is only a very young vent of less than 10 ka. Three eruptive phases can be recognized, defined by the composition of the lava flows and the nature of the scoria cone. This chapter will begin by discussing the pre-eruptive topography before outlining the three phases and the eruptive products that correlate to them. Figure 5.1 illustrates these three eruptive phases. This will provide a clear sequence of events of how Red Crater has behaved over its short lifetime.

5.1 PRE-ERUPTION TOPOGRAPHY

Prior to the instigation of the Red Crater vents, the topography in central Tongariro would have been quite different. The sketches shown below in Figure 5.2 show the generalized lay of the land around 9.7 ka ago.

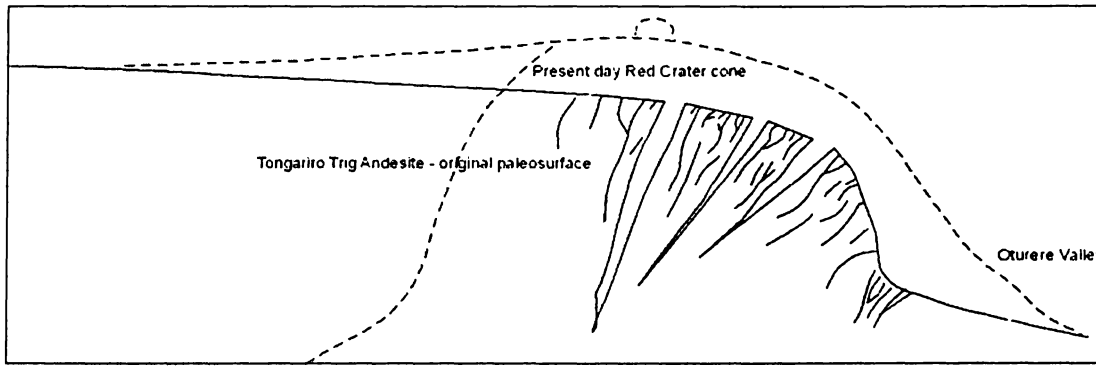

Figure 5.2 – Pre-eruptive topography of the central Tongariro area.

The current location of Red Crater is at the eastern end of a ridge of Tongariro Trig andesitic lavas that were emplaced between 115 and 65 ka, during the fifth phase of cone building at Tongariro (Hobden, 2000). The Tongariro Trig cone which these andesites originated from was very productive during this phase, erupting 0.3 km^3/ka (Hobden, 2000).

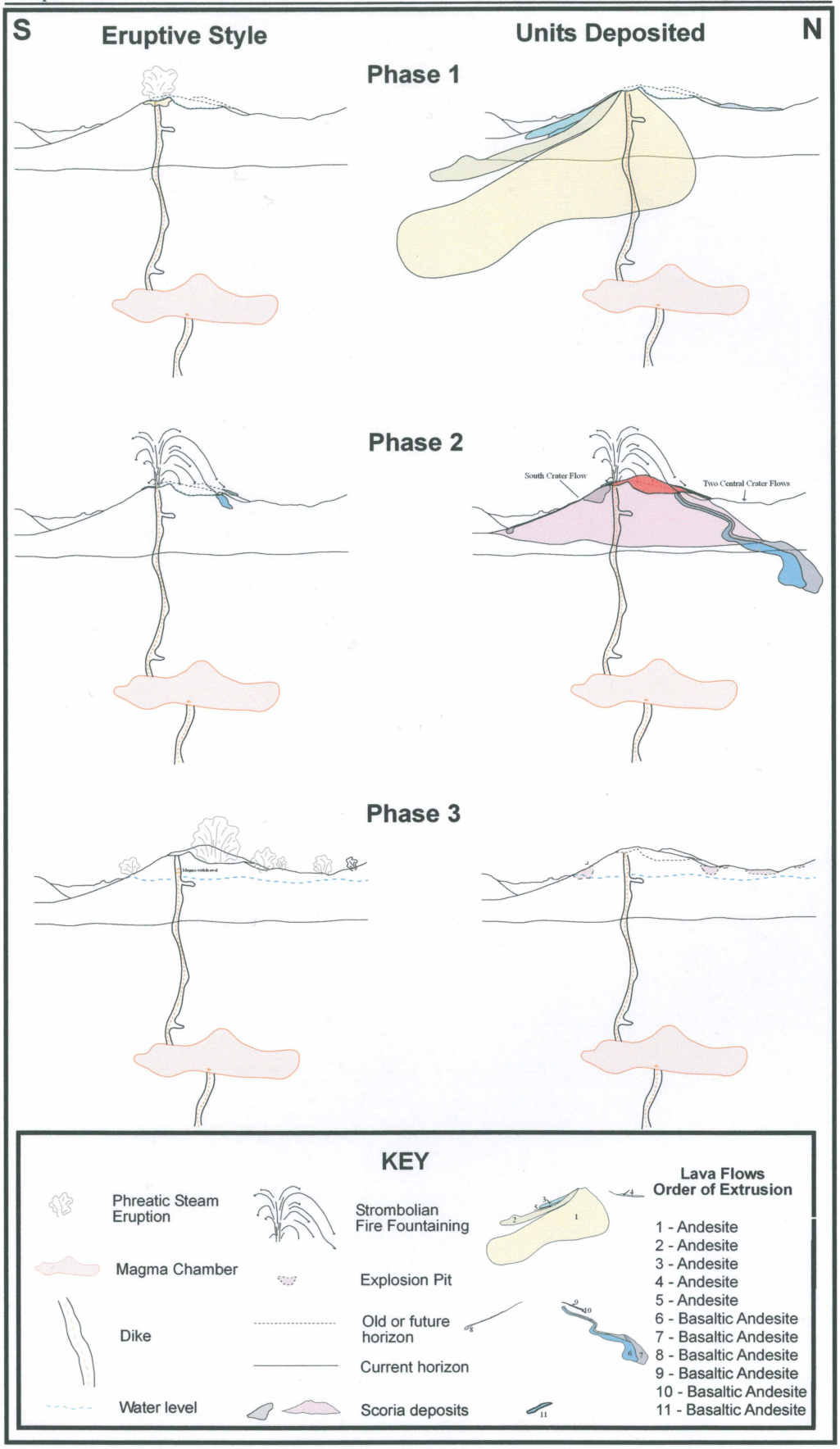

Figure 5.1 - The three eruptive phases of Red Crater, Tongariro. The dike depicted actually strikes NE-SW at depth and NW-SE at the surface, so an accurate picture would show a single flat sheet.

5.2 PHASE ONE

Somewhere between 9.7ka and 3.4ka, fresh magma was injected into a magma chamber beneath Tongariro, causing increased pressure within the chamber resulting in the initiation and propagation of a dike. This dike intruded beneath the present day location of Red Crater. As it approached the surface it came into contact with groundwater causing flashing to steam and a violent phreatic eruption. This phreatic eruption blasted away part of the old ridge of Tongariro Trig andesites, creating a path to the surface for the dike. This initial phreatic eruption also decreased the volatile content in the magma so effusive activity took over. A sustained magma discharge (effusion) rate enabled effusive activity to continue for months to years, during which time, the large andesitic flow into Oturere Valley was erupted. Recorded as flow 1 in Red Craters history, this is also the single largest lava flow still preserved within the entire Tongariro Volcanic complex, extending for approximately 7 kilometers with an estimated volume of c. 371-640 million cubic metres (Stevens, 2002). A number of authors, namely Stevens (2002), Hobden (1997) and Topping (1974), have all thought that this initial flow may have represented a near emptying of the magma chamber which feed it. The age of this flow was deemed by Topping (1974) to be between 9700 and 3500 years BP because both the Mangamate Tephra and Papakai Tephras are not found upon it, yet are seen elsewhere on Tongariro, which constrains the oldest possible age to between these limits.

Fresh injections of andesitic magma into the chamber between 3.4 ka and 1.8 ka trigger the effusive deposition of the remaining andesitic flows into Oturere Valley and along the current emerald lakes ridge. Flows 2, 3, 4 and 5 have systematically decreasing lengths and volumes perhaps representing the decreasing andesitic source magma, indicating that the volume of each of the andesitic flows represents the total volume in the magma chamber(s) at the time of the eruption. Continuous but irregular magma discharge rates dominated during this effusive phase of the eruptions. While there is a period of approximately 1600 years before the second phase of eruptive activity begins, it is likely that the andesitic lava flows just discussed would have being erupted within 100 years of each other due to the similarities in composition

and crystal size. If the magma had sat for longer periods in the chamber prior to each flow being erupted, then crystals would have being able to grow to varying sizes.

5.3 PHASE TWO

The onset of phase two marks a big change in the magma composition and hence the eruptive style. While the previous 1600 years were dominated by effusive andesitic volcanism, post 1.85 ka was dominated by strombolian basaltic andesitic volcanism. This phase of Red Craters eruptive history represents the major cone building stage.

Injection of basaltic magma into the magma chamber is the trigger for this phase, with this fresh gas charged magma causes an increase in volatile percentages. This increasing gas content occurred as a two-phase slug flow, where pulses or slugs of coalescing gas bubbles tore up the dike causing strombolian fire fountaining and discrete gas bursts. Throughout the duration of this initial stage, the scoria cone facies were deposited from the fountain. As the sketch in Figure 5.3 shows the inner part of the fountain was feeding the basaltic andesite aa lava flows that were emplaced during the time taken to construct the scoria cone.

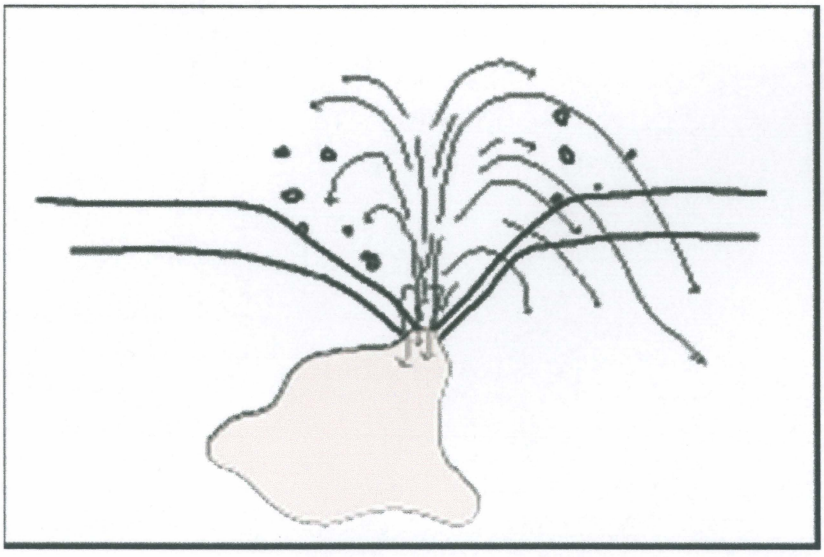

Figure 5.3 – Scoria deposits and lava flows from a fire fountain.

While initially high, the magma discharge rate decreased during the deposition of this unit, before a further injection deep into the chamber causes the discharge rate to increase again, depositing Unit 2. The deposition of Unit 2 resulted from the second highest discharge rate of the entire cone. These waxing and waning magma discharge rates continue throughout the deposition of the eleven units recorded in the eastern crater wall, and may represent new batches of fresh gas-charged magma entering the magma chamber.

Unit 2's high discharge rate is immediately followed by a sharp discharge rate decline during the deposition of Unit 3. The way Unit 4 is deposited reflects the changing heights of the fire fountain which are caused by the changing discharge rates. Figure 5.4 below illustrates how the wedged shaped deposit on Unit 4 was deposited.

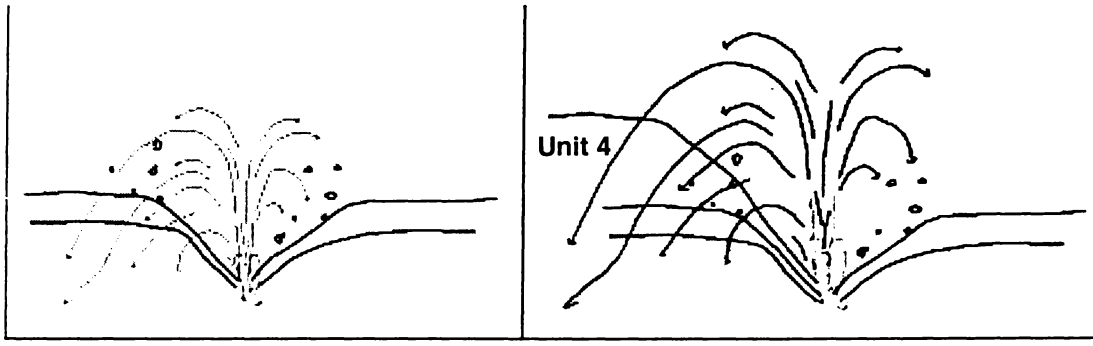

Figure 5.4 – Changing fire fountaining heights resulting in the wedged shaped deposit of Unit 4, Eastern inner-wall section.

Initially the discharge rate was low following the decline recorded in Unit 3, so the fire fountain was small, depositing scoria closer to the vent. As the discharge rate increased during deposition of this unit, the fountain grew, depositing scoria further away from the vent, creating the wedged deposit. The increasing discharge rate throughout Unit 4 reached a maximum for the entire eastern wall sequence during the deposition of Unit 5. As the discharge rate is unable to continue peaking without constant magma recharge, the four units following this, Units 6 , 7, 8 and 9 were all deposited during a declining magma discharge rate recorded in the increasing vesicularity ranges (Houghton and Wilson, 1989).

Unit 9 marked the lowest magma discharge rate of the sequence. There was brief increase in discharge rate during the deposition of Units 10 and 11 as new magma entered the system, but the low vesicularities and higher densities recorded in Units A and B, which are stratigraphically above the eastern wall section, show this magma did not mix as much in the chamber, but rather was erupted very close to the time of injection because the scoria has not had time to reach as close to peak vesiculation as previous units had. This entire cone sequence was probably constructed within 24 to 48 hours, based on comparisions made with Mexico's Paricutin volcano, with the three decreases in discharge rate representing the end of three fountaining events during this time frame. The basaltic andesite aa lava flows 6, 7, 8, 9, 10 and 11 were all emplaced during the deposition of the scoria cone. The dike exposed in the western crater wall was injected late in the cone building history.

Injection of more basaltic magma continued, this time erupting as another strombolian fire fountain or discrete gas explosion which was restricted to the southern rim of the crater. This focus of eruption is probably due to the wind direction which concentrated the fire fountain in this area. The magma discharge rate started high, initially depositing unit SCR1 while simultaneously feeding the dribble of a basaltic andesite aa lava flow into South Crater. Discharge rates declined steadily during the deposition of Units SCR2 – SCR6, to their lowest point during the deposition of unit SCR7. A slight increase resulted in the deposition of unit SCR8, but this was the final episode in the construction of the scoria cone.

5.4 PHASE THREE

Magma withdrawal from the dike caused de-pressurisation within the conduit and allowed cracks to form, which groundwater could then penetrate. This withdrawing magma came into contact with water at depth causing another violent phreatic eruption which blasted out the NE trending explosion pits of the emerald lakes and the explosion pit on the south face of the cone. The same phreatic eruption also removed a substantial section of the cone itself, revealing the inner eastern and

western crater walls and completely destroying the northern crater wall. This phreatic eruption has to have occurred at this point in time because the lava flow which fed the upper Central Crater flow, plus the SE Oturere basaltic andesite aa flow have both been excavated by these explosions. There is also andesitic blocks and hydrothermally altered blocks on top of the Central Crater flows and around the upper eastern and south-eastern rims of the cone.

The removal of the northern crater wall by this phreatic eruption weakened the northern portion of the eastern crater wall, causing the slumping of a large portion of it. The order of extrusion of the aa basaltic andesite flows in phases two, was determined by Topping (1974), who also stated that these flows would have all being deposited within 600 years of the 1.85 ka Taupo eruption. While minor steam and ash eruptions have being recorded in the late 1800's and the fumaroles around Red Crater are still very active, no major eruptions have occurred from Red Crater in the past 100 years.

CHAPTER SIX

SUMMARY

6.0 INTRODUCTION

Subduction beneath the North Island of the Pacific Plate along the Hikurangi trench is the dominant control on late Cenozoic volcanism within New Zealand. This subduction setting has rotated south over time, currently fuelling the Taupo Volcanic Zone (TVZ). The TVZ can be subdivided into northern, central and southern regions with rhyolitic eruptions dominating the central region, while predominantly andesitic magmas have being erupted in the northern and southern regions (Wilson et al., 1995). During the 1.6 ma that the central region has being active approximately 20,000 km^3 of material has been erupted (Wilson et al., 1995).

The Tongariro volcanic complex extends for approximately 55 km and is dominated by the two andesitic composite cones of Ruapehu and Tongariro. Tongariro is a dominantly andesitic composite cone complex, yet located at its centre is Red Crater, a basaltic andesite vent with an eruptive nature in striking contrast to the rest of Tongariro. The oldest lava flows at Tongariro were dated at ~ 275 ka, but evidence of gravels underlying the 0.34 ma Whakamaru ignimbrite suggest activity is at least this old (Hobden et al., 1996).

Evidence for glaciers on the slopes of Tongariro was noted by Matthews (1967). The entire cone complex can be subdivided into three age groups based on there relationship to the timing of these glaciations. The vents within the Tongariro cone complex form two lineaments, one trending NW-SE and extending for 10 km, while the other trends NE-SW and includes all the vents on both Tongariro and Ruapehu. Faulting within the Tongariro cone complex is mostly limited to the outer flanks of the volcano.

Previous workers on Tongariro have both observed past eruptions and carried out experiments and research to determine different aspects of how the cone complex was formed.

Red Crater is part of a line of explosion pits trending NE along the same alignment as the volcanic vents within the complex. The Emerald Lakes to the north and the explosion pit on the south face of Red Crater are included in this explosion line. The exposed drained dike in the eastern crater wall is the most recognized feature of Red Crater. A lateral extension of this dike occurs in the western crater wall, occurring in a NW-SE trending lineament, cutting across the NE trending vent lineament.

6.1 STRATIGRAPHY

Red Crater displays a complex and variable stratigraphy, with units often showing little continuity between the east, west and southern inner crater walls. This cone stratigraphy was the main focus of this research, with the associated lava flows and explosion pits also being investigated. The Red Crater scoria cone is perched on the edge of a glacially eroded slope at the head of the Oturere Valley. Within the past 10 ka, the Red Crater vent has been one of the most active and productive post-glacial vents within the Tongariro complex, with an eruptive rate of 0.1 km^3/ka (Hobden and Houghton, 2000).

The scoria deposits within Red Crater were described in sections based on their localities, including the Eastern inner-wall section; Eastern crater rim sections and Southern crater rim sections. The Eastern inner-wall section is the most comprehensive of those described, covering a 52 metre section through the entire eastern inner wall of the cone which represents the outer wall facies in an idealized scoria cone model. The eleven units within this section vary in thickness, grain size, colour and vesicularity which enables an approximate magma discharge rate curve to be interpreted. A further two sections on the Eastern crater rim were described, with some of these units correlating with the units seen in the Eastern inner-wall section. Eight units were described on the Southern crater rim, which were the final scoria units to be deposited during the cone construction. These eight units are limited to the Southern crater rim as a result of localized strombolian gas bursts concentrating deposits in close proximity to the vent. The Eastern inner-crater wall and Southern crater rim sections together provide a section through the entire preserved scoria cone

thickness. The western crater wall is a chaotic mix of steeply dipping agglutinated scoria fall deposits, unwelded scoria deposits and a dike.

Associated with the Red Crater are eleven lava flows which have been erupted over the last c.9.7 ka. These flows can be divided into two groups: 1) those erupted prior to 1.85 ka (Taupo eruption) which are andesitic in composition and, 2) those erupted post 1.85 ka, which are basaltic andesite in composition. The andesitic flows only occur in Oturere Valley, while the basaltic andesite flows are emplaced in Central Crater, South Crater, NE Oturere Valley and SE Oturere Valley. The first flow (flow 1) to be erupted from Red Crater is the single largest preserved flow on the entire Tongariro cone complex and extends for 7 km down valley from the vent, infilling the full width of the Oturere Valley. The volume of this single flow (0.3 km^3) is an order of magnitude greater than the total volume of all the remaining Red Crater flows (0.034 km^3) possibly representing a significant emptying of the magma chamber (Hobden, 1997; Stevens, 2002).

Phreatic explosion craters are a feature of the Red Crater vent system. Explosion craters occur on the outer south wall of Red Crater and a line of five craters extends NE of the scoria cone, three of which are occupied by the ~ 5m deep Emerald Lakes. The Red Crater cone has also been excavated by phreatic explosions, to reveal the Tongariro Trig lavas on which the cone is constructed. Ballistic blocks are located on and around the rims of these pits, blown out during phreatic explosions associated with scoria cone construction..

6.2 TEXTURAL AND COMPONENTRY ANALYSIS

Vesicularity analysis, SEM analysis, grain size analysis and petrography were all used to gain an understanding of the lava flows and scoria deposits erupted from this vent. Sampling of each unit within the Eastern inner-wall section enabled the vesicularity of clasts within individual units to be determined. Clast vesicularities calculated from the Red Crater deposits range from 41 – 85%, with average vesicularities of this Eastern inner-wall deposit between 62% and 75%, which

classifies them as highly vesicular (Houghton and Wilson, 1989). There are no obvious time breaks in the deposition of the scoria cone, but the changing ranges of vesicularities for each unit enable an approximate magma discharge curve to be drawn, with larger ranges in vesicularity reflecting a decrease in the discharge rate (Houghton and Wilson, 1989). An essentially continuous eruption may have deposited the scoria cone, but two peaks and three declines in magma discharge rate indicate that fluctuations were occurring within the magma conduit. Grain size analysis enabled an approximate grain size curve to be interpreted with decreasing grain sizes coinciding with decreasing magma discharge rates.

Thin section analysis on all the Red Crater lava flows and also on a scoria bomb from the cone, helped to link the eruption of the lava flows with the production of the scoria cone, while also providing evidence for magma mixing and mingling at depth. Plagioclase was found to be the dominant phenocryst in all Red Crater lava flows, with the abundance of olivine being high in the basaltic andesite flows and lower in the andesitic flows. Comparisons of the percentages of different phenocrysts between the lava flows allowed compositional groupings to be made. Two groups of lava flows are seen at Red Crater, the andesites and the basaltic andesites. Petrographic analysis confirmed these groups, and indicates the composition of the scoria cone is similar to that of the basaltic andesite flows. Oscillatory, patchy and reverse zoning and sieve textures in Plagioclase are seen within all the Red Crater lava flows, indicating discrete batches of magma had been mixed and mingled before eruption at the surface.

By plotting various physical parameters of the lava flows, relationships between each of the flows can be seen, with all the andesite flows plotting together, separate from the basaltic andesite flows. This reflects both the differences in eruption style and the change in magmatic composition. The profiles of three of the Red Crater flows emphases that slope angles were not the controlling factor on the length of the lava flows, with the basaltic andesite flow into South Crater (flow 11) being emplaced on a 23° slope angle and yet not reaching the valley floor. This indicates that the magma discharge rate was the key to the sizes of the Red Crater lava flows.

Deep basement xenoliths of quartz and metasedimentary greywacke sampled from the crater rims of the scoria cone show the depth (~ 10 – 15 km) that the magma was sourced from.

6.3 ERUPTIVE PROCESSES

Three main eruptive processes have occurred over the lifetime of the Red Crater vent. Phreatic eruptions, effusive activity and strombolian eruptions have all produced the Red Crater cone. Phreatic eruptions cleared the way for initial dike intrusion which was followed by effusive activity erupting the five andesitic lava flows into Oturere Valley. These andesitic lava flows are blocky in nature, with flow fronts thicker than the interior of the flow. Phreatic eruptions were caused by the interaction of groundwater with the intruding dike, flashing the water to steam and creating a violent phreatic eruption.

A change from andesitic to basaltic andesite magma occurred around the time of 1.85 ka, with a change in eruption style to strombolian style eruptions also occurring. Strombolian eruptions explode scoria clasts out of the vent in discrete gas explosions, and if the frequency of the gas slugs which feed these discrete gas explosions is high enough, then a fire fountain can also occur, highlighting the transitional nature between hawaiian and strombolian style eruptions. The most common eruptive product of a strombolian eruption are the scoria clasts, which rapidly accumulated to form the scoria cone. Observations of Paricutin in Mexico and the "Laghetto" scoria cone on Mt Etna showed that scoria cones of similar height to Red Crater can be constructed within 48 hours (Calvari, 2003; Luhr and Simkin, 1993). Inner and outer wall crater facies can be seen within the Red Crater cone. Unwelded massive and weakly-bedded scoria units, lava bombs and agglutinated scoria fall units are the three eruptive products of strombolian eruptions which all construct the cone seen at Red Crater.

The lava flows into Central Crater, South Crater, NE Oturere Valley and SE Oturere Valley all occurred in conjunction with the scoria cone construction and are clastogenic flows, feed by agglutination of accumulating molten scoria clasts rather than directly from the vent. Aa flows with cauliflower texture define the basaltic andesite flows erupted from Red Crater.

Two dikes are clearly exposed within the Red Crater cone. One, on the eastern wall, is partially drained, and second is a bulbous dike within in the western outer-wall. The alignment of these two dikes (NW-SE) suggests they are remnant of a once continuous structure that cuts across the regional and local structural trend (NE-SW). This probably reflects shallow level structural control on the intrusion, the shape of the cone and the underlying topography.

6.4 ERUPTIVE HISTORY

The eruptive history of Red Crater displays an abrupt shift in eruptive style and yet is only a very young vent of less than 10 ka. It is situated on the eastern end of a ridge of Tongariro Trig andesitic lavas which were emplaced between 115 and 65 ka, during the fifth phase of cone building at Tongariro (Hobden and Houghton, 2000; Hobden et al., 1996).

The eruptive history of Red Crater can be separated into three phases of activity. Phase One began with the intrusion of a dike from the magma chamber, which while on its way to the surface, interacted with groundwater, flashing it to steam and causing a violent phreatic eruption which cleared the way to the surface for this dike. A large amount of the volatiles within this magma column would have been expelled during the phreatic eruption, therefore effusive activity took over when the dike reached the surface, erupting the andesitic lava flows (flows 1, 2, 3, 4 and 5) into Oturere Valley.

Phase Two was marked by a stark change in the magma composition and eruptive style. Injection of basaltic andesite magma into the conduit triggered the start of phase

two. The high level of retained volatiles and rapid ascent of this new magma batch fuelled the eruption. Strombolian style discrete gas explosions dominated this phase, with the construction of the scoria cone on top of the older Tongariro Trig andesites. During the construction of the cone, the basaltic andesite lava flows 6, 7, 8, 9, 10 and 11 were all deposited as clastogenic flows, meaning they were derived from rapidly accumulating hot scoria, molten enough to flow away, which was deposited from highly frequent discrete gas explosions. The dike exposed in the western wall has occurred from a lateral injection of magma from the main dike (now exposed in the eastern wall), intruding into the scoria units already emplaced.

Phase Three saw another change in eruptive style, with the withdrawal of magma within the dike, with possible depressurization creating cracks in the conduit wall. At depth this draining magma interacted with water, generating a large, violent phreatic eruption which tore apart the explosion pits filled by the Emerald Lakes and the explosion pit of the south face of the Red Crater cone. Evidence of this phreatic eruption is seen around the rims of Red Crater and the Emerald Lakes in the form of ballistic blocks. Lava flows 8 and 9 have also been blown apart by this eruption.

Apart from a few minor steam and ash eruptions late in the 18th Century, Red Crater has been mostly quite, with the fumaroles surrounding the crater the main evidence that the system is still very much potentially active, and likely to be the site of eruptions in the future.

REFERENCES

REFERENCES

Acocella, V., Neri, M., 2003. What makes flank eruptions? The 2001 Etna eruption and its possible triggering mechanisms. *Bulletin of Volcanology*, 65: 517-529.

Behncke, B., Neri, M., 2003. The July-August 2001 eruption of Mt. Etna (Sicily). *Bulletin of Volcanology*, 65: 461-476.

Bibby, H.M., Caldwell, T.G., Davey, F.J., Webb, T.H., 1995. Geophysical evidence on the structure of the Taupo Volcanic Zone and its hydrothermal circulation. *Journal of Volcanology and Geothermal Research*, 68: 29 - 58.

Calvari, S., Neri, M., Pinkerton, H., 2002. Effusion rate estimations during the 1999 summit eruption on Mount Etna, and growth of two distinct lava flow fields. *Journal of Volcanology and Geothermal Research*, 119: 107-123.

Calvari, S., Pinkerton, H., 2003. Birth, growth and morphologic evolution of the 'Laghetto' cinder cone during the 2001 Etna eruption. *Journal of Volcanology and Geothermal Research*, 3008: 1-15.

Carrigan, C.R., 2000. Plumbing Systems. In: H. Sigurdsson (Editor), *Encyclopedia of Volcanology*. Academic Press, San Diego, pp. 1417.

Cas, R.A.F., Wright, J.V.,, 1987. *Volcanic successions, modern and ancient.* Allen and Urwin, London, 528 pp.

Cashman, K.V., Thornber, C., Kavahikaua, J.P., 1999. Cooling and crystallization of lava in open channels, and the transition of Pahoehoe lava to Aa. *Bulletin of Volcanology*, 61: 306-323.

Chouet, B., Saccorotti, G., Dawson, P., Martini, M., Scarpa, R., De Luca, G., Milana, G., Cattaneo, M., 1999. Broadband measurements of the sources of explosions at Stromboli Volcano, Italy. *Geophysical Research Letters*, 26: 1937-1940.

Chovet, B., Saccorotti, G., Dawson, P., Martini, M., Scarpa, R., De Luca, G., Milana, G., Cattaneo, M., 1999. Broadband measurements of the sources of explosions at Stromboli Volcano, Italy. *Geophysical Research Letters*, 26: 1937-1940.

Cole, J.W., 1978. Andesites of the Tongariro Volcanic Centre. *Journal of Volcanology and Geothermal Research*, 3: 121-153.

Cole, J.W., Cashman, K.V., Rankin, P.C., 1983. Rare-earth element geochemistry and the origin of andesites and basalts of the Taupo Volcanic Zone, NZ. *Chemical Geology*, 38: 255-274.

Cronin, S.J., Neall, V.E., 1997. A late Quaternary stratigraphic framework for the north eastern Ruapehu and eastern Tongariro ring plains, NZ. *NZ Journal of Geology and Geophysics*, 40: 185-197.

Dibble, R.R., Nairn, I.A., Neall, V.E., 1985. Volcanic hazards of North Island, New Zealand - overview. *Journal of Geodynamics*, 3: 369-396.

Donoghue, S., Neall, V.E., 1996. Tephrostratigraphic studies at Tongariro Volcanic Centre, New Zealand: an overview. *Quaternary International*, 34-36: 13-20.

Donoghue, S., Neall, V.E., Palmer, A.S., 1995. Stratigraphy and chronology of late Quaternary andesitic tephra deposits, Tongariro Volcanic Centre, New Zealand. *Journal of the Royal Society of New Zealand*, 25(2): 115-206.

Fisher, R.V., Heiken, G., Hulen, J.B., 1997. *Volcanoes - Crucibles of Change.* Princeton University Press, New Jersey, 317 pp.

Francalanci, L., Tommasini, S., Conticelli, S., Davies, G.R., 1999. Sr isotope evidence for short magma residence time for the 20th Century activity at Stromboli volcano, Italy. *Earth and Planetary Science Letters*, 167: 61-69.

Francis, P., 1993. *Volcanoes - A planetary perspective.* Oxford University Press, New York, 443 pp.

Gamble, J.A., Price, R.C., 2000. Tectonic setting and andesitic volcanoes of the central North Island of New Zealand. In: R.C. Price, Gamble, J.A., Hobden, B.J. (Editor), *State of the Arc 2000. Processes and time scales in the genesis and evolution of arc magmas.* Guidebook for field excursions on Ruapehu and Tongariro Volcanoes. The Royal Society of New Zealand, Wellington, pp. 52.

Graham, I.J., Grapes, R.H., Kifle, K., 1988. Buchitic metagreywacke xenoliths from Mount Ngauruhoe, Taupo Volcanic Zone, New Zealand. *Journal of Volcanology and Geothermal Research*, 35: 205-216.

Gregg, D.R., 1961a. The tectonic setting of the Tongariro volcanoes, New Zealand, *Proceedings of the Ninth Pacific. Sci. Congr.*, pp. 218-224.

Gregg, D.R., 1961b. Volcanoes of Tongariro National Park. *A NZ Geological Survey Handbook*, 28: 83.

Gutmann, J.T., 1979. Structure and eruptive cycle of cinder cones in the pinacate volcanic field and the controls of strombolian activity. *Journal of Geology*, 87: 448-454.

Hagerty, M., Benites, R., 2003. Tornillos beneath Tongariro Volcano, New Zealand. *Journal of Volcanology and Geothermal Research*, 125: 151-169.

Harris, S.L., 2000. Archaeology and Volcanism. In: H. Sigurdsson (Editor), *Encyclopedia of Volcanology*. Academic Press, San Diego, pp. 1417.

Hector, J.D., 1870. Eruption of the volcano Tongariro, NZ. *Nature*, 2.

Hill, H., 1893. The volcanic outburst at Te Mari, Tongariro, in November 1892. *Transactions of the NZ Institute*, 26: 388-392.

Hobden, B.J., 1997. Modelling magmatic trends in time and space: eruptive and magmatic history of Tongariro volcanic complex, New Zealand. *Ph.D. thesis, University of Canterbury.*

Hobden, B.J., Houghton, B.F., Davidson, J.P., Weaver, S.D., 1999. Small and short-lived magma batches at composite volcanoes: time windows at Tongariro Volcano, New Zealand. *Journal of the Geological Society*, London, 156: 865-868.

Hobden, B.J., Houghton, B.F., Lanphere, M.A., Nairn, I.A., 1996. Growth of the Tongariro volcanic complex: new evidence from K-Ar age determinations. *New Zealand Journal of Geology and Geophysics*, 39: 151-154.

Hobden, B.J., Houghton, B.F., 2000. Geology of the Tongariro Volcano Traverse. In: R.C. Price, Gamble, J.A., Hobden, B.J. (Editor), *State of the Arc 2000. Processes and time scales in the genesis and evolution of arc magmas.* Guidebook for field excursions on Ruapehu and Tongariro Volcanoes. The Royal Society of New Zealand, Wellington, pp. 52.

Hobden, B.J., Houghton, B.F., Nairn, I.A., 2002. Growth of a young, frequently active composite cone: Ngauruhoe volcano, New Zealand. *Bulletin of Volcanology*, 64: 392-409.

Hochstein, M., 1985. Steaming ground at Red Crater and in the Te Mari Craters, Mount Tongariro geothermal system (NZ), *Proceedings of the 7th NZ Geothermal Workshop*, pp. 177-180.

Houghton, B.F., Wilson, C.J.N., 1989. A vesicularity index for pyroclastic deposits. *Bulletin of Volcanology*, 51: 451-462.

Houghton, B.F., Wilson, C.J.N., McWilliams, M.O., Lanphere, M.A., Weaver, S.D., Briggs, R.M., Pringle, M.S., 1995. Chronology and dynamics of a large silicic magmatic system: Central Taupo Volcanic Zone, New Zealand. *Geology*, 23(1): 13-16.

Houghton, B.F., Wilson, C.J.N., Smith, I.E.M., 1999. Shallow-seated controls on styles of explosive basaltic volcanism: a case study from New Zealand. *Journal of Volcanology and Geothermal Research*, 91: 97-120.

Hucks, J.P., 2000. Reconstructing the pre-glacial cone growth of the Tongariro Volcanic Complex, North East Oturere Valley. *MSc Thesis, University of Waikato*, Hamilton.

Hyndman, D.W., Alt, D., 1987. Radial dykes, laccoliths and gelatine models. *Journal of Geology*, 95: 763-774.

Ingham, M., Zeng, Y., 1993. AMT soundings to determine electrical structure in Tongariro National Park, *Proceedings 15th NZ Geothermal Workshop* 1993, pp. 373-379.

James, M.R., Lane, S.J., Chovet, B., Gilbert, J.S., 2003. Pressure changes associated with the ascent and bursting of gas slugs in liquid-filled vertical and inclined conduits. *Journal of Volcanology and Geothermal Research*, 2669: 1-22.

Jaupart, C., 1998. Gas loss from magmas through conduit walls during eruption. In: J.S. Gilbert, Sparks, R.S.J. (Editor), *The Physics of Explosive Volcanic Eruptions*. The Geological Society, London, pp. 73-90.

Jaupart, C., Vergniolle, S., 1988. Laboratory models of Hawaiian and Strombolian eruptions. *Nature*, 331: 58-60.

Kilburn, C.R.J., 2000. Lava flows and flow fields. In: H. Sigurdsson (Editor), *Encyclopedia of Volcanology*. Academic Press, San Diego, pp. 1417.

Kilburn, C.R.J., Guest, J.E., 1993. Aa lavas of Mount Etna, Sicily. In: C.R.J. Kilburn, Luongo, G. (Editor), *Active lavas: monitoring and modelling.*. UCL Press, London, pp. 73-106.

Kilburn, C.R.J., Lopes, R.M.C., 1990. Surfaces of aa flow-fields on Mount Etna, Sicily; Morphology, rheology, crystallization and scaling phenomena. In: J.H. Fink (Editor), *Lava flows and domes*. Springer, Berlin Heidelberg New York, pp. 73-106.

Kilburn, C.R.J., Lopes, R.M.C., 1991. General patterns of flow field growth: Aa and Blocky lavas. *Journal of Geophysical Research*, 96: 19,721-19,732.

Lecointre, J.A., Neall, V.E., Cleland Wallace, R., Prebble, W.M., 2002. The 55- to 60-ka Te Whaiau Formation: a Catastropic, avalanche-induced, cohesive debris-flow deposit from Proto-Tongariro volcano, New Zealand. *Bulletin of Volcanology*, 63: 509-525.

Linneman, S.R., Borgia, A., 1993. The blocky andesitic lava flows of Arenal volcano, Costa Rica. In: C.R.J. Kilburn, Luongo, G. (Editor), *Active lavas: monitoring and modelling*. UCL Press, London, pp. 374.

Luhr, J.F., Simkin, T. (Eds), 1993. *Paricutin: The volcano born in a Mexican cornfield.* Geoscience Press, Inc, Phoenix, 427 pp.

MacDonald, G.A., 1972. *Volcanoes.* Prentice-Hall, New Jersey, 510 pp.

Marsh, B.D., 2000. Magma Chambers. In: H. Sigurdsson (Editor), *Encyclopedia of Volcanology.* Academic Press, San Diego, pp. 1417.

Mathews, W.H., 1967. A contribution to the geology of the Mount Tongariro massif, North Island, New Zealand. *New Zealand Journal of Geology and Geophysics*, 10: 1027-1038.

McLeod, P., Tait, S., 1999. The growth of dykes from magma chambers. *Journal of Volcanology and Geothermal Research*, 92: 231-245.

Moore, P.R., Brock, S.L., 1981. A physical and chemical survey of Ketetahi Hot Springs, Mt Tongariro, NZ. *NZ Journal of Science*, 24: 161-177.

Nairn, I.A., 1976. Atmospheric shock waves and condensation clouds from Ngauruhoe explosive eruptions. *Nature,* 259: 190-192.

Nairn, I.A., Kobayashi, T., Nakagawa, M., 1998. The ~10ka Multiple vent pyroclastic eruption sequence at Tongariro Volcanic Centre, TVZ, NZ: Part 1. Eruptive processes during regional extension. *Journal of Volcanology and Geothermal Research*, 86: 19-44.

Nakagawa, M., Nairn, I.A., Kobayashi, T., 1998. The ~10ka Multiple vent pyroclastic eruption sequence at Tongariro Volcanic Centre, TVZ, NZ: Part 2. Petrological insights into magma storage and transport during regional extension. *Journal of Volcanology and Geothermal Research*, 86: 45-65.

Ollier, C., 1988. *Volcanoes.* Basil Blackwell, Oxford, 228 pp.

Parfitt, E.A., Wilson, L., 1995. Explosive volcanic eruptions - IX. The transition between Hawaiian-style lava fountaining and Strombolian explosive activity. *Geophys. J. Int.*, 121: 226-232.

Parfitt, E.A., Wilson, L., 2004. A discussion of the mechanisms of explosive basaltic eruptions. *Journal of Volcanology and Geothermal Research*, In Press.

Price, R.C., Gamble, J.A., Hobden, B.J., 2000. Geology of the Tongariro Traverse. *State of the Arc 2000. Guide Book for field excursions on Ruapehu and Tongariro Volcanoes.*

Price, R.C., Hobden, B.J., Smith, R.T., Briggs, R.M., Gleadow, A.J.W., Kunz, P., 2003. *Volcanology of the Tongariro Crossing: A virtual field trip on CD-ROM.* The University of Waikato, Hamilton, New Zealand.

Rittmann, A., 1962. *Volcanoes and their activity.* John Wiley & Sons, New York, 305 pp.

Rogan, W., Blake, S., 1994. Trace element zonation of phenocrysts from Ngauruhoe Volcano, New Zealand: constraints on magmatic processes. *Mineral Magazine*, 58A: 783-784.

Spera, F.J., 2000. Physical properties of Magma. In: H. Sigurdsson (Editor), *Encyclopedia of Volcanoes*. Academic Press, San Diego, pp. 1417.

Stevens, N.F., 2002. Emplacement of the large andesite lava flow in the Oturere stream valley, Tongariro Volcano, from airborne interferometric radar. *New Zealand Journal of Geology and Geophysics*, 45: 387-394.

Tibaldi, A., 2003. Influence of cone morphology on dykes, Stromboli, Italy. *Journal of Volcanology and Geothermal Research*, 126: 79-95.

Topping, W.W., 1974. Some aspects of Quaternary history of Tongariro Volcanic Centre. *Ph.D. thesis, Victoria University*, Wellington.

Vergniolle, S., Brandeis, G., 1996. Strombolian explosions 1. A large bubble breaking at the surface of a lava column as a source of sound. *Journal of Geophysical Research*, 101(20,433-20,447).

Vergniolle, S.a.M., M., 2000. Hawaiian and Strombolian Eruptions. In: H. Sigurdsson (Editor), *Encyclopedia of Volcanoes*. Academic Press, San Diego, pp. 1417.

Vespermann, D., Schmincke, H. -V., 2000. Scoria cones and tuff rings. In: H. Sigurdsson (Editor), *Encyclopedia of volcanoes*. Academic Press, San Diego, pp. 683-696.

Wilcoxson, K.H., 1966. *Chains of Fire - The story of volcanoes*. Chilton Company, Philadelphia, 235 pp.

Williams, H., McBirney, A.R., 1979. *Volcanology*. Freeman, Cooper and Company, San Francisco, 397 pp.

Williams, K., 2001. *Volcanoes of the South Wind - A field guide to the Volcanoes and Landscape of Tongariro National Park*. Tongariro Natural History Society, 148 pp.

Wilson, C.J.N., Houghton, B.F., McWilliams, M.O., Lanphere, M.A., Weaver, S.D., Briggs, R.M., 1995. Volcanic and structural evolution of Taupo Volcanic Zone, New Zealand: a review. *Journal of Volcanology and Geothermal Research*, 68: 1-28.

Wohletz, K. and Heiken, G., 1992. *Volcanology and Geothermal Energy*. University of California Press, Berkeley, 432 pp.

Wolff, J.A., Sumner, J.M., 2000. Lava fountains and their products. In: H. Sigurdsson (Editor), *Encyclopedia of Volcanoes*. Academic Press, San Diego, pp. 1417.

Zeng, Y., Ingham, M., 1993. Modelling of gravity data from Tongariro National Park, *15th New Zealand Geothermal Workshop*, Geothermal Institute, University of Auckland.

APPENDIX ONE

METHODOLOGY FOR CALCULATING VESICULARITIES

METHODOLOGY FOR CALCULATING VESICULARITY

Modified from Houghton and Wilson (1989).

i) Where possible, select at least 15 juvenile clasts (the more clasts available for the procedure the more representative the result will be) which are between 4-10 cm.

ii) Back in the laboratory, clean and dry these samples.

iii) Set up a balance with a weighing stand on it as shown below in Figure A1.

iv) Tare the balance and weigh each individual clast (W_{clast}^{air}).

v) Cut out a 5 x 5 cm piece of parafilm and weigh in water. This averages out at ~0.03g (W_{sheet}^{water}).

vi) Wrap the clast in the parafilm sheets. Mould the parafilm into the surface irregularities which are not vesicles and across the edges of larger vesicles.

vii) Lower the arm of the stand so the wire basket is in the water but not touching the sides or bottom of the beaker.

viii) Lift the wire basket off the arm, place the clast in the basket and replace it. Shake in water to dislodge any small air bubbles. Record the weight ($W_{clast + sheet}^{water}$).

ix) Remove the wire basket and remove the clast.

NOTE: Any clasts which floated were ballasted with a sinker which was weighed in water (W_{sinker}^{water}).

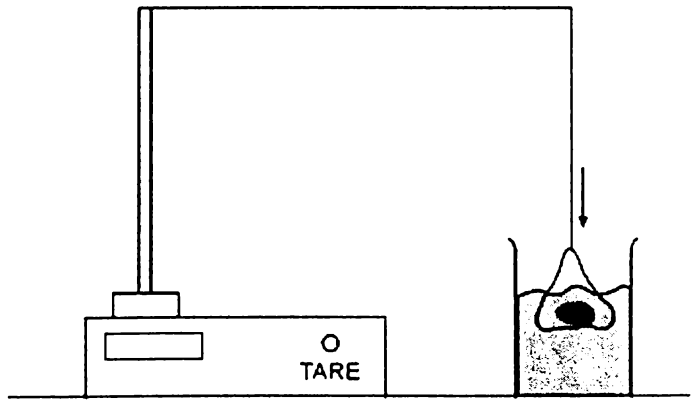

Figure A1 – Illustration of equipment and setup used to obtain weights for vesicularity calculations.

Calculations

Clast Specific Gravity (S.G)

$$(S.G.) = \frac{(W_{clast}^{air})}{(W_{clast}^{air}) + (W_{sheet}^{water}) - (W_{clast+sheet}^{water})}$$

If a lead weight was also used, then this becomes:

$$S.G. = \frac{(W_{clast}^{air})}{(W_{clast}^{air}) + (W_{sheet}^{water}) - ((W_{clast+sheet}^{water} + {}_{sinker}^{water}) - (W_{sinker}^{water}))}$$

From this the vesicularity of each clast can then be calculated using this formula:

$$V(\%) = \frac{100\ (\text{D.R.E density} - \text{clast density})}{\text{D.R.E density}}$$

The D.R.E or dense rock equivalent value used for the basaltic scoria density was 2.74 g/cm^{-3} (Wohletz and Heiken, 1992).

APPENDIX TWO

RED CRATER VESICULARITY RAW DATA

Sample Number	**58/01**	**58/03**	**67/3**	**67/4**	**59/02**
Locaility	SCR8 Southern Crater Rim	SCR7 Southern Crater Rim	SCR7 Southern Crater Rim	SCR6 Southern Crater Rim	SCR3 Southern Crater Rim
Waypoint	001 (15/5/03)	001 (15/5/03)	003 (13/6/03)	003 (13/6/03)	001 minus 4m (15/5/03)
Mean mass (g)	47.88	35.29	44.78	26.24	18.87
Standard Deviation Mass	35.92	35.21	38.33	22.93	31.50
Maximum mass (g)	122.44	149.90	194.28	103.70	158.77
Minimum Mass (g)	9.53	7.02	7.31	4.60	2.61
Mean Vesicularity (%)	69.23	64.03	67.87	72.89	75.38
Standard Deviation Vesicularity	5.59	8.29	6.93	4.62	2.96
Maximum Vesicularity (%)	80.66	79.31	78.28	80.26	80.55
Minimum Vesicularity (%)	59.49	47.04	41.06	62.23	65.80
Average 3 minimum Vesicularity (%)	60.54	47.32	51.61	63.24	68.63
Average 3 maximum Vesicularity (%)	78.69	77.53	77.09	79.24	79.96
Mean Density (g cm^{-3})	0.84	0.99	0.88	0.74	0.67
Standard Deviation Density	0.15	0.23	0.19	0.13	0.08
Maximum Density (g cm^{-3})	1.11	1.45	1.62	1.04	0.94
Minimum Density (g cm^{-3})	0.53	0.57	0.60	0.54	0.53
Average 3 minimum Density (g cm^{-3})	0.58	0.62	0.63	0.57	0.55
Average 3 maximum Density (g cm^{-3})	1.08	1.44	1.33	1.01	0.86

Summary Statistics for Vesicularity Measurements - Red Crater, Tongariro

Sample Number	60/01	67/6	60/02	100/1	100/2
Locaility	Eastern Crater Rim - ECR-a2	Eastern Crater Rim - ECR-a1	Unit A - Eastern inner-wall	Unit 11-Eastern inner-wall	Unit 10-Eastern inner-wall
Waypoint		004 (13/6/03)	002 (15/5/03)	005 (11/1/04)	005 (11/1/04)
Mean mass (g)	33.55	57.05	66.52	55.28	68.74
Standard Deviation Mass	20.49	43.05	42.55	35.07	45.42
Maximum mass (g)	89.25	207.53	158.07	171.03	196.86
Minimum Mass (g)	7.52	3.55	12.04	17.77	15.20
Mean Vesicularity (%)	74.02	76.84	51.54	68.22	65.91
Standard Deviation Vesicularity	5.01	5.10	7.95	5.54	5.24
Maximum Vesicularity (%)	80.88	82.08	70.58	75.95	76.93
Minimum Vesicularity (%)	60.91	62.88	30.47	53.58	56.13
Average 3 minimum Vesicularity (%)	63.30	65.13	36.09	56.71	57.72
Average 3 maximum Vesicularity (%)	80.43	81.91	66.94	75.51	75.17
Mean Density (g cm^{-3})	0.71	0.63	1.31	0.87	0.93
Standard Deviation Density	0.14	0.14	0.20	0.15	0.14
Maximum Density (g cm^{-3})	1.07	1.02	1.91	1.27	1.20
Minimum Density (g cm^{-3})	0.52	0.49	0.81	0.66	0.63
Average 3 minimum Density (g cm^{-3})	0.54	0.50	0.91	0.67	0.68
Average 3 maximum Density (g cm^{-3})	1.01	0.96	1.55	1.19	1.16

Summary Statistics for Vesicularity Measurements - Red Crater, Tongariro

Sample Number	100/3	100/4	100/7	100/8	100/9
Locality	Unit 9-Eastern inner-wall	Unit 7-Eastern inner-wall	Unit 5-Eastern inner-wall	Unit 4-Eastern inner-wall	Unit 3-Eastern inner-wall
Waypoint	005 (11/1/04)	005 (11/1/04)	005 (11/1/04)	005 (11/1/04)	005 (11/1/04)
Mean mass (g)	61.75	48.94	32.89	38.58	51.94
Standard Deviation Mass	48.93	54.89	33.29	31.18	72.01
Maximum mass (g)	191.66	231.56	152.21	134.73	371.70
Minimum Mass (g)	3.00	2.64	4.58	2.53	6.04
Mean Vesicularity (%)	62.28	66.03	72.48	69.13	67.01
Standard Deviation Vesicularity	7.42	8.30	3.60	4.63	6.54
Maximum Vesicularity (%)	73.61	77.77	77.55	78.50	76.39
Minimum Vesicularity (%)	47.74	46.13	62.37	59.45	51.97
Average 3 minimum Vesicularity (%)	49.38	49.29	64.28	61.03	53.57
Average 3 maximum Vesicularity (%)	73.21	76.99	77.20	77.04	75.44
Mean Density (g cm^{-3})	1.03	0.93	0.75	0.85	0.90
Standard Deviation Density	0.20	0.23	0.10	0.13	0.18
Maximum Density (g cm^{-3})	1.43	1.48	1.03	1.11	1.32
Minimum Density (g cm^{-3})	0.72	0.61	0.62	0.59	0.65
Average 3 minimum Density (g cm^{-3})	0.73	0.63	0.62	0.63	0.67
Average 3 maximum Density (g cm^{-3})	1.39	1.39	0.98	1.07	1.27

Summary Statistics for Vesicularity Measurements - Red Crater, Tongariro

Sample Number **Locaility** **Waypoint**	**100/10** Unit 2-Eastern inner-wall 005 (11/1/04)	**100/11** Unit 1-Eastern inner-wall 005 (11/1/04)	**100/12** Unit 1-Eastern inner-wall 005 (11/1/04)
Mean mass (g)	35.58	40.72	43.89
Standard Deviation Mass	36.97	34.33	34.63
Maximum mass (g)	196.52	157.15	152.81
Minimum Mass (g)	3.47	7.25	7.00
Mean Vesicularity (%)	71.50	67.63	67.93
Standard Deviation Vesicularity	4.81	7.15	6.52
Maximum Vesicularity (%)	78.14	78.47	77.88
Minimum Vesicularity (%)	60.11	48.21	54.89
Average 3 minimum Vesicularity (%)	61.51	50.77	55.96
Average 3 maximum Vesicularity (%)	77.69	77.88	77.03
Mean Density (g cm^{-3})	0.78	0.88	0.88
Standard Deviation Density	0.13	0.18	0.18
Maximum Density (g cm^{-3})	1.09	1.15	1.24
Minimum Density (g cm^{-3})	0.60	0.59	0.61
Average 3 minimum Density (g cm^{-3})	0.61	0.61	0.63
Average 3 maximum Density (g cm^{-3})	1.05	1.26	1.21

Summary Statistics for Vesicularity Measurements - Red Crater, Tongariro

Sample 58/01
Locality <-5 phi sampled from SCR8
Date Collected 5/15/2003

Clast No.	Air (g)	Water (g)	Ballast (g)	Wax (sheets)	S.G. (g cm^{-3})	Vesicularity(%)
18	37.847	129.03	162.14	13.5	0.530	80.66
20	13.070	152.93	162.14	5.5	0.582	78.76
31	12.236	155.43	162.14	5.5	0.640	76.64
22	43.176	140.47	162.14	10.5	0.663	75.80
14	23.543	152.58	162.14	7.0	0.698	74.53
26	20.544	153.84	162.14	7.0	0.707	74.20
24	30.686	150.43	162.14	8.0	0.720	73.72
8	9.532	158.58	162.14	4.0	0.721	73.69
2	56.133	140.96	162.14	12.5	0.723	73.61
29	50.022	145.06	162.14	14.5	0.741	72.96
9	10.914	158.79	162.14	4.0	0.759	72.30
5	41.827	149.41	162.14	10.5	0.762	72.19
3	27.380	154.28	162.14	9.0	0.771	71.86
10	44.086	149.57	162.14	11.0	0.773	71.79
16	15.448	158.11	162.14	6.0	0.786	71.31
33	17.431	158.30	162.14	6.0	0.813	70.33
7	102.378	139.82	162.14	17.0	0.818	70.15
13	121.090	136.18	162.14	20.5	0.820	70.07
27	21.023	158.08	162.14	6.5	0.832	69.64
17	14.052	160.05	162.14	5.0	0.863	68.50
12	18.079	160.81	162.14	5.0	0.924	66.28
15	21.824	161.38	162.14	6.0	0.959	65.00
11	35.543	160.87	162.14	7.5	0.960	64.96
21	71.374	160.27	162.14	12.5	0.970	64.60
25	122.440	161.09	162.14	16.0	0.988	63.94
28	105.754	161.68	162.14	18.0	0.991	63.83
32	109.808	162.52	162.14	15.0	0.999	63.54
6	43.895	162.44	162.14	8.5	1.001	63.47
30	99.990	165.06	162.14	15.0	1.025	62.59
23	38.803	164.00	162.14	8.0	1.044	61.91
19	27.568	1.80	0	6.0	1.062	61.24
4	98.376	7.02	0	14.5	1.072	60.88
1	74.282	7.72	0	11.5	1.110	59.49

Sample 58/03
Locality Sampled SCR7
Date Collected 5/15/2003

Clast No.	Air (g)	Water (g)	Ballast (g)	Wax (sheets)	S.G. (g cm^{-3})	Vesicularity (%)
37	42.666	129.90	162.14	11.5	0.567	79.31
13	74.132	119.76	162.14	15.5	0.634	76.86
8	18.158	152.38	162.14	6.5	0.646	76.42
28	7.964	158.09	162.14	4.5	0.656	76.06
5	27.112	149.38	162.14	9.0	0.675	75.36
19	15.071	157.30	162.14	5.5	0.751	72.59
18	15.275	3.44	0.00	4.0	0.783	71.42
15	21.360	157.77	162.14	6.5	0.824	69.93
34	17.153	158.88	162.14	5.5	0.834	69.56
35	13.013	159.84	162.14	4.5	0.842	69.27
14	20.916	158.89	162.14	6.0	0.859	68.65
24	26.040	158.11	162.14	6.3	0.861	68.58
6	11.802	160.40	162.14	4.0	0.864	68.47
17	21.684	158.99	162.14	6.0	0.867	68.36
36	7.023	161.19	162.14	3.5	0.869	68.28
12	9.019	160.92	162.14	3.5	0.872	68.18
38	56.304	157.28	162.14	11.0	0.916	66.57
30	21.453	160.51	162.14	6.0	0.922	66.35
11	20.932	160.57	162.14	5.5	0.923	66.31
3	22.337	160.97	162.14	5.0	0.944	65.55
31	26.130	161.17	162.14	6.5	0.957	65.07
26	12.647	161.75	162.14	4.5	0.960	64.96
1	36.009	161.18	162.14	7.0	0.969	64.64
25	20.096	161.93	162.14	6.0	0.981	64.20
32	50.734	2.68	0.00	8.5	1.050	61.68
10	11.080	0.76	0.00	3.5	1.063	61.20
9	147.829	171.55	162.14	18.0	1.064	61.17
16	32.468	165.08	162.14	6.5	1.092	60.15
21	29.323	3.95	0.00	6.0	1.148	58.10
27	18.627	2.57	0.00	4.0	1.151	57.99
40	12.420	1.81	0.00	4.0	1.158	57.74
4	111.891	179.23	162.14	15.0	1.175	57.12
2	107.920	179.50	162.14	13.0	1.187	56.68
22	23.342	3.91	0.00	5.0	1.192	56.50
20	12.949	2.20	0.00	3.5	1.193	56.46
23	40.627	9.85	0.00	7.5	1.310	52.19
7	40.788	172.47	162.14	7.5	1.329	51.50
39	21.744	6.72	0.00	4.5	1.434	47.66
33	149.899	46.59	0.00	14.5	1.445	47.26
29	35.513	11.21	0.00	5.5	1.451	47.04

Sample 59/02
Locality Sampled from SCR3
Date Collected 5/15/2003

Clast No.	Air (g)	Water (g)	Ballast (g)	Wax (sheets)	S.G. (g cm^{-3})	Vesicularity (%)
23	20.333	144.57	162.14	9.0	0.533	80.55
31	30.496	137.19	162.14	12.0	0.546	80.07
38	3.468	159.58	162.14	2.5	0.568	79.27
2	3.098	159.88	162.14	2.5	0.570	79.20
12	7.185	156.83	162.14	4.0	0.570	79.20
27	17.354	150.10	162.14	8.0	0.586	78.61
16	3.516	159.88	162.14	2.5	0.606	77.88
4	3.376	160.08	162.14	3.0	0.611	77.70
1	2.902	160.37	162.14	2.0	0.613	77.63
24	7.500	157.53	162.14	4.0	0.613	77.63
21	11.348	155.28	162.14	5.5	0.618	77.46
36	3.998	159.81	162.14	2.5	0.624	77.23
11	6.981	158.32	162.14	4.0	0.639	76.68
26	21.712	150.45	162.14	8.0	0.645	76.46
34	7.699	158.29	162.14	4.0	0.653	76.17
5	5.784	159.22	162.14	3.5	0.657	76.02
28	6.191	8.89	162.14	3.5	0.658	75.99
40	5.047	159.62	162.14	3.0	0.659	75.95
22	12.199	156.20	162.14	6.0	0.666	75.69
18	2.607	10.67	11.90	2.0	0.669	75.58
32	9.215	157.89	162.14	4.5	0.678	75.26
6	158.770	89.26	162.14	29.0	0.683	75.07
7	85.768	124.39	162.14	17.0	0.692	74.74
33	15.326	155.63	162.14	6.0	0.696	74.60
14	5.188	159.98	162.14	3.0	0.697	74.56
17	3.401	160.74	162.14	2.5	0.697	74.56
20	8.408	158.61	162.14	4.0	0.697	74.56
37	5.191	160.06	162.14	4.0	0.702	74.38
19	3.707	160.68	162.14	2.0	0.709	74.12
15	3.059	10.74	11.90	2.0	0.715	73.91
10	6.826	159.72	162.14	3.5	0.730	73.36
9	50.093	144.07	162.14	13.5	0.731	73.32
39	3.503	10.68	162.14	2.0	0.732	73.28
8	103.362	128.48	162.14	18.5	0.751	72.59
30	8.338	159.55	162.14	4.0	0.755	72.45
25	42.017	149.25	162.14	11.5	0.760	72.26
3	10.474	159.96	162.14	5.0	0.818	70.15
13	8.190	160.51	162.14	4.0	0.824	69.93
35	22.238	160.81	162.14	5.5	0.937	65.80
29	10.933	155.32	162.14	5.5		

Sample 60/01
Locality Eastern Crater Rim - ECR-a2
Date Collected 5/15/2003

Clast No.	Air (g)	Water (g)	Ballast (g)	Wax (sheets)	S.G. (g cm^{-3})	Vesicularity (%)
1	47.448	119.56	162.14	15.0	0.524	80.88
29	36.837	130.42	162.14	12.0	0.535	80.47
9	45.805	125.11	162.14	13.5	0.550	79.93
19	16.130	150.17	162.14	6.0	0.570	79.20
20	8.943	155.71	162.14	4.0	0.577	78.94
13	48.386	128.08	162.14	15.5	0.583	78.72
10	25.752	145.55	162.14	6.0	0.606	77.88
30	61.716	122.85	162.14	15.0	0.608	77.81
17	12.896	154.04	162.14	5.5	0.609	77.77
15	28.804	145.45	162.14	9.0	0.629	77.04
2	56.074	129.84	162.14	12.5	0.632	76.93
28	14.514	153.98	162.14	6.0	0.635	76.82
12	17.041	152.83	162.14	6.0	0.642	76.57
6	20.398	151.76	162.14	7.0	0.658	75.99
31	25.180	149.70	162.14	8.5	0.665	75.73
25	19.986	152.95	162.14	7.0	0.680	75.18
11	45.039	141.67	162.14	12.0	0.684	75.04
33	21.019	153.17	162.14	7.0	0.696	74.60
8	7.520	159.07	162.14	4.0	0.702	74.38
14	20.526	153.73	162.14	7.5	0.704	74.31
32	45.116	144.60	162.14	12.0	0.716	73.87
23	39.120	148.01	162.14	10.0	0.731	73.32
3	32.696	151.37	162.14	8.0	0.748	72.70
26	42.766	148.45	162.14	10.0	0.754	72.48
22	85.652	135.20	162.14	19.0	0.757	72.37
7	19.528	157.30	162.14	6.0	0.796	70.95
21	24.930	156.21	162.14	7.0	0.802	70.73
16	8.700	161.09	162.14	4.0	0.881	67.85
5	34.564	157.75	162.14	8.0	0.882	67.81
24	10.686	161.33	162.14	4.5	0.919	66.46
18	54.255	157.91	162.14	11.5	0.922	66.35
4	89.252	164.65	162.14	15.0	1.024	62.63
27	39.932	2.89	0	8.5	1.071	60.91

Sample 60/02
Locality Unit A - Eastern inner-wall
Date Collected 5/15/2013

Clast No.	Air (g)	Water (g)	Ballast (g)	Wax (sheets)	S.G. (g cm^{-3})	Vesicularity (%)
23	12.039	159.37	162.14	4.0	0.806	70.58
18	22.179	161.24	162.14	6.0	0.954	65.18
22	27.008	161.07	162.14	6.5	0.957	65.07
26	25.722	3.06	0.00	5.5	1.127	58.87
20	31.858	3.84	0.00	6.0	1.130	58.76
30	15.525	2.01	0.00	4.0	1.139	58.43
11	32.523	5.30	0.00	6.0	1.187	56.68
7	57.514	10.12	0.00	9.5	1.206	55.99
4	63.774	11.90	0.00	10.0	1.222	55.40
13	97.298	18.62	0.00	13.5	1.230	55.11
21	25.039	5.06	0.00	5.0	1.244	54.60
8	112.268	23.76	0.00	12.0	1.263	53.91
10	19.509	4.41	0.00	4.5	1.281	53.25
5	127.916	32.06	0.00	12.0	1.329	51.50
24	64.137	16.29	0.00	8.5	1.333	51.35
27	52.385	13.67	0.00	8.0	1.345	50.91
29	17.244	4.67	0.00	4.0	1.358	50.44
31	28.832	7.91	0.00	5.5	1.367	50.11
9	112.396	30.60	0.00	11.5	1.368	50.07
1	158.071	43.75	0.00	14.0	1.378	49.71
15	116.329	33.12	0.00	12.0	1.392	49.20
2	128.227	37.12	0.00	12.0	1.402	48.83
16	64.809	19.14	0.00	8.5	1.411	48.50
28	56.556	17.40	0.00	7.5	1.436	47.59
6	57.569	17.92	0.00	7.0	1.444	47.30
3	82.361	26.19	0.00	10.0	1.458	46.79
14	106.358	33.98	0.00	11.5	1.463	46.61
17	93.801	31.74	0.00	9.5	1.505	45.07
25	67.662	22.93	0.00	8.0	1.505	45.07
32	44.517	16.48	0.00	6.0	1.578	42.41
19	51.948	8.06	0.00	8.0	1.177	35.40
12	155.390	74.22	0.00	14.0	1.905	30.47

Sample 67/3
Locality SCR7 Southern Crater Rim
Date Collected 6/13/2003

Clast No.	Air (g)	Water (g)	Ballast (g)	Wax (sheets)	S.G. (g cm^{-3})	Vesicularity (%)
3	50.628	127.96	162.14	11.5	0.595	78.28
35	19.213	151.47	162.14	6.5	0.639	76.68
28	10.979	156.33	162.14	4.5	0.649	76.31
42	7.306	158.80	162.14	3.5	0.680	75.18
7	19.168	153.40	162.14	6.5	0.682	75.11
21	28.610	150.42	162.14	8.0	0.705	74.27
6	47.997	143.21	162.14	12.5	0.713	73.98
40	28.551	146.85	162.14	8.5	0.647	73.81
22	14.811	156.69	162.14	5.5	0.725	73.54
11	12.886	157.66	162.14	4.5	0.736	73.14
13	48.324	145.16	162.14	11.5	0.736	73.14
4	54.331	143.22	162.14	11.5	0.738	73.07
41	21.778	154.74	162.14	6.0	0.742	72.92
19	20.579	155.77	162.14	6.5	0.758	72.34
24	54.714	146.03	162.14	11.0	0.769	71.93
18	15.503	157.92	162.14	5.5	0.780	71.53
8	14.018	158.73	162.14	5.0	0.797	70.91
23	11.744	159.89	162.14	4.0	0.832	69.64
27	12.762	159.99	162.14	5.5	0.846	69.12
37	122.600	141.27	162.14	20.5	0.851	68.94
2	44.230	155.01	162.14	9.5	0.856	68.76
16	27.108	157.92	162.14	6.5	0.860	68.61
32	98.512	149.14	162.14	16.0	0.880	67.88
12	31.015	158.50	162.14	8.0	0.889	67.55
9	18.635	160.02	162.14	5.5	0.891	67.48
1	73.780	154.62	162.14	11.5	0.904	67.01
14	27.121	159.76	162.14	6.5	0.913	66.68
39	101.682	153.73	162.14	19.5	0.919	66.46
5	23.381	160.35	162.14	6.5	0.922	66.35
26	33.939	160.83	162.14	7.5	0.957	65.07
29	16.872	161.75	162.14	4.5	0.970	64.60
25	37.356	161.46	162.14	8.0	0.976	64.38
36	45.515	162.18	162.14	8.0	0.996	63.65
33	51.621	2.08	0.00	10.0	1.036	62.19
31	42.881	1.88	0.00	8.0	1.040	62.04
15	47.195	2.14	0.00	8.0	1.042	61.97
38	131.260	8.18	0.00	16.5	1.062	61.24
10	30.771	2.36	0.00	6.0	1.076	60.73
20	29.211	3.16	0.00	5.5	1.114	59.34
34	194.275	29.07	0.00	22.0	1.171	57.26
30	72.926	12.02	0.00	9.5	1.192	56.50
17	85.026	32.64	0.00	8.5	1.615	41.06

Sample 67/4
Locality SCR6 Southern Crater Rim
Date Collected 6/13/2003

Clast No.	Air (g)	Water (g)	Ballast (g)	Wax (sheets)	S.G. (g cm^{-3})	Vesicularity (%)
13	58.584	112.89	162.14	16.0	0.541	80.26
32	41.464	132.75	162.14	13.5	0.582	78.76
24	11.292	154.23	162.14	5.0	0.584	78.69
25	52.149	127.20	162.14	16.5	0.595	78.28
28	14.012	152.78	162.14	6.0	0.595	78.28
7	12.198	154.16	162.14	5.0	0.600	78.10
1	11.107	155.02	162.14	5.0	0.604	77.96
14	10.012	155.78	162.14	5.0	0.606	77.88
18	103.696	103.10	162.14	21.5	0.635	76.82
35	51.434	135.78	162.14	12.5	0.658	75.99
10	12.339	156.02	162.14	4.5	0.664	75.77
4	7.732	158.58	162.14	4.0	0.678	75.26
15	14.430	155.72	162.14	6.0	0.686	74.96
3	9.851	157.80	162.14	4.0	0.688	74.89
17	9.556	157.94	162.14	4.0	0.689	74.85
26	17.394	154.51.	162.14	6.5	0.690	74.82
31	25.783	151.43	162.14	7.5	0.702	74.38
5	8.730	158.64	162.14	4.0	0.707	74.20
37	23.779	152.58	162.14	7.0	0.709	74.12
38	14.349	156.44	162.14	5.0	0.710	74.09
21	9.615	158.63	162.14	4.0	0.726	73.50
34	20.659	154.80	162.14	6.5	0.733	73.25
36	32.706	151.31	162.14	8.0	0.747	72.74
30	37.516	149.80	162.14	9.0	0.748	72.70
12	29.875	152.70	162.14	7.5	0.756	72.41
2	16.058	157.78	162.14	6.0	0.780	71.53
19	39.392	151.77	162.14	10.0	0.787	71.28
20	23.866	156.03	162.14	6.0	0.791	71.13
33	80.634	144.19	162.14	17.0	0.814	70.29
29	28.817	156.23	162.14	7.5	0.824	69.93
40	81.920	145.18	162.14	15.0	0.825	69.89
11	5.234	161.26	162.14	2.5	0.846	69.12
16	19.470	158.87	162.14	6.0	0.849	69.01
9	4.603	161.66	162.14	2.0	0.895	67.34
27	12.611	161.12	162.14	4.0	0.917	66.53
6	14.921	162.04	162.14	4.5	0.984	64.09
23	19.406	162.13	162.14	4.5	0.993	63.76
8	6.073	162.18	162.14	2.5	0.994	63.72
22	29.944	1.21	0.00	7.0	1.035	62.23
39	104.782			22.0		

Sample 67/6
Locality Eastern Crater Rim - ECR-a1
Date Collected 6/13/2003

Clast No.	Air (g)	Water (g)	Ballast (g)	Wax (sheets)	S.G. (g cm^{-3})	Vesicularity (%)
3	25.568	135.96	162.14	9.5	0.491	82.08
16	51.369	110.51	162.14	14.5	0.497	81.86
24	26.228	136.07	162.14	8.0	0.499	81.79
31	4.784	8.03	11.90	3.0	0.512	81.31
4	56.244	109.76	162.14	17.0	0.515	81.20
11	9.548	153.81	162.14	6.0	0.529	80.69
23	22.241	143.47	162.14	8.5	0.540	80.29
22	60.213	111.61	162.14	16.5	0.541	80.26
27	101.649	80.94	162.14	22.0	0.554	79.78
7	43.749	127.56	162.14	12.0	0.566	79.71
21	48.708	124.45	162.14	12.5	0.561	79.53
15	41.755	130.08	162.14	10.0	0.563	79.45
1	78.651	105.98	162.14	17.5	0.573	79.09
28	70.392	110.17	162.14	16.5	0.573	79.09
2	48.790	126.44	162.14	12.0	0.575	79.01
5	78.063	105.74	162.14	19.5	0.578	78.91
9	47.823	128.40	162.14	12.5	0.584	78.69
19	40.878	133.68	162.14	11.5	0.587	78.58
18	32.131	141.25	162.14	10.0	0.603	77.99
25	154.768	63.02	162.14	28.0	0.609	77.77
32	3.547	9.73	11.9	3.0	0.611	77.70
12	56.245	132.14	162.14	13.0	0.649	76.31
20	3.560	10.82	11.90	2.0	0.672	75.47
30	115.645	110.16	162.14	19.5	0.688	74.89
29	72.537	133.57	162.14	14.5	0.714	73.94
10	40.726	148.71	162.14	9.5	0.748	72.70
6	30.948	156.27	162.14	8.0	0.835	69.53
26	69.828	149.69	162.14	12.5	0.845	69.16
8	68.249	153.38	162.14	11.5	0.882	67.81
17	56.092	160.55	162.14	10.5	0.967	64.71
14	207.534	166.45	162.14	25.5	1.017	62.88
13	128.952			22.5		

Sample 100/1
Locality Unit 11-Eastern inner-wall
Date Collected 11/1/2004

Clast No.	Air (g)	Water (g)	Ballast (g)	Wax (sheets)	S.G. (g cm^{-3})	Vesicularity (%)
17	129.784	121.23	187.56	25.0	0.659	75.95
11	61.921	158.48	187.56	13.5	0.677	75.29
21	21.755	177.39	187.56	7.0	0.677	75.29
5	105.466	138.32	187.56	21.0	0.679	75.22
9	43.781	169.34	187.56	12.0	0.702	74.38
14	30.778	176.27	187.56	10.0	0.726	73.50
7	33.516	175.53	187.56	10.0	0.731	73.32
12	66.352	167.25	187.56	14.0	0.762	72.19
19	25.589	180.49	187.56	9.0	0.777	71.64
20	45.486	175.98	187.56	11.5	0.792	71.09
3	65.576	171.27	187.56	16.0	0.796	70.95
26	19.887	183.11	187.56	6.0	0.811	70.40
6	53.220	177.59	187.56	11.5	0.838	69.42
10	67.378	175.61	187.56	14.0	0.845	69.16
4	43.538	180.16	187.56	11.0	0.849	69.01
22	33.734	181.81	187.56	8.5	0.849	69.01
8	72.811	177.22	187.56	14.5	0.871	68.21
15	57.766	179.90	187.56	13.5	0.877	67.99
13	31.847	183.66	187.56	8.5	0.885	67.70
28	17.773	186.07	187.56	6.0	0.914	66.64
1	171.026	173.42	187.56	24.5	0.920	66.42
23	34.296	185.02	187.56	10.0	0.924	66.28
25	23.195	186.86	187.56	6.0	0.963	64.85
27	30.891	187.44	187.56	8.0	0.988	63.94
18	85.698	189.18	187.56	13.5	1.014	62.99
2	99.411	189.68	187.56	16.5	1.017	62.88
24	23.528	188.22	187.56	6.0	1.021	62.74
30	67.669	8.04	-	11.0	1.129	58.80
16	39.421	193.18	187.56	8.0	1.158	57.74
29	55.444	12.16	-	10.0	1.272	53.58

Sample 100/2
Locality Unit 10-Eastern inner-wall
Date Collected 11/1/2004

Clast No.	Air (g)	Water (g)	Ballast (g)	Wax (sheets)	S.G. (g cm^{-3})	Vesicularity (%)
6	86.968	137.42	187.56	17.0	0.632	76.93
30	26.610	175.47	187.56	9.0	0.683	75.07
4	110.720	146.41	187.56	20.0	0.726	73.50
23	17.749	181.69	187.56	6.0	0.746	72.77
11	65.005	170.74	187.56	13.5	0.791	71.13
12	38.512	179.10	187.56	10.5	0.814	70.29
9	58.234	174.92	187.56	11.5	0.818	70.15
20	43.353	179.25	187.56	10.0	0.834	69.56
26	15.740	184.66	187.56	6.5	0.836	69.49
16	39.610	180.13	187.56	9.5	0.837	69.45
17	66.916	176.59	187.56	12.5	0.855	68.80
24	38.855	183.00	187.56	10.0	0.889	67.55
19	48.684	182.05	187.56	11.0	0.893	67.41
13	62.346	181.29	187.56	12.0	0.904	67.01
29	26.269	185.28	187.56	8.0	0.912	66.72
10	94.868	181.69	187.56	15.5	0.937	65.80
18	112.991	181.18	187.56	18.0	0.942	65.62
22	30.319	187.52	187.56	8.0	0.911	63.83
27	15.198	187.62	187.56	4.0	0.996	63.65
25	57.608	187.79	187.56	12.0	0.998	63.58
3	103.424	188.62	187.56	14.0	1.006	63.28
5	55.103	188.19	187.56	10.0	1.006	63.28
31	35.099	188.22	187.56	8.0	1.012	63.07
21	56.664	191.27	187.56	9.5	1.064	61.17
1	170.156	11.82	-	24.0	1.070	60.95
2	196.859	15.57	-	24.0	1.082	60.51
14	91.944	195.02	187.56	14.0	1.083	60.47
15	102.402	199.12	187.56	14.0	1.122	59.05
28	53.644	6.54	-	8.5	1.133	58.65
7	49.738	6.39	-	9.0	1.140	58.39
8	159.255	27.29	-	17.0	1.202	56.13

Sample 100/3
Locality Unit 9-Eastern inner-wall
Date Collected 11/1/2004

Clast No.	Air (g)	Water (g)	Ballast (g)	Wax (sheets)	S.G. (g cm^{-3})	Vesicularity (%)
36	5.806	185.44	187.56	3.5	0.723	73.61
39	4.143	186.07	187.56	2.0	0.728	73.47
30	14.730	182.88	187.56	6.0	0.752	72.55
11	35.315	176.27	187.56	9.5	0.753	72.52
6	133.322	153.85	187.56	22.5	0.795	70.99
35	8.196	185.65	187.56	4.0	0.801	70.77
34	6.299	186.43	187.56	3.0	0.838	69.42
16	15.882	184.75	187.56	6.5	0.841	69.31
4	100.479	169.28	187.56	17.5	0.842	69.27
38	3.000	187.07	187.56	2.0	0.845	69.16
9	60.400	179.65	187.56	12.0	0.880	67.88
37	4.744	186.98	187.56	2.0	0.881	67.85
23	44.276	183.03	187.56	10.0	0.902	67.08
31	29.399	184.87	187.56	7.5	0.910	66.79
15	61.080	182.60	187.56	11.5	0.920	66.42
19	37.136	184.93	187.56	9.0	0.928	66.13
32	13.350	187.01	187.56	5.0	0.950	65.33
3	42.732	185.82	187.56	8.0	0.956	65.11
13	59.171	187.66	187.56	10.5	0.996	63.65
10	39.085	187.76	187.56	8.5	0.999	63.54
18	49.294	187.87	187.56	9.5	1.001	63.47
21	26.580	2.17	-	7.0	1.080	60.58
5	61.539	5.54	-	10.5	1.093	60.11
17	148.345	15.70	-	17.5	1.114	59.34
14	117.254	14.61	-	14.5	1.138	58.47
28	47.869	6.08	-	9.0	1.138	58.47
25	74.157	11.47	-	11.0	1.177	57.04
2	125.091	19.81	-	15.5	1.183	56.82
33	28.518	4.71	-	6.0	1.189	56.61
22	47.243	8.39	-	8.5	1.213	55.73
12	191.657	34.90	-	18.5	1.218	55.55
20	71.169	13.17	-	11.0	1.220	55.47
26	82.092	15.67	-	11.0	1.230	55.11
29	61.248	13.20	-	10.0	1.267	53.76
27	85.418	21.01	-	12.0	1.319	51.86
1	133.370	33.32	-	14.0	1.327	51.57
8	159.631	40.28	-	17.0	1.332	51.39
7	129.595	37.29	-	14.5	1.397	49.01
24	49.516	15.18	-	8.0	1.432	47.74

Sample 100/4
Locality Unit 7-Eastern inner-wall
Date Collected 11/1/2004

Clast No.	Air (g)	Water (g)	Ballast (g)	Wax (sheets)	S.G. (g cm^{-3})	Vesicularity (%)
5	26.227	171.00	187.56	10.0	0.609	77.77
30	17.047	178.02	187.56	7.0	0.636	76.79
6	77.924	145.49	187.56	19.0	0.646	76.42
35	2.955	186.13	187.56	2.0	0.665	75.73
33	5.826	184.95	187.56	4.0	0.681	75.15
11	16.824	180.28	187.56	8.0	0.691	74.78
24	23.024	177.65	187.56	8.0	0.694	74.67
37	3.647	186.06	187.56	2.0	0.700	74.45
20	17.593	180.96	187.56	7.0	0.721	73.69
23	19.020	181.20	187.56	6.0	0.744	72.85
19	28.677	178.13	187.56	8.0	0.748	72.70
38	3.602	186.41	187.56	2.0	0.749	72.66
31	16.857	182.31	187.56	6.0	0.756	72.41
14	105.015	155.37	187.56	20.0	0.762	72.19
28	61.811	169.33	187.56	13.0	0.768	71.97
4	31.859	180.02	187.56	9.0	0.803	70.69
8	20.709	183.18	187.56	8.0	0.818	70.15
16	48.953	178.71	187.56	11.0	0.842	69.27
34	11.604	186.27	187.56	6.0	0.888	67.59
29	46.003	183.26	187.56	11.5	0.908	66.86
15	44.553	184.79	187.56	9.5	0.936	65.84
17	51.747	184.90	187.56	11.0	0.945	65.51
18	38.449	186.40	187.56	8.5	0.965	64.78
12	77.227	185.58	187.56	14.5	0.970	64.60
3	28.150	187.10	187.56	8.0	0.976	64.38
25	147.437	3.47	-	18.5	1.020	62.77
39	3.001	186.72	187.56	2.0	1.034	62.26
1	99.593	4.09	-	17.0	1.043	61.93
22	136.959	13.43	-	18.0	1.050	61.68
7	63.768	3.46	-	13.0	1.051	61.64
32	6.307	0.66	-	3.0	1.099	59.89
40	2.638	186.87	187.56	2.0	1.105	59.67
36	14.286	1.64	-	4.0	1.119	59.16
21	8.007	188.59	187.56	2.5	1.135	58.58
13	52.288	9.75	-	8.0	1.222	55.40
26	52.635	11.16	-	8.0	1.262	53.94
27	61.525	14.40	-	10.0	1.297	52.66
10	25.673	6.34	-	6.0	1.316	51.97
2	231.564	63.90	-	21.0	1.376	49.78
9	226.732	73.66	-	19.0	1.476	46.13

Sample 100/7
Locality Unit 5-Eastern inner-wall
Date Collected 11/1/2004

Clast No.	Air (g)	Water (g)	Ballast (g)	Wax (sheets)	S.G. (g cm^{-3})	Vesicularity (%)
5	259.126	-	-	38.0	-	-
2	89.880	131.82	187.56	16.0	0.615	77.55
28	9.296	182.19	187.56	5.0	0.627	77.12
6	42.262	163.52	187.56	18.0	0.632	76.93
12	29.026	172.89	187.56	8.0	0.661	75.88
38	8.125	183.53	187.56	4.0	0.662	75.84
17	12.824	181.26	187.56	5.0	0.665	75.73
10	35.548	170.69	187.56	11.0	0.674	75.40
37	10.519	182.62	187.56	5.0	0.674	75.40
8	49.463	164.53	187.56	10.5	0.679	75.22
16	64.286	158.29	187.56	14.0	0.684	75.04
27	13.305	181.69	187.56	6.0	0.687	74.93
13	32.753	173.76	187.56	13.0	0.698	74.53
15	52.396	165.38	187.56	14.0	0.699	74.49
29	8.366	184.11	187.56	4.0	0.701	74.42
22	57.713	163.61	187.56	14.0	0.703	74.34
11	71.422	158.65	187.56	14.0	0.709	74.12
24	12.099	182.82	187.56	5.0	0.712	74.01
34	6.509	185.18	187.56	4.0	0.722	73.65
7	26.741	177.69	187.56	9.0	0.725	73.54
33	6.622	185.30	187.56	4.0	0.736	73.14
36	5.596	185.83	187.56	4.0	0.752	72.55
4	75.444	163.81	187.56	15.5	0.757	72.37
21	18.212	181.97	187.56	6.0	0.759	72.30
25	22.214	180.78	187.56	8.0	0.760	72.26
35	6.461	185.65	187.56	4.0	0.761	72.23
32	4.948	186.30	187.56	2.5	0.788	71.24
26	12.325	184.42	187.56	4.0	0.791	71.13
19	27.472	181.24	187.56	8.5	0.807	70.55
9	17.378	183.76	187.56	5.0	0.815	70.26
31	4.577	186.69	187.56	2.0	0.831	69.67
1	152.211	158.85	187.56	24.0	0.838	69.42
23	19.988	183.93	187.56	7.0	0.839	69.38
30	13.829	186.12	187.56	5.0	0.897	67.26
20	26.567	184.92	187.56	7.5	0.903	67.04
18	27.544	185.67	187.56	8.0	0.928	66.13
14	25.775	187.21	187.56	8.5	0.977	64.34
3	117.363	191.69	187.56	19.5	1.031	62.37

Sample 100/8
Locality Unit 4-Eastern inner-wall
Date Collected 11/1/2004

Clast No.	Air (g)	Water (g)	Ballast (g)	Wax (sheets)	S.G. (g cm^{-3})	Vesicularity (%)
18	88.079	126.37	187.56	18.0	0.589	78.50
23	14.941	178.92	187.56	6.0	0.629	77.04
17	31.091	172.46	187.56	8.5	0.669	75.58
32	15.802	180.85	187.56	6.5	0.696	74.60
28	24.438	177.24	187.56	7.0	0.699	74.49
30	13.303	182.69	187.56	5.0	0.726	73.50
8	39.234	174.41	187.56	10.5	0.744	72.85
14	37.985	175.59	187.56	9.0	0.756	72.41
26	2.526	186.79	187.56	1.5	0.756	72.41
4	66.169	166.72	187.56	12.0	0.757	72.37
20	38.720	176.16	187.56	10.5	0.768	71.97
25	31.313	178.41	187.56	9.5	0.768	71.97
19	57.378	170.72	187.56	14.0	0.769	71.93
21	22.878	181.54	187.56	8.0	0.785	71.35
1	91.379	163.53	187.56	19.0	0.788	71.24
12	19.433	183.36	187.56	6.0	0.816	70.22
22	16.603	184.02	187.56	5.0	0.818	70.15
5	26.969	181.96	187.56	7.0	0.823	69.96
29	14.312	184.68	187.56	4.5	0.826	69.85
24	15.705	184.67	187.56	6.0	0.836	69.49
2	104.337	170.19	187.56	20.0	0.853	68.87
34	11.562	186.10	187.56	4.0	0.880	67.88
13	24.506	184.97	187.56	7.0	0.897	67.26
11	25.086	185.13	187.56	6.0	0.906	66.93
27	11.788	186.78	187.56	4.5	0.928	66.13
15	17.893	186.49	187.56	6.5	0.934	65.91
31	36.063	185.37	187.56	8.5	0.937	65.80
36	7.118	187.25	187.56	3.0	0.947	65.44
9	104.104	183.58	187.56	15.0	0.959	65.00
3	43.826	186.71	187.56	9.0	0.975	64.42
16	36.773	186.97	187.56	8.0	0.978	64.31
6	43.740	187.69	187.56	8.0	0.997	63.61
10	134.733	193.46	187.56	17.0	1.042	61.97
33	16.723	188.38	187.56	5.0	1.042	61.97
35	46.860	190.05	187.56	8.0	1.050	61.68
7	55.379	193.40	187.56	9.5	1.111	59.45

Sample 100/9
Locality Unit 3-Eastern inner-wall
Date Collected 11/1/2004

Clast No.	Air (g)	Water (g)	Ballast (g)	Wax (sheets)	S.G. (g cm^{-3})	Vesicularity (%)
24	77.735	145.54	187.56	16.0	0.647	76.39
17	63.131	158.50	187.56	14.5	0.682	75.11
23	14.601	181.12	187.56	4.0	0.690	74.82
7	65.391	159.29	187.56	15.5	0.695	74.64
31	14.012	181.58	187.56	4.5	0.696	74.60
21	19.694	179.19	187.56	6.0	0.697	74.56
20	15.558	180.95	187.56	4.5	0.698	74.53
19	33.978	174.63	187.56	9.0	0.720	73.72
32	10.646	184.27	187.56	3.0	0.759	72.30
29	10.420	184.53	187.56	4.0	0.768	71.97
5	13.053	183.92	187.56	5.0	0.775	71.72
8	9.235	185.09	187.56	4.0	0.781	71.50
34	14.046	183.78	187.56	4.5	0.782	71.46
6	17.852	184.00	187.56	5.5	0.827	69.82
35	16.261	184.90	187.56	4.0	0.854	68.83
11	80.304	174.56	187.56	15.5	0.856	68.76
28	10.082	186.02	187.56	3.0	0.861	68.58
26	14.089	186.13	187.56	4.0	0.901	67.12
13	148.481	174.39	187.56	23.0	0.915	66.61
18	13.857	186.71	187.56	4.0	0.935	65.88
14	40.450	185.29	187.56	8.5	0.941	65.66
4	81.274	184.12	187.56	13.0	0.955	65.15
25	35.227	186.71	187.56	6.0	0.972	64.53
3	202.765	185.68	187.56	22.0	0.988	63.94
22	32.573	187.57	187.56	8.0	0.993	63.76
30	6.035	187.72	187.56	2.0	1.017	62.88
33	17.552	0.45	-	4.0	1.019	62.81
12	24.313	188.46	187.56	6.0	1.031	62.37
15	48.871	2.16	-	8.5	1.041	62.01
2	126.918	7.52	-	17.0	1.058	61.39
9	117.217	201.89	187.56	14.5	1.134	58.61
1	371.703	45.91	-	32.0	1.138	58.47
27	17.018	3.36	-	4.0	1.235	54.93
16	8.770	1.90	-	2.0	1.266	53.80
10	24.682	193.63	187.56	5.0	1.316	51.97

Sample 100/10
Locality Unit 2-Eastern inner-wall
Date Collected 11/1/2004

Clast No.	Air (g)	Water (g)	Ballast (g)	Wax (sheets)	S.G. (g cm^{-3})	Vesicularity (%)
32	7.897	182.39	187.56	4.0	0.599	78.14
38	5.965	183.77	187.56	3.0	0.606	77.88
37	12.598	180.32	187.56	6.5	0.629	77.04
26	3.474	185.60	187.56	2.5	0.631	76.97
1	32.720	169.66	187.56	9.5	0.643	76.53
25	17.369	178.15	187.56	5.5	0.645	76.46
20	8.612	183.03	187.56	3.5	0.650	76.28
8	13.936	180.61	187.56	4.5	0.663	75.80
15	15.048	180.42	187.56	6.0	0.673	75.44
6	54.813	161.39	187.56	12.0	0.674	75.40
7	11.562	182.15	187.56	4.5	0.676	75.33
18	41.939	167.80	187.56	10.5	0.676	75.33
24	20.289	178.12	187.56	8.5	0.677	75.29
19	64.894	157.48	187.56	16.0	0.680	75.18
17	69.726	160.04	187.56	17.5	0.717	73.83
31	23.994	178.86	187.56	8.0	0.729	73.39
3	96.777	155.65	187.56	20.0	0.749	72.66
27	4.974	185.98	187.56	2.5	0.750	72.63
10	41.658	174.66	187.56	10.0	0.759	72.30
30	8.964	184.86	187.56	5.0	0.759	72.30
34	13.922	183.35	187.56	5.5	0.761	72.23
14	70.795	166.24	187.56	14.0	0.765	72.08
23	87.849	161.43	187.56	14.0	0.768	71.97
11	9.268	185.37	187.56	3.5	0.802	70.73
13	38.675	178.99	187.56	10.0	0.813	70.33
22	87.523	168.68	187.56	16.0	0.819	70.11
4	41.045	179.04	187.56	8.5	0.824	69.93
2	196.521	146.51	187.56	26.0	0.825	69.89
28	20.686	183.57	187.56	5.5	0.833	69.60
35	17.938	184.90	187.56	6.5	0.863	68.50
16	17.494	185.10	187.56	4.5	0.871	68.21
33	4.862	187.27	187.56	2.5	0.930	66.06
12	20.161	186.27	187.56	6.0	0.932	65.99
5	54.569	184.11	187.56	11.0	0.935	65.88
21	51.291	185.78	187.56	10.5	0.961	64.93
9	51.618	188.33	187.56	10.0	1.009	63.18
36	9.242	187.89	187.56	3.5	1.025	62.59
29	19.788	1.02	-	5.0	1.046	61.82
39	17.078	189.17	187.56	5.0	1.093	60.11

Sample 100/11
Locality Unit 1-Eastern inner-wall
Date Collected 11/1/2004

Clast No.	Air (g)	Water (g)	Ballast (g)	Wax (sheets)	S.G. (g cm^{-3})	Vesicularity (%)
31	32.339	165.36	187.56	10.0	0.590	78.47
11	18.416	176.15	187.56	9.0	0.612	77.66
8	23.878	172.98	187.56	10.5	0.616	77.52
37	9.635	182.13	187.56	5.0	0.633	76.90
25	13.548	180.92	187.56	5.0	0.666	75.69
28	58.146	160.51	187.56	13.0	0.679	75.22
4	36.226	171.47	187.56	11.0	0.688	74.89
17	12.739	182.70	187.56	4.5	0.718	73.80
18	24.047	178.51	187.56	8.5	0.721	73.69
29	49.408	168.78	187.56	11.5	0.721	73.69
27	50.579	169.69	187.56	12.0	0.735	73.18
36	8.513	184.94	187.56	4.0	0.756	72.41
41	12.341	184.11	187.56	5.0	0.774	71.75
26	15.621	183.30	187.56	5.5	0.779	71.57
6	59.788	172.75	187.56	14.0	0.797	70.91
24	22.210	182.37	187.56	6.5	0.805	70.62
12	47.661	176.48	187.56	13.0	0.806	70.58
5	116.863	160.96	187.56	20.0	0.811	70.40
38	9.696	185.73	187.56	4.0	0.833	69.60
34	20.066	183.78	187.56	6.0	0.835	69.53
43	13.463	185.36	187.56	4.0	0.853	68.87
14	23.585	184.27	187.56	6.0	0.872	68.18
33	16.461	185.56	187.56	4.0	0.886	67.66
3	127.884	171.87	187.56	18.0	0.887	67.63
20	8.297	186.62	187.56	3.0	0.890	67.52
9	42.178	182.72	187.56	10.0	0.891	67.48
16	40.368	183.28	187.56	9.0	0.899	67.19
19	59.752	184.20	187.56	12.0	0.941	65.66
21	7.246	187.24	187.56	3.0	0.946	65.47
10	51.279	185.27	187.56	11.5	0.951	65.29
2	48.381	185.62	187.56	11.5	0.955	65.15
39	35.336	186.88	187.56	7.0	0.975	64.42
22	34.312	187.59	187.56	9.0	0.993	63.76
30	51.014	187.43	187.56	8.5	0.993	63.76
23	31.175	187.94	187.56	7.0	1.005	63.32
42	32.122	189.10	187.56	6.0	1.044	61.90
35	16.995	1.19	-	4.5	1.066	61.09
13	122.356	8.28	-	16.0	1.068	61.02
15	50.941	8.83	-	9.0	1.202	56.13
32	22.626	3.97	-	5.0	1.203	56.09
7	78.985	17.64	-	11.0	1.281	53.25
40	37.239	9.78	-	6.0	1.347	50.84
1	157.145	20.92	-	19.0	1.149	48.21

Sample 100/12
Locality Unit 1-Eastern inner-wall
Date Collected 11/1/2004

Clast No.	Air (g)	Water (g)	Ballast (g)	Wax (sheets)	S.G. (g cm^{-3})	Vesicularity (%)
20	40.089	161.82	187.56	12.5	0.606	77.88
32	8.991	182.22	187.56	4.0	0.622	77.30
21	53.900	160.18	187.56	13.0	0.660	75.91
13	14.958	180.24	187.56	5.0	0.667	75.66
19	40.009	168.33	187.56	10.0	0.672	75.47
15	29.687	174.58	187.56	9.0	0.691	74.78
4	80.592	152.21	187.56	14.0	0.693	74.71
18	22.915	178.71	187.56	6.5	0.717	73.83
8	35.875	174.44	187.56	12.0	0.727	73.47
29	50.661	170.14	187.56	12.0	0.740	72.99
24	43.368	173.55	187.56	11.0	0.752	72.55
6	14.500	183.02	187.56	5.0	0.756	72.41
33	11.576	183.99	187.56	5.0	0.757	72.37
22	17.429	182.20	187.56	5.0	0.760	72.26
28	22.597	181.75	187.56	6.5	0.790	71.17
34	6.997	185.96	187.56	2.5	0.807	70.55
30	46.247	182.25	187.56	11.0	0.891	67.48
35	16.194	185.74	187.56	4.0	0.893	67.41
23	57.135	181.37	187.56	12.0	0.897	67.26
26	16.600	185.88	187.56	5.0	0.901	67.12
25	61.560	181.35	187.56	11.0	0.904	67.01
11	14.388	186.52	187.56	5.0	0.924	66.28
10	99.134	181.63	187.56	14.0	0.940	65.69
16	48.899	185.01	187.56	11.0	0.944	65.55
7	78.845	184.72	187.56	14.5	0.960	64.96
12	19.013	187.82	187.56	5.5	1.005	63.32
27	17.063	188.58	187.56	4.0	1.056	61.46
17	76.434	4.67	-	11.0	1.060	61.31
5	129.620	195.75	187.56	15.5	1.063	61.20
3	70.072	4.68	-	12.0	1.066	61.09
31	10.342	188.53	187.56	4.0	1.090	60.22
9	36.339	191.86	187.56	6.5	1.127	58.87
2	72.268	11.76	-	11.0	1.188	56.64
1	152.806	25.74	-	22.0	1.196	56.35
14	19.136	3.80	-	5.0	1.236	54.89

APPENDIX THREE

SEM METHODOLOGY

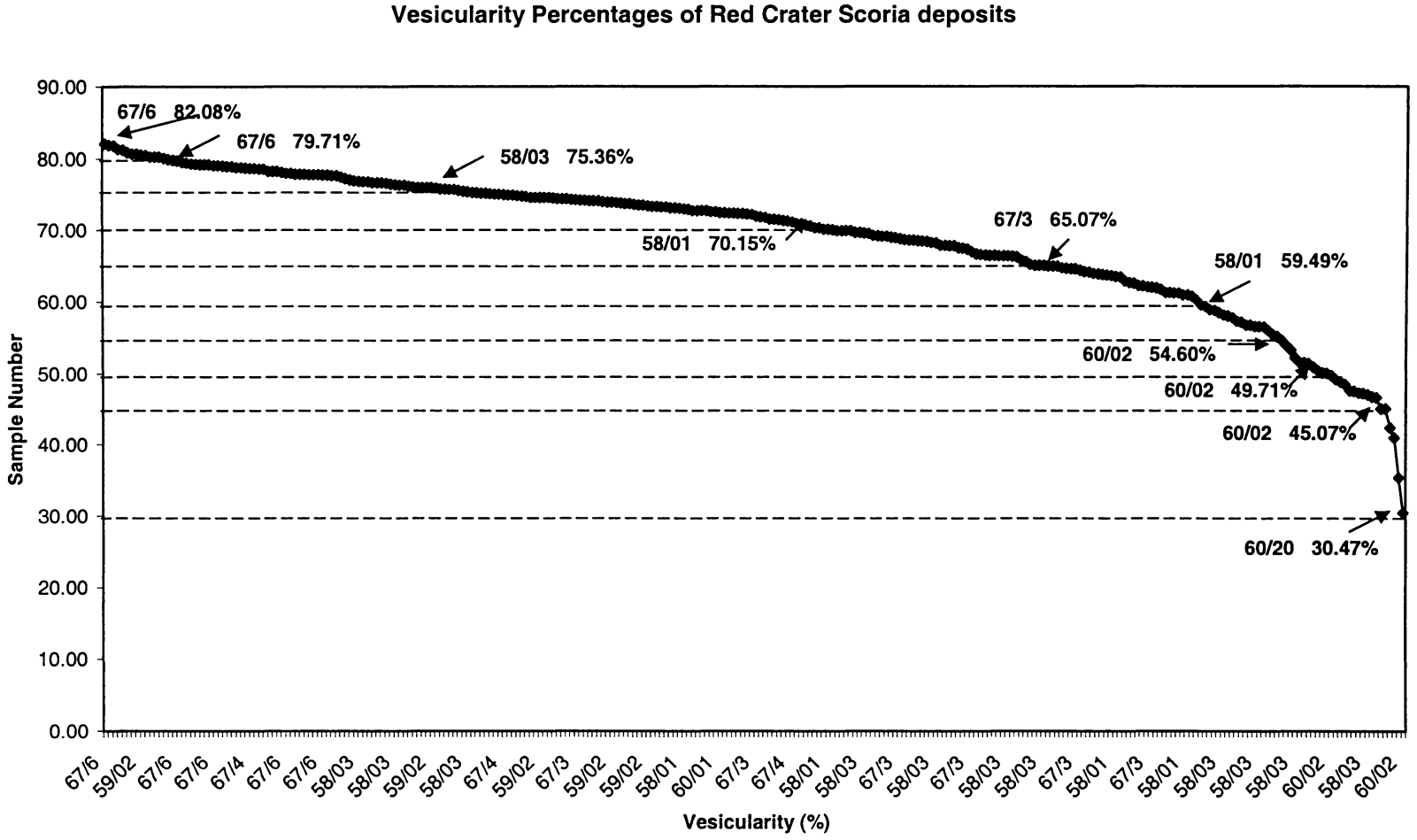

Appendix 3a - Each line intersects a point which corresponds with a unit sampled and the clast within that unit.

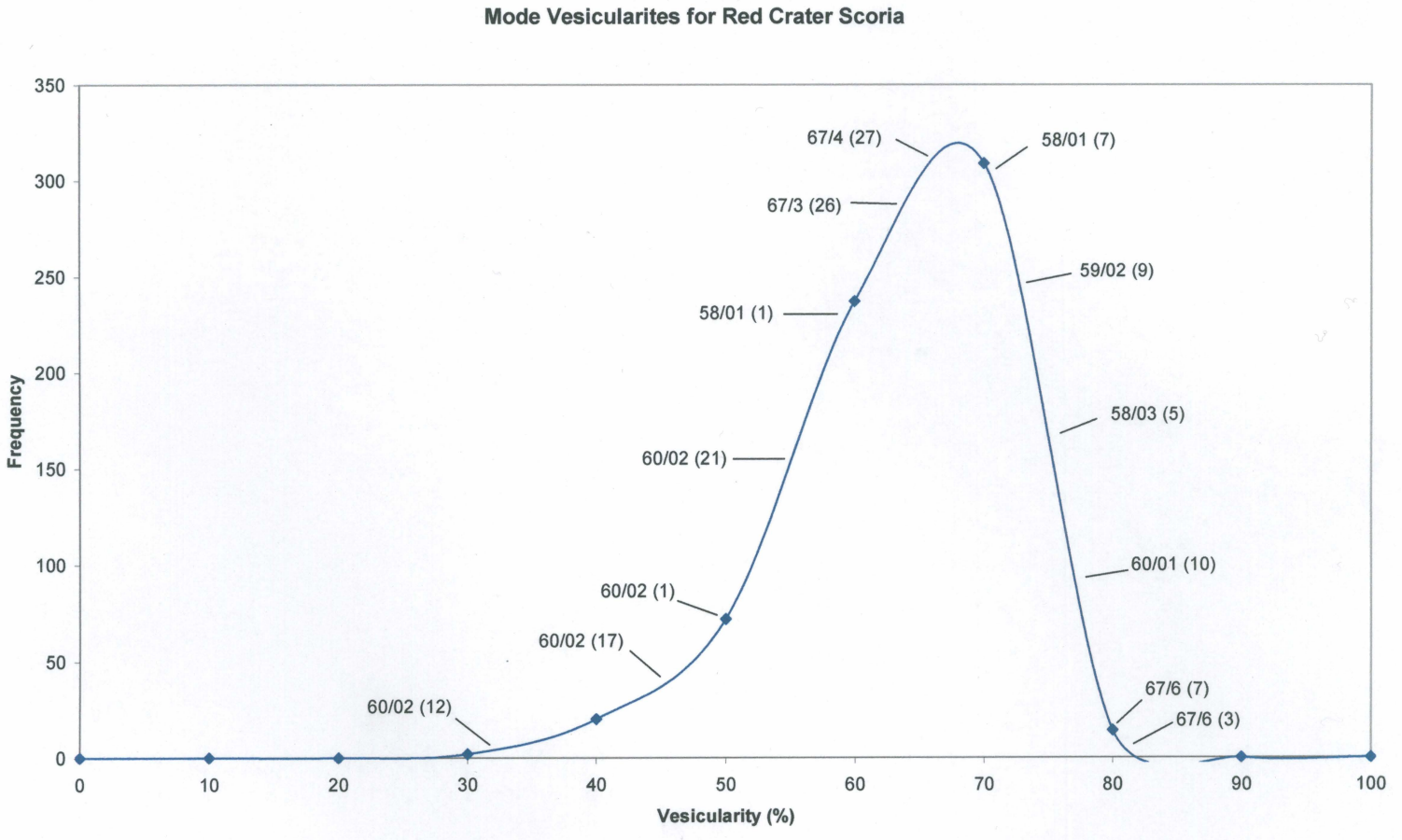

Appendix 3b – Frequency curve of the Red Crater samples showing where the selected 13 clasts fit into this curve.

APPENDIX FOUR

SEM AND THIN SECTION PREPARATION

SEM AND THIN SECTION PREPARATION

(modified from Dept. of Earth Science Instruction Sheet)

This methodology can be followed for samples designated to both SEM and Thin Section analysis.

1 Cut rock sample into a block (~3.5 x 2.4 x 2.4 cm) with a rock saw and write the sample number on the block.

2 If the sample is soft (or porous), dry it on the hot plate (70°C) for approximately three hours, or longer if required. Then either surface impregnate or fully impregnate (depending on just how porous it is) it with Araldite K142 glue, using a ratio of 2 grams (resin): 0.4 grams (hardener) for two thin sections.

3 Grind one side of the sample until no saw marks can be seen. Use #600 polish powder on a large frosted glass plate. Frost a glass slide (4.5 x 2.7 cm) with the diamond disco grinder (Struers Discoplan –TS). Then dry samples on the hot plate (70°) for approximately three hours.

4 Mount the sample on the glass with Hillquist glue using a ratio of 0.7g (resin): 0.3g (hardener) for approximately four thin sections. Make sure all bubbles are removed from between the sample and the glass. Then cure on the hot plate (60°C) for approximately two hours or longer if required.

5 For SEM analysis: Trim the sample to ~ 3-4mm with the diamond disco saw (Struers Discoplan –TS), then polish to ~3mm. This is the final step in preparing samples for SEM work. Samples will be analysised using a paper grinder. The samples are then taken to a SEM laboratory where samples are coated with platinum to make them conductive using a Hitachi E-1030 Sputter Coater. They are then put into a Hitachi S-4000 Field Emission Scanning Electron Microscope where they can be viewed and photographed.

For Thin section analysis: Trim the sample to ~ 1mm (less than the glass thickness) with the diamond disco saw (Struers Discoplan –TS) and write sample number on the glass using a diamond pen.

6 Using the discoplan, grind the samples with a progress rate of two small divisions (20 mμ) from the beginning to 50 small divisions, then with a progress rate of 1.5 small divisions from 50 to ~130 small divisions. When you can see the light through the sample, grind the sample with a progress rate of 0.5 or 1 small divisions (5 or 10 mμ) and check the slide frequently (every 1 or 2 small divisions) by comparing the mineral (quartz, feldspar or calcite) colour (at a thickness of ~ 40 mμ) of the sample with the mineral table or the mineral colour of a standard thin section. Then grind it a little to ~ 30 mμ with paper (#1200) grinder or on the frosted glass slide. Move the sample slowly over the grinding wheel (speed of the moving handle).

7 Put one drip of Petropoxy on the sample (using a ratio of 1 ml resin: 0.1 mls hardener by volume for ~ 10 thin sections) and then put a cover slip on top, make sure there are no bubbles between the cover slip and the sample. Do not cover samples that are intended for cathodoluminescence (CL), microscopy, elemental microprobing or any other surface analysis techniques.

8 Clean glue on the thin section with a blade or acetone, and number the slide using a diamond pen.

APPENDIX FIVE

PETROGRAPHY RAW DATA

Sample Locality	18/2 Flow 11	24/2 Flow 11	34/1 Tong. Trig Lava - ECR	34/3 Tong. Trig Lava Ballistic	34/3 Tong. Trig Lava Ballistic
Hand Speciman					
Colour	Grey	Grey	Light grey	Grey	Light grey
Mafic : Felsic ratio	85:15	85:15	70:30	70:30	70:30
Fabric	Porphyritic	Porphyritc	Porphyritic	Porphyritic	Porphyritic
Crystals visable	Plag, Olivine	Plag, Olivine	Plag, Hyp	Plag, Hyp	Plag, Hyp
Crystal volume %	30%	45%	60%	70%	70%
Crystal Sizes	0.5 - 6mm	0.5 - 4mm	0.33 - 3mm	1 - 5mm	1 - 5mm
Grain Size	Medium	Medium	Medium	Medium	Medium
Comments					
Vesicularity					
Shape of vesicles	Subrounded	Subrounded	-	Subangular	Subangular
Min and Max sizes	1 - 12mm	0.5 - 4mm	-	1 - 2mm	1 - 2mm
Coalascence	Yes	Yes	-	No	No
Vesicularity %	70%	80%	0%	5%	5%
Thin Section					
Groundmass	Intergrannular Plag laths Blebs Oliv, Hyp, Aug Fine grained	Intergranular Plag laths Fine grained	Intersertal Plag laths Fine grained	Intergrannular Plag laths Blebs Hyp Fine grained	Intergranular Plag laths Blebs Hyp Fine grained
Phenocrysts	Plag > Oliv > Hyp > Aug	Plag > Oliv > Aug	Plag > Hyp > Aug	Plag > Hyp > Aug > Oliv > Titn	Plag > Aug > Hyp > Oliv > Opaq
Shape	All Subhedral	All Subhedral	Euh > Subh > Subh	Euh > Sub > Sub > Euh > Sub	All Subhedral
Proportion (of crystals)	80% > 10% > 5% > 3%	80% > 10% > 10%	70% > 15% > 10%	90% > 8% > 2% > 1% > 1%	90% > 5% > 4% > 2% > 1%
Maximum sizes	100 > 50 > 25 > 12	80 > 40 > 38	12 > 10 > 20	25 > 15 > - > 4 > 3	32 > 12 > 5
Point Count done	Yes	No	Yes	Yes	No
Comments	Poorly sorted	Olivine clusters	Plagioclase twining Intergrown plag	Oscillitory zoning/twining in plag	9 x 7 mm lithic present

Sample Locality	36/1 Tong. Trig in SF Exp. Pit	38/1 Flow 9	38/1 Flow 9	39/1 Flow 9
Hand Speciman				
Colour	Light grey	Dark brown/grey	Dark brown/grey	Dark grey
Mafic : Felsic ratio	70:30	95:5	95:5	90:10
Fabric	Porphyritic	Porphyritic	Porphyritic	Porphyritic
Crystals visable	Plag, Olivine	Plag, Olivine	Plag, Olivine	Plag, Olivine
Crystal volume %	75%	50%	50%	40%
Crystal Sizes	1 - 3mm	1 - 4mm	1 - 4mm	0.5 - 3mm
Grain Size	Medium	Medium	Medium	Medium
Comments				
Vesicularity				
Shape of vesicles	Subrounded	Rounded	Rounded	Rounded
Min and Max sizes	0.5 - 1mm	0.5 - 6mm	0.5 - 6mm	0.5 - 7mm
Coalascence	No	Yes	Yes	Very minor amounts
Vesicularity %	1%	70%	70%	80-90%
Thin Section				
Groundmass	Intergranular Plag laths Blebs Olivine Fine grained	Intergranular Plag laths Blebs Olivine Fine grained	Intergranular Plag laths Fine grained	Intergranular Plag laths Fine grained
Phenocrysts	Plag > Aug > Oliv > Hyp > Opaq	Plag > Oliv > Aug	Plag > Oliv > Aug	Plag > Oliv > Aug
Shape	All Subhedral	All Subhedral	All Subhedral	All Subhedral
Proportion (of crystals)	80% > 8% > 5% > 3% > 2%	70% > 10% > 10%	80% > 10% > 1%	80% > 10% > 5%
Maximum sizes	130 > 70 > 25 > 35	52 > 20 > 15	85 > 25 > 8	95 > 25 > 28
Point Count done	Yes	No	No	Yes
Comments	Broken, intertwined Plagioclase	Oscillitory zoning in Plag	Oscillitory zoning in Plag	Blebs Oliv in some plag Agglom Olivine - Plag

Sample Locality	39/1 Flow 9	40/1 Lava channel of Flow 9	40/2 Lava channel of Flow 9	46/3 Loose clast from crater floor
Hand Speciman				
Colour	Dark grey	Dark grey/black	Grey	Dark Red
Mafic : Felsic ratio	90:10	90:10	80:20	90:10
Fabric	Porphyritic	Porphyritic	Porphyritic	Porphyritic
Crystals visable	Plag, Olivine	Plag, Olivine	Plag, Olivine	Plag
Crystal volume %	40%	35%	30%	40%
Crystal Sizes	0.5 - 3mm	1 - 4mm	0.5 - 1mm	0.5 - 4mm
Grain Size	Medium	Medium	Medium	Medium
Comments				Contains a 6 x 5mm lithic, green in colour, wall rock.
Vesicularity				
Shape of vesicles	Rounded	Subrounded	Subrounded	Subrounded
Min and Max sizes	0.5 - 7mm	0.5 - 6mm	0.5 - 4mm	0.5 - 10mm
Coalascence	Very minor amounts	Yes	Yes	Yes
Vesicularity %	80-90%	75%	70%	70%
Thin Section				
Groundmass	Intergrannular Plag laths Blebs Oliv, Aug, Hyp	Intergranular Plag laths Blebs of Oliv, Hyp, Aug fine grained	Intergrannular Plag laths Fine grained	
Phenocrysts	Plag > Oliv > Hyp > Aug	Plag > Oliv > Aug > Hyp	Plag > Oliv > Aug > Hyp > Opaq	
Shape	All Subhedral	All Subhedral	All Subhedral	
Proportion (of crystals)	80% > 10% > 5% > 5%	70% > 15% > 11% > 5%	80% > 8% > 5% > 1% > 1%	
Maximum sizes	65 > 20 > 70 > 30	65 > 130 > 15 > 35		
Point Count done	No	Yes	No	
Comments		Oliv/Hyp agglomerate Limited oscillitory zoning	Rock fragment - Full 2-4 Plag	

Sample Locality	46/3 Loose clast left dike, crater floor	47/1 Flow 7	47/4 Lava Channel Flow 7	47/5 Lava Channel Flow 6
Hand Speciman				
Colour	Red	Grey	Light grey/brown	Light grey
Mafic : Felsic ratio	60:40	85:15	85:15	70:30
Fabric	Porphyritic	Porphyritic	Porphritic	Porphyritic
Crystals visable	Plag, Olivine	Plag, Olivine	Plag, Olivine	Plag
Crystal volume %	15%	50%	40%	35%
Crystal Sizes	0.5 - 3mm	1 - 4mm	1 - 3mm	0.5 - 3mm
Grain Size	Medium	Medium	Medium	Medium
Comments	Contains inclusion (45 x 25mm) of re-worked scoria, honeycomb like texture, black, Plag rich			
Vesicularity				
Shape of vesicles	Subrounded	Subrounded	Subangular	Subangular
Min and Max sizes	0.5 - 15mm	0.5 - 7mm	0.5 - 9mm	0.5 - 2mm
Coalascence	Yes	Yes	Yes	Yes
Vesicularity %	70%	85%	50%	20%
Thin Section				
Groundmass		Glassy Matrix - 16.8% Microlite Matrix - 32.2%	Intergranular Plag laths Blebs of Oliv	Intergrannular Plag laths Iddingsite Fine grained
Phenocrysts		Plag > Oliv > Aug > Hyp	Plag > Oliv > Aug	Plag > Oliv > Aug
Shape			All Subhedral	All Subhedral
Proportion (of crystals)		10% > 6.4% > 6% > 0.8%	80% > 7% > 2%	80% > 15% > 10%
Maximum sizes			75 > 20 > 32	40 > 20 > 32
Point Count done		Yes	Yes	No
Comments		27.8% vesicles in thin section	Oscillitory zoning in Plag	

Sample Locality	48/2 Lava Channel Flow 6	49/1 Lava Channel Flow 6	49/2 Flow 6	50/1 Upper lobe Flow 2
Hand Speciman				
Colour	Light grey	Light grey	Medium grey/brown	Grey
Mafic : Felsic ratio	70:30	80:20	90:10	60:40
Fabric	Porphyritic	Porphyritic	Porphyritic	Porphyritic
Crystals visable	Plag, Olivine	Plag, Olivine	Oliv, Plag	Plag, Oliv, Hyp
Crystal volume %	40%	30%	40%	90%
Crystal Sizes	1 - 2mm	0.5 - 7mm	0.5 - 4mm	0.5 - 9mm
Grain Size	Medium	Medium	Medium	Medium-Coarse
Comments				
Vesicularity				
Shape of vesicles	Subrounded, elongated	Subrounded to elongate	Rounded, elongate	Irregular
Min and Max sizes	0.5 - 10mm	1 - 7mm	0.5 - 3mm	0.5 - 20mm
Coalascence	Yes	Yes	Yes	Yes
Vesicularity %	50%	75%	50%	10%
Thin Section				
Groundmass	Intergrannular Plag laths Blebs Oliv, Hyp, Aug Fine grained	Intergranular Plag laths Blebs Plag, Aug, Oliv Fine grained	Intergrannular Plag laths Fine grained	Intergrannular Plag laths
Phenocrysts	Plag > Oliv > Hyp > Aug	Plag > Aug > Oliv	Plag > Oliv > Aug > Hyp	Plag > Aug > Oliv > Hyp > Opaq
Shape	All Subhedral	All Subhedral	All Subhedral	All Subhedral
Proportion (of crystals)	70% > 15% > 5% > 5%	80% > 10% > 5%	75% > 10% > 10% > 5%	60% > 15% > 10% > 5% > 5%
Maximum sizes	150 > 42 > 38 > 15	60 > 60 > 30	65 > 22 > 32 > 70	100 > 65 > 150 > 50
Point Count done	Yes	Yes	No	Yes
Comments	Complex plagioclase twin Compositional zoning (hypersthene, olivine rim)	Oscillitory zoning Plag 7mm Olivine crystal	Agglomerocryst Oliv, Aug	Lithic 5 x 5mm present - pumice? Smaller olivine clusters

Sample Locality	51/1 Flow 5	51/2 Middle lobe Flow 2	51/3 Flow 8	52/1 Middle lobe Flow 2
Hand Speciman				
Colour	Light grey	Grey	Medium grey	Light grey
Mafic : Felsic ratio	60:40	80:20	70:30	70:30
Fabric	Porphyritic	Porphyritic	Porphyritic	Porphyritic
Crystals visable	Plag, Hyp	Plag, Oliv, Hyp	Plag, Olivine	Oliv, Hyp, Plag
Crystal volume %	90%	75%	50%	85%
Crystal Sizes	1 - 5mm	1 - 5mm	0.5 - 4mm	1 - 4mm
Grain Size	Medium	Medium	Medium	Medium
Comments				
Vesicularity				
Shape of vesicles	Subangular	Irregular	Subangular, elongated	Irregular shapes
Min and Max sizes	0.5 - 1.5mm	0.5 - 3mm	0.5 - 4mm	0.5 - 4mm
Coalascence	No	Yes	Yes	Yes
Vesicularity %	5%	15%	10%	10%
Thin Section				
Groundmass	Intergranular Plag laths Fine grained	Intergranular Plag laths Blebs of Oliv, Aug Fine grained	Intergranular Plag laths Blebs Oliv, Hyp, Aug Fine grained	Intergranular Plag laths
Phenocrysts	Plag > Hyp > Aug > Oliv	Plag > Oliv > Aug > Opaq	Plag > Oliv > Aug > Hyp	Plag > Oliv > Hyp > Aug > Opaq
Shape	All Subhedral	All Subhedral	All Subhedral	All Subhedral
Proportion (of crystals)	85% > 10% > 4% > 1%	75% > 15% > 5% > 5%	70% > 20% > 5% > 2%	70% > 20% > 5% > 1% > 1%
Maximum sizes	60 > 10 > 50 > 10	80 > 40 > 52	90 > 20 > 20 > 33	150 > 40 > 35 > 135
Point Count done	Yes	Yes	Yes	Yes
Comments	Oscillatory zoning in Plag Inter-penetrating twins of Hyp and Oliv	Oscillitory zoning in Plag	Oscillatory zoning in Plag	Opaques within olivine crystals

Sample Locality	56/2 Flow 10	57/1 Flow 9	62/1 Tong. Trig Sth face	65/2 Flow 10
Hand Speciman				
Colour	Light grey	Light grey	Light grey	Black
Mafic : Felsic ratio	80:20	70:30	70:30	98:2
Fabric	Porphyritic	Porphyritic	Porphyritic	Porphyritic
Crystals visable	Plag, Oliv, Hyp	Plag, Oliv	Plag, Oliv, Hyp	Plag
Crystal volume %	20%	65%	85%	40%
Crystal Sizes	0.5 - 3mm	0.5 - 4mm	0.5 - 6mm	0.5 - 4mm
Grain Size	Medium	Medium	Medium	Medium
Comments				
Vesicularity				
Shape of vesicles	Elongated, Subrounded	Subrounded, Elongated	Subrounded	Rounded, Subrounded
Min and Max sizes	0.5 - 16mm	0.5 - 10mm	0.5 - 2mm	0.5 - 6mm
Coalascence	Yes	Yes	No	Yes
Vesicularity %	80%	70%	1%	15%
Thin Section				
Groundmass	Intergrannular Plag laths Iddingsite, Blebs Oliv, Hyp, Aug Fine grained	Intergranular Plag laths Fine grained	Intergrannular Plag laths Iddingsite	Intergranular Plag laths Iddingsite Fine grained
Phenocrysts	Plag > Oliv > Aug > Hyp > Opaq	Plag > Oliv > Aug > Hyp	Plag > Hyp > Oliv > Aug	Plag > Aug > Oliv > Opaq > Hyp
Shape	All Subhedral	All Subhedral	All Subhedral	All Subhedral
Proportion (of crystals)	60% > 15% > 10% > 10% > 5%	80% > 10% > 5% > 3%	70% > 10% > 10% > 10%	80% > 8% > 5% > 2% > 1%
Maximum sizes	75 > 45 > 11 > 45	93 > 100 > 65 > 40	100 > 32 > - > 70	120 > 34 > 50 > - > 10
Point Count done	Yes	No	Yes	Yes
Comments	Oscillatory zoning in Plag	Oscillitory zoning in Plag	Agglomerate of Plag, Aug, Oliv, Opaqs, from 5 - 50	Blebs of opaques within many crystals - resorption?

Sample Locality	52/3 Flow Front Flow 2	53/1 Flow 1	53/2 Flow 1	53/2 Flow 1
Hand Speciman				
Colour	Medium grey	Mottled dark grey/white/red	Dark grey/red	Dark grey/red
Mafic : Felsic ratio	80:20	80:20	80:20	80:20
Fabric	Porphyritic	Porphyritic	Porphyritic	Porphyritic
Crystals visable	Plag, Oliv, Hyp	Plag, Oliv, Hyp		
Crystal volume %	85%	90%	85%	85%
Crystal Sizes	1 - 4mm	0.5 - 4mm	1 - 5mm	1 - 5mm
Grain Size	Medium	Medium	Medium	Medium
Comments				
Vesicularity				
Shape of vesicles	Subrounded	Subrounded	Subangular	Subangular
Min and Max sizes	0.5 - 4mm	0.5 - 2mm	0.5 - 3mm	0.5 - 3mm
Coalascence	Yes	No	Yes	Yes
Vesicularity %	30%	2%	5%	5%
Thin Section				
Groundmass	Intergrannular Plag laths Fine grained	Iddingsite Plag laths	Intergranular Plag laths Red heamitite Fine grained	Intergranular 50% Iddingsite, 50% Plag laths Blebs Hyp, Olivine Fine grained
Phenocrysts	Plag > Opag > Oliv > Hyp > Aug	Plag > Oliv > Aug	Plag > Oliv	Plag > Oliv > Hyp > Aug > Opaq
Shape	All Subhedral	All Subhedral	All Subhedral	All Subhedral
Proportion (of crystals)	70% > 10% > 5% > 5% > 5%	45% > 35% > 15%	40% > 5%	80% > 10% > 5% > 1% > 1%
Maximum sizes	58 > - > 40 > 18	120 > 120 > 60	100 > 70	90 > 130 > 82 > 12
Point Count done	Yes	Yes	No	Yes
Comments	Agglomerocrysts of Aug, Plag, Opaq	No alteration at margins, formed in magma chamber	Heamatite rock inclusion	Oliv, Hyp twin

Sample Locality	65/3 Flow 10
Hand Speciman	
Colour	Grey
Mafic : Felsic ratio	80:20
Fabric	Porphyritic
Crystals visable	Plagioclase
Crystal volume %	60%
Crystal Sizes	0.5 - 3mm
Grain Size	Medium
Comments	
Vesicularity	
Shape of vesicles	Subrounded, Irregular
Min and Max sizes	0.5 -4mm
Coalascence	Yes
Vesicularity %	40%
Thin Section	
Groundmass	Intergrannular Plag laths Iddingsite, Blebs Oliv, Hyp, Aug Fine grained
Phenocrysts	Plag > Oliv > Aug > Hyp > Opaq
Shape	All Subhedral
Proportion (of crystals)	60% > 15% > 10% > 10% > 5%
Maximum sizes	75 > 45 > 11 > 45
Point Count done	Yes
Comments	Oscillatory zoning in Plag

APPENDIX SIX

GRAIN SIZE RAW DATA

Sample 18/1
Locality South Red Crater face - track up to ridge
Date Collected 21/1/03

Phi Ø	Weight (g)	Weight (g) Cummulative	Weight % Cummulative	Weight %
= -5.0	33.30	33.30	5.00	5.00
-4.5	14.10	47.40	7.12	2.12
-4.0	52.40	99.80	14.99	7.87
-3.5	64.30	164.10	24.65	9.66
-3.0	91.90	256.00	38.45	13.80
-2.5	96.90	352.90	53.01	14.56
-2.0	74.00	426.90	64.12	11.12
-1.5	60.30	487.20	73.18	9.06
-1.0	44.20	531.40	79.82	6.64
-0.5	29.59	560.99	84.27	4.44
0.0	20.40	581.39	87.33	3.06
0.5	14.40	595.79	89.49	2.16
1.0	14.54	610.33	91.68	2.18
1.5	12.94	623.27	93.62	1.94
2.0	11.70	634.97	95.38	1.76
2.5	11.00	645.97	97.03	1.65
3.0	10.20	656.17	98.56	1.53
3.5	5.20	661.37	99.34	0.78
4.0	2.43	663.80	99.71	0.37
> 4.0	1.94	665.74	100.00	0.29

Actual Total Weight (g) 666.30

Sample 18/3
Locality Southern crater rim
Date Collected 21/1/03

Phi Ø	Weight (g)	Weight (g) Cummulative	Weight % Cummulative	Weight %
= -5.0	11.50	11.50	2.08	2.08
-4.5	23.80	35.30	6.39	4.31
-4.0	20.10	55.40	10.03	3.64
-3.5	47.70	103.10	18.67	8.64
-3.0	81.70	184.80	33.47	14.80
-2.5	89.60	274.40	49.69	16.23
-2.0	63.80	338.20	61.25	11.55
-1.5	51.30	389.50	70.54	9.29
-1.0	38.10	427.60	77.44	6.90
-0.5	29.30	456.90	82.75	5.31
0.0	20.44	477.34	86.45	3.70
0.5	13.90	491.24	88.97	2.52
1.0	15.50	506.74	91.77	2.81
1.5	12.80	519.54	94.09	2.32
2.0	9.30	528.84	95.77	1.68
2.5	8.30	537.14	97.28	1.50
3.0	7.00	544.14	98.55	1.27
3.5	4.18	548.32	99.30	0.76
4.0	2.00	550.32	99.66	0.36
> 4.0	1.85	552.17	100.00	0.36

Actual Total Weight (g) 553.60

Sample 18/4
Locality Southern crater rim
Date Collected 21/1/03

Phi Ø	Weight (g)	Weight (g) Cummulative	Weight % Cummulative	Weight %
= -5.0	87.70	87.70	13.52	13.52
-4.5	78.40	166.10	25.60	12.08
-4.0	42.90	209.00	32.21	6.61
-3.5	65.20	274.20	42.26	10.05
-3.0	73.80	348.00	53.64	11.37
-2.5	67.70	415.70	64.07	10.43
-2.0	50.40	466.10	71.84	7.77
-1.5	39.30	505.40	77.90	6.06
-1.0	32.80	538.20	82.95	5.06
-0.5	24.90	563.10	86.79	3.84
0.0	18.70	581.80	89.67	2.88
0.5	13.00	594.80	91.68	2.00
1.0	13.60	608.40	93.77	2.10
1.5	10.60	619.00	95.41	1.63
2.0	8.60	627.60	96.73	1.33
2.5	7.40	635.00	97.87	1.14
3.0	6.70	641.70	98.91	1.03
3.5	3.80	645.50	99.49	0.59
4.0	1.60	647.10	99.74	0.25
> 4.0	1.70	648.80	100.00	0.26

Actual Total Weight (g) 649.50

Sample 20/1
Locality Eastern crater rim - ECR-a1
Date Collected 21/1/03

Phi Ø	Weight (g)	Weight (g) Cummulative	Weight % Cummulative	Weight %
= -5.0	52.30	52.30	7.58	7.58
-4.5	0.00	52.30	7.58	0.00
-4.0	45.20	97.50	14.13	6.55
-3.5	40.40	137.90	19.99	5.86
-3.0	54.40	192.30	27.87	7.89
-2.5	81.70	274.00	39.72	11.84
-2.0	55.60	329.60	47.78	8.06
-1.5	47.80	377.40	54.70	6.93
-1.0	38.00	415.40	60.21	5.51
-0.5	35.10	450.50	65.30	5.09
0.0	33.60	484.10	70.17	4.87
0.5	34.20	518.30	75.13	4.96
1.0	41.40	559.70	81.13	6.00
1.5	33.90	593.60	86.04	4.91
2.0	25.70	619.30	89.77	3.73
2.5	28.90	648.20	93.96	4.19
3.0	25.30	673.50	97.62	3.67
3.5	7.40	680.90	98.70	1.07
4.0	5.30	686.20	99.46	0.77
> 4.0	3.70	689.90	100.00	0.54

Actual Total Weight (g) 691.90

Sample 33/4
Locality SCR7 - Southern crater rim
Date Collected 5/3/2003

Phi Ø	Weight (g)	Weight (g) Cummulative	Weight % Cummulative	Weight %
= -5.0	19.90	19.90	3.75	3.75
-4.5	15.50	35.40	6.67	2.92
-4.0	21.40	56.80	10.70	4.03
-3.5	43.30	100.10	18.86	8.16
-3.0	67.70	167.80	31.62	12.76
-2.5	83.60	251.40	47.37	15.75
-2.0	49.90	301.30	56.77	9.40
-1.5	47.50	348.80	65.72	8.95
-1.0	40.40	389.20	73.34	7.61
-0.5	33.20	422.40	79.59	6.26
0.0	24.50	446.90	84.21	4.62
0.5	17.10	464.00	87.43	3.22
1.0	17.80	481.80	90.79	3.35
1.5	16.00	497.80	93.80	3.01
2.0	11.60	509.40	95.99	2.19
2.5	8.90	518.30	97.66	1.68
3.0	6.30	524.60	98.85	1.19
3.5	3.10	527.70	99.43	0.58
4.0	1.80	529.50	99.77	0.34
> 4.0	1.20	530.70	100.00	0.23

Actual Total Weight (g) 530.40

Sample 35/2
Locality Eastern crater rim - ECR-a4
Date Collected 5/3/2003

Phi Ø	Weight (g)	Weight (g) Cummulative	Weight % Cummulative	Weight %
= -5.0	0.00	0.00	0.00	0.00
-4.5	0.00	0.00	0.00	0.00
-4.0	29.40	29.40	9.21	9.21
-3.5	40.30	69.70	21.83	12.62
-3.0	57.40	127.10	39.81	17.98
-2.5	50.10	177.20	55.50	15.69
-2.0	36.90	214.10	67.06	11.56
-1.5	24.30	238.40	74.67	7.61
-1.0	18.40	256.80	80.44	5.76
-0.5	12.40	269.20	84.32	3.88
0.0	9.00	278.20	87.14	2.82
0.5	6.54	284.74	89.19	2.05
1.0	7.23	291.97	91.45	2.26
1.5	6.90	298.87	93.61	2.16
2.0	6.20	305.07	95.56	1.94
2.5	5.63	310.70	97.32	1.76
3.0	4.20	314.90	98.63	1.32
3.5	1.90	316.80	99.23	0.60
4.0	1.50	318.30	99.70	0.47
> 4.0	0.96	319.26	100.00	0.30

Actual Total Weight (g) 319.10

Sample 67/1
Locality SCR4 - Southern crater rim
Date Collected 13/6/03

Phi Ø	Weight (g)	Weight (g) Cummulative	Weight % Cummulative	Weight %
= -5.0	10.40	10.40	0.79	0.79
-4.5	40.60	51.00	3.26	3.07
-4.0	77.20	123.20	9.31	5.84
-3.5	167.30	290.50	21.96	12.65
-3.0	228.20	518.70	39.21	17.25
-2.5	246.30	765.00	57.83	18.62
-2.0	129.20	894.20	67.60	9.77
-1.5	103.80	998.00	75.45	7.85
-1.0	76.00	1074.00	81.19	5.75
-0.5	59.70	1133.70	85.70	4.51
0.0	40.70	1174.40	88.78	3.08
0.5	27.20	1201.60	90.84	2.06
1.0	32.20	1233.80	93.27	2.43
1.5	26.30	1260.10	95.26	1.99
2.0	19.40	1279.50	96.73	1.47
2.5	16.70	1296.20	97.99	1.26
3.0	12.40	1308.60	98.93	0.94
3.5	6.70	1315.30	99.43	0.51
4.0	4.30	1319.60	99.76	0.33
> 4.0	3.20	1322.80	100.00	0.24

Actual Total Weight (g) 1327.10

Sample 67/2
Locality SCR3 - Southern crater rim
Date Collected 13/6/03

Phi Ø	Weight (g)	Weight (g) Cummulative	Weight % Cummulative	Weight %
= -5.0	142.30	142.30	9.42	9.42
-4.5	110.10	252.40	16.71	7.23
-4.0	240.70	493.10	32.64	15.43
-3.5	189.10	682.20	45.16	12.52
-3.0	224.20	906.40	60.00	14.84
-2.5	186.00	1092.40	72.31	12.31
-2.0	93.80	1186.20	78.52	6.21
-1.5	60.60	1246.80	82.53	4.01
-1.0	48.10	1294.90	85.72	3.18
-0.5	40.30	1335.20	88.38	2.67
0.0	31.10	1366.30	90.44	2.06
0.5	24.10	1390.40	92.04	1.60
1.0	32.30	1422.70	94.17	2.14
1.5	23.40	1446.10	95.72	1.55
2.0	19.70	1465.80	97.03	1.30
2.5	16.70	1482.50	98.13	1.11
3.0	13.20	1495.70	99.01	0.87
3.5	7.50	1503.20	99.50	0.50
4.0	3.80	1507.00	99.76	0.25
> 4.0	3.70	1510.70	100.00	0.24

Actual Total Weight (g) 1510.60

Sample 100/5
Locality Unit 6 - Eastern inner-wall
Date Collected 11/1/2004

Phi Ø	Weight (g)	Weight (g) Cummulative	Weight % Cummulative	Weight %
= -5.0	22.00	22.00	2.35	2.35
-4.5	76.90	98.90	10.55	8.20
-4.0	64.40	163.30	17.41	6.87
-3.5	86.40	249.70	26.63	9.21
-3.0	102.90	352.60	37.60	10.97
-2.5	135.40	488.00	52.04	14.44
-2.0	86.90	574.90	61.30	9.27
-1.5	61.40	636.30	67.85	6.55
-1.0	45.30	681.60	72.68	4.83
-0.5	39.30	720.90	76.87	4.19
0.0	31.40	752.30	80.22	3.35
0.5	25.30	777.60	82.92	2.70
1.0	30.80	808.40	86.20	3.28
1.5	29.30	837.70	89.33	3.12
2.0	24.10	861.80	91.90	2.57
2.5	22.50	884.30	94.30	2.40
3.0	20.40	904.70	96.47	2.18
3.5	13.80	918.50	97.94	1.47
4.0	9.80	928.30	98.99	1.04
> 4.0	9.50	937.80	100.00	1.01

Actual Total Weight (g) 938.50

Sample 100/13
Locality Unit 1 - Eastern inner-wall
Date Collected 11/1/2004

Phi Ø	Weight (g)	Weight (g) Cumulative	Weight % Cumulative	Weight %
-4.5	139.60	139.60	16.78	4.61
-4.0	132.70	272.30	32.73	4.39
-3.5	78.70	351.00	42.19	2.60
-3.0	80.50	431.50	51.86	2.66
-2.5	70.10	501.60	60.29	2.32
-2.0	60.00	561.60	67.50	1.98
-1.5	44.50	606.10	72.85	1.47
-1.0	34.70	640.80	77.02	1.15
-0.5	29.80	670.60	80.60	0.98
0.0	25.70	696.30	83.69	0.85
0.5	22.94	719.24	86.45	0.76
1.0	23.60	742.84	89.28	0.78
1.5	23.00	765.84	92.05	0.76
2.0	17.56	783.40	94.16	0.58
2.5	15.50	798.90	96.02	0.51
3.0	-	-	96.02	-
3.5	19.78	818.68	98.40	0.65
4.0	6.60	825.28	99.19	0.22
> 4.0	6.72	832.00	100.00	0.22

Actual Total Weight (g) 832.00

Sample 58/1b
Locality SCR8 - Southern crater rim
Date Collected 15/5/03

Phi Ø	Weight (g)	Weight (g) Cummulative	Weight % Cummulative	Weight %
-8.0	4505.00	4505.00	28.11	28.11
-7.0	875.00	5380.00	33.57	5.46
-6.0	4420.00	9800.00	61.14	27.58
-5.0	4290.00	14090.00	87.91	26.77
-4.5	448.50	14538.50	90.71	2.80
-4.0	478.20	15016.70	93.69	2.98
-3.5	233.30	15250.00	95.15	1.46
-3.0	150.30	15400.30	96.09	0.94
-2.5	98.97	15499.27	96.70	0.62
-2.0	93.86	15593.13	97.29	0.59
-1.5	83.90	15677.03	97.81	0.52
-1.0	74.50	15751.53	98.28	0.46
-0.5	66.65	15818.18	98.69	0.42
0.0	31.58	15849.76	98.89	0.20
0.5	28.96	15878.72	99.07	0.18
1.0	31.00	15909.72	99.26	0.19
1.5	32.38	15942.10	99.47	0.20
2.0	25.10	15967.20	99.62	0.16
2.5	23.10	15990.30	99.77	0.14
3.0	20.10	16010.40	99.89	0.13
3.5	9.04	16019.44	99.95	0.06
4.0	4.60	16024.04	99.98	0.03
> 4.0	3.70	16027.74	100.00	0.02

Actual Total Weight (g) 16027.74

APPENDIX SEVEN

UNIVERSITY OF WAIKATO CATALOG NUMBERS FOR ALL SAMPLES

CJB SAMPLE NO	UOW CATALOG NO	PURPOSE	EASTING/NORTHING
51/1	W04 0901	Thin section	E2739417/NZ N6225777
34/3	W04 0902	Thin section	E2739031/NZ N6226207
34/1	W04 0903	Thin section	E2739167/NZ N6226207
34/3	W04 0904	Thin section	E2739031/NZ N6226207
53/2	W04 0905	Thin section	E2740263/NZ N6225013
38/1	W04 0906	Thin section	E2739663/NZ N6227269
39/1	W04 0907	Thin section	E2739434/NZ N6227096
38/1	W04 0908	Thin section	E2739663/NZ N6227269
53/2	W04 0909	Thin section	E2740263/NZ N6225013
47/4	W04 0910	Thin section	E2740176/NZ N6226105
52/1	W04 0911	Thin section	E2739449/NZ N6225498
36/1	W04 0912	Thin section	E2738994/NZ N6226018
51/3	W04 0913	Thin section	E2739213/NZ N6225506
53/1	W04 0914	Thin section	E2740232/NZ N6224955
51/2	W04 0915	Thin section	E2739384/NZ N6225764
49/1	W04 0916	Thin section	E2740207/NZ N6226211
49/2	W04 0917	Thin section	E2740436/NZ N6226197
39/1	W04 0918	Thin section	E2739434/NZ N6227096
52/3	W04 0919	Thin section	E2739698/NZ N6225052
18/2	W04 0920	Thin section	E2738900/NZ N6226244
48/2	W04 0921	Thin section	E2740089/NZ N6226200
56/2	W04 0922	Thin section	North face of Red Crater
62/1	W04 0923	Thin section	E2739162/NZ N6226152
47/5	W04 0924	Thin section	E2740136/NZ N6226201
65/2	W04 0925	Thin section	North face of Red Crater
47/1	W04 0926	Thin section	E2740835/NZ N6225719
40/1	W04 0927	Thin section	E2739129/NZ N6226632
24/2	W04 0928	Thin section	E2738748/NZ N6226217
40/2	W04 0929	Thin section	E2739124/NZ N6226628
65/3	W04 0930	Thin section	North face of Red Crater
57/1	W04 0931	Thin section	Lava Flow 10
50/1	W04 0932	Thin section	E2739754/NZ N6225757
40/2	W04 0933	Thin section	E2739124/NZ N6226628
18/5a	W04 0934	Thin section	E2739073/NZ N6226227
19/3	W04 0935	Thin section	E2739409/NZ N6226460
100/15	W04 0936	Thin section	Inside Red Crater
60/01 (10)	W04 0937	SEM	Eastern Crater Rim - ECR-a2
60/02 (1)	W04 0938	SEM	E2739234/NZ N6226236
67/4 (27)	W04 0939	SEM	E2739117/NZ N6226234
60/02 (12)	W04 0940	SEM	E2739117/NZ N6226234
60/02 (17)	W04 0941	SEM	E2739117/NZ N6226234
60/02 (21)	W04 0942	SEM	E2739117/NZ N6226234
58/01 (1)	W04 0943	SEM	E2739126/NZ N6226225
67/3 (26)	W04 0944	SEM	E2739117/NZ N6226234
58/01 (7)	W04 0945	SEM	E2739126/NZ N6226225
59/02 (9)	W04 0946	SEM	E2739126/NZ N6226225

CJB SAMPLE NO	UOW CATALOG NO	PURPOSE	EASTING/NORTHING
58/03 (5)	W04 0947	SEM	E2739126/NZ N6226225
67/6 (7)	W04 0948	SEM	E2739179/NZ N6226231
67/6 (3)	W04 0949	SEM	E2739179/NZ N6226231
58/01	W04 0950	Clast density	E2739126/NZ N6226225
58/03	W04 0951	Clast density	E2739126/NZ N6226225
67/3	W04 0952	Clast density	E2739117/NZ N6226234
67/4	W04 0953	Clast density	E2739117/NZ N6226234
59/02	W04 0954	Clast density	E2739126/NZ N6226225
60/01	W04 0955	Clast density	Eastern Crater Rim - ECR-a2
67/6	W04 0956	Clast density	E2739179/NZ N6226231
60/02	W04 0957	Clast density	E2739117/NZ N6226234
100/1	W04 0958	Clast density	E2739219/NZ N6226236
100/2	W04 0959	Clast density	E2739219/NZ N6226236
100/3	W04 0960	Clast density	E2739219/NZ N6226236
100/4	W04 0961	Clast density	E2739219/NZ N6226236
100/7	W04 0962	Clast density	E2739219/NZ N6226236
100/8	W04 0963	Clast density	E2739219/NZ N6226236
100/9	W04 0964	Clast density	E2739219/NZ N6226236
100/10	W04 0965	Clast density	E2739219/NZ N6226236
100/11	W04 0966	Clast density	E2739219/NZ N6226236
100/12	W04 0967	Clast density	E2739219/NZ N6226236
100/13	W04 0968	Grain size	E2739219/NZ N6226236
100/5	W04 0969	Grain size	E2739219/NZ N6226236
67/2	W04 0970	Grain size	E2739125/NZ N6226227
67/1	W04 0971	Grain size	E2739186/NZ N6226241
58/1b	W04 0972	Grain size	E2739126/NZ N6226225
35/2	W04 0973	Grain size	E2739210/NZ N6226246
33/4	W04 0974	Grain size	E2739116/NZ N6226228
20/1	W04 0975	Grain size	E2739200/NZ N6226230
18/4	W04 0976	Grain size	E2739064/NZ N6226235
18/3	W04 0977	Grain size	E2739064/NZ N6226235
18/1	W04 0978	Grain size	E2738876/NZ N6226182